



University of
Sheffield

Investigating the role of *DOCK6* and *EOGT* in Cardiac Development and Congenital Heart Disease

Emma Louise Armitage

A thesis submitted in partial fulfilment of the requirements for
the degree of Doctor of Philosophy

The University of Sheffield
Department of Biosciences

April 2023

Table of Contents

Acknowledgements	VI
Abstract	VIII
Abbreviations	IX
List of tables and figures	XII
Declaration	XV
1. Introduction	1
1.1 Congenital heart defects	1
1.2 Human heart development	2
1.3 Adams-Oliver Syndrome	6
1.4 NOTCH signalling.....	10
1.5 NOTCH signalling in cardiovascular development	12
1.6 RAC1/CDC42 signalling	17
1.7 RAC1/CDC42 signalling in cardiovascular development	20
1.8 <i>DOCK6</i> and <i>EOGT</i> are mutated in autosomal recessive AOS.....	25
1.9 EGF domain-specific <i>O</i> -GlcNAc Transferase (<i>EOGT</i>).....	26
1.10 Deducator of Cytokinesis 6 (<i>DOCK6</i>)	27
1.11 Animal models of AOS.....	31
1.12 Using zebrafish as a model to study human heart development	32
1.13 Zebrafish heart development	34
1.14 Rationale and Aims	37
2. Materials and Methods	39
2.1 Zebrafish husbandry	39
2.1.1 Zebrafish lines	39
2.1.2 Zebrafish care.....	39
2.1.3 Zebrafish embryo collection and staging	40
2.2 Embryo manipulation	40
2.2.1 Embryo fixation	40
2.2.2 Microinjection	40
2.3 Molecular techniques	41
2.3.1 Isolation of total genomic DNA	41
2.3.2 Isolation of total RNA	41
2.3.3 Generation of complementary DNA	42
2.3.4 Polymerase Chain Reaction (PCR)	42
2.3.5 TOPO-TA cloning	44
2.3.6 Bacterial transformation	44
2.4 mRNA <i>in situ</i> hybridisation	46
2.4.1 mRNA <i>in situ</i> hybridisation probe synthesis	46
2.4.2 mRNA <i>in situ</i> hybridisation probes.....	47
2.4.3 mRNA <i>in situ</i> hybridisation protocol	48
2.4.4 mRNA <i>in situ</i> hybridisation antibody pre-incubation.....	50

2.4.5 mRNA <i>in situ</i> hybridisation solutions	50
2.4.6 Imaging mRNA <i>in situ</i> hybridisations	51
2.4.7 Quantification and statistical analysis of heart area and heart looping from mRNA <i>in situ</i> hybridisation images	51
2.4.8 Genotyping post mRNA <i>in situ</i> hybridisation	52
2.5 Generation of CRISPR/Cas9 promoter-less mutant zebrafish lines	52
2.5.1 gRNA design	52
2.5.2 gRNAs used	52
2.5.3 Microinjection to generate CRISPR/Cas9 promoter-less stable mutant zebrafish lines	53
2.5.4 CRISPR/Cas9 primers.....	54
2.6 Generation of CRISPR/Cas12a AOS disease specific knock-in mutant zebrafish lines.....	55
2.6.1 crRNA design.....	55
2.6.2 crRNAs used	56
2.6.3 Designing single stranded oligonucleotides for homology directed repair	56
2.6.4 Single stranded oligos used.....	57
2.6.5 Microinjection to generate CRISPR/Cas12a knock-in mutant zebrafish lines.....	58
2.6.6 CRISPR/Cas12a primers.....	59
2.7 Cloning coding sequences for over-expression experiments	60
2.7.1 Designing primers to amplify open reading frames	60
2.7.2 Generation of <i>eogt</i> sense and antisense and <i>isg15</i> sense over-expression constructs.....	61
2.7.3 Microinjection of <i>eogt</i> and <i>isg15</i> over-expression RNA.....	63
2.8 Immunohistochemistry	63
2.8.1 Immunohistochemistry protocol	63
2.8.2 Immunohistochemistry imaging	64
2.8.3 Quantification of Notch positive cells	64
2.8.4 Statistical analysis	65
2.9 Light-sheet imaging and analysis	65
2.9.1 Imaging embryos on the Light-sheet microscope	65
2.9.2 Genotyping embryos following Light-sheet imaging	66
2.9.3 MorphoHeart image analysis.....	66
2.9.4 Statistical analysis	67
2.10 Genotyping and raising homozygous mutant embryos to adulthood	67
2.11 Quantitative PCR (qPCR).....	67
2.11.1 RNA extraction and cDNA synthesis for qPCR experiments.....	67
2.11.2 Primer design and efficiency testing	68
2.11.3 qPCR primers.....	68
2.11.4 qPCR protocol	69
2.11.5 qPCR statistical analysis	69
2.12 Adult behavioural analysis	70
2.12.1 Adult behavioural analysis protocol.....	70
2.12.2 Statistical analysis	70
3. Creating zebrafish models of Adams-Oliver Syndrome	71
3.1 Introduction.....	71
3.2 Humans and zebrafish share conserved <i>DOCK6</i> transcripts.....	72
3.3 Zebrafish <i>dock6</i> transcripts are expressed in distinct tissues during cardiac development ..	74
3.4 Generating zebrafish <i>dock6</i> mutant models using CRISPR genome editing	78
3.5 <i>dock6-201</i> promoter-less mutant CRISPR/Cas9-mediated genome editing strategy	79

3.6 <i>dock6-201</i> AOS disease-specific knock-in mutant CRISPR/Cas12a-mediated genome editing strategy	81
3.7 Humans and zebrafish share conserved <i>EOGT</i> transcripts.....	88
3.8 Identification of a zebrafish <i>eogt</i> antisense transcript expressed in the heart during cardiac development	89
3.9 Generating zebrafish <i>eogt</i> mutant models using CRISPR genome editing.....	92
3.10 <i>eogt-201</i> AOS disease-specific knock-in mutant CRISPR/Cas12a-mediated genome editing strategy	94
3.11 Discussion	97
4. Investigating the role of <i>dock6</i> in Cardiac Development and Congenital Heart Disease	110
4.1 Introduction	110
4.2 <i>dock6-RI1</i> retained intron mutations overlap with active enhancer methylation marks.....	112
4.3 <i>dock6-RI1^{ins41}</i> retained intron insertion mutation results in reduced expression of both <i>dock6</i> transcripts	113
4.4 <i>dock6-RI1^{A28}</i> retained intron deletion mutation has no effect on <i>dock6-201</i> or <i>dock6-RI1</i> expression	116
4.5 <i>dock6-RI1</i> retained intron mutations have no effect on cardiac development	118
4.6 <i>dock6-RI1^{ins41}</i> retained intron insertion mutation has no effect on adult behaviour	125
4.7 Investigating potential compensation mechanisms in <i>dock6</i> mutants – <i>isg15</i> expression is heterogeneous during early development	127
4.8 Over-expressing <i>isg15</i> mRNA in <i>dock6-RI1^{ins41}</i> retained intron insertion mutant embryos leads to cardiac abnormalities	129
4.9 <i>dock6-201^{ins36Δ65}</i> coding sequence mutation has no effect on <i>dock6-201</i> expression or cardiac development	138
4.10 Discussion	140
5. Investigating the role of <i>eogt</i> in Cardiac Development and Congenital Heart Disease 153	
5. 1 Introduction	153
5.2 Strategy to over-express <i>eogt</i> sense and antisense RNA to investigate their effects on heart development and Notch signalling.....	154
5.3 Over-expressing <i>eogt</i> sense or antisense RNA has no effect on cardiac development.....	158
5.4 Notch signalling pathway components are expressed in the ventricle and OFT during early cardiac development	161
5.5 Over-expressing <i>eogt</i> sense or antisense RNA has no effect on OFT development.....	163
5.6 Over-expressing <i>eogt</i> sense or antisense RNA has no effect on Notch signalling in the developing heart.....	167
5.7 <i>eogt-201^{A28}</i> coding sequence mutant has no effect on <i>eogt</i> sense or antisense expression	169
5.8 <i>eogt-201^{A28}</i> coding sequence mutant has no effect on cardiac development	171
5.9 <i>eogt-201^{A28}</i> coding sequence mutant has no effect on Notch signalling in the developing heart.....	175

5.10 Discussion	178
6. Discussion	187
6.1 Why is AOS associated with such varied feature severity?	187
6.2 How do phenotypes in AOS arise?	191
6.3 Are non-coding mutations involved in the pathogenesis of AOS?	195
6.4 Future perspectives.....	199
7. Bibliography	202

Acknowledgements

Firstly, I want to thank Joshua Griffiths for all his help and support over the past 3 years, and in particular the last 4 stressed months of thesis writing and job applications. I appreciate you sitting through endless practice talks and acting enthusiastic when I tell you about an exciting paper I've just read, even though you probably have no idea what I am talking about. And for bringing me McDonald's or pizza to try to cheer me up, I hope to return the favour when you are writing your thesis!

I want to give a special shout out to my group of friends (otherwise known as the Chimney Bees Support Group) for providing me with motivational speeches and many curry nights at Prithiraj, and to Josie Gibson for the coffee walks around the park. I would also like to give a special thank you to my lovely mum and dad who are always so supportive and understanding, and Mollie dog for the cuddles when I've been stressed.

Most importantly, I would like to thank Emily Noël for being an excellent supervisor, my PhD would not have been anywhere near as enjoyable without being in such a brilliant lab. Emily is patient, helpful, enthusiastic and goes above and beyond to ensure everyone in her lab is happy and supported. The Noël lab meetings were a highlight of my week, and I appreciate being able to use these meetings to ask all of my stupid questions, of which there have been many. I feel extremely lucky to have done my PhD in such a friendly and welcoming lab and I am very sad to be leaving.

In addition to Emily, I couldn't have completed my PhD without the support of the rest of the Noël Lab. I want to thank Chris Derrick for helping me so much while we were working in bubble cohorts during the COVID pandemic, and in particular for staying with me in the aquarium while I was outcrossing my first mutant founders, which took me so long I thought we would never leave. I want to thank Juliana Sánchez Posada for putting up with my constant questions about MorphoHeart and for being so patient with me even though it was going in one ear and out of the other. I also want to thank Eric Pollitt, who I am convinced is a cloning genius, for all his help and guidance with anything molecular biology related.

In the wider department, I would like to thank Iwan Evans for teaching me all the science basics, without his help I am sure the start of my PhD would have been much harder. I would also like to thank Tim Chico and Chun Guo for your help and advice during advisory meetings. I am grateful to all the aquarium staff, who do an excellent job taking care of the fish, and to Lisa Van Hateren for all your help with Zeg/3dpf finclips. I would like to thank Darren Robinson for his help over the years with all of my microscope related problems, and finally I would like to give a special shout out to Stone Elworthy, who has endless knowledge when it comes to anything CRISPR related, and I appreciate all of your help.

Finally, I would like to thank all remaining members of C21 (special shout out to Gideon Hughes and Nahal Shahidan for being great lab friends!) and all additional friends in other labs I have made over the years, I've had the best time working with you all.

Abstract

Congenital Heart Defects (CHDs) are structural malformations that occur during development and affect around 1% of live births worldwide. Correct heart development requires tight spatiotemporal control of both the RAC1/CDC42 and NOTCH signalling pathways, and mutations in components or regulators of both pathways can lead to CHDs. Adams-Oliver Syndrome (AOS) is a multisystemic disorder in which 20% of patients also suffer from CHDs. All known causative mutations in AOS have been identified in RAC1/CDC42 or NOTCH signalling pathway components, including autosomal recessive mutations in *DOCK6* and *EOGT* which regulate RAC1/CDC42 and NOTCH signalling respectively. However, it is unknown how mutations in these genes lead to the onset of this disease. I aim to understand how mutations in *DOCK6* and *EOGT* lead to dysregulation of RAC1/CDC42 and NOTCH signalling during heart development and cause CHDs in patients with AOS, using zebrafish as a model.

I find that mRNA of both *dock6* and *eogt* is expressed transiently during early zebrafish cardiovascular development. *eogt* mRNA expression is restricted to a subset of developing vascular structures, while *dock6* exhibits slightly broader expression. Unexpectedly, both genes also have non-coding transcripts which are expressed in the myocardium during early heart morphogenesis: a *dock6-R11* retained intron transcript and an *eogt-201* antisense transcript. Using CRISPR mediated genome editing I have created zebrafish models of AOS with mutations in both *dock6* and *eogt*, in which I assess cardiac morphology throughout development. In addition, I investigate whether non-coding transcripts of *dock6* and *eogt* play a role in heart development, or the onset of CHDs in AOS patients. Finally, I investigate a cell intrinsic compensation mechanism identified in human cells which activates RAC1/CDC42 in the absence of *DOCK6* and assess whether this compensation mechanism could be active in *dock6-R11* retained intron mutants which have reduced *dock6* expression.

Abbreviations

acana	aggrecan a
ACC	aplasia cutis congenita
amhc	atrial myosin heavy chain
AOS	Adams-Oliver Syndrome
ARHGAP31	Rho GTPase activating protein 31
Arp2/3	actin related protein 2/3
AVC	atrioventricular canal
bp	base pairs
CADASIL	cerebral autosomal dominant arteriopathy with subcortical infarcts and leukoencephalopathy
CHD	congenital heart defect
CHIP-seq	chromatin immunoprecipitation sequencing
CMTC	cutis marmorata telangiectatica congenita
CNC	cardiac neural crest
CRISPR	clustered regularly interspaced short palindromic repeats
crRNA	CRISPR RNA
CSL	CBF1/RBPJ/Su(H)/Lag-1
DA	dorsal aorta
DDD	Dowling Degos Disease
DH domain	dbl homology domain
DHR1	DOCK homology region 1
DHR2	DOCK homology region 2
DLL4	delta-like ligand 4
DOCK6	dedicator of cytokinesis 6
dpf	days post fertilisation
ECM	extracellular matrix
EGF	epidermal growth factor-like
EMT	epithelial-mesenchymal transition
EOGT	EGF domain-specific O-GlcNAc Transferase
ER	endoplasmic reticulum
F-actin	filamentous actin

FHF	first heart field
G-actin	globular actin
GAP	GTPase activating protein
GDI	GTPase dissociation inhibitors
GDP	guanosine-5'-diphosphate
GEF	guanine exchange factor
gRNA	guide RNA (crRNA + tracrRNA)
GTP	guanosine-5'-triphosphate
GXYLT1/2	glucoside xylotransferases 1 and 2
HDR	homology-directed Repair
hpf	hours post fertilisation
Hsp70	heat shock protein 70
ISG15	interferon stimulated gene 15
ISVs	intersegmental vessels
IQGAP1	IQ motif containing GTPase activating protein 1
klf2a	krüppel-like factor 2a
LFNG	lunatic fringe
LIMK	LIM-kinase
lncRNA	long non-coding RNA
LOF	loss-of-function
ltbp3	latent transforming growth factor beta binding protein 3
MAML	mastermind-like
MCeV	mid cerebral vein
miRNA	microRNA
MRFT	Myocardin related Transcription Factor
myl7	myosin light chain 7
NICD	notch intracellular domain
NTD	notch transmembrane domain
OFT	outflow tract
O-GlcNAc	O-linked-N-acetylglucosamine
ORF	open reading frame
PAK	P21-activating kinase
PAM	protospacer adjacent motif

PCV	posterior cardinal vein
PH domain	pleckstrin homology domain
POFLUT1	protein O-fucosyltransferase 1
POGLUT1	protein O-glucosyltransferase 1
POGLUT2/3	protein O-glucosyltransferase 2/3
RACE	rapid amplification of cDNA ends
RBPJ	recombination signal binding protein for immunoglobulin kappa J region
sgRNA	single guide RNA
SHF	second heart field
SRF	serum response factor
TALEN	transcription activator like effector nucleases
ToF	Tetralogy of Fallot
tracrRNA	transactivating RNA
TTLD	terminal transverse limb defects
VASP	vasodilator-stimulated phosphoprotein
vmhc	ventricular myosin heavy chain
VSMC	vascular smooth muscle cell
WRC	WASP-related WAVE regulatory complex
ZFN	zinc finger nuclease

List of tables and figures

Figure 1.1. Human heart development	4
Figure 1.2. Common phenotypes associated with AOS	7
Table 1.1. Summary of genetic mutations in AOS with associated phenotypes	9
Figure 1.3. NOTCH signalling pathway	10
Table 1.2. Roles of NOTCH signalling pathway components during heart development	12
Figure 1.4. RAC1/CDC42 signalling pathways	17
Table 1.3. Roles of RAC1/CDC42 during heart development	22
Figure 1.5. A cell intrinsic adaptation mechanism to a chronic loss of <i>DOCK6</i>	29
Figure 1.6. Zebrafish heart development	36
Table 2.1. Zebrafish Lines	39
Table 2.2. Primers to sequence orientation of insert in PCR TOPO-II vector	46
Table 2.3. mRNA <i>in situ</i> hybridisation probe primers	47
Table 2.4. mRNA <i>in situ</i> hybridisation probes generated in this study	47
Table 2.5. mRNA <i>in situ</i> hybridisation probes previously made	48
Table 2.6. <i>in situ</i> hybridisation solutions	50
Table 2.7. gRNAs used in this study	52
Table 2.8. CRISPR/Cas9 Genotyping	54
Table 2.9. crRNAs used in this study	56
Table 2.10. Single Stranded Oligos for CRISPR knock-in	57
Table 2.11. CRISPR/Cas12a Genotyping	59
Table 2.12. Primers to amplify <i>eogt</i> coding sequence	60
Table 2.13. Primers to amplify <i>isg15</i> coding sequence	60
Table 2.14. Ligating <i>eogt</i> coding sequence into the PCS2+ vector	62
Table 2.15. Ligating <i>isg15</i> coding sequence into the PCS2+ vector	62
Table 2.16. Primary antibody solutions for Immunohistochemistry	63
Table 2.17. Secondary antibody solutions for Immunohistochemistry	64
Table 2.18. Housekeeping qPCR primers	68
Table 2.19. Experimental qPCR Primers	68
Figure 3.1. Human <i>DOCK6</i> gene structure	73
Figure 3.2. Zebrafish <i>dock6</i> gene structure	75

Figure 3.3. Zebrafish <i>dock6-201</i> and <i>dock6-R11</i> expression throughout zebrafish development	77
Figure 3.4. Zebrafish <i>dock6-201</i> and <i>dock6-R11</i> sense RNA expression and controls at 24hpf	80
Figure 3.5. Zebrafish <i>dock6-201</i> LOF CRISPR/Cas9 gene editing strategy and the recovered <i>dock6-R11</i> retained intron mutants	82
Figure 3.6. Location of AOS <i>DOCK6</i> mutations	84
Figure 3.7. Zebrafish <i>dock6-201</i> AOS disease-specific knock-in CRISPR/Cas12a gene editing strategy and the recovered <i>dock6-201</i> coding sequence mutant	86
Figure 3.8. Human <i>EOGT</i> gene structure	89
Figure 3.9. Zebrafish <i>eogt</i> gene structure	91
Figure 3.10. Zebrafish <i>eogt</i> sense and antisense RNA expression patterns throughout development	92
Figure 3.11. Location of AOS <i>EOGT</i> mutations	94
Figure 3.12. Zebrafish <i>eogt-201</i> AOS disease-specific knock-in CRISPR/Cas12a gene editing strategy and the recovered <i>eogt-201</i> coding sequence mutant	96
Figure 4.1. <i>dock6-R11</i> retained intron mutants overlap with active enhancer methylation marks	110
Figure 4.2. <i>dock6-R11^{ins41}</i> mutation results in reduced expression of both <i>dock6</i> transcripts	112
Figure 4.3. <i>dock6-R11^{Δ28}</i> mutation has no effect on <i>dock6</i> expression	114
Figure 4.4. <i>dock6-R11^{ins41}</i> mutation has no effect on cardiac morphology	116
Figure 4.5. <i>dock6-R11^{Δ28}</i> mutation has no effect on cardiac morphology	118
Figure 4.6. MorphoHeart analysis of cardiac morphology and size in <i>dock6-R11^{ins41}</i> mutant embryos	119
Figure 4.7. MorphoHeart analysis of myocardial thickness in <i>dock6-R11^{ins41}</i> mutant embryos	121
Figure 4.8. <i>dock6-R11^{ins41}</i> mutation has no effect on adult behaviour	123
Figure 4.9. <i>isg15</i> expression is heterogeneous during zebrafish development.	125
Figure 4.10. <i>isg15</i> coding sequence cloning strategy and RNA over-expression in zebrafish embryos	127
Figure 4.11. Over-expressing <i>isg15</i> mRNA in <i>dock6-R11^{ins41}</i> mutant embryos leads to chamber orientation defects	129

Figure 4.12. Over-expressing <i>isg15</i> mRNA in <i>dock6-R11^{ins41}</i> mutant embryos has no effect on OFT morphology	131
Figure 4.13. Over-expressing <i>isg15</i> mRNA in <i>dock6-R11^{ins41}</i> mutant embryos has no effect on myocardial tissue thickness	132
Figure 4.14. Over-expressing <i>isg15</i> mRNA in <i>dock6-R11^{ins41}</i> mutant embryos has no effect on heart size but does cause reduced myocardial ballooning	134
Figure 4.15. <i>dock6-201^{ins36Δ65}</i> mutation has no effect on <i>dock6-201</i> expression or heart morphology	136
Figure 5.1. <i>eogt</i> sense and antisense coding sequence cloning strategy and RNA over-expression in zebrafish embryos	153
Figure 5.2. Over-expressing <i>eogt</i> sense or antisense RNA has no effect on cardiac size	156
Figure 5.3. Components of the Notch signalling pathway are expressed in the primitive ventricle and OFT of the developing heart.	159
Figure 5.4. Over-expressing <i>eogt</i> sense or antisense RNA has no effect on OFT morphology	161
Figure 5.5. Over-expressing <i>eogt</i> sense or antisense RNA has no effect on early vascular development	163
Figure 5.6. Over-expression of <i>eogt</i> sense or antisense RNA has no effect on Notch signalling in the developing heart	165
Figure 5.7. <i>eogt-201^{Δ28}</i> mutation has no effect on <i>eogt</i> sense or antisense RNA expression	167
Figure 5.8. <i>eogt-201^{Δ28}</i> mutation has no effect on OFT morphology	169
Figure 5.9. MorphoHeart analysis of cardiac morphology in <i>eogt-201^{Δ28}</i> mutant embryos	171
Figure 5.10. <i>eogt-201^{Δ28}</i> mutation has no effect on cardiac development	173
Figure 5.11. <i>eogt-201^{Δ28}</i> mutation has no effect on Notch signalling in the developing heart	174

Declaration

I, the author, confirm that the Thesis is my own work. I am aware of the University's Guidance on the Use of Unfair Means (www.sheffield.ac.uk/ssid/unfair-means). This work has not been previously been presented for an award at this, or any other, university.

1. Introduction

1.1 Congenital heart defects

Congenital heart defects (CHDs) are structural malformations that arise during development and affect around 1% of live births worldwide (Alankarage et al., 2019). Despite surgical interventions being available to correct some CHDs, patients can still suffer from lifelong complications (Wang et al., 2019). The causes of CHDs can vary from genetic to environmental, with only 15% of CHDs having a known cause (Bouma and Mulder, 2017). Understanding the cause of CHDs can be made even more complicated due to genetic heterogeneity and incomplete penetrance, as although some individuals can share the same genetic mutation, this can result in very different phenotypes, with some people suffering from severe CHDs while others have no disease at all (Williams et al., 2019).

To date around 400 genes have been linked to the development of CHDs, ranging from genes which encode transcription factors to chromatin modifiers, and it is thought that proteins encoded by these genes interact in larger functional networks (Williams et al., 2019). Around 10% of CHDs are associated with chromosomal abnormalities, such as in patients with Down syndrome, while around 5% of CHDs are associated with single genetic mutations in other diseases such as Alagille syndrome, where patients often present with additional defects alongside cardiac malformations (Bouma and Mulder, 2017). Additionally, around 2% of CHDs are considered to be caused by environmental factors, with increased risk being associated with maternal diabetes, maternal obesity, and exposure to certain drugs or alcohol (Bouma and Mulder, 2017).

CHDs can comprise numerous different malformations, and not all of them have one known cause, making it likely that a combination of genetic mutations alongside environmental factors contribute to the development of certain CHDs (Lagendijk et al., 2010). CHDs are generally classified into categories depending on severity, for example severe CHDs are those which cause serious illnesses with a risk of death, such as Tetralogy of Fallot (ToF) and truncus arteriosus; moderate CHDs are likely to require medical care but do not cause serious illness like those in the severe category, such as large atrial septal defects; and mild CHDs are often undetected as patients can be asymptomatic, and include small atrial and ventricular septal defects which can resolve themselves without treatment or interventions (Hoffman and Kaplan, 2002).

Life expectancy of patients with CHDs depends on the CHD severity, and although life expectancy of patients suffering from CHDs has improved over time, these patients often experience complications later in life, such as heart disease, and will often require further operations (Bouma and Mulder, 2017). Therefore, research into how CHDs arise and how to prevent them is important to help people make informed decisions around reproduction, and to help clinicians understand the risk and severity associated with a particular CHD. By defining the genetic pathways and morphological processes underlying heart development, this helps to improve the understanding of how this process goes wrong. Furthermore, mutations linked to heart development could also be important for adult heart function and so it is useful to understand the risk certain mutations pose for CHD patients throughout the remainder of their life.

1.2 Human heart development

The heart is the first functioning organ to develop during embryogenesis, transporting oxygen and nutrients to the rapidly developing embryo (Buckingham et al., 2005). Two weeks into development cardiac precursors emerge from the mesoderm and begin to migrate anteriorly where they form two pools on either side of the embryonic midline (Luxán et al., 2016). These mesodermal cells then differentiate into cardiomyocytes (Buijtenlijk et al., 2020), migrate together and fuse to form the cardiac crescent, spanning the embryonic midline (Günthel et al., 2018). Alongside cardiomyocyte differentiation and migration, another population of cells undergo endothelial to mesenchymal transition (EMT) to form the endocardial cells, which localise with the myocardial cells at the cardiac crescent (Buijtenlijk et al., 2020) (Fig. 1.1 A). As the embryo begins folding, the posterior cardiac crescent then undergoes further fusion resulting in formation of the cardiac tube (Srivastava and Olson, 2000), which is composed of an inner endocardial layer and an outer myocardial layer, separated by extracellular matrix (ECM) (Günthel et al., 2018) (Fig. 1.1 B). Once the heart tube has formed the heart begins to beat by peristaltic contraction from venous to arterial poles to ensure blood flows in one direction before the formation of valves (Sylva et al., 2014).

During the cardiac crescent stage of heart development, two distinct populations of cells contribute to the developing heart myocardium: the first heart field (FHF) and the second heart field (SHF) (Pater et al., 2009). The linear heart tube is composed of

cells derived from the FHF, which in the adult heart contributes only to the left ventricle (Schleich et al., 2013). The SHF is situated in the mesoderm surrounding the heart tube, and these cells proliferate rapidly and are added to either pole of the heart to facilitate further heart growth (Kelly et al., 2014). Lineage tracing in mice demonstrates that the SHF contributes to the remaining structures of the adult heart, a process thought to be conserved in humans (Schleich et al., 2013). Furthermore, mutations in genes required for SHF addition in mice such as *Fgf8*, *Tbx1* and *Mef2c* (Buckingham et al., 2005) have been found to be mutated in human patients which present with CHDs (Zhou et al., 2020; Parisot et al., 2011; Qiao et al., 2017).

Concomitant with SHF addition, the heart undergoes a complex process termed cardiac looping, in which asymmetric morphogenesis changes the shape of the heart from a linear tube to a helical loop (Lombardo et al., 2019) (Fig. 1.1 C). This process is essential for the correct formation of subsequent structures such as the outflow tract (OFT), valves and chambers, along with the correct alignment of the chambers with surrounding vasculature (Desgrange et al., 2018). Studies in mice show that tissue remodelling which underlies heart looping begins with a rightward bending of the arterial pole and a leftward bending of the venous pole, causing the heart tube to form first a “C” shape, and then an “S” shape, shortening the distance between the inflow and outflow tracts while the heart tube lengthens (Garrec et al., 2017). As the heart loops, cardiomyocytes at the outer curvatures begin to proliferate in a process called cardiac ballooning, which is important for distinct chambers to emerge from the heart tube (Günthel et al., 2018). At this stage the formation of distinct cardiac structures has been strongly linked to heart function, as blood flow and contractility have been shown to be required for endocardial cell proliferation during endocardial ballooning (Dietrich et al., 2014) and required to activate expression of the flow responsive gene *klf2a* in developing valve tissue, as loss of blood flow induced *klf2a* expression leads to defective valve morphogenesis (Vermot et al., 2009).

Once the heart tube has undergone initial morphogenesis, more precise and regionalised development can proceed (Lin et al., 2012) (Fig. 1. 1 D). Cardiac septation and valve formation is essential for the formation of the dual circulatory system, as together valves and septa ensure the correct flow of blood through the heart and into the correct circulatory pathways, preventing mixing of oxygenated and

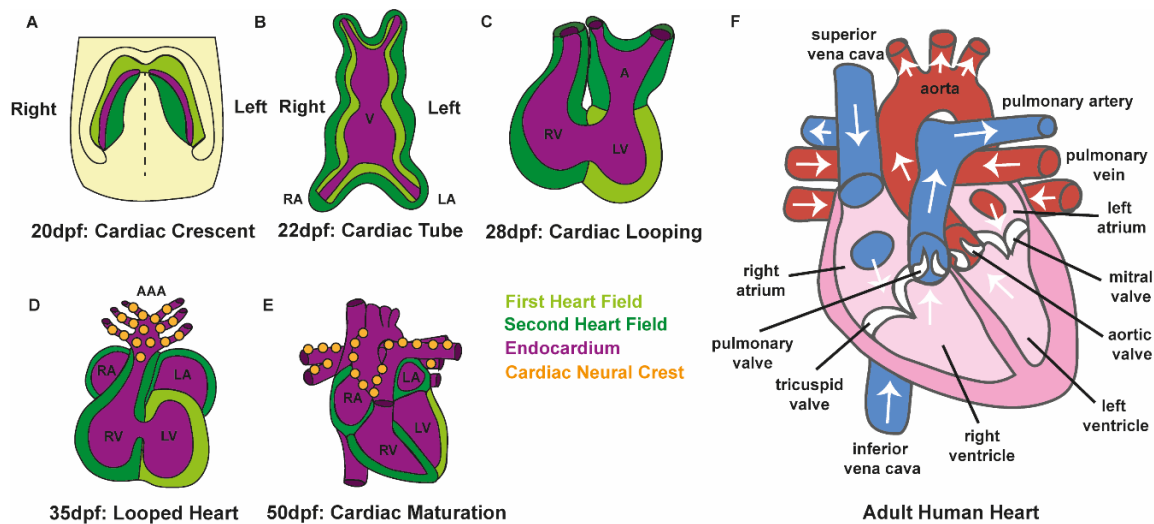


Figure 1.1. Human heart development. (A) At 20dpf, cardiac precursors which have emerged from the mesoderm migrate together to form the cardiac crescent spanning the embryonic midline. Three populations of cardiac cells localise at the cardiac crescent, the first heart field (FHF; light green), the second heart field (SHF; dark green) and endocardial cells (EC; magenta). (B) Following cardiac crescent formation, the embryo begins folding, resulting in formation of the cardiac tube at around 22dpf, which is composed of an inner layer of ECs (magenta), and an outer myocardial layer of mainly FHF cells (light green). SHF cells (dark green) are situated in the mesoderm surrounding the linear heart tube and undergo proliferation before migrating into either pole of the heart to facilitate growth. (C) Following SHF addition the heart begins cardiac looping, an asymmetric process whereby the atrial pole bends right and ventral pole bend left, shortening the distance between the two poles of the heart. (D) Cardiac looping continues, with cardiomyocytes at the outer curvatures of the heart beginning to proliferate to facilitate cardiac ballooning, during which distinct cardiac chambers begin to emerge. During this time, cardiac neural crest cells (CNC; orange) begin migrating into the aortic arch arteries and outflow tract (OFT) to assist formation of the great heart arteries and septation of the OFT to separate blood flow. (E) During cardiac maturation precise and regionalised development occurs, with septation of the atria and ventricles, septation of the OFT, and valve formation occurring to form the final structures of the adult heart. In the adult heart, the FHF mainly contributes to the formation of the left ventricle, while the SHF contributes to the right ventricle and both atria. The CNC cells mainly

contribute to the main heart arteries. (F) The adult human heart, which has two atria, two ventricles and a separated OFT tract to facilitate a dual circulatory system. White arrows indicate direction of blood flow. V: ventricle; A: atrium; RV: right ventricle; LV: left ventricle; RA: right atrium; LA: left atrium; AAA: aortic arch arteries; dpf: days post fertilisation. Figure adapted from Buckingham et al., 2005.

deoxygenated blood (Srivastava and Olson, 2000). OFT and atrioventricular valves form through the expansion of cardiac ECM to produce cardiac cushions, and signalling between the myocardial and endocardial tissue layers surrounding cardiac cushions leads to endocardial cells undergoing epithelial to mesenchymal transition (EMT) (Lin et al., 2012). After EMT, endothelial cells migrate into the cushions where they proliferate to form the valve leaflets which separate the chambers and prevent retrograde blood flow (Srivastava and Olson, 2000). Valves, along with establishment of a pacemaker and conduction system ensure unidirectional blood flow via initiation of contraction at the inflow tract (Schleich et al., 2013). Further septation occurs between the chambers, with the atria being separated by the development of the septum primum, a mesenchymal structure which grows from the roof of the atria and extends down towards the centre of the heart (Schleich et al., 2013). Ventricular separation occurs through the formation of a thick muscular septal ridge in the floor at the centre of the two ventricles, called the interventricular septum which subsequently grows upwards towards the centre of the heart and fuses with both the AV cushions to separate both the ventricles, and the OFT cushions to separate blood flow out of each ventricle (Lin et al., 2012). Additionally, the ventricles undergo a process called trabeculation, in which myocardial cells are extruded into the ventricular lumen and form muscular ridges to increase the surface area for blood oxygen exchange prior to the development of coronary arteries (Schleich et al., 2013). Following trabeculation, the myocardium forms a thick compact layer through proliferation and differentiation of ventricular cardiomyocytes by 8 weeks post fertilisation, and in the adult heart formation of compact myocardium is essential for correct heart function (Buijtendijk et al., 2020). Furthermore, the epicardium forms from a villous population of proepicardial cells which are located at the venous pole of the linear heart tube before contacting the outer surface of the heart and spreading to cover the whole heart (Sylva et al., 2014). Epicardial cells then undergo EMT, producing the sub-epicardial mesenchyme

layer between the epicardium and myocardium, from which the coronary vasculature develops (Buijtenlijk et al., 2020).

To separate the systemic and pulmonary circulation, in addition to ventricular septation the OFT needs to be further divided to form the aorta and the pulmonary trunk (Katano et al., 2019). The OFT is a myocardial tube that runs from the ventricles to the aortic sac, which connects the heart to the pharyngeal arch arteries (Sylva et al., 2014). This septation is driven by the addition of a third population of cells called the cardiac neural crest (CNC) cells (Schleich et al., 2013). The neural crest is a migratory population of cells that arise in the neural tube and migrate throughout the embryo and differentiate into numerous different cell types such as bone, nerves and muscle (Keyte et al., 2014). The CNC is a subpopulation of neural crest cells which migrate to the developing heart, and enter the pharyngeal arch arteries to assist with formation of the main heart arteries, and also migrate into the OFT to assist formation of OFT valves and septation (Erhardt et al., 2021) (Fig. 1.1 D). CNC cells signal to and coordinate with SHF cells to promote SHF addition into the OFT to enable elongation and growth (Schleich et al., 2013). The CNC cells then migrate into the distal OFT, where they become the mesenchyme of the truncal cushions of the OFT, which fuse and separate the OFT into the aorta and pulmonary trunk (Lin et al., 2012) (Fig. 1.1 E). The proximal OFT divides via formation of the conal cushions, which are formed through EMT of endothelial cells, which again fuse in order to separate the OFT into the left and right ventricular outlets (Lin et al., 2012). The conal and truncal cushions of the OFT then fuse together, resulting in OFT separation and development of the main heart vasculature (Lin et al., 2012). The embryonic heart now resembles the adult organ, with four separate chambers and the separation of blood into a parallel circulatory system (Sylva et al., 2014) (Fig. 1.1 F).

1.3 Adams-Oliver Syndrome

Adams-Oliver syndrome (AOS) is a rare developmental disorder affecting 1 in 225,000 live births (Algaze et al., 2013). Diagnosis of AOS is by either the presence of two major features, or one major feature and one minor feature (Snape et al., 2009). Major features include aplasia cutis congenita (ACC), a thinning of the skin on the scalp and underlying skull tissue (Fig. 1.2 A); and terminal transverse limb defects (TTLD), which are characterised by a loss of digits (Fig. 1.2 B). An additional feature used to aid

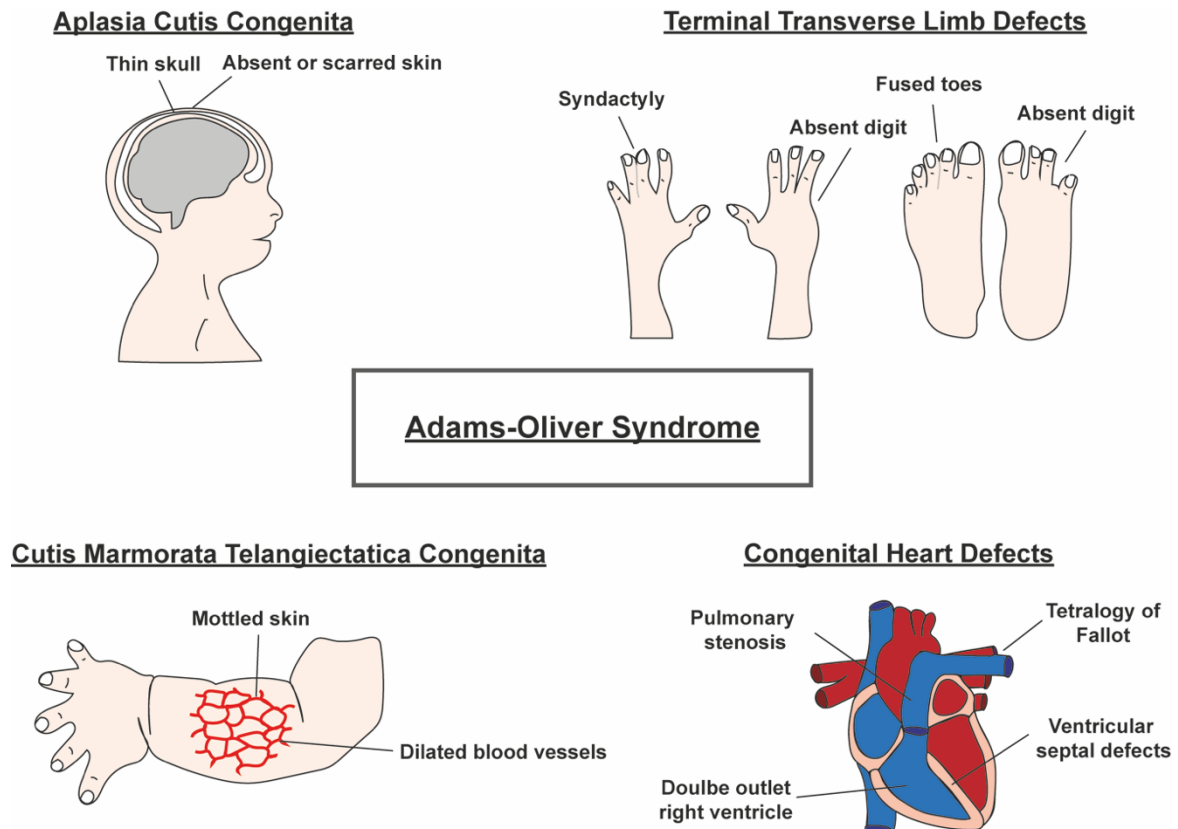


Figure 1.2. Common phenotypes associated with AOS. AOS is diagnosed by either the presence of two major features (ACC, TTLD or family history of AOS), or one major feature and one minor feature (CMTC, CHDs or vascular anomalies). (A) Aplasia cutis congenita (ACC) is a thinning of skin on top of the head, which can also be accompanied by thinning of the underlying skull tissue. (B) Terminal transverse limb defects (TTLD) is characterised by a loss of digits, fusion of digits, loss of fingernails/toenails or complete loss of limbs in extreme cases. (C) Cutis marmorata telangiectatica congenita (CMTC) is the presence of dilated blood vessels and mottled skin. (D) Congenital heart defects (CHDs) are structural malformations of the heart which arise during development, and the most common CHDs associated with AOS include Tetralogy of Fallot, pulmonary stenosis, double outlet right ventricle and ventricular septal defects. Figure adapted from Mašek and Andersson, 2017.

diagnosis also includes a family history of AOS (Algaze et al., 2013). Minor features include: cutis marmorata telangiectatica congenita (CMTC), which causes dilated

blood vessels and mottled skin (Fig. 1.2 C); CHDs (Fig. 1.2 D) or vascular anomalies (Snape et al., 2009).

While little is known about the origin and progression of the disease, mutations in six genes have been identified as causative of AOS: *EOGT*, *DOCK6*, *ARHGAP31*, *NOTCH1*, *DLL4* and *RBPJ*, all of which are involved in either the NOTCH or RAC1/CDC42 signalling pathways, with *NOTCH1* being the most commonly mutated gene associated with AOS (Hassed et al., 2017). Mutations in *EOGT* and *DOCK6* have been identified in autosomal recessive forms of AOS, (Sukalo et al., 2015), whereas mutations in *ARHGAP31*, *NOTCH1*, *DLL4* and *RBPJ* are linked with autosomal dominant forms of the disease (Stittrich et al., 2014, Meester et al., 2015, Southgate et al., 2011, Hassed et al., 2012). Furthermore, while most cases of AOS are gained through autosomal inheritance, non-familial spontaneous cases have also been reported (Mašek and Andersson, 2017). Since mutations in the six genes outlined above only represent approximately 50% of known AOS patients, this suggests there is significantly more to be understood about the genetic origins of AOS, and it is likely more causative genes will be identified in future studies (Sukalo et al., 2015).

Patients with AOS can present with a varying severity of phenotypes, ranging from debilitating defects such as a complete loss of limbs to less severe phenotypes such as a patch of missing hair (Tashima and Okajima, 2018). This is also true for cardiac abnormalities, which only occur in 20% of AOS patients (Algaze et al., 2013) with some patients having no CHDs to others suffering from severe CHDs such as truncus arteriosus (Hassed et al., 2017). Alongside varying severity of phenotypes, defects which arise can also vary depending on the genetic mutation a patient has (Table 1.1). It has been found that TTLD is particularly common in patients with autosomal recessive mutations in *DOCK6* and *EOGT*, which occurred in 94% and 95% of reported patients with mutations in these genes respectively (Hassed et al., 2017). Neurological abnormalities seem to be specifically associated with *DOCK6* mutations, affecting 69% of reported patients, but do arise rarely in AOS patients with mutations in *NOTCH1*, *DLL4* and *EOGT* (Hassed et al., 2017). These neurological defects include structural anomalies of the brain such as atrophy of the corpus callosum, ocular defects such as retinal detachment and intellectual disabilities such as autistic behaviour (Sukalo et al., 2015). Additionally, CHDs are mostly associated with

	Percentage of patients identified from current literature (%)																	
	Hassed et al., 2017 (398 individuals)						Meester et al., 2018 (194 probands/families)						Dudoignon et al., 2019 (25 individuals)					
	NOTCH1	DLL4	DOCK6	EOGT	ARHGAP31	RBPJ	NOTCH1	DLL4	DOCK6	EOGT	ARHGAP31	RBPJ	NOTCH1	DLL4	DOCK6	EOGT	ARHGAP31	RBPJ
Patients with identified mutations (total cohorts)	6	5	4	5	7	2	9.8	6.2	5.7	3.1	3.1	2.1	28	8	12	8	0	0
ACC	78	89	94	95	24	100	100	100	100	100	75	75	100	100	100	100	100	-
CMTC	13	28	12	6	-	-	100	75	100	100	0	50	86	100	67	50	-	-
TTLD	83	33	100	26	100	100	77	58	100	50	100	100	29	50	100	100	-	-
Congenital heart defects	43	11	31	16	-	-	69	83	50	0	0	100	83	50	67	0	-	-
Brain anomalies	13	6	69	11	-	-	27	75	100	33	0	50	33	0	67	0	-	-

Table 1.1. Summary of genetic mutations in AOS with associated phenotypes. A summary of phenotypes associated with identified AOS patient mutations in published literature to date from the three most recent reviews. Percentages of patients with identified mutations from all studies were calculated based on total cohorts representing all AOS patients, not just mutation positive patients. Percentages from Meester et al., 2018 were calculated only from reported presence and absence of phenotypes, any cases where phenotypes were unknown were not included when calculating averages. Percentages from Hassed et al., 2017 were taken directly as calculated in the papers. Percentages from Dudoignon et al 2019 were calculated based on new cases identified only in that study. – indicates unknown/unreported data. ACC: Aplasia Cutis Congenita; CMTC: Cutis Marmorata Telangiectatica Congenita; TTLD: Terminal Transverse Limb Defects. Table adapted from Hassed et al., 2017, Meester et al., 2018 and Dudoignon et al., 2019.

NOTCH1 mutations, occurring in 43% of patients, but rare in patients with mutations in *EOGT*, occurring in only 16% of patients reported (Hassed et al., 2017). It is currently unclear whether certain CHDs are associated with specific mutations in AOS, but common CHDs that arise in AOS patients include ventricular septal defects, double outlet right ventricle, Tetralogy of Fallot and pulmonary stenosis (Algaze et al., 2013).

As all identified causative genes of AOS are involved in the NOTCH and RAC1/CDC42 signalling pathways, this suggests dysregulation of these pathways drive disease progression (Dudoignon et al., 2019). Therefore, improving our understanding of the how these pathways are regulated in heart development will provide insight into how CHDs arise.

1.4 NOTCH signalling

NOTCH signalling is required for the formation of many organs during embryonic development, often playing distinct roles in different tissues (Meester et al., 2019a). Prior to activation of the NOTCH signalling pathway via interaction of NOTCH receptors and ligands at the cell surface, receptors and ligands first undergo a series of post-translational modifications (Siebel and Lendahl, 2017) (Fig. 1.3). NOTCH receptors are transmembrane proteins containing extracellular regions of 36 epidermal growth factor-like (EGF) repeats, which are glycosylated at specific residues by the enzymes Protein *O*-fucosyltransferase 1 (POFUT1), Protein *O*-glycosyltransferase 1 (POGLUT1) and EGF domain-specific *O*-GlcNAc Transferase (EOGT) in the endoplasmic reticulum (ER) (Zhou et al., 2022). While glycosylation of NOTCH receptors is known to be important for mediating receptor/ligand interactions, NOTCH ligands are also glycosylated on their extracellular EGF repeats, but it is unknown whether glycosylation affects ligand function (D'Souza et al., 2008). Following glycosylation, NOTCH receptors are then translocated to the golgi apparatus, where they undergo proteolytic cleavage at site 1 (S1) by a Furin-like protease, producing the functional NOTCH receptor (Kopan and Ilagan, 2009) and further modifications by Fringe enzymes which extend the glycosylation modifications, which encourage the NOTCH receptors to interact with specific ligands (Siebel and Lendahl, 2017). Mature NOTCH receptors are then presented on the surface of cells and the canonical NOTCH signalling pathway is activated in neighbouring cells when a NOTCH receptor on one cell binds to a NOTCH ligand on a cell nearby (Mašek and

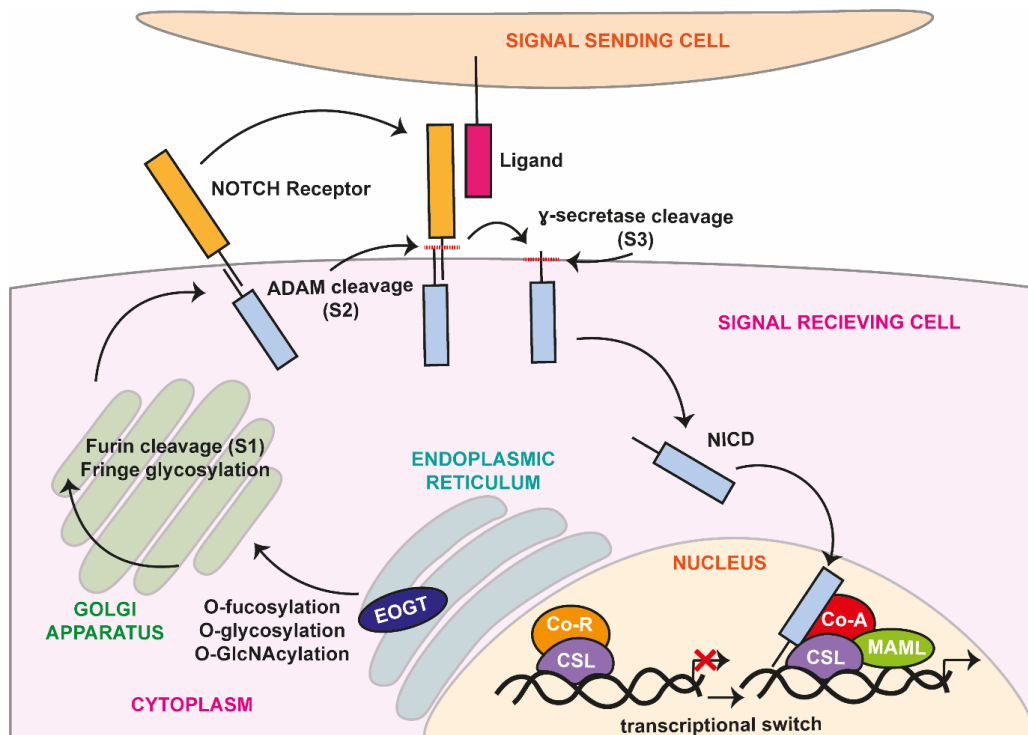


Figure 1.3. NOTCH signalling pathway. The NOTCH signalling pathway is activated by binding of a NOTCH receptor on one cell to a NOTCH ligand on a neighbouring cell. Before NOTCH receptors reach the cell surface they undergo a series of post-translational modifications, including O-fucosylation, O-glycosylation and O-GlcNAcylation in the endoplasmic reticulum. Receptors then travel to the golgi apparatus where they undergo further modifications by Fringe enzymes, and Furin proteolytic cleavage at site S1. Mature receptors then translocate to the cell surface where they can interact with NOTCH ligands on neighbouring cells. Following receptor/ligand interaction, the NOTCH receptor is cleaved by the matrix metalloprotease ADAM at site S2, releasing the part of the NOTCH receptor which is bound to the ligand, which will be endocytosed by the signal sending cell. The NOTCH receptor then undergoes further cleavage by γ -secretase at site S3, releasing the NOTCH intracellular domain (NICD) from the cell surface, which can then translocate to the nucleus of the signal receiving cell. Once in the nucleus, the NICD can form a complex with the DNA binding protein CSL, Mastermind-Like (MAML) and co-activators (Co-A), which together activate transcription of NOTCH target genes. EOGT: EGF domain-specific O-GlcNAc Transferase; Co-R: co-repressors; CSL: CBF1/RBPJ/Su(H)/Lag-1. Figure adapted from Kopan and Ilagan, 2009.

Andersson, 2017). Following NOTCH-ligand binding, the ligand is endocytosed by the ligand expressing cell, and this results in a conformational change to the bound NOTCH receptor, exposing site 2 (S2), a cleavage site for the ADAM metalloprotease to cleave (Kopan and Ilagan, 2009). Cleavage of S2 triggers a further conformational change of the NOTCH receptor, exposing site 3/4 (S3/4) which undergoes cleavage by the γ -secretase enzyme, releasing the NOTCH intracellular domain (NICD) (Kopan and Ilagan, 2009). The NICD then translocates to the nucleus where it interacts with the DNA binding protein CSL (CBF1/RBPJ/Su(H)/Lag-1), recruiting mastermind-like (MAML) and co-activators and promoting transcription of NOTCH target genes such as *HES1* and *HEY1* (Zhou et al., 2022). The NOTCH signalling pathway is highly conserved from *C.elegans* to humans, however the components of NOTCH signalling pathway differ between species (Bray, 2006). While *Drosophila* only have one Notch receptor (Notch), *C.elegans* have two Notch receptors (LIN-12 and GLP-1) and vertebrates have four (NOTCH 1-4) (Zhou et al., 2022). Similarly, while *Drosophila* only have two Notch ligands (Delta and Serrate), *C.elegans* have four (APX-1,LAG-2,ARG-1 and DSL-1) and vertebrates have six (DLL1-4 and JAG 1-2) (Bray, 2006).

1.5 NOTCH signalling in cardiovascular development

NOTCH signalling can act in different ways during development, and these modes of action are broken down into three categories: lateral inhibition, where Notch signalling amplifies differences in signalling between otherwise similar cell types; lineage decisions, where two daughter cells inherit different amounts of NOTCH signalling components; and inductive signalling, where different levels of NOTCH signalling amongst two adjacent populations of cells triggers different cell fates along a boundary (Bray, 2006). Studies in mice have shown that during cardiovascular development, NOTCH signalling is essential at multiple timepoints and in numerous cell types (MacGrogan et al., 2018) with expression dynamics of relevant NOTCH pathway components outlined in Table 1.2. In early heart development, NOTCH signalling is required during cardiac cell fate decisions, with *Notch1* expression downregulated in early cardiomyocytes and upregulated in early endothelial cells (Lescroart et al., 2018). During cardiac looping and the formation of the atrioventricular canal (AVC), NOTCH1-DLL4 signalling is required in the endocardium surrounding the developing AVC to restrict BMP signalling to the myocardium and to initiate EMT required to form the endothelial valve cushions (Papoutsis et al., 2018). Additionally, *Notch1* signalling

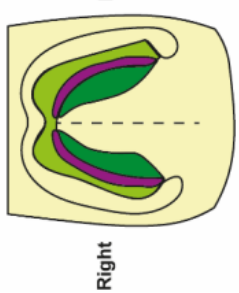
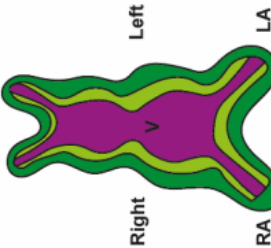
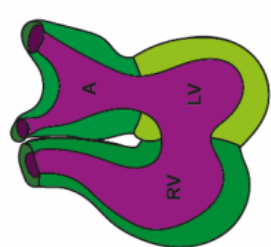
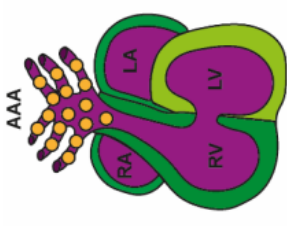
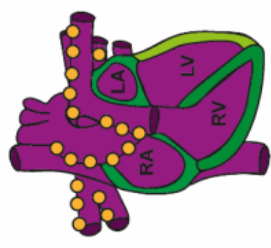
	A	B	C	D	E	
	 <p>20dpf: Cardiac Crescent E7.5: Cardiac Crescent</p>	 <p>22dpf: Cardiac Tube E8: Cardiac Tube</p>	 <p>28dpf: Cardiac Looping E8.5: Cardiac Looping</p>	 <p>35dpf: Looped Heart E10.5: Looped Heart</p>	 <p>50dpf: Cardiac Maturation E14.5: Cardiac Maturation</p>	
JAG1						<p>Expressed in ventricular myocardial cells to facilitate trabeculation (D'Amato et al., 2016)</p> <p>Required for CNC differentiation in vascular smooth muscle cells during OFT septation (Varadkar et al., 2008)</p> <p>Maintains vascular smooth muscle cell proliferation around OFT and aortic arch arteries (Varadkar et al., 2008)</p>
NOTCH2						<p>Low expression in ventricular myocardium to facilitate formation of the compact myocardium (Yang et al., 2012)</p>
DLL4						<p>Expressed in endocardial cells at the base of trabeculae to facilitate trabeculation (D'Amato et al., 2016)</p> <p>Expressed in endocardial cells at the base of trabeculae to facilitate trabeculation (D'Amato et al., 2016)</p>
NOTCH1	<p>Required in endocardial cell precursors for endocardial cell differentiation (Lescroart et al., 2018)</p>	<p>Expressed in SHF progenitors to restrict proliferation and promote differentiation (MacGrogan et al., 2018)</p>	<p>Expressed in endocardium overlaying the AVC to facilitate endocardial cell EMT to form valve leaflets (Papoutsi et al., 2018)</p>	<p>Expressed in endocardium overlaying the AVC to facilitate endocardial cell EMT to form valve leaflets (Papoutsi et al., 2018)</p>	<p>Expressed in endocardial cells at the base of trabeculae to facilitate trabeculation (D'Amato et al., 2016)</p>	<p>Required for arterial endothelial differentiation and vessel wall maturation in developing coronary arteries (del Monte et al., 2011)</p>

Table 1.2. Roles of NOTCH signalling pathway components during heart development. Roles of JAG1, NOTCH2, DLL4 and NOTCH1 throughout cardiac development. **(A)** During the cardiac crescent stage, NOTCH1 is expressed in endocardial cell progenitors to steer them towards an endocardial cell fate. **(B)** At the cardiac tube stage NOTCH1 is expressed in the second heart field (SHF) progenitor population to restrict proliferation and promote SHF differentiation. **(C)** During cardiac looping DLL4 and NOTCH1 are expressed in the endocardium of the atrioventricular canal (AVC) to facilitate endocardial cell epithelial-to-mesenchymal transition (EMT) to form the valve leaflets. **(D)** In the looped heart, JAG1 is expressed in ventricular myocardial cells to facilitate trabeculation and is also required in cardiac neural crest cells (CNC) to aid their differentiation into vascular smooth muscle cells during outflow tract (OFT) septation. In the looped heart, NOTCH2 is required to maintain vascular smooth muscle cell proliferation around the OFT and aortic arch arteries. At this stage, NOTCH1 and DLL4 are both required in endocardial cells at the base of developing trabeculae to facilitate trabeculation. **(E)** During cardiac maturation, NOTCH2 is required at low levels in the ventricular myocardium to facilitate formation of the compact myocardium, while NOTCH1 is required for arterial endothelial differentiation and vessel wall maturation in developing coronary arteries. V: ventricle; A: atrium; RA: right atrium; LA: left atrium; RV: right ventricle; LV: left ventricle; AAA: aortic arch arteries; dpf: days post fertilisation. Table adapted from Mašek and Andersson, 2017.

is required within the SHF progenitor population to restrict SHF proliferation and promote differentiation (MacGrogan et al., 2018). NOTCH signalling is also important for trabeculation, which requires communication facilitated by NOTCH signalling between the endocardium and ventricular myocardium, with *Notch1* and *Dll4* expressed in the endocardial cells at the base of developing trabeculae, while *Jag1* is expressed in the neighbouring myocardial cells which form the trabeculae (D'Amato et al., 2016). Finally, NOTCH signalling is important during ventricular compaction, as JAG1- and JAG2-mediated NOTCH signalling is required for myocardial to endocardial communication to ensure correct patterning and maturation of the ventricular walls (MacGrogan et al., 2018).

During vascular development, NOTCH signalling has been shown to play important roles in arterial/venous endothelial cell differentiation in mammalian cell culture experiments, with components of the NOTCH signalling pathway such as *NOTCH1* and *DLL4* being expressed in arterial endothelial cells, but not in venous endothelial cells, indicating NOTCH signalling defines arterial identity while also inhibiting venous identity (Gridley, 2007). Additionally, studies in mammalian cell lines show that specific NOTCH signalling components seem to be important for determining endothelial cell or vascular smooth muscle cell (VSMC) identity, with NOTCH3-JAG1 appearing to play important roles in VSMC specification, while NOTCH1-4 and Dll4/JAG2 are mainly involved in defining endothelial cell identity (Iso et al., 2003). At later developmental stages once the initial vascular networks have formed, new vessels form via angiogenesis (Herbert and Stainier, 2011). Studies from both mice and zebrafish show that during angiogenesis, tip cells extend filopodia and migrate towards angiogenic cues, and often express high levels of *DLL4*, while stalk cells, which provide support the extending tip cells, generally express higher levels of *NOTCH1* (Naito et al., 2020). The expression of different NOTCH components in tip and stalk cells is important for determining correct cell fate decisions and aiding correct angiogenic sprouting (Herbert and Stainier, 2011).

It is unsurprising given the numerous roles of NOTCH signalling during cardiac development that mutations in components of the NOTCH signalling pathway have been implicated in many human disorders associated with CHDs (Luxán et al., 2016). Alagille syndrome is a multisystemic disorder associated with cardiac defects along with bile duct paucity, skeletal and craniofacial defects, ocular defects and liver disease (Meester et al., 2019). It is linked to mutations in *NOTCH2* and *JAG1*, and like AOS it commonly presents with highly variable phenotypes indicating incomplete penetrance (Meester et al., 2019). CHDs associated with Alagille syndrome include ToF, pulmonary artery stenosis and aortic valve stenosis (Ayoub and Kamath, 2020), but again like AOS, severity of CHDs vary between patients with some patients having no cardiac defects, to others suffering from severe cardiac structural malformations (Meester et al., 2019). As NOTCH2-JAG1 signalling is required for development of multiple structures of the heart, it is thought cardiac defects arise in patients with Alagille syndrome due to a range of processes going wrong (Mašek and Andersson, 2017). In mice, loss of *Jag1* expression in the endocardium is linked to defects similar

to those observed in Alagille syndrome, such as ToF and aortic valve stenosis (Meester et al., 2019). Additionally, it is thought that JAG1 and NOTCH2 are required in the CNC to encourage differentiation and proliferation of CNC cells into vascular smooth muscle cells in and around the aortic arch arteries and the OFT, as *Jag1* and *Notch2* knockdown in mice CNC cells results in OFT defects (Varadkar et al., 2008). Furthermore, it has been proposed that the range of phenotypes arising in Alagille syndrome, including cardiac defects, which mainly affect the heart vasculature and OFT, could be due to defects in vasculogenesis as mice with *Jag1* loss-of-function (LOF) are embryonic lethal and display vascular defects (Meester et al., 2019).

A further disorder caused by mutations in *NOTCH2* is Hajdu-Cheney syndrome, which is characterised by craniofacial defects, CHDs, neurological defects, and polycystic kidneys (Siebel and Lendahl, 2017). Unlike Alagille syndrome, which is thought to be due to loss of NOTCH2 function, Hajdu-Cheney syndrome is considered to be caused by over-expression of the *NOTCH2* receptor (Isidor et al., 2011). Common CHDs associated with Hajdu-Cheney syndrome include patent-ductus arteriosus, aortic valve defects and atrial and ventricular septal defects (Canalis and Zanotti, 2014), and although it is still unknown how these defects arise in this syndrome, studies in mice have shown that constitutively active *Notch2* in the myocardium can result in hyper-trabeculation and ventricular septal defects (Yang et al., 2012). Similarly, mutations in *NOTCH3* are found in patients with CADASIL (Cerebral autosomal dominant arteriopathy with subcortical infarcts and leukoencephalopathy) syndrome, which is characterised by build-up of granular osmiophilic material in vascular smooth muscle cells, and is associated with recurrent subcortical infarctions, migraines and neurodegenerative disorders (Meester et al., 2019). Unlike AOS, CADASIL syndrome shows complete penetrance, but it is unsure how mutations in *NOTCH3* are causative of CADASIL, as *Notch3* LOF mice do not display the phenotypes associated with the syndrome (Siebel and Lendahl, 2017). Additionally, CADASIL syndrome is not generally associated with CHDs, as it mainly affects the vascular smooth muscle cells in the brain, causing them to deteriorate and result in strokes or neuronal degeneration at a young age (Meester et al., 2019).

Further cardiac diseases associated with mutations in *NOTCH* signalling pathway components are bicuspid aortic valve syndrome and hypoplastic left heart syndrome (Siebel and Lendahl, 2017) which are thought to be caused by mutations in *NOTCH1*,

and result in valve defects due to disorganised proliferation and apoptosis during endocardial cushion remodelling and valve formation (Wang et al., 2021). Together these examples indicate the importance of the NOTCH signalling pathway during cardiac development and indicate the numerous different CHDs that can arise upon NOTCH dysregulation.

1.6 RAC1/CDC42 signalling

Like the NOTCH signalling pathway, Rho GTPases such as RAC1 and CDC42 are involved in a vast range of processes during embryonic development (Duquette and Lamarche-Vane, 2014) which typically involve tight regulation of cytoskeletal dynamics, for example cell migration, cell-cell adhesions and cell polarity (Denk-Lobnig and Martin, 2019). There are currently 20 known Rho GTPases in humans, which act as molecular switches and cycle from an inactive guanosine-5'-diphosphate (GDP) bound state, which is facilitated by GTPase activating proteins (GAPs), and an active guanosine-5'-triphosphate (GTP) bound state, which is facilitated by guanine exchange factors (GEFs) (Denk-Lobnig and Martin, 2019). Further GTPase regulation can be achieved through GTPase dissociation inhibitors (GDIs) which bind GTPases and sequester them in their inactive states in the cytosol (Denk-Lobnig and Martin, 2019).

When GTPases are in their inactive GDP-bound state, dissociation from GDP happens very slowly, and can be facilitated by the action of GEFs to activate the GTPase (Bos et al., 2007). Within the GTPase, the GDP nucleotide sits between two loops called switch 1 and switch 2, alongside a phosphate binding loop called the P loop (Bos et al., 2007). Following GEF binding to the GTPase, conformational changes occur in the loop structures leading to release of the bound GDP molecule, and due to higher cell concentration of GTP compared to GDP, this then increases the likelihood of GTP binding (Bos et al., 2007). Upon binding of a new GTP molecule, this converts the GTPase into its active GTP-bound state, and decreases the affinity of GEF binding, resulting in release of the GEF from the GTPase (Bos et al., 2007). To inactivate the GTPase, bound GTP needs to undergo hydrolysis, but as GTP hydrolysis by GTPases is very slow, GAPs are required to speed up the process (Mosaddeghzadeh and Ahmadian, 2021). To do this, GAPs bind to the GTPase and insert a conserved arginine finger into the nucleotide binding domain, which in turn

Figure 1.4. RAC1/CDC42 signalling pathways. RAC1/CDC42 are involved in numerous processes during development, such as the formation of cell-cell adhesions (**A**), establishing cell polarity (**B**) and cell migration (**C**). (**A**) RAC1/CDC42 (turquoise) assist in the formation of cell-cell adhesions through the formation of adherens junctions, which involve cadherin (light blue) interacting with α -catenin (yellow) and β -catenin (pink) molecules which then bind to the actin cytoskeleton (orange) and form strong adhesions between cells. Active RAC1/CDC42 can bind and regulate the effector IQGAP1 (purple), preventing it from interacting with β -catenin. However, when RAC1/CDC42 are in their inactive GDP bound states, IQGAP1 is free to bind to β -catenin, preventing β -catenin from interacting with α -catenin and the actin cytoskeleton, resulting in weak cell adhesions. (**B**) RAC1/CDC42 have been found to be important for regulating cell polarity via spatiotemporal activation within cells. RAC1 (turquoise) and CDC42 (light green) are active on the apical side of cells and regulate Par protein localisation to ensure spatial regulation of the actin cytoskeleton for maintenance of cell shape and cell junction formation. (**C**) Active RAC1 (turquoise) and CDC42 (light green) regulate cell migration through the WASP-related regulatory complex, which activates the Arp2/3 complex resulting in polymerisation of branched actin structures in the form of lamellipodia and filopodia which bind to underlying cells or extracellular matrix via focal adhesions to pull the cell forwards, in combination with actomyosin contraction to detach the rear of the cell. C: cadherin; β : beta-catenin; α : alpha-catenin; TJ: tight junction; AJ: adherens junction; GDP: guanosine-5'-diphosphate; GTP: guanosine-5'-triphosphate; LIMK: Lim kinase; VASP: vasodilator-stimulated phosphoprotein. Figures adapted from Fukata et al., 1999, Mack and Georgiou, 2014, [Benson and Southgate, 2021](#).

makes the GTP a better substrate for nucleophilic attack by water, resulting in GTP hydrolysis into GDP and a phosphate molecule (Bos et al., 2007). Following GTP hydrolysis, the Rho GTPase is now once again in its inactive GDP-bound state (Duquette and Lamarche-Vane, 2014).

Once in an active GTP-bound state, GTPases can then remodel the actin cytoskeletal (Hall, 1998). The actin cytoskeleton forms from the assembly of globular actin (G-actin) into filamentous actin (F-actin) structures such as filopodia, which are finger-like

structures composed of long tight bundles of actin filaments; lamellipodia, which are sheet-like protrusions commonly found at the edges of cells, and stress fibres which are actin bundles that connect the actin cytoskeleton to the extracellular matrix through focal adhesions (Van Aelst and D'Souza-Schorey, 1997). Actin cytoskeletal remodelling via the formation and disassembly of F-actin structures is important to allow the cell to carry out a range of functions such as cell migration, maintaining cell polarity and shape, undergoing cell division and forming cell-cell adhesions (Rottner et al., 2017). RAC1 activation has been linked to the formation of lamellipodia, while CDC42 activation is important for filopodia formation, and RHO activation for the formation of stress fibres (Van Aelst and D'Souza-Schorey, 1997). Whilst RAC1 and RHO often work antagonistically, RAC1 and CDC42 commonly work together (Mack and Georgiou, 2014).

1.7 RAC1/CDC42 signalling in cardiovascular development

RAC1 and CDC42 are implicated in numerous processes during cardiac development, such as the formation of cell-cell adhesions (Fig. 1.4 A), establishing cell polarity (Fig. 1.4 B) and cell migration (Fig. 1.4 C) (Abu-Issa, 2015; Leung et al., 2016; Leung et al., 2014). During heart development, migration of both SHF and CNC cells are essential for right ventricle formation and septation of the OFT, with defects in cell migration resulting in the onset of CHDs (Di Felice and Zummo, 2009). RAC1 and CDC42 coordinate cell migration via actin polymerisation at the leading edge of cells, where they regulate the formation of lamellipodia and filopodia which bind to underlying cells or ECM to pull cells forward, in combination with detachment of the rear of the cell via actomyosin contraction (Ridley, 2015). Following RAC1 activation, it binds to the WASP-related WAVE regulatory complex (WRC) (Benson and Southgate, 2021), triggering WRC conformational change which in turn activates the actin related protein 2/3 (Arp2/3) complex (Marei and Malliri, 2016). The Arp2/3 complex activation then results in polymerisation of branched actin structures (Rottner et al., 2017), and extension of these structures is regulated by elongation factors such as the uncapping protein vasodilator-stimulated phosphoprotein (VASP) and formin, which add G-actin to the ends of growing filaments and inhibits capping proteins (Haga and Ridley, 2016) in order to form lamellipodia (Benson and Southgate, 2021). Similarly, CDC42 activation is thought to trigger formation of filopodia via one of two mechanisms: the convergent elongation model suggests CDC42 also activates the

Arp2/3 complex following on from lamellipodia formation, and elongation factors such as VASP and formin continue the elongation of branched actin filaments, resulting in extension of several parallel actin filaments which are then cross-linked by fascin and form filopodial protrusions (Yang and Svitkina, 2011). Alternatively, the tip nucleation model suggests actin polymerisation in filopodia is driven by formin, which clusters at the plasma membrane and nucleates and elongates several actin filaments which are then cross-linked (Yang and Svitkina, 2011). Additionally, both RAC1 and CDC42 activate the serine-threonine P21-activating kinase (PAK) family which also contribute to actin polymerisation in both lamellipodia and filopodia via downstream effectors such as LIM-kinase (Benson and Southgate, 2021). As actin polymerisation is a highly dynamic process involving rapid turnover of actin filaments, actin depolymerisation in both lamellipodia and filopodia is carried out by cofilin which binds to and disassembles actin filaments (Pollard and Borisy, 2003).

Cell-cell adhesion is important to ensure tissue integrity, particularly in the heart as the cardiac tissue undergoes constant stretching in order to function correctly (Jieli Li et al., 2017). In the heart myocardium, adherens junctions, which are protein complexes that form strong adhesions between cells (Mack and Georgiou, 2014), are mainly composed of cadherin2/N-cadherin (Bagatto et al., 2006) which interact with the downstream effectors β -catenin and α -catenin in order to form stable cell adhesions (Jieli Li et al., 2017). In the developing endocardium, adherens junctions are mainly formed of VE-cadherin, which like N-cadherin connects to the actin cytoskeleton via β -catenin and α -catenin in order to form stable adhesions between cells (Lagendijk et al., 2014). Kaibuchi et al., suggest that RAC1 and CDC42 along with IQ Motif GTPase Activating Protein 1 (IQGAP1) regulate the formation of cadherin cell-cell adhesions, as when RAC1 and CDC42 are in their active GTP bound state, they bind IQGAP1 preventing it from interacting with β -catenin, and establish stable cadherin- β -catenin cell adhesions (Fig.1.4 A). However, when RAC1 and CDC42 are inactive, IQGAP1 is free to bind to β -catenin, resulting in weak cadherin- β -catenin cell adhesions. This shows RAC1, CDC42 and IQGAP1 have opposing effects which regulate cadherin mediated cell adhesions (Kaibuchi et al., 1999).

In order for cells to carry out specific functions, they need to establish correct cellular polarity, which requires asymmetric localisation of subcellular components and the formation of cell-cell interactions (Mack and Georgiou, 2014) (Fig.1.4 B). During heart

development there is evidence to suggest that correct establishment of apical-basal polarity is required for cardiac precursors to migrate to the embryonic midline for correct development of the linear heart tube, as mutations in cell polarity proteins results in disorganized cardiomyocytes and defective heart tube formation (Henderson and Chaudhry, 2011). Polarity protein localisation has mainly been studied in *Drosophila* epithelial cells, and there is evidence it is important for establishing the apical and basal sides of cells. Par proteins such as Par3, aPKC and Par6, and Crumbs complex proteins such as Crumbs, Stardust and Patj are localised at the apical sides of cells, while Scribble complex proteins such as Lgl, Dlg and Scrib, and Yrt/Cora proteins being localised to the basal side of the cell (Mack and Georgiou, 2014). RAC1 has been found to play important roles in apical polarity by having altered activity along the apical-basal axis and displaying higher levels of activity at adherens junctions compared to tight junctions (Mack and Georgiou, 2014). CDC42 also regulates apical polarity through activation at the apical side of the cell where it recruits aPKC and Par6, and this interaction is required for correct adherens junction formation between cells (Mack and Georgiou, 2014).

Studies in mice have shown that RAC1/CDC42 are involved in numerous processes during cardiovascular development (Table 1.3). Following explant of mice hearts with *Rac1* mutations in the SHF cells, they found a reduction in SHF cell migration, decreased lamellipodia formation, and decreased expression of components of the WAVE and Arp2/3 complex, indicating RAC1 is required in the SHF for this population to migrate during development (Leung et al., 2014). Additionally, it has been shown in mice that mutating *Rac1* in the SHF cell population results in a reduction in *Sema3c* expression, a chemoattractant that attracts CNC cells, which results in a decrease in CNC cell migration to the developing OFT (Leung et al., 2016). Similarly, CDC42 has been shown to be important for CNC cell migration into the OFT during development, and CNC-specific deletion of *Cdc42* resulted in OFT defects such as persistent truncus arteriosus and defects in patterning of the aortic arch arteries (Liu et al., 2013). Furthermore, gain-of-function mutations in *ARHGAP31* (a GAP which switches RAC1 and CDC42 into their inactive states) in fibroblast cells resulted in decreased cell migration, indicating the importance of active RAC1 and CDC42 for cell migration during heart development (Southgate et al., 2011).

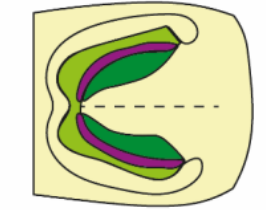
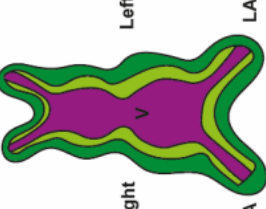
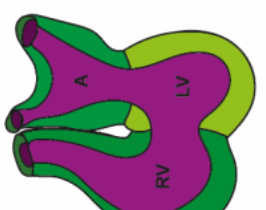
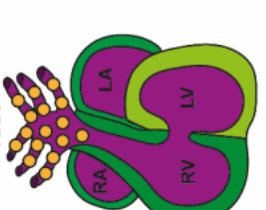
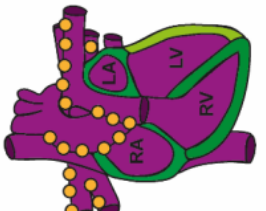
<p>First Heart Field Second Heart Field Endocardium Cardiac Neural Crest</p>	<p>A</p>  <p>20dpf: Cardiac Crescent E7.5: Cardiac Crescent</p>	<p>B</p>  <p>22dpf: Cardiac Tube E8: Cardiac Tube</p>	<p>C</p>  <p>28dpf: Cardiac Looping E8.5: Cardiac Looping</p>	<p>D</p>  <p>35dpf: Looped Heart E10.5: Looped Heart</p>	<p>E</p>  <p>50dpf: Cardiac Maturation E14.5: Cardiac Maturation</p>
<p>RAC1</p>	<p>Required for SHF migration (Leung et al., 2014)</p>	<p>Required for SHF cell proliferation and cell polarity (Leung et al., 2014) Required for SHF cell adhesions (Leung et al., 2016) Required for ventricular myocardium proliferation (Leung et al., 2021)</p>	<p>Required for SHF cell proliferation and cell polarity (Leung et al., 2014) Required for SHF cell adhesions (Leung et al., 2016) Required for ventricular myocardium proliferation (Leung et al., 2021)</p>	<p>Required for cell polarity during ventricular myocardium development (Leung et al., 2014) (Leung et al., 2021) Promotes SHF cell survival (Leung et al., 2014) Required for SHF cell migration into OFT mesenchyme to begin OFT separation (Leung et al., 2016) Mediates release of <i>Sema3c</i> by SHF cells to attract CNC cells (Leung et al., 2016) Required for cell adhesion in cardiomyocytes (Abu-Issa, 2015)</p>	<p>Required for cell adhesion in cardiomyocytes (Jieli Li et al., 2017)</p>
<p>CDC42</p>	<p>Required for SHF migration (Leung et al., 2014)</p>	<p>Required for SHF cell proliferation and cell polarity (Leung et al., 2014) Required for SHF cell adhesions (Leung et al., 2016) Required for ventricular myocardium proliferation (Leung et al., 2021)</p>	<p>Required for SHF cell proliferation and cell polarity (Leung et al., 2014) Required for SHF cell adhesions (Leung et al., 2016) Required for ventricular myocardium proliferation (Leung et al., 2021)</p>	<p>Required for cell polarity during ventricular myocardium development (Leung et al., 2014) (Leung et al., 2021) Promotes SHF cell survival (Leung et al., 2014) Required for SHF cell migration into OFT mesenchyme to begin OFT separation (Leung et al., 2016) Mediates release of <i>Sema3c</i> by SHF cells to attract CNC cells (Leung et al., 2016) Required for cell adhesion in cardiomyocytes (Abu-Issa, 2015)</p>	<p>Required for cell adhesion in cardiomyocytes (Jieli Li et al., 2017)</p>

Table 1.3. Roles of RAC1/CDC42 during heart development. (A) Neither RAC1 or CDC42 have been found to be required at the cardiac crescent stage of development, with only active RAC1 being found to be required for second heart field (SHF) migration at cardiac tube stage (B). (C) During cardiac looping, active RAC1 is required for SHF cell proliferation, polarity, and cell-cell adhesion, in addition to being required in the ventricle to aid myocardial cell proliferation. (D) In the looped heart, active RAC1 is required for establishing cell polarity during ventricular myocardium development and establishing cell-cell adhesions between myocardial cells. Additionally, active RAC1 regulates SHF cell survival and migration into the outflow tract (OFT) mesenchyme to begin OFT septation, alongside regulating SHF expression of *Sema3c* which attracts cardiac neural crest cells (CNC) to the OFT. In the looped heart, active CDC42 is required in CNC cells to facilitate their migration into the OFT and AAA, alongside being required for establishing cell polarity in migrating pro-epicardial cells. (E) During cardiac maturation, CDC42 is required for stable cell-cell adhesions between cardiomyocytes. V: ventricle; A: atrium; RA: right atrium; LA: left atrium; RV: right ventricle; LV: left ventricle; AAA: aortic arch arteries; dpf: days post fertilisation.

Both RAC1 and CDC42 have been shown to be important for adherens junction formation in the developing heart, with knock-out of *Rac1* in mouse cardiomyocytes resulting in cell-cell adhesion and cell-ECM adhesion defects (Abu-Issa, 2015) (Table 1.3). Similarly, knock-out of *Cdc42* in cardiomyocytes results in defective cell-cell adhesion, with disorganised N-cadherin and decreased β -catenin at cell-cell junctions (Jieli Li et al., 2017). Furthermore, *Rac1* mutations in the SHF in mice resulted in reduced β -catenin expression at cell junctions in the right ventricular myocardium, indicating that the cardiac abnormalities observed in this study, such as thin ventricular myocardial tissue and ventricular septal defects, could be due to defects in cell-cell adhesion (Leung et al., 2014). Together this data indicates the important roles of RAC1/CDC42 for the formation of cell adhesions during cardiac development, and how disrupted cell-adhesions can result in CHDs.

Correct polarity during heart development is crucial in order to form complex structures via the coordination of multiple cell types (Leung et al., 2016). Mutations in *Rac1* in the SHF in mice results in loss of cell organization and apical-basal polarity in SHF

cells, which failed to organise themselves correctly in relation to one another (Leung et al., 2016). Additionally, *Rac1* mutations in the SHF resulted in decreased expression of the cell polarity protein SCRIB, and cells exhibited disrupted cytoskeletal organisation, resulting in cardiac defects such as septal defects and thin ventricular myocardium (Leung et al., 2014). Furthermore, active CDC42 is required to establish polarity in pro-epicardial cells, which along with microtubule organisation is required for their migration to the heart, as pro-epicardial *Cdc42* knock-out cells from mice had disrupted polarity and cell migration, resulting in defective epicardium formation (Jingjing Li et al., 2017).

During vascular development, angiogenesis occurs via endothelial tip cell migration towards vascular endothelial growth factor (VEGF) cues which encourage vessel branching (le Noble et al., 2008). VEGF signalling has been shown to be upstream of activated RAC1 and CDC42, triggering the formation of lamellipodia and filopodia respectively to drive endothelial tip cell migration (De Smet et al., 2009). Additionally, RAC1 and CDC42 have also been shown to be important for regulating asymmetrical polarization of the actin cytoskeleton in endothelial cells to facilitate lumen formation, which is required to allow blood to flow through the developing vasculature (Norden et al., 2016). Furthermore, CDC42 is also required for the formation of cell-cell adhesions in the developing vasculature through the extension of filopodia between cells, which associate with VE-cadherin to form strong cell adhesions and maintain vascular integrity (Barry et al., 2015).

1.8 *DOCK6* and *EOGT* are mutated in autosomal recessive AOS

DOCK6 and *EOGT* are commonly mutated in the autosomal recessive form of AOS, with *DOCK6* mutations accounting for 4% of all known AOS patient mutations and *EOGT* mutations account for 5% (Hassed et al., 2017) (Table 1.1). These genes may regulate distinct signalling pathways involved in heart development, as *DOCK6* is a GEF regulating RAC1 and CDC42 activity (Sukalo et al., 2015), and *EOGT* is a post translational modification enzyme which has been shown to regulate the NOTCH signalling pathway (Schröder et al., 2019). Despite mutations in these genes regulating different signalling pathways, patients with mutations in either gene commonly display similar AOS phenotypes such as ACC and TTLD, with 94% and 100% of patients with *DOCK6* mutations presenting these phenotypes respectively,

and 95% and 26% of patients with mutations in *EOGT* (Hassed et al., 2017). Despite this similarity in the classical hallmark features of AOS, mutations in these genes are also associated with specific phenotypes, for example 69% of reported patients with mutations in *DOCK6* had neurological abnormalities, compared to only 11% of patients with mutations in *EOGT* (Hassed et al., 2017). Similarly, CHDs are more common in patients with mutations in *DOCK6*, reported in 31% of patients compared to only 16% of patients with mutations in *EOGT* (Hassed et al., 2017). However, it is currently unknown how mutations in these two genes are causative of specific phenotypes that arise in AOS patients (Hassed et al., 2017).

1.9 EGF domain-specific O-GlcNAc Transferase (EOGT)

EGF domain-specific O-GlcNAc transferase (EOGT) is a post translational modification enzyme that transfers an N-acetylglucosamine (O-GlcNAc) to specific sequences on serine and threonine residues located between the fifth and sixth cysteines on epidermal growth factor-like (EGF) repeats of membrane proteins (Varshney and Stanley, 2017). EOGT was originally identified to modify the EGF repeats of *Drosophila* Notch and the extracellular matrix protein Dumpy (Sakaidani et al., 2012). EOGT is highly conserved between species, with 11 of 36 of the EGF O-GlcNAc consensus sites in NOTCH1 being conserved between mice, rats and humans (Varshney and Stanley, 2017). EOGT has been found to act on over 1,000 proteins, which are involved in numerous processes such as cell signalling, transcriptional regulation, and cell differentiation (Ogawa et al., 2015). In mammals, alongside NOTCH receptors, further proteins have been identified to be O-GlcNAc targets of EOGT including heparin sulfate proteoglycan 2 (HSPG2), neural EGFL like 1 (NELL1) and laminin subunit alpha 5 (LAMA5) (Varshney and Stanley, 2017).

The roles of EOGT during cardiovascular development have mainly been studied in the context of vascular development. In mice, EOGT is required for retinal vascular development, and *Eogt* LOF results in defective vascular integrity, although mice are otherwise viable and do not display other phenotypes associated with AOS, such as ACC or TTLD (Sawaguchi et al., 2017). Additionally, the mutations observed in *Eogt* LOF mice are similar to those seen in *Notch1* or *Rbpj* heterozygous mutant mice, and double mutants for *Eogt* with either heterozygous *Notch1* or *Rbpj* have enhanced phenotypes compared to *Eogt* recessive mutations alone, suggesting EOGT is

important for regulating NOTCH signalling in mice during retinal vasculogenesis (Ogawa and Okajima, 2019). Furthermore, in mice endothelial cells EOGT-mediated O-GlcNAcylation was found to be required specifically for NOTCH1-DLL4 mediated NOTCH signalling, but is not required for NOTCH1-JAG1 interactions (Sawaguchi et al., 2017). In *Drosophila*, *Eogt* LOF is incompatible with survival past the second instar larval stage, with any animals surviving up to this point displaying defects associated with mutations in genes required for epithelial-cell matrix interactions, such as wing and tracheal abnormalities (Varshney and Stanley, 2017). Furthermore, loss of *Eogt* specifically in the wing resulted in wing blistering phenotypes which are also associated with defective epithelial-cell matrix interactions, suggesting in *Drosophila* *Eogt* primarily regulates regulated genes associated with epithelial-cell matrix interactions (Sakaidani et al., 2011). Additionally, *Eogt* LOF *Drosophila* did not display phenotypes associated with defective Notch signalling, providing further support that in *Drosophila* the primary target of *Eogt* is more likely to be an extracellular matrix protein such as Dumpy, rather than the Notch receptor (Varshney and Stanley, 2017).

In humans, it is currently unknown how mutations in *EOGT* result in the phenotypes observed in AOS, or whether these phenotypes arise due to disruption in NOTCH signalling (Shaheen et al., 2013). All current known AOS patient mutations in *EOGT* have been found to result in loss of enzyme activity (Ogawa and Okajima, 2019), and although disrupted NOTCH signalling hasn't been shown in AOS patients with mutations in *EOGT*, it has been shown that NOTCH1 is a target of EOGT in pancreatic cancer cells (Yang et al., 2021). This data, together with the evidence that other NOTCH signalling pathway components are commonly mutated in AOS, suggests phenotypes in AOS patients with *EOGT* mutations could be due to dysregulated NOTCH signalling, although further investigation into EOGT target proteins or NOTCH pathway activity upon *EOGT* LOF is required to demonstrate this conclusively (Shaheen et al., 2013).

1.10 Dedicator of Cytokinesis 6 (DOCK6)

Dedicator of cytokinesis 6 (DOCK6) is an atypical GEF which activates RAC1 and CDC42 by cycling them from their inactive GDP bound state to their active GTP bound state (Gadea and Blangy, 2014). There are two families of GEFs, the typical Dbl family and the atypical DOCK family, which have differing GEF domains (Marei and Malliri,

2016). The Dbl homology family of GEFs have a Dbl homology or DH domain which is required for GEF activity, and a pleckstrin homology or PH domain which binds to phosphorylated phosphoinositides and proteins and is thought to be involved in regulating GEF cellular localisation, mainly to the plasma membrane (Schmidt and Hall, 2002). DOCK GEFs on the other hand have two highly conserved domains called DOCK homology region 1 (DHR1) which is required for membrane localisation within the cell via phospholipid binding (Kunimura et al., 2020), and the DOCK homology region 2 (DHR2) which is required for GEF activity (Boland et al., 2022). While both families of GEFs contain GEF domains, it is noteworthy that both the DH domain and DHR domain share little structural similarity (Miyamoto and Yamauchi, 2010). While Dbl family GEFs activate a range of Rho GTPases (Schmidt and Hall, 2002), DOCK GEFs specifically activate RAC1 and CDC42 (Goicoechea et al., 2014).

There are 11 members of the DOCK family, which are split into 4 subgroups based on their sequences and substrate specificity (Kunimura et al., 2020). The DOCK-A subfamily is composed of DOCK1, 2 and 5, and contain an N-terminal Src homology domain-3 (SH3), a helix domain, an armadillo repeat motif and a C-terminal proline rich domain, alongside the DHR1 and DHR2 domains (Benson and Southgate, 2021). The DOCK-B subgroup, which includes DOCK3 and DOCK4 shares similar domains, all except for the helix domain (Benson and Southgate, 2021), and both DOCK-A and -B GEFs have a specificity for activating RAC1 (Gadea and Blangy, 2014). DOCK-C comprises of DOCK6, 7 and 8, which have only 3 recognisable domains which are the DHR1 and DHR2 domains and the armadillo repeat motif (Benson and Southgate, 2021). DOCK-C GEFs have dual GEF activity and are able to activate both RAC1 and CDC42 (Gadea and Blangy, 2014). Finally, the DOCK-D subfamily consists of DOCK9, 10 and 11, and alongside the DHR1 and DHR2 domains they contain a PH domain and the armadillo repeat motif (Benson and Southgate, 2021), and specifically activate CDC42 (Gadea and Blangy, 2014).

The roles of DOCK6 have mainly been studied in the context of neuronal migration, where it has been shown in mice that DOCK6 regulates RAC1/CDC42 activity during neurite outgrowth (Miyamoto et al., 2007). During the axonal growth and branching which occur in the development of dorsal root ganglion neurons, it was found that the phosphorylation state of DOCK6 could regulate its activity, with Akt-mediated phosphorylation of DOCK6 at Ser1194 resulting in DOCK6 inhibition, and

dephosphorylation by PP2A removing this inhibition to allow DOCK6 to activate RAC1/CDC42 and promote in axon growth (Miyamoto et al., 2013). Additionally it has been observed that *Dock6* is expressed in the developing limb buds and heart of a mouse embryo at stage E10.5 (Shaheen et al., 2011a).

In humans, how mutations in *DOCK6* lead to dysregulation of the RAC1/CDC42 and result in AOS phenotypes is currently unknown (Jones et al., 2017). *DOCK6* mutations identified in patients often result in loss of DOCK6 function, with many disrupting the DHR2 domain preventing DOCK6 GEF activity (Benson and Southgate, 2021). In AOS patient-derived fibroblast cells with mutations in *DOCK6*, the actin cytoskeletal defects observed matched phenotypes seen in RAC1 and CDC42 mutant fibroblasts, suggesting that DOCK6 is regulating RAC1/CDC42 activity in humans (Shaheen et al., 2011a). Furthermore, heterozygous gain-of-function mutations in ARHGAP31, a GAP which cycles RAC1 and CDC42 into their inactive GDP bound states, have also been identified in AOS patients, providing further evidence that AOS can arise from RAC1/CDC42 signalling dysregulation (Southgate et al., 2011).

Interestingly, in fibroblast cells taken from AOS patients with mutations in *DOCK6*, the actin cytoskeleton displayed defects less severe than in fibroblast cells which had an acute knock-down of *DOCK6* (Cerikan and Schiebel, 2019). In a study conducted by Cerikan et al., they found that under wild-type conditions, DOCK6 activates RAC1 and CDC42 by cycling them from their inactive GDP-bound states to their active GTP-bound states (Fig. 1.5 A). When there is acute *DOCK6* depletion, RAC1 and CDC42 are in their inactive GDP-bound states, resulting in a decrease in RAC1 and CDC42 activity and cytoskeletal defects (Fig. 1.5. B). However, under prolonged *DOCK6* depletion in *DOCK6* CRISPR/Cas9 knock-out cells, these cells were able to adapt to a loss of *DOCK6*, rescuing the actin cytoskeletal defects (Cerikan et al., 2016) (Fig.1.5 C). In this study, they found that under chronic *DOCK6* depletion this resulted in an increased level of globular actin in the cell, which in turn can regulate gene expression. Genes which are sensitive to the actin polymerisation state of a cell include serum response factors (*SRF*) and myocardin related transcription factors (*MRTF*), which when in the presence of increase globular actin levels are bound and sequestered in the cytoplasm. This lack of SRF/MRTF translocation into the nucleus results in a loss of expression of the small ubiquitin like modifier interferon stimulated gene 15 (*ISG15*) which is regulated by SRF/MRTF. Under normal conditions, ISG15 would ubiquitinate

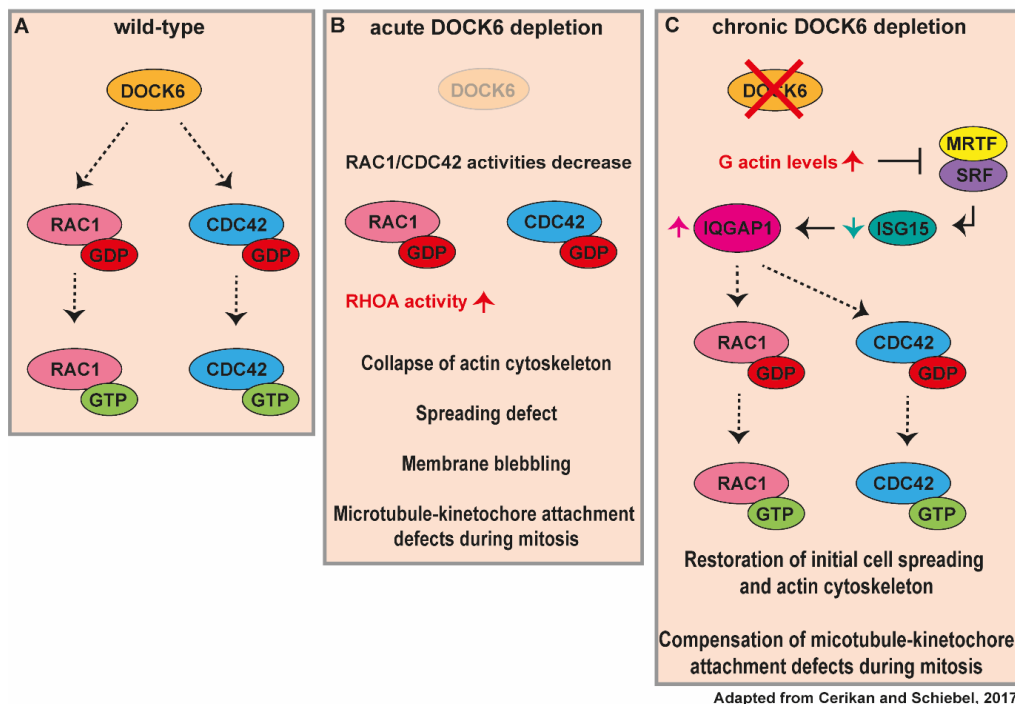


Figure 1.5. A cell intrinsic adaptation mechanism to a chronic loss of *DOCK6*.

Human fibroblast cells derived from AOS patients with *DOCK6* mutations displayed a cell intrinsic adaptation mechanism to overcome a chronic loss of *DOCK6*. **(A)** Under wild-type conditions, *DOCK6* activates RAC1 and CDC42 by cycling them from their inactive GDP-bound states to their active GTP-bound states. **(B)** Under acute *DOCK6* knock-down, RAC1 and CDC42 remain in their inactive GDP-bound states, resulting in a decrease in RAC1/CDC42 activity, and an increase in RHOA activity. This leads to collapse of the actin cytoskeleton, cell spreading defects, membrane blebbing and microtubule-kinetochore attachment defects during mitosis. **(C)** Under chronic *DOCK6* depletion, globular actin levels within the cell increase and bind to MRTF/SRF and sequester them in the cytoplasm. As MRTF/SRF regulate the expression of the small ubiquitin like modifier *ISG15*, upon their inhibition *ISG15* levels decrease. Decrease of *ISG15* results in an increase of IQGAP1, which is normally targeted for degradation by *ISG15*. An increase in IQGAP1 results in stabilisation of RAC1 and CDC42 in their active GTP-bound states and restores cytoskeletal defects. *DOCK6*: dedicator of cytokinesis 6; GDP: guanosine-5'-diphosphate; GTP: guanosine-5'-triphosphate; G actin: globular actin; MRTF: myocardin related transcription factors; SRF: serum response factors; *ISG15*: interferon stimulated gene 15; IQGAP1: IQ motif containing GTPase activating protein 1.

a further gene called IQ motif containing GTPase activating protein 1 (IQGAP1) and target it for degradation, however when this compensation mechanism is active and there is a loss of ISG15, IQGAP1 levels increase. IQGAP1 regulates the actin cytoskeleton and can stabilise RAC1 and CDC42 in their active GTP bound states in the absence of DOCK6. This results in RAC/CDC42 activation and recovery of actin cytoskeletal defects in the absence of DOCK6 in order to adapt to a loss of DOCK6 expression (Cerikan et al., 2016). This compensation mechanism and the accompanying data in animal models suggests the importance of DOCK6 for regulating RAC1/CDC42 during actin cytoskeleton remodelling. However, how mutations in DOCK6 are resulting in defective RAC1/CDC42 activity and leading to defects in AOS patients is still unknown and requires further investigation.

1.11 Animal models of AOS

Both RAC1/CDC42 and NOTCH signalling pathways are implicated in AOS, and while numerous studies have provided insights into the roles of both RAC1/CDC42 and NOTCH during cardiovascular development, little is still known about AOS aetiology. There are currently very few animal models designed to understand how CHDs arise in AOS, one of which being a SHF specific deletion of *Dll4* in mice, utilised to understand how cardiac defects arise in AOS patients with mutations in *DLL4* (Zoysa et al., 2020). This study found that knock-out of *Dll4* in the SHF resulted in a reduction in cell proliferation and an increase in apoptosis, greatly reducing the SHF cell population, and resulting in a small right ventricle and OFT defects (Zoysa et al., 2020). Another study found that heterozygous mutations in *Dll4* in mice resulted in lethality in most embryos by embryonic day E10.5, with mutant mice suffering from pericardial edema and vascular defects such as stenosis of the aorta (Gale et al., 2004). Interestingly, a subset of the *Dll4* heterozygous mutant mice survive and were indistinguishable from the wild-type counterparts, indicating that like in humans, *Dll4* mutations exhibit incomplete penetrance in mice depending on their genetic backgrounds (Gale et al., 2004). Heterozygous mutations in *Notch1* in mice have been found to cause aortic valve stenosis, a cardiac abnormality also observed in some AOS patients, however these mice did not display any of the hallmark features of AOS (ACC, TTLD) (Nigam and Srivastava, 2009). Like *Notch1* mutant mice, *Rbpj* heterozygous mutant mice also develop aortic valve disease but do not display other classical features of AOS (Nus et al., 2011). Additionally, *Rbpj* mutations identified in

AOS patients caused decreased *Rbpj* DNA binding in *Drosophila* disease models, resulting in decreased Notch signalling due to a failure of Rbpj to activate downstream Notch target genes (Gagliani et al., 2022). Interestingly, they also found that the specific *Rbpj* variant was predictive of how severe the Notch phenotype in *Drosophila* would be, depending on how it impacted Rbpj protein function, and, like mice models of *Dll4* mutations, the genetic background of individual *Drosophila* could vary how severe the Notch phenotype caused by the same variant could be (Gagliani et al., 2022). To date there are no reported mice models to understand how loss-of-function mutations in *Dock6* and gain-of-function mutations *Arhgap31* result in CHDs in AOS, however there is an *Arhgap31* loss-of-function mouse model which displays vascular defects, indicating an important role for this gene in vascular development (Caron et al., 2016). Furthermore, there is only one mouse model to understand the role of *Eogt* in vascular development, which found that *Eogt* null mice have defects in retinal vasculogenesis, but otherwise do not display the hallmark features of AOS (Sawaguchi et al., 2017). Due to a lack of phenocopying AOS features, this data suggests that mice models might not be the most suitable to study AOS (Ristori et al., 2021), revealing an area of exploration for a more suitable animal model to study this disease. As very little is still known about the roles of DOCK6 and EOGT in cardiovascular development, and as there are currently limited animal models to investigate the role these genes play during the onset of AOS, further animal models would be useful to investigate these genes in more detail.

1.12 Using zebrafish as a model to study human heart development

Zebrafish first started being used as a model to study genetic disorders in the mid-1990s in the first forward genetic screens to identify morphological defects similar to those seen in human genetic disorders (Ota and Kawahara, 2014). Zebrafish are an excellent model to study heart development (Bowley et al., 2021) as the heart develops rapidly - the contractile tube forms by 24 hours post fertilisation (hpf) and heart looping is complete by 72hpf (Bakkers, 2011), compared to 8 and 10.5 days respectively in mice (Savolainen et al., 2009), or 21 days and 28 days in humans (Srivastava and Olson, 2000). Additionally, zebrafish embryos can survive without a fully functional cardiovascular system for the first week of life, as due to their small size oxygen can enter embryos via passive diffusion, enabling the observations of mutations which lead to cardiovascular system defects without embryonic lethality

(Bakkers, 2011). While the zebrafish heart comprises only two chambers, early heart development is highly conserved using the same developmental signalling pathways and morphological processes underlying early human heart development (Giardoglou and Beis, 2019). As the zebrafish embryo develops externally and is relatively transparent, we can combine fluorescent transgenic reporters with confocal and high resolution microscopy to image specific cell types in live embryos *in vivo*, a process which still remains challenging in higher vertebrate systems (Bakkers, 2011). Zebrafish are also easy to genetically manipulate in reverse genetic approaches thanks to genome editing tools, facilitating generation of LOF models of genes of interest (Li et al., 2016), in addition to knock-in of human mutations (Tessadori et al., 2018) furthering our understanding of the genetic basis of cardiac development and human disease.

Genome editing involves the insertion, deletion or substitution of a region of DNA in an organism or cell (Paul and Montoya, 2020). Previously used reverse genetic approaches include zinc finger nuclease (ZFN) and transcription-activator like effector nucleases (TALEN), which both work in similar ways utilising the endonuclease *Fok1* by guiding it to a specific region within the DNA where it then creates double stranded breaks (Gupta et al., 2019). Despite playing an important role in the evolution of genome editing technologies, ZFN and TALENs are associated with several limitations, such as difficulties with design and synthesis, the cost of using these technologies, and the complexities faced when using them, such as being unable to guarantee they will work *in vivo*, and their actions depending on DNA methylation states (Li et al., 2016). Therefore a new technology which would allow cheaper, easier and more precise genome editing would be beneficial, and this led to the discovery and appropriation of the CRISPR-Cas9 system (Gupta et al., 2019), which was first adopted in zebrafish in 2013 (Woong Y Hwang et al., 2013).

The clustered regularly interspaced short palindromic repeats (CRISPR)-Cas system involves a family of endonucleases identified in bacteria that has been adapted for precise genome editing in research (van der Oost et al., 2009), and the best studied system involves the Cas9 enzyme which was discovered in the *Streptococcus pyrogenes* bacteria (Li et al., 2016). This process works via a CRISPR RNA (crRNA) forming a complex along with a transactivating RNA (tracrRNA) which together guide the Cas9 endonuclease to a specific location within the genome where it cleaves a

double stranded break in the DNA (Ma et al., 2014). The specificity of where in the genome the Cas9 endonuclease cuts arises from a complementary sequence of around 20bp in the crRNA, along with a short DNA sequence recognised by the Cas9 enzyme called the protospacer adjacent motif (PAM) (Li et al., 2016). This process has been adapted for genome editing in multiple different organisms, via designing a single guide RNA (sgRNA) composed of approximately 20 nucleotides of complementary sequence to where the desired mutation is to be created in the genome, flanked by the PAM recognition site (5'-NGG-3' in the case of Cas9) (Ma et al., 2014). Following co-injection of the sgRNA and the Cas9 enzyme, the sgRNA will guide Cas9 to the desired target site, where it will create a double stranded break at a precise location (Gupta et al., 2019).

Alongside the discovery of Cas9, further Cas enzymes have been discovered with varying properties which can be adapted for different genome editing techniques (Pickar-Oliver and Gersbach, 2019). Another Cas enzyme, called Cas12a/Cpf1, was identified in the *Francisella novicida* bacteria (Paul and Montoya, 2020). In comparison to Cas9, Cas12a does not need to form a complex with tracrRNA in order to bind and activate the Cas endonuclease, and it recognises a different PAM sequence (5'-TTTN-3') (Paul and Montoya, 2020). Furthermore, Cas12a produces staggered double stranded breaks outside of the PAM site, producing overhang regions, while Cas9 creates blunt end double stranded breaks at the PAM site, and the overhang regions created by Cas12a have proved useful, for example in aiding homology directed repair (HDR) (Li et al., 2019). CRISPR genome editing can be used to knock-out specific genes, for example by designing sgRNAs which would flank the annotated promoter and ATG translational start sites, which then act together to excise a portion of DNA containing both these elements thus preventing transcription and translation (Li et al., 2016). Alternatively, CRISPR can be used to knock-in desired mutations, for example knocking-in human mutations when carrying out disease modelling experiments (Pickar-Oliver and Gersbach, 2019). This can be achieved by co-injecting the sgRNA and Cas enzyme, alongside a single stranded oligonucleotide which contains the mutation to be knocked-in to the genome, alongside flanking homologous regions of DNA which will facilitate HDR (Tessadori et al., 2018).

1.13 Zebrafish heart development

Zebrafish have a single circulatory system composed of an atria, ventricle and unseparated OFT (Olson, 2006). The zebrafish heart begins to develop around 12hpf when the cardiac progenitors differentiate from the mesoderm (Staudt and Stainier, 2012) and migrate to the anterior of the embryo where they reside bilaterally either side of the embryonic midline (Bakkers, 2011). These progenitor populations subsequently fuse across the midline to form the cardiac disc, a structure similar to the cardiac crescent in vertebrates (Desgrange et al., 2018), with the atrial myocardial progenitors and ventricle myocardial progenitors forming distinct separate populations (Bakkers, 2011). Endocardial cells form from the anterior lateral plate mesoderm, and migrate to the embryonic midline just before the myocardial cells, where they coalesce in the centre of the cardiac disc, surrounded by myocardial cells (Bakkers, 2011) (Fig. 1.6 A). Cells comprising the heart disc migrate asymmetrically to form the linear heart tube at 26hpf which comprises an inner endocardial layer, and an outer myocardial layer separated by cardiac ECM (McFadden and Olson, 2002) (Fig.1.6 B).

Similar to human heart development, the zebrafish heart grows through addition of the SHF, a population of cells derived from the pharyngeal mesoderm which contribute to the formation of the ventricle and OFT (Liu and Stainier, 2012). Following SHF addition, the heart tube grows, and similar to vertebrate heart development loops to the right to ensure correct chamber alignment (Lombardo et al., 2019) (Fig. 1.6 C). Following cardiac looping, the chambers of the heart become distinguishable, which is further enhanced by a process called cardiac ballooning (Bakkers, 2011). Cardiac ballooning occurs through a combination of cell proliferation and addition of differentiating cells, defining the inner and outer curvatures of the chambers (Dietrich et al., 2014). In order to form the cardiac valves in the zebrafish heart, endocardial cells in the AV canal begin expressing an adhesion molecule called Dm-grasp and extend protrusions into the ECM (Bakkers, 2011). Unlike in mammalian heart development, it is thought that valves in the zebrafish heart form through invagination of endocardial cells, rather than EMT, with the valve leaflets completely formed by 7dpf (Staudt and Stainier, 2012). Like human hearts, developing zebrafish hearts also possess trabeculae in the ventricle, with cardiomyocytes beginning migration into the ventricular lumen around 60hpf (Tu and Chi, 2012). Trabeculae continue to mature up to 15dpf (Liu et al., 2010), before forming a compact layer by 4 weeks post fertilisation (Hu et al., 2000). Similar to human heart development, the epicardial cells are derived

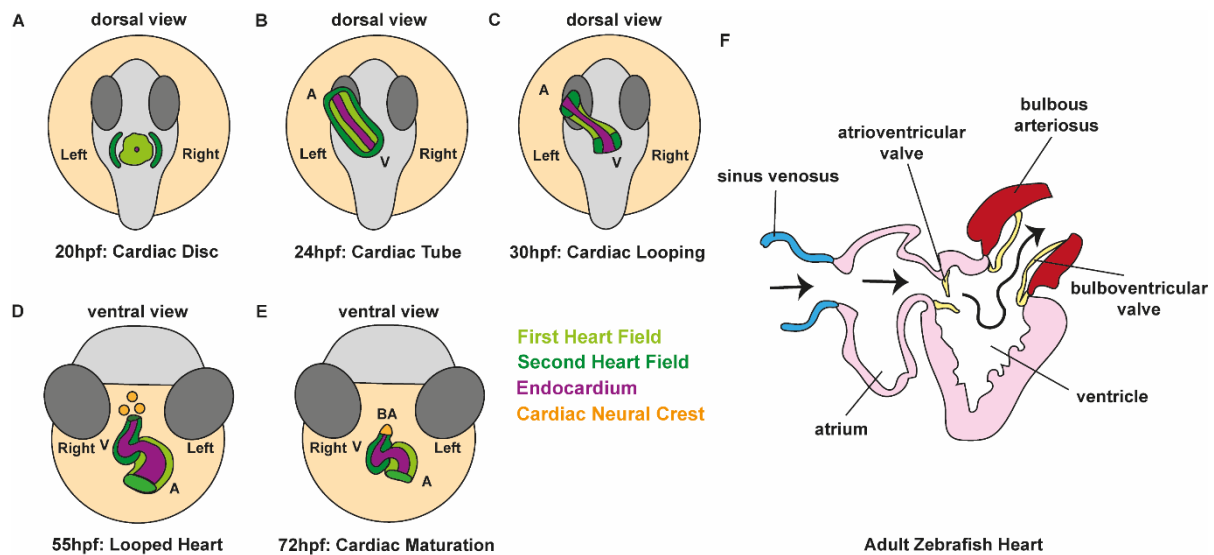


Figure 1.6. Zebrafish heart development. (A) At 20hpf, cardiac precursors emerge from the mesoderm and migrate together to form the cardiac disc, with endocardial cells at the centre, surrounded by first heart field cells (FHF; light green), with second heart field cells (SHF; dark green) arising from the surrounding mesoderm. (B) Around 24hpf, cells making up the cardiac disc begin migrating asymmetrically to form the linear heart tube which has an inner layer of endocardium and an outer layer of myocardium. SHF cells from the surrounding mesoderm begin proliferating and migrating into the linear heart tube to assist heart growth. (C) At 30hpf, the heart tube grows and begins undergoing cardiac looping to ensure correct alignment of the heart chambers. (D) Around 55hpf the heart has looped, and cardiac ballooning occurs at the outer curvatures of the chambers to assist chamber growth. Cardiac neural crest cells (CNC; orange) begin migrating into the heart to contribute to myocardial thickness in the ventricle and formation of the outflow tract (OFT). (E) During cardiac maturation, the atrioventricular canal forms, along with ventricular trabeculation and formation of the bulbous arteriosus (BA). The atrium is mainly composed of FHF cells, the ventricle is mainly composed of SHF cells and the undivided OFT is composed of both SHF and CNC cells (F) The adult zebrafish heart is composed of one atrium, one ventricle and an undivided OFT called the bulbous arteriosus. Black arrows indicate direction of blood flow. V: ventricle; A: atrium; BA: bulbous arteriosus; hpf: hours post fertilisation. Figure adapted from Bakkers, 2011 and Poon and Brand, 2013.

from pro-epicardial cells which are located next to the ventral wall of the looped heart, and at 72hpf migrate to cover the whole outer surface of the heart (Bakkers, 2011).

Similarly to humans, CNC cells also contribute to the formation of the zebrafish heart, however as the OFT is unseparated, the roles of CNCs differs between humans and zebrafish (George et al., 2020). It is thought the CNC supports zebrafish heart development by migrating into the heart and contributing to the myocardial thickness of the ventricle and OFT, which in turn assists cardiac looping (Li et al., 2003) (Fig. 1.6 D). During cardiac maturation, features of the adult zebrafish heart become visible with the FHF mainly contributing to the atrium, the SHF mainly contributing to the ventricle and the cardiac neural crest contributing to formation of the ventricle and OFT (Liu and Stainier, 2012) (Fig.1.6 E). The adult zebrafish heart is composed of a single atrium, ventricle, and unseparated OFT called the bulbous arteriosus, with a single circulatory system (Poon and Brand, 2013) (Fig.1.6 F). Despite the differences in adult heart morphology, the similarities between zebrafish and human early heart development, such as cardiac tube formation, heart looping, ballooning and valve and trabeculae formation makes the zebrafish a suitable model for studying these processes. Furthermore, the signalling pathways which drive cardiac development are also conserved between zebrafish and humans, making this a useful organism to model human genetic disorders (Bowley et al., 2021; Ota and Kawahara, 2014).

1.14 Rationale and Aims

Despite previous studies which have identified some of the processes that the RAC1/CDC42 and NOTCH signalling pathways regulate during cardiac development, mechanistic studies linking mutations in AOS patients to defects in these processes are limited. Although it is known that recessive mutations in *DOCK6* and *EOGT* are identified in patients with AOS, it is also unknown how these mutations lead to the dysregulation of the RAC1/CDC42 and NOTCH signalling pathways respectively, and how this leads to the onset of CHDs. Furthermore, limited animal models have been generated to investigate the roles of *DOCK6* and *EOGT* during cardiac development, with no animal models created for either of these genes to look directly at the impact AOS mutations are having on cardiac development. Given the advantages described above of zebrafish as an organism to study heart development, a *DOCK6* and *EOGT*

zebrafish mutant model would prove invaluable to investigate the roles these genes are playing in the formation of different cardiac structures and the onset of CHDs.

In this thesis I aimed to create zebrafish mutant models for *dock6* and *eogt*, both in the form of LOF mutations and AOS disease-specific models by inserting human AOS patient mutations into the zebrafish genome. Additionally, I aimed to investigate the impact of these mutations on cardiac development and understand the regulatory roles for *dock6* and *eogt* in Rac1/Cdc42 and Notch signalling during cardiac development. In Chapter 3 I explain how I created novel zebrafish mutant models for both *dock6* and *eogt*: a coding sequence mutant model for both genes, and two retained intron mutant models for *dock6*, alongside identifying non-coding transcripts for both genes which are expressed in the heart myocardium during early heart development. In Chapter 4, I carry out in depth analysis on cardiac morphology for each of the *dock6* mutant models and show an intronic mutation in the *dock6-202* retained intron transcript results in the reduction of *dock6-201* protein coding transcript gene expression and investigate a cell intrinsic compensation mechanism which adapts to a chronic loss of *dock6*. Finally, in Chapter 5 I investigate the role of an *eogt* antisense transcript and assess whether it has any effect on heart development or Notch signalling in the developing heart when over-expressed, alongside in-depth analysis on cardiac morphology for the *eogt* coding sequence mutant. Together, I present the first reported zebrafish mutant models for both *dock6* and *eogt* and identify non-coding transcripts for both genes which are expressed in the heart myocardium at a key early stage of zebrafish heart development.

2. Materials and Methods

2.1 Zebrafish husbandry

2.1.1 Zebrafish lines

The following zebrafish lines were used in this study:

Line	Reference
Wild-type (AB)	-
Wild-type (TL)	-
<i>Tg(myf7:eGFP)</i>	Huang et al., 2003
<i>Tg(-5.1myf7:Ds-red2-NLS)^{f2}</i>	Rottbauer et al., 2002
<i>Tg(myf7:LifeActGFP)</i>	Reischauer et al., 2014
<i>Tg(fli1a:AC-tagRFP)^{sh511}</i>	Savage et al., 2019
<i>Tg(myf7:LifeActGFP;Tg(Tp1bglob:hmgb1-mCherry)^{jh11}</i>	Parsons et al., 2009
<i>Tg(fli1a:EGFP)^{y1}</i>	Roman et al., 2002
<i>Tg(dll4in3:GFP)^{icr1}</i>	Sacilotto et al., 2013
<i>Tg(flk1:ras-Cherry)^{s896}</i>	Chi et al., 2008
<i>dock6-RI1^{Δ28}</i>	Generated in this study
<i>dock6-RI1^{ins41}</i>	
<i>dock6-201^{ins36Δ65}</i>	
<i>eogt-201^{Δ28}</i>	

2.1.2 Zebrafish care

Adult zebrafish were kept in circulating water at a temperature of 28.5°C with a 14-hour day, 10-hour night cycle. Fish were fed twice daily.

2.1.3 Zebrafish embryo collection and staging

Adult male and female zebrafish were paired overnight physically separated by dividers. Following pair mating, fertilised embryos were collected from 30 minutes to 1 hour after pulling the dividers. Embryos were then staged according to Kimmel et al., 1995, and were maintained in 1X E3 media (5mM NaCl, 0.17mM KCl, 0.33mM CaCl₂, 0.33mM MgSO₄) at 28.5°C at a density of no more than 60 embryos per dish. When necessary, embryo development was delayed by transferring embryos to lower temperatures of 23°C after gastrulation, and before being staged. For embryos older than 24hpf which would be used in experiments such as immunohistochemistry, *in situ* hybridisation and light-sheet microscopy, embryos were transferred into 1X E3 media containing 0.003% 1-phenyl 2-thiourea (PTU, Sigma P7629) to block pigment formation for imaging purposes.

2.2 Embryo manipulation

2.2.1 Embryo fixation

Before fixation, embryos which were still in their chorion were dechorionated by hand using forceps (Dumont no.5). Dechorionated embryos were then then fixed overnight in 2mL 4% Paraformaldehyde (PFA, Cell Signalling Technology #12606) diluted in 1X phosphate-buffered saline (PBS, OXOID BR0014G). The following day embryos were washed three times in phosphate-buffered saline with 0.2% Tween20 (PBST, Sigma P2287) for 5 minutes at room temperature to remove fixative and then gradually washed into 100% methanol (30%, 50%, 70% methanol diluted in PBST) for storage at -20°C.

2.2.2 Microinjection

Glass injection needles were created from Borosilicate Glass Capillaries (World Precision Instruments) using a P-1000 Flaming/Brown Micropipette Puller. Microloader tips (Eppendorf, ZT1262621S) were used to load needles, which were then attached to a PV820 Pneumatic PicoPump (World Precision Instruments). The

2. Materials and Methods

needle was calibrated by breaking the tip with forceps and measuring the droplet size by placing the tip into mineral oil (Sigma M5904) on a graticule (Agar Scientific L4201). The droplet size was then adjusted to 1nL volume by adjusting ejection time and measuring droplet diameter against the graticule scale.

Embryos to be injected were collected after 20 minutes of adult zebrafish pair mating and placed into troughs in a 1.5% agarose gel mould made with 1X E3 media. 1nL volume of injection mix was injected into the yolk of one cell stage embryos which were then transferred into fresh 1X E3 media. Later that day, any embryos which were unfertilised or dead were removed, with the remaining embryos kept at 28.5°C until the required stage for either fixation or imaging.

2.3 Molecular techniques

2.3.1 Isolation of total genomic DNA

Genomic DNA (gDNA) was extracted from dechorionated embryos by placing individual embryos in 50µL SEL buffer (50mM KCl, 2.5mM MgCl₂, 10mM Tris pH8.3, 0.005% NP40, 0.005% Tween-20, 0.001% Gelatine) with 100µg/mL Proteinase K (Ambion AM2542) and incubating for 1 hour at 65°C followed by 15 minutes at 95°C to denature the Proteinase K. 1µL of gDNA was then used in a PCR reaction.

2.3.2 Isolation of total RNA

At the relevant developmental stage approximately 60 dechorionated embryos were placed into a 1.5mL Eppendorf with 200µL TriReagent (Invitrogen AM9738) and homogenised with a pipette tip. 40µL of chloroform was added and mixed well. After 5 minutes incubating at room temperature the aqueous and organic phases were separated by centrifugation at 15,000rpm for 15 minutes at 4°C, and approximately 100µL of aqueous phase was removed to a fresh Eppendorf with an equal volume of isopropanol. The aqueous phase and isopropanol were mixed and left to incubate for 15 minutes at room temperature. The RNA was then pelleted by centrifugation at

2. Materials and Methods

15,000rpm for 15 minutes at 4°C, and the pelleted RNA was washed in 75% ethanol and then left to air dry at room temperature for 10 minutes. The RNA was resuspended in 30µL RNase free water (Invitrogen 111538646) and stored at -80°C.

2.3.3 Generation of complementary DNA

Complementary DNA (cDNA) was created by reverse transcription using Superscript IV Reverse Transcriptase (ThermoFisher 18090010) using 2µg of RNA template. 2µL Anchored Oligo(dT)₂₀ primer (Invitrogen 12577011) and 2µL of 10mM dNTPs were added to the RNA template, along with RNase free water giving a final volume of 16µL. The Anchored Oligo(dT)₂₀ mix was then incubated at 65°C for 5 minutes to allow the primer to anneal to the RNA template. The reverse transcription mix composed of 8µL of First Strand Buffer, 8µL of 25mM MgCl₂, 4µL of 0.1mM DTT and 2µL RNaseOut (Invitrogen 10777-019) was added to the RNA-OligoDT complex and incubated at 42°C for 2 minutes before adding 2µL Superscript RT IV enzyme and incubated at 42°C for 50 minutes, followed by 70°C for 15 minutes. Then 2µL of RNaseH (ThermoFisher EN0201) was added at 37°C for 20 minutes to degrade the original RNA template. cDNA was diluted 1:2 in 40µL RNase free water, with 1µL used in subsequent PCR reactions.

2.3.4 Polymerase Chain Reaction (PCR)

2.3.4.1 Primer design

Primers were designed using Primer3 (<https://primer3.ut.ee/>) or designed manually if necessary, with annealing temperatures checked using the NEB Tm Calculator (<https://tmcalculator.neb.com>). Primers were ordered from Integrated DNA Technologies, resuspended at a 100µM concentration in water and stored at -20°C.

2.3.4.2 BioMix Red PCR reaction

Standard PCRs were 10µL Biomix Red reactions with 5µL Biomix Red (Meridian BIO-25006), 3µL water, 0.5µL of both the forward and reverse primers at a 10µM

concentration and 1µL of gDNA/cDNA. PCR cycling programmes were carried out in a BioRad T100 Thermocycler as shown below:

98°C for 3 minutes
98°C for 30 seconds
55-58°C for 30 seconds/kb
72°C for 1 minute
Repeat steps 2-4 30 times
72°C for 5 minutes
4°C for 5 minutes

PCR was then assessed using TAE or TBE agarose gel electrophoresis.

2.3.4.3 Phusion Taq PCR reaction

PCR reactions to amplify full length coding sequences were generated using Phusion Taq polymerase (NEB M0530S) in a 50µL reaction with 1µL Phusion Taq polymerase, 10µL 5X High Fidelity Buffer, 1µL 10mM dNTPs, 1µL of both the forward and reverse primers at a 10µM concentration and 1µL gDNA/cDNA. The PCR cycling programme was carried out in a BioRad T100 Thermocycler as shown below:

98°C for 3 minutes
98°C for 30 seconds
55-58°C for 30 seconds/kb
72°C for 1 minute
Repeat steps 2-4 30 times
72°C for 10 minutes
4°C for 5 minutes

PCR was then assessed using TAE or TBE agarose gel electrophoresis.

2.3.4.4 Sequencing

2. Materials and Methods

To sequence PCR products, a 60µl BioMix Red reaction was carried out and purified using the QIAGEN PCR Purification Kit (QIAGEN 28016) with PCR products eluted in 30µL of water. Purified PCR products were sequenced using Genewiz Sanger sequencing service (<https://clims4.genewiz.com>).

2.3.5 TOPO-TA cloning

The DNA sequence to be cloned was amplified in a 10µL BioMix Red PCR reaction (see section 2.3.4.2) using cDNA obtained from the relevant stage of wild-type embryos (see section 2.3.3) using sequence specific primers. 5µL of the resulting PCR product was assessed using 1% TAE gel electrophoresis to determine whether the amplification reaction had worked, while the remaining 5µL was reserved for use in TOPO-TA Cloning.

The PCR product was blunt-end ligated into the PCRII-TOPO vector (ThermoFisher 450640) by combining 1µL of PCR product with 0.5µL PCRII-TOPO vector, 0.5µL salt solution and 1µL water in a 0.2mL PCR tube at room temperature for 5 minutes. 1µL of the ligation reaction was then used immediately for transformation into TOP10 cells (ThermoFisher C404003).

2.3.6 Bacterial transformation

50µL aliquots of TOP10 cells were thawed on ice for 30 minutes before 1µL of ligation reaction was added, gently mixed, and incubated on ice for 30 minutes. Cells were heat-shocked at 42°C for 30 seconds, then incubated on ice for a further 2 minutes. 250µL of SOC media (Sigma S1797) was then added before placing cells horizontally in a shaking incubator at 37°C for 60 minutes.

Cells were pelleted by centrifugation at 3000rpm for 5 minutes at room temperature, followed by removal of 200µL of SOC supernatant and resuspension of the cells in the remaining 50µL of SOC media. Cells were spread onto pre-heated LB agar plates (Sigma L7025) containing Ampicillin at 100µg/mL (Sigma A0166). For blue/white screening, plates were spread with IPTG (0.1M, Merck I6758) and X-Gal (20mg/mL,

2. Materials and Methods

ThermoFisher R0404) 30 minutes before cells were added. Plates were then incubated overnight at 37°C.

The following day, colony PCR was performed to identify colonies containing the plasmid with successful ligation of the desired PCR product, which involved picking 7 white colonies into 10µL of water and including one water-only negative control. 5µL of the colony in water was used as a template for a 20µL colony PCR reaction using primers which were designed to amplify the original PCR fragment. The 20µL colony PCR reaction contained 10µL of BioMix Red, 4.2µL of water, 0.4µL of either the forward or reverse primer at a concentration of 10µM, and 5µL of the colony in water. The PCR cycling programme was carried out in a BioRad T100 Thermocycler as shown below:

94°C for 2 minutes

94°C for 20 seconds

60°C for 20 seconds (dropping 1°C per cycle)

72°C for 45 seconds

Repeat steps 2-4 9 times

94°C for 20 seconds

50°C for 20 seconds

72°C for 45 seconds

Repeat steps 6-8 14 times

72°C for 3 minutes

10°C for 5 minutes

10µL of the colony PCR reaction was assessed using 1% TAE agarose gel electrophoresis, and for colonies containing the plasmid with successful ligation of the desired PCR product the remaining 5µL of the colony in water was inoculated in 50mL of LB broth (Sigma L72275) with 100µg/mL ampicillin and grown overnight in a shaking incubator at 37°C. The following day the plasmid containing the desired PCR fragment was extracted from cells using a QIAGEN Midi-Prep kit (QIAGEN 12143). Sanger sequencing (Genewiz) was used to identify the orientation of the insert into the vector using the M13 forward and M13 Reverse primers (see Table 2.2), to allow transcription of RNA in the correct orientation.

The following primers were used to sequence the insert orientation into the PCR TOPO-II vector:

Table 2.2. Primers to sequence orientation of insert in PCR TOPO-II vector	
Primer	Sequence
M13 Reverse	CAGGAAACAGCTATGACC
M13 Forward	TGTAAAACGACGGCCAGT

2.4 mRNA *in situ* hybridisation

2.4.1 mRNA *in situ* hybridisation probe synthesis

To create mRNA *in situ* hybridisation probes, 10µg of plasmid DNA was linearised overnight in a 50µL reaction using 0.5µL of the relevant restriction enzyme, 5µL of Cutsmart buffer, and made up to 50µL final volume with water. The digest reaction was then purified using a QIAGEN PCR Purification kit and eluted in 30µL of water. To check the plasmid was completely linearised a 1:5 dilution of digested plasmid was assessed alongside a 1:10 dilution of undigested plasmid via gel electrophoresis, with the presence of a single band for the linearised plasmid confirming successful linearisation. The concentration of the linearised plasmid was then measured using a NanoDrop, and the plasmid was stored at -20°C.

The linearised plasmid was used as a template in a transcription reaction to transcribe the mRNA *in situ* hybridisation probes. The transcription reaction consisted of 1µg of linearised plasmid, with 2µL of the appropriate RNA polymerase, 2µL transcription buffer, 2µL digoxigenin-UTP labelling mix (Roche 11277073910), 1µL RNaseOUT and water up to a final volume of 20µL. The transcription reaction was incubated for 2 hours at 37°C in a BioRad T100 Thermocycler followed by the addition of 3µL of TURBO DNase (Invitrogen AM2238) and incubated for another 30 minutes at 37°C. The RNA probe was then purified using overnight ammonium acetate precipitation,

2. Materials and Methods

followed by centrifugation at 15,000rpm for 15 minutes at 4°C the next day. The RNA pellet was resuspended in 10-20µL RNase free water depending on pellet size, and a 1:5 dilution of the RNA probe was assessed via gel electrophoresis to confirm successful RNA transcription. Depending on brightness of the band following gel electrophoresis, the RNA probe was diluted in either 20µL or 40µL of Hyb- (see Table 2.6) and stored at -20°C.

2.4.2 mRNA *in situ* hybridisation probes

The following primers were used to generate *in situ* hybridisation probes in this study:

Table 2.3. mRNA <i>in situ</i> hybridisation probe primers		
Primer	Gene	Sequence
EA-L10	<i>dock6-201</i> sense and antisense	AAACCTCCACCCAGCTACTC
EA-R10	<i>dock6-201</i> sense and antisense	TGGGACATGCTCTTCACCAT
EA-L32	<i>dock6-RI1</i> sense and antisense	TCGGTTCACTGCCTCTCAAT
EA-R32	<i>dock6-RI1</i> sense and antisense	GATGCACGCGTCTCCTTTAG
EA-L16	<i>eogt-201</i> sense and antisense	AACAACCTCCTTCAGCCGTGA
EA-R16	<i>eogt-201</i> sense and antisense	TGTTTAGCTCTCCAGTCCGG
EA-L53	<i>isg-15</i> sense	ATGCAGCTGACTGTAAACTGC
EA-R53	<i>isg-15</i> sense	TTATCCTCCTCGTAGACGGAGA

The following restriction enzymes and RNA polymerases were used to generate *in situ* hybridisation probes in this study:

Table 2.4. mRNA <i>in situ</i> hybridisation probes generated in this study
--

Probe	Restriction Enzyme	RNA Polymerase
<i>dock6-201</i> antisense	SpeI	T7
<i>dock6-201</i> sense	NotI	SP6
<i>dock6-RI1</i> antisense	SpeI	T7
<i>dock6-RI1</i> sense	NotI	SP6
<i>eogt-201</i> antisense	NotI	SP6
<i>eogt-201</i> sense	SpeI	T7
<i>isg-15 antisense</i>	NotI	SP6

The following pre-made *in situ* hybridisation probes were used in this study:

Probe	Reference	Restriction Enzyme	RNA Polymerase
<i>myl7 (cmlc2)</i>	Yelon et al., 1999	NotI	T7
<i>myh7 (vmhc)</i>	Bakkers Lab	NotI	T7
<i>myh6 (amhc)</i>		PstI	T7
<i>notch1a</i>	Rob Wilkinson (unpublished)	BamHI	T3
<i>notch1b</i>	Rob Wilkinson (unpublished)	HindIII	T7
<i>acana</i>	Chris Derrick (unpublished)	NotI	SP6
<i>klf2a</i>	Novodvorsky et al., 2015	From T. Chico	
<i>ltbp3</i>	Derrick et al., 2021	EcoRI	SP6
<i>fli1a</i>	Brown et al., 2000	XbaI	T3

2.4.3 mRNA *in situ* hybridisation protocol

Embryos fixed and stored in methanol were rehydrated gradually into 0.2% PBST (70%, 50%, 30% methanol diluted in 0.2% PBST) and then washed in PBST four times

2. Materials and Methods

for 5 minutes at room temperature. Embryos were then permeabilised in 10µg/mL Proteinase K in PBST for a specific amount of time dependant on embryonic stage as follows:

Blastula and gastrula: 0 minutes

Early somitogenesis: 1 minute

Late somitogenesis (14-22 somites): 3 minutes

24hpf: 5 minutes

36/48hpf: 10 minutes

55hpf: 12 minutes

72hpf: 15 minutes

96hpf: 15 minutes in 20µg/mL Proteinase K

120hpf: 15 minutes in 20µg/mL Proteinase K

Following Proteinase K treatment, embryos were re-fixed in 10% Formalin for 20 minutes at room temperature, followed by five washes in PBST for 5 minutes at room temperature. Embryos were then pre-hybridised in Hyb+ (Hyb- (see Table 2.6) with 50µg/mL Heparin (Merck 2106) and 550µg/mL yeast tRNA (Invitrogen 15401-29)) for a minimum of 1 hour at 70°C. Hyb+ was then removed and replaced with dig-labelled mRNA probes diluted in Hyb+ and incubated overnight at 70°C. After removal of the probes, embryos were gradually washed from Hyb- into 2X SSCT (1:10 20X SSC (see Table 2.6) with 0.2% Tween20) at 70°C, and then washed twice in 0.2X SSCT (1:100 20X SSC (see Table 2.6) with 0.2% Tween20) at 70°C with all wash solutions pre-heated to 70°C. Embryos were subsequently gradually washed out of 0.2X SSCT into 0.2% PBST at room temperature, and then transferred from Eppendorfs into a 24 well microtitre plate, where they were placed into blocking buffer (PBST with 2% sheep serum (Sigma S3772) and 2mg/mL bovine serum albumin (Sigma A9418)) for a minimum of 2 hours at room temperature. Blocking buffer was then removed and replaced with a 1:50 dilution of anti-digoxigenin-AP conjugated pre-incubated antibody (1:5000 (Roche 11093274910); see section 2.4.4) in blocking buffer, and the embryos were incubated overnight in the antibody solution at 4°C. The antibody solution was removed from the embryos the following day with two quick PBST washes followed by eight 15 minute PBST washes at room temperature. Embryos were then washed three times for 5 minutes in staining buffer (see Table 2.6), followed

2. Materials and Methods

by incubation in 1:50 Nitro-blue tetrazolium/5-bromo-4-chloro-3-inodyl phosphate (NBT/BCIP (Roche 11681451001)) diluted in staining buffer at room temperature, with embryos kept in the dark for the remainder of the experiment. After allowing enough time for staining to develop, embryos were washed out of the staining solution using PBST and fixed overnight in 10% Formalin. Embryos were then gradually washed into 100% methanol for storage at -20 °C prior to imaging. When investigating differing levels of gene expression in embryos undergoing different manipulations, all embryos for each probe were fixed at the same time point post staining.

2.4.4 mRNA *in situ* hybridisation antibody pre-incubation

To create the anti-digoxigenin-AP conjugated pre-incubation antibody around 200 embryos from different stages of development were washed in PBST at room temperature and then homogenised in 1mL PBST using a fine needle and syringe. Once sufficiently homogenised, 10µL (1:100 dilution) of anti-DIG antibody was added to the homogenised embryos in PBST and left to incubate for 1 hour at room temperature. The embryo and antibody solution was then centrifuged at 15,000rpm for 15 minutes at 4°C to pellet the homogenised embryos, while the supernatant containing the pre-incubated antibody was removed to a new Eppendorf tube. The supernatant was then stored at 4°C with 0.02% Sodium Azide (1:100 from stock solution (Sigma S8032)).

2.4.5 mRNA *in situ* hybridisation solutions

The following solutions were used during *in situ* hybridisation:

Solution	Composition				
Hyb- (50mL)	25mL Formamide (50%) (Sigma 47671)	12.5mL 20X SSC (5X SSC)	500µL 10% Tween20 (0.1%)	460µl 1M Citric Acid (9.2mM pH 6.0)	10.54mL water

20X SSC (500mL) pH 7.0	87.5g NaCl (Sigma S7653)	44.1g Sodium Citrate (VWR 27833.360)	500mL water		
Staining Buffer (50mL)	5mL 1M Tris-HCl pH 9.5 (10mM Tris-HCl) (Sigma T1503)	2.5mL 1M MgCl ₂ (50mM MgCl ₂)	1mL 5M NaCl (100mM NaCl)	500µL 10% Tween20 (0.1% Tween20)	41mL water

2.4.6 Imaging mRNA *in situ* hybridisations

Embryos were dissected and mounted between a glass slide (VWR ROTH870.1) and a glass coverslip (Mezel Gläser 15787582) and imaged in BBA (2:1 Benzyl Benzoate (Sigma B6630): Benzoic Acid (Sigma 402834)) using an Olympus BX51 microscope.

2.4.7 Quantification and statistical analysis of heart area and heart looping from mRNA *in situ* hybridisation images

To prevent bias, images were blinded using the ImageJ Blind_Analysis plugin (https://github.com/quantixed/imagej-macros/blob/master/Blind_Analysis.ijm) prior to data analysis. Heart area/chamber area was measured in FIJI using *myl7* to label the whole heart area, and *amhc* and *vmhc* to label the atrium and ventricle respectively (see Figure. 4.4). Heart looping was assessed by calculating the looping ratio, by dividing the looped heart length by the linear heart length, as measured in FIJI using *myl7* to label the heart (see Figure. 4.4).

Heart area and looping ratios were analysed in Prism and checked for normal distribution using the Shapiro-Wilks normality test. Looping ratios and areas are

displayed showing the mean and standard deviation of the mean, with non-parametric tests and multiple comparisons applied where appropriate (specific tests used for comparative statistics are named in relevant figure legend). Each embryo is an individual data point, with a minimum of 2 biological repeats.

2.4.8 Genotyping post mRNA *in situ* hybridisation

Once imaged, embryos which required genotyping were transferred individually into 50µL SEL with 1:100 proteinase K to extract the genomic DNA (see section 2.3.1), of which 1µL was then used in a BioMix Red PCR reaction (see section 2.3.4.2).

2.5 Generation of CRISPR/Cas9 promoter-less mutant zebrafish lines

2.5.1 gRNA design

gRNAs were designed on CHOPCHOP (<https://chopchop.cbu.uib.no/>) using the danRer11/GRCz11 assembly of the zebrafish genome. gRNAs flanking the annotated promoter regions of both zebrafish *dock6* and *eogt* as described on the eukaryotic promoter database (<https://epd.epfl.ch//index.php>) were chosen, taking into consideration minimal off-target scores.

2.5.2 gRNAs used

The following gRNAs were used to attempt to make CRISPR/Cas9 promoter-less mutants:

Table 2.7 gRNAs used in this study			
Gene target	gRNA sequence (PAM)	Injected alone/co-injected	Short name
<i>dock6</i> promoter 1	AATGTTGAGGTGTCGTGCTGTGG	Injected alone	<i>dock6-23</i>

<i>eogt</i> promoter exon 1-1	GCGGTGGCTGAAAGTAAGACTGG	Co-injected	<i>eogt</i> exon 1-2
<i>eogt</i> promoter exon 1-2	TGCTTTTTCCCGCTAGTAAAGG	Co-injected	<i>eogt</i> exon 1-6
<i>eogt</i> promoter exon 2-1	TGTCTCTTGTGAATGACTGTAGG	Co-injected	<i>eogt</i> exon 2-21
<i>eogt</i> promoter exon 2-2	CTGCAATAATAAAACCGTCTCGG	Co-injected	<i>eogt</i> exon 2-19

2.5.3 Microinjection to generate CRISPR/Cas9 promoter-less stable mutant zebrafish lines

To attempt to generate *dock6* promoter-less mutants, an injection mixture containing 1µL of 21.4µM *dock6*-23 gRNA, 1µL of 122.5nM tracrRNA, 1µL of 6.67µM Cas9 protein and 1µL of phenol red was prepared and incubated at 37°C. Immediately following incubation, 1nL of injection mix was injected into the yolks of wild-type embryos at one cell stage. A similar strategy was used to make *eogt* promoter-less mutants however 4 gRNAs equalling a total volume of 1µL were co-injected at the same time (*eogt* exon 1-2, *eogt* exon 1-6, *eogt* exon 2-21, *eogt* exon 2-19).

Following microinjection, embryos were genotyped to determine the efficiency with which the gRNAs guide Cas9 to cut the DNA, by designing PCR primers which flank the cut sites. gDNA was extracted from individual embryos at 24hpf in 50µL SEL buffer with 100µg/mL Proteinase K (see section 2.3.1). 1µL of gDNA was then used in a BioMix Red PCR reaction, and 5µL of the PCR reaction assessed on a 4% TBE (89mM Tris-HCl, 89mM Boric Acid, 2mM EDTA) gel to detect the presence of heteroduplexes in the PCR product, indicating successful targeted DNA cutting and imperfect DNA repair.

2. Materials and Methods

Once gRNA efficiency had been determined, injected embryos were raised to adulthood (F0) and once at breeding age, these F0 founders were out-crossed to wild-type fish to identify founders transmitting the desired mutation through the germline, using the PCR method described above to screen F1 embryos for mutations. Once transmission of mutations through the germline had been confirmed, Sanger sequencing (Genewiz) was used to confirm the exact mutation being transmitted, and suitable F0 founders were then out-crossed to establish stable mutant F1 lines. In further F1 and F2 generations, gDNA extracted from fin biopsies was used to determine heterozygous mutant fish.

2.5.4 CRISPR/Cas9 primers

The following primers were used to genotype whether gRNAs guided Cas9 to cut the genome efficiently during CRISPR/Cas9 promoter-less mutant strategies:

Table 2.8 CRISPR/Cas9 Genotyping		
Primer	Sequence	Genotyping
EA-L13	CTGTAAGGAGCTCTG CCTGTTT	<i>dock6-23</i> gRNA cut site: PCR heteroduplexes indicates targeted DNA cut <i>dock6-R11</i> ⁴²⁸ and <i>dock6-R11</i> ^{ins41} : reveals differences in size of PCR product
EA-R13	TGGCGGATCTTCTCT TTATCTC	<i>dock6-23</i> gRNA cut site: PCR heteroduplexes indicates targeted DNA cut <i>dock6-R11</i> ⁴²⁸ and <i>dock6-R11</i> ^{ins41} : reveals differences in size of PCR product
EA-L3	CAAGCCATTA AAAATTT TCCACC	<i>eogt exon 1-2</i> gRNA cut site: PCR heteroduplexes indicates targeted DNA cut
EA-R3	GGAATTGCTGAGAAA AAGATGC	<i>eogt exon 1-2</i> gRNA cut site: PCR heteroduplexes indicates targeted DNA cut
EA-L4	TCCAAGGAGGTAAGC GTACAAT	<i>eogt exon 1-6</i> gRNA cut site: PCR heteroduplexes indicates targeted DNA cut
EA-R4	GATTGACACGTTGCC AAAATAA	<i>eogt exon 1-6</i> gRNA cut site: PCR heteroduplexes indicates targeted DNA cut

EA-L5	CACATGGAGTAAGAT CCGTTCA	<i>eogt exon 2-21</i> gRNA cut site: PCR heteroduplexes indicates targeted DNA cut
EA-R5	TGTTGTAGTCTAGCT GTGGCGT	<i>eogt exon 2-21</i> gRNA cut site: PCR heteroduplexes indicates targeted DNA cut
EA-L6	GGAGTAAGATCCGTT CATTGTC	<i>eogt exon 2-19</i> gRNA cut site: PCR heteroduplexes indicates targeted DNA cut
EA-R6	AGCCAGGCTGTTGTA GTCTAGC	<i>eogt exon 2-19</i> gRNA cut site: PCR heteroduplexes indicates targeted DNA cut
EA-L8	GCCATTAAAATTTTCC ACCAGCT	<i>eogt exon 1</i> cut out region (from <i>eogt exon 1-2</i> and <i>1-6</i> gRNA co-injection): multiple bands indicate cut out region and both gRNAs are working well together
EA-R8	ACTCCTGCAGAAAGT GAATCA	<i>eogt exon 1</i> cut out region (from <i>eogt exon 1-2</i> and <i>1-6</i> gRNA co-injection): multiple bands indicate cut out region and both gRNAs are working well together
EA-L9	TGCCAAATACAGCCA ACCAC	<i>eogt exon 1</i> cut out region (from <i>eogt exon 2-21</i> and <i>2-19</i> gRNA co-injection): multiple bands indicate cut out region and both gRNAs are working well together
EA-R9	TTAAAAGGGCAAAGC GGGTC	<i>eogt exon 1</i> cut out region (from <i>eogt exon 2-21</i> and <i>2-19</i> gRNA co-injection): multiple bands indicate cut out region and both gRNAs are working well together

2.6 Generation of CRISPR/Cas12a AOS disease specific knock-in mutant zebrafish lines

2.6.1 crRNA design

crRNAs were designed to guide Cas12a to cut as close as possible to the genomic location where human AOS disease-specific mutations were going to be knocked into

the zebrafish genome (see Chapter 3, Figures 3.7 and 3.12). crRNAs were designed using the Deep CRISPR crRNA design tool (<http://deepcrispr.info/>) considering minimal off target effects.

2.6.2 crRNAs used

The following crRNAs were used to attempt to make CRISPR/Cas12a AOS disease-specific knock-in mutants:

Table 2.9 crRNAs used in this study		
Gene target	crRNA sequence (PAM)	Short name
<i>dock6</i> exon 37	TTTCTATAAGCCAAGTTAATCATC	<i>dock6</i> crRNA 3
<i>eogt</i> exon 6	TTTACACAGGCCTCTGTTAGTTAC	<i>eogt</i> crRNA 1

2.6.3 Designing single stranded oligonucleotides for homology directed repair

Single stranded oligonucleotides were designed based on recommendations from Fernandez et al., 2018. Oligos were designed based on the opposite strand to where the crRNA targets to increase the efficiency of homology directed repair (HDR), with a longer Pam proximal arm and a shorter PAM distal arm, which were designed based on the homologous sequences flanking the point mutation I intended to knock into the genome. The point mutation to be introduced was included in the single stranded oligonucleotide, along with silent mutations along the crRNA binding site and PAM site to prevent re-cutting of the DNA following successful incorporation of the oligonucleotide. A restriction site was also introduced using silent mutations to facilitate genotyping of successful oligonucleotide incorporation. Oligos were ordered from Integrated DNA Technologies as a custom ultramer (standard purity) with the first 2 and last 2 bases phosphorothioated.

2.6.4 Single stranded oligos used

The following single stranded oligonucleotides were used to attempt to make CRISPR/Cas12a AOS disease-specific knock-in mutants:

Table 2.10 Single Stranded Oligos for CRISPR knock-in			
Gene Target	Point mutation introduced	Restriction site introduced	Short name
<i>dock6</i>	G>T Nonsense mutation Lehman et al., 2014	SpeI	<i>dock6</i> ss oligo 1
<i>eogt</i>	G>C Missense mutation Shaheen et al., 2013	SphI	<i>eogt</i> ss oligo 2

(Point mutation, crRNA binding site, PAM, restriction site, ▲ cut site, homology arms)

***dock6-201* original target sequence**

AGCGCCTCGCTCTACCTTCTCATGAGACAGAACTTCGAGATCGGAAACGTAAGT
CACAAAAAAGCCCAGATGATTAACCTGGCTTATAGAAAAGGTTAAATGTGACAA
GTGAATTGCTGT ▲

***dock6* single stranded oligonucleotide (*dock6* ss oligo 1)**

AGCGCCTCGCTCTACCTTCTCATGAGACAGAACTTCAGATCGGAAACGTAAGT
CACAAAAAAGCCCAATGATCAATTTAGCATACAGGAAAAGGTTAAATGTGACTA
GTGAATTGCTGT ▲

***eogt-201* original target sequence**

AGGCAGAAGGGACACATAAGAGTCCCCTACAGTCTTGTA ACTAACAAAGGCC
TGTGTAACACATATTAATTCTTTGATTTTAATCAGTCTTCAGTTAATGAAACAAT
GTCAATTCAAGA ▼

eogt single stranded oligonucleotide (eogt ss oligo 2)

AGGCAGAAGGGACACATAAGAGTCCCCTACAGTCTT**C**GTAGCTCACCAAAGCA
TGCGTCAAGCATATTAATTCTTTGATTTTAATCAGTCTTCAGTTTAATGAAACAAT
GTCAATTCAAGA

2.6.5 Microinjection to generate CRISPR/Cas12a knock-in mutant zebrafish lines

Microinjection and testing crRNA efficiency was carried out the same as described above for generating CRISPR/Cas9 promoter-less mutant lines (see section 2.5.3) with an injection mix composed of 1µL of 200µM crRNA, 0.2µL 10X NEB 2.1 Buffer, 0.5µL 100µM Cas12a protein (NEB M0653T) and 0.3µL phenol red which is incubated for 10 minutes at 25°C and then injected immediately into the yolk of 1 cell stage embryos. Once crRNA efficiency had been determined, the same injection mixture as described above plus 1µL of the relevant 3µM single stranded oligonucleotide was injected, to attempt to knock-in the desired mutation into the zebrafish genome via HDR. gDNA was extracted from individual embryos, and 1µL of gDNA was used in a BioMix Red PCR reaction with primers flanking the crRNA target site. Successful knock-in was determined using restriction digest of the PCR amplified knock-in region, using the knocked-in restriction site. Following BioMix Red PCR amplification of the knock-in region, 5µL of PCR product was digested using 0.3µL of the appropriate restriction enzyme, with 1µL of Cutsmart buffer and 3.7µL of water. The PCR product was digested for 3 hours at 37°C and then assessed on a 4% TBE gel alongside uncut PCR product to determine whether the oligo, and therefore the restriction site, had been successfully incorporated. Alternatively, successful incorporation of single stranded oligo could be detected via knock-in PCR, using a primer designed to bind to the SNPs introduced into the genome to prevent the crRNA guiding the Cas12a to recut the DNA when the oligo had been incorporated, and therefore would only amplify a PCR product if the knock-in had been successful.

Once successful knock-in was confirmed, injected embryos were raised to adulthood (F0) and subsequent F1 were screened as described above for generation of CRISPR/Cas9 mutant lines.

2.6.6 CRISPR/Cas12a primers

The following primers were used to genotype whether crRNAs guided Cas12a to cut the genome efficiently, and whether the single stranded oligonucleotides were incorporated during CRISPR/Cas12a AOS disease-specific mutant strategies:

Table 2.11 CRISPR/Cas12a Genotyping		
Primer	Sequence	Genotyping
EA-L19	G TTCAGGTCAACTCT GGCTTCT	<i>dock6 crRNA 3</i> cut site: PCR heteroduplexes indicates targeted DNA cut <i>dock6-201^{ins36Δ65}</i> genotyping: reveals differences in size of PCR product
EA-R19	TTCTACAGAATGGGA GGGAAAA	<i>dock6 crRNA 3</i> cut site: PCR heteroduplexes indicates targeted DNA cut <i>dock6-201^{ins36Δ65}</i> genotyping: reveals differences in size of PCR product
EA-L20	TAAAGAGGATTCCT GGAGCAG	<i>eogt crRNA 1</i> cut site: PCR heteroduplexes indicates targeted DNA cut <i>eogt-201^{Δ28}</i> genotyping: reveals differences in size of PCR product
EA-R20	AAAAGGAAGGCAACA TCTTCTG	<i>eogt crRNA 1</i> cut site: PCR heteroduplexes indicates targeted DNA cut <i>eogt-201^{Δ28}</i> genotyping: reveals differences in size of PCR product
EA-L47	TTCAGGTCAACTCTG GCTTC	<i>dock6</i> knock-in PCR: will only amplify a PCR product if oligo has been incorporated successfully
EA-R47	TTCCTGTATGCTAAAT TGATCATT	<i>dock6</i> knock-in PCR: will only amplify a PCR product if oligo has been incorporated successfully
EA-L44	TGACCGAAGCATGCG TGAAG	<i>eogt</i> knock-in PCR: will only amplify a PCR product if oligo has been incorporated successfully

EA-R44	TGTGCAGCCCTAGTG GTAAC	<i>eogt</i> knock-in PCR: will only amplify a PCR product if oligo has been incorporated successfully
--------	--------------------------	---

2.7 Cloning coding sequences for over-expression experiments

2.7.1 Designing primers to amplify open reading frames

As the *eogt* coding sequence is too long (1560bp) to undergo accurate BioMix Red amplification and TOPO-TA cloning, the coding sequence was amplified via Phusion Taq Polymerase PCR with the addition of restriction sites at either end, before being cloned into the PCS2+ vector. The following primers were used to amplify the *eogt* coding sequence flanked by *ecoRI* restriction sites and a Kozak sequence to increase transcription efficiency (Kozak, 1987):

Table 2.12 Primers to amplify <i>eogt</i> coding sequence	
Primer	Sequence (addition, <i>ecoRI</i>, Kozak, sequence specific)
EA-L21	CGGAATTCACCATGCTGCTTCTGGTAG
EA-R21	CCGGAATTCCTACAGTTCTTCTCGACTTT

Due to the shorter length of the *isg15* coding sequence (474bp), *isg15* underwent BioMix red PCR amplification and TOPO-TA cloning (see section 2.3.5) before being cloned into the PCS2+ vector. The following primers were used to amplify the *isg15* coding sequence:

Table 2.13 Primers to amplify <i>isg15</i> coding sequence	
Primer	Sequence
EA-L21	ATGCAGCTGACTGTAAACTGC
EA-R21	TTATCCTCCTCGTAGACGGAGA

2.7.2 Generation of *eogt* sense and antisense and *isg15* sense over-expression constructs

The coding sequence of *eogt* was amplified from 24hpf cDNA using a Phusion Taq Polymerase PCR reaction (see section 2.3.4.3) and assessed via TAE gel electrophoresis, with the relevant sized band extracted and purified using a QIAGEN gel purification column (QIAGEN 28704). The *isg15* coding sequence was amplified via BioMix Red PCR reaction (see section 2.3.4.2) and underwent TOPO-TA cloning before being excised from the TOPO-TA vector using the *ecoRI* restriction enzyme (NEB R3101S). To clone both the *eogt* and *isg15* coding sequences into the PCS2+ vector, 5µg of both the PCR product and the PCS2+ vector were digested with the 0.5µL of *ecoRI* restriction enzyme (NEB R3101S) along with 5µL of Cutsmart buffer, with the reaction made up to 50µL with water and incubated overnight at 37°C. Digested products were assessed via gel electrophoresis alongside undigested plasmid to ensure linearisation, and the PCS2+ vector dephosphorylated with 2.5µL of rSAP (NEB M0371L) for 30 minutes at 37°C to prevent relegation, followed by 5 minutes at 65°C to denature the enzyme. The digested plasmid and PCR product were then ligated together using either a 1:1, 1:3 or 1:7 ratio of vector to insert (see Table 2.14 and Table 2.15) with all ligation ratios calculated using the NEB online ligation calculator (<https://nebiocalculator.neb.com/#!/ligation>). Ligation reactions were incubated overnight at 16°C, with 1µL of the resulting ligation being used to transform TOP10 cells the following day (see section 2.3.6). Colony PCR was used to detect colonies with plasmids containing the *eogt* or *isg15* coding sequences and midi-preps of positive colonies were carried out as previously described (see section 2.3.6). Positive plasmids then underwent Sanger sequencing (Genewiz) to ensure no SNPs were introduced into the coding sequences, and to determine the orientation that the sequence had been inserted into the PCS2+ vector.

Once orientation and fidelity of sequence had been confirmed, plasmids containing *eogt* in both the forward and reverse orientations, and *isg15* in the forward orientation were chosen and digested with the *NotI*-HF restriction enzyme (NEB R3189S), cleaned up using the QIAGEN PCR clean up kit and eluted in 30µL of water. The linearized plasmids were then used as templates to transcribe RNA using the SP6

2. Materials and Methods

mMessage mMachine kit (ThermoFisher AM1340). A reaction mix containing 1µg of linearised plasmid, 2µL of SP6 enzyme mix, 2µL 10X reaction buffer, 10µL 2X NTP/CAP and water up to 20µL was incubated for 2 hours at 37°C. 1µL of TURBO DNase (ThermoFisher AM2238) was then added for 15 minutes at 37°C to remove any remaining DNA from the sample. RNA was precipitated using Lithium Chloride precipitation method, with 30µL of lithium chloride and 30µL water added to the sample before being chilled overnight at -20°C. The RNA was pelleted by centrifugation for 15 minutes at 15,000RPM at 4°C, before washing the pellets in 70% ethanol and letting them air dry, and then resuspending in 10µL of RNase free water. A 1:10 dilution of each RNA was then assessed on a NanoDrop to determine the concentration and a 1:5 dilution assessed via gel electrophoresis to confirm RNA integrity. The remaining RNA was diluted to 0.4µg/mL concentration, and aliquoted for storage at -80°C.

Table 2.14 Ligating <i>eogt</i> coding sequence into the PCS2+ vector		
Vector:Ligand ratio		
Component	Amount (µL) in Vector:Ligand ratio	
	1:3	1:7
PCS2+ Vector (108.4ng/µL)	1	1
<i>eogt</i> insert (285.9ng/µL)	3.57	8.38
T4 DNA Ligase Buffer	2	2
T4 DNA Ligase	1	1
Water	Up to 20	Up to 20

Table 2.15 Ligating <i>isg15</i> coding sequence into the PCS2+ vector		
Vector:Ligand ratio		
Component	Amount (µL) in Vector:Ligand ratio	
	1:1	1:3
PCS2+ Vector (Xng/µL)	1	1
<i>isg15</i> insert (Xng/µL)	0.6	1.98
T4 DNA Ligase Buffer	2	2
T4 DNA Ligase	1	1
Water	Up to 20	Up to 20

2.7.3 Microinjection of *eogt* and *isg15* over-expression RNA

To over-express *eogt* sense and antisense RNA or *isg15* RNA, the RNA was diluted to 0.1µg/mL by combining 1µL of the 0.4µg/mL stock with 2µL of water and 1µL of phenol red. A 1nL volume was injected into the yolks of embryos of the relevant genetic background at one cell stage, and embryos were then fixed at the appropriate stage for *in situ* hybridisation or immunohistochemistry, or used live in light-sheet microscopy.

2.8 Immunohistochemistry2.8.1 Immunohistochemistry protocol

Fixed embryos stored in methanol were gradually washed into PBS-Triton (0.2% Triton-X-100 (Sigma T8787) in PBS) (70%, 50%, 30% methanol diluted in PBS-triton) and washed three times for 5 minutes at room temperature in PBS-Triton. Embryos were then blocked using blocking buffer (10% goat serum (Invitrogen 10000C) in PBS-Triton) for 45 minutes before being placed into primary antibody solutions (see Table 2.16) made up in blocking buffer with 1% DMSO and incubated overnight at 4°C. The following day the primary antibody solution was removed followed by 3 washes in PBS-Triton for 5 minutes at room temperature, and then followed by 4 longer PBS-Triton washes throughout the remainder of the day. Secondary antibody solutions (see Table 2.17) were diluted 1:200 in blocking buffer with 1% DMSO, and added to embryos overnight at 4°C, with protection from light from this point onwards. Following removal of the secondary antibody solutions, embryos were washed 4 times for 5 minutes at room temperature and stored in PBS-Triton at 4°C before being prepared for imaging.

The following primary antibodies were used in immunohistochemistry in this study:

Table 2.16 Primary antibody solutions for Immunohistochemistry			
Antigen	Species	Dilution	Reference
GFP	Chicken	1:500	Aves Labs, Inc. GFP697986

DM-Grasp (zn-8)	Mouse	1:100	DSHB AB_531904
anti-Fli1B	Rabbit	1:500	Kerafast ES1005

The following secondary antibodies were used in immunohistochemistry in this study:

Table 2.17 Secondary antibody solutions for Immunohistochemistry			
Raised Against	Species	fluorophore	Reference
Chicken	Donkey	Cy2	Jackson Immuno Research Europe LTD 703-225-155
Mouse	Goat	Cy5	Jackson Immuno Research Europe LTD 115-165-146
Rabbit	Goat	Cy5	Jackson Immuno Research Europe LTD 111-175-144

2.8.2 Immunohistochemistry imaging

Embryos were dissected and mounted between a glass slide (VWR ROTH870.1) and a glass coverslip (Mezel Gläser 15787582) in VectaShield (Vecta Laboratories (H-1000)). Slides were imaged on a Nikon A1 Inverted Confocal Microscope (Wolfson Light Microscopy Facility).

2.8.3 Quantification of Notch positive cells

Zebrafish carrying the transgenes *Tg(Tp1bglob:hmgb1-mCherry);Tg(fli1a:eGFP)* were injected with *eogt* sense or antisense RNA as previously described (see section

2.7.3) and fixed at 26hpf. Embryos underwent immunohistochemistry as described above (see 2.8.1) with the anti-DM-Grasp primary antibody to label the heart, and embryos were imaged to quantify the number of Notch positive cells in the endocardium (see Chapter 5, Section 5.6). Additionally, embryos of the genotype *eogt-201^{Δ28}/Tg(myI7:LifeActGFP);Tg(Tp1bglob:hmgb1-mCherry)* were fixed at 26hpf and underwent immunostaining with the anti-Fli1b antibody to label endocardial cell nuclei, and were imaged to quantify the number of Notch positive cells in the endocardium (see Chapter 5, Section 5.9). Prior to analysis, images were blinded using the ImageJ Blind_Analysis plugin (https://github.com/quantixed/imagej-macros/blob/master/Blind_Analysis.ijm) to prevent quantification bias. Blinded images were opened in FIJI and the number of Notch positive cells (labelled by *Tg(Tp1bglob:hmgb1-mCherry)* in the endocardium (labelled by *Tg(fli1a:eGFP)* or the anti-Fli1b antibody) were counted by scrolling through the Z stack of each heart (see Figures 5.6 and 5.11).

2.8.4 Statistical analysis

The number of Notch positive cells was analysed in Prism and checked for normal distribution using the Shapiro-Wilks normality test. All data is displayed showing the mean and standard deviation of the mean, with non-parametric tests and multiple comparisons applied where appropriate (specific tests used for comparative statistics are named in relevant figure legend). Each embryo is an individual data point, with 3 technical repeats on embryos laid on 3 separate days.

2.9 Light-sheet imaging and analysis

2.9.1 Imaging embryos on the Light-sheet microscope

Heterozygous F2 zebrafish of the different mutant lines were raised in the *Tg(myI7:LifeActGFP);Tg(fli1a:AC-TagRFP)* background and in-crossed to obtain a selection of wild-type, heterozygous and homozygous mutant embryos. Embryos were treated with PTU at 24hpf to block development of pigmentation and screened for both green and red fluorophores labelling the myocardium and endocardium respectively

at 55hpf, before being imaged at 72hpf or 5dpf. Embryos were anaesthetised using Tricaine (Merck 10521) in E3 media and mounted in 1% low melting temperature agarose (Sigma A9414), with 72hpf embryos mounted in black capillaries with a 1mm diameter, and 5dpf embryos mounted in green capillaries with a 1.5mm diameter. Embryos were imaged using a Zeiss light-sheet Z.1 system using dual side lasers and capturing the green channel with the 488 laser and the red channel with the 561 laser, obtaining cross sections through the whole heart for 72hpf and the top of the ventricle and outflow tract for 5dpf embryos. Data was acquired using Zeiss ZEN software.

2.9.2 Genotyping embryos following Light-sheet imaging

Following imaging, the capillaries containing embryos were carefully labelled, allowing extraction of DNA from individual embryos to be matched to the heart image taken from that embryo. gDNA was extracted from individual embryos in 50µL SEL with 1:100 Proteinase K as described above (see section 2.3.1) and then 1µL of extracted DNA was used in a BioMix Red PCR reaction as described above (see section 2.3.4.2) and assessed using TAE gel electrophoresis to identify wild-type or homozygous mutant embryos for analysis of their heart morphology.

2.9.3 MorphoHeart image analysis

Heart morphology was analysed using MorphoHeart, a custom-built image analysis pipeline developed by Juliana Sánchez-Posada (Sánchez-Posada, 2022). Light-sheet images of wild-type and homozygous mutant hearts were processed using Arivis to remove background and sharpen the contours of the myocardial and endocardial tissue layers as labelled with the *Tg(myI7:LifeActGFP)* and *Tg(fli1a:AC-TagRFP)* transgenes respectively. Once processed, masks were made for each heart layer in FIJI, and these masks were loaded into MorphoHeart to facilitate an in-depth analysis of heart morphology. Using MorphoHeart, the contours of both the myocardial and endocardial tissue layers were selected for each heart to create 3D reconstructions of each tissue layer. The 3D reconstructions were cropped at both the inflow and outflow tracts, and centrelines through the tissue automatically calculated. MorphoHeart then assessed parameters such as heart/chamber size, heart/chamber geometry, tissue

thickness for each of the tissue layers and heart/chamber ballooning, providing qualitative heat maps and quantitative measurements for all parameters measured.

2.9.4 Statistical analysis

MorphoHeart quantitative data was analysed in Prism and checked for normal distribution using the Shapiro-Wilks normality test. All data is displayed showing the mean and standard deviation of the mean, with non-parametric tests and multiple comparisons applied where appropriate (specific tests used for comparative statistics are named in relevant figure legend). Each embryo is an individual data point, with a minimum of 2 technical repeats.

2.10 Genotyping and raising homozygous mutant embryos to adulthood

Homozygous mutant embryos for each of the different mutant lines were genotyped by either Zeg (Danilab) or 3dpf finclip by the University of Sheffield Genotyping Facility (<https://www.sheffield.ac.uk/bateson/zebrafish/information#4>). gDNA obtained by Zeg or 3dpf finclip were then used in BioMix Red PCR reactions (see section 2.3.4.2) to identify homozygous mutant and wild-type sibling embryos which were separated and raised to adulthood.

2.11 Quantitative PCR (qPCR)

2.11.1 RNA extraction and cDNA synthesis for qPCR experiments

RNA was extracted from embryos at the relevant stage of development depending on the expression dynamics of the gene being analysed. To investigate gene expression in *eogt* over-expression conditions, embryos were injected with either *eogt* sense or antisense RNA as described previously (see section 2.7.3) and RNA extracted as described above (see section 2.3.2) once they had reached the relevant stage of development. To obtain *dock6-R11^{ins41}* homozygous mutant and wild-type sibling RNA, homozygous *dock6-R11^{ins41}* adults or wild-type sibling adults were in-crossed and RNA

2. Materials and Methods

extracted from the embryos at 24hpf. RNA was quantified using a NanoDrop and only RNA with a 260/280 ratio of ~2, and a 260/230 ratio between 2 and 2.2 used in qPCR experiments to ensure the RNA was pure. 2µg of RNA was used in each cDNA transcription with Superscript IV for consistency (see section 2.3.3) with three separate transcriptions carried out on three different batches of embryos.

2.11.2 Primer design and efficiency testing

qPCR primers were designed using the Integrated DNA Technologies PrimerQuest Tool (<https://www.idtdna.com/pages/tools/primerquest>). Primers were tested for efficiency using a serial dilution of wild-type cDNA (1:10 – 1:10,000) and only primer pairs with an efficiency between 90-110% were selected for use.

2.11.3 qPCR primers

The following housekeeping control primers were used for qPCR in this study:

Table 2.18 Housekeeping qPCR primers		
Primer	Gene	Sequence
EA-L58	<i>ef1a</i>	TCATCAAGAGCGTTGAGAAGAA
EA-R58		AACGGTGTGATTGAGGGAAA
EA-L56	<i>Sc125a5</i>	CTGGGTAAGTCTTGGTAAAGA
EA-R56		CGAAGTAGGCAGCTCTGTAAAT

The following experimental primers were used for qPCR in this study:

Table 2.19 Experimental qPCR Primers		
Primer	Gene	Sequence
EA-L64	<i>klf2a</i>	CTCAGGACATTTCCGGAGTGTATC
EA-R64		GTTGCCCTCTTGTTTGACTTTG

EA-L60	<i>fli1a</i>	GAACTATTAAGGAGGCGCTGTC
EA-R60		CAGTCATGTCTGTCTTGGGTA
EA-L69	<i>dock6-201</i>	GCAGACATAGCCAGCAGATA
EA-R69		ATGAGAGAGAGCAGGTCATTAAG
EA-L70	<i>dock6-R11</i>	CAACCATCTACCCTTCCTCAA
EA-R70		CTGCCCATCACTATGTCTAACC

2.11.4 qPCR protocol

qPCR reactions were assembled as a 20µL SYBR green master mix to avoid pipetting error. Each reaction contained 10µL SYBR green (ThermoFisher 4309155), 6µL water, 0.5µL of both the forward and reverse primers at a 10µM concentration and 3µL of cDNA at a 1:10 dilution in water. Each PCR reaction had 3 technical repeats per plate, alongside PCR reactions using control primers for housekeeping genes (*ef1α* and *slc25a5*) and a negative control using water. PCR cycling programmes were carried out in a BioRad CFX96 Real-Time Thermocycler as shown below:

97°C for 7 minutes

95°C for 15 seconds

58°C for 30 seconds

Repeat steps 2-3 40 times

95°C for 30 seconds

Melt curve: increase from 65°C to 95°C by 0.5°C every 5 seconds

2.11.5 qPCR statistical analysis

2. Materials and Methods

Δ CT values were calculated for each cDNA condition, and the $2^{-\Delta\Delta CT}$ values calculated for each cDNA condition by normalising to the housekeeping genes. Any CT values with more than 0.2 difference were eliminated from quantification. $2^{-\Delta\Delta CT}$ values were analysed in Prism and checked for normal distribution using the Shapiro-Wilks normality test. All data is displayed showing the mean and standard deviation of the mean, with non-parametric tests and multiple comparisons applied where appropriate (specific tests used for comparative statistics are named in relevant figure legend). Each data point is the $2^{-\Delta\Delta CT}$ value from 3 plate repeats, with each plate using cDNA generated from separate batches of embryos.

2.12 Adult behavioural analysis

2.12.1 Adult behavioural analysis protocol

Adult fish were transported to the behavioural analysis room and placed into individual tanks filled with aquarium water. The tanks were then stacked in front of a light source and camera in the adult fish behavioural analysis booth, before being recorded swimming around for 8 hours using the ViewPoint Behavioural analysis software (<https://www.viewpoint.fr/en/home>). The system tracks the fish and records “inactivity” (movement of less than 5cm/sec), “average speed” (movement of between 5-7cm/sec) and “hyperactivity” (movement of more than 7cm/sec).

2.12.2 Statistical analysis

Averages of time spent inactive or hyperactive were calculated per fish and then analysed in Prism, checking for normal distribution using the Shapiro-Wilks normality test. All data is displayed showing the mean and standard deviation of the mean, with non-parametric tests and multiple comparisons applied where appropriate (specific tests used for comparative statistics are named in relevant figure legend). Each embryo is an individual data point, with differing icons representing 3 technical repeats, each repeat conducted using different fish.

3. Creating zebrafish models of Adams-Oliver Syndrome

3.1 Introduction

Adams-Oliver syndrome (AOS) is a multisystemic disorder which affects around 1 in 225,000 live births (Meester et al., 2019), and is characterised by aplasia cutis congenita (ACC), a thinning of the skin on top of the head and underlying skull tissue, and terminal transverse limb defects (TTLD), for example fusion of digits or complete loss of digits in extreme cases (Sukalo et al., 2015). Congenital heart defects (CHDs) are also present in some AOS patients, which occur in around 20% of patients (Algaze et al., 2013). Very little is currently known about AOS disease progression, and to-date mutations have been identified in six genes that lead to AOS: *NOTCH1*, *DLL4*, *RBPJ*, *EOGT*, *ARHGAP31* and *DOCK6*, which are all involved in either the NOTCH or RAC1/CDC42 signalling pathways (Dudoignon et al., 2019). Mutations in any of these six genes have only been identified in around 50% of AOS patients, so it is likely that more causative genes will be identified in the future (Sukalo et al., 2015), either in other genes associated with the NOTCH or RAC1/CDC42 signalling pathways, genes associated with other signalling pathways, or additional mutations within non-coding transcripts or regulatory regions of the six genes already identified. Whilst *NOTCH1*, *DLL4*, *RBPJ* and *ARHGAP31* are linked with autosomal dominant forms of the disease, *DOCK6* and *EOGT* have been identified in autosomal recessive forms of the disease (Mašek and Andersson, 2017). *DOCK6* and *EOGT* are thought to be involved in the regulation of the RAC1/CDC42 and NOTCH signalling pathways respectively, and although we have a greater understanding of the roles these signalling pathways play more generally during cardiac development, it is still unclear how mutations in these specific genes lead to the dysregulation of these pathways and subsequently to the defects observed in patients with AOS (Hassed et al., 2017). I specifically chose to study the role of *DOCK6* and *EOGT* in the pathology of AOS, as recessive mutations are likely to be loss-of-function (LOF) and allow easier modelling using zebrafish, due to the ability to raise healthy heterozygous carriers to adulthood, and in-crossing them to observe autosomal recessive phenotypes in embryos. By studying autosomal recessive mutations for *dock6* and *eogt* in zebrafish embryos I hope to improve the

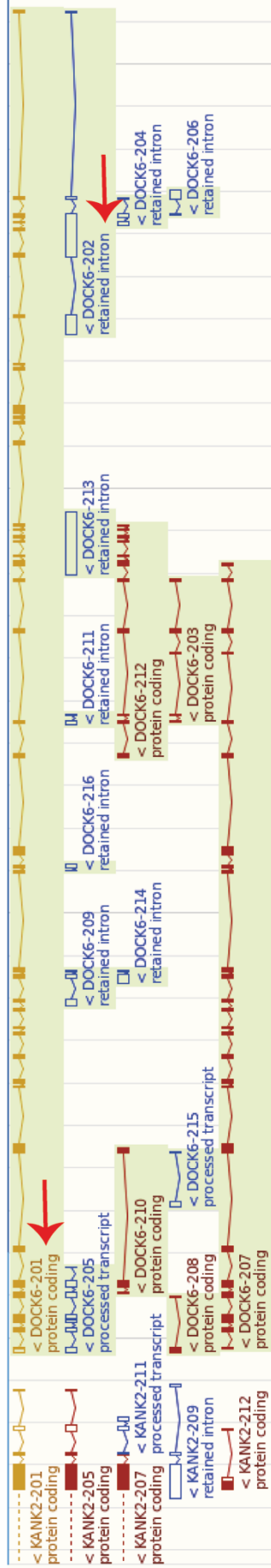
understanding of how these mutations regulate Rac1/Cdc42 and Notch signalling in the context of both development and disease.

To date there are only a few animal models which have been created to try to understand the aetiology of AOS (De Zoysa et al., 2021, Caron et al., 2016). *Dock6* mutant mice models have been reported (Mallon et al., 2012; Miyamoto et al., 2013), however none of them have been used to study AOS, and only one mouse model has been created to understand the role of *Eogt* in the AOS (Sawaguchi et al., 2017). Zebrafish are easy to genetically manipulate using CRISPR/Cas9 genome editing (Li et al., 2016), and the fact that the embryos develop externally and are relatively transparent (Liu and Stainier, 2012) facilitates imaging early heart development in live embryos (Giardoglou and Beis, 2019). Combined with a high conservation of gene function, this makes them an excellent model to investigate human diseases and particularly to study CHDs. Therefore, a zebrafish model would provide us with a powerful model to elucidate the roles these genes play during heart development and the onset of CHDs in AOS. In this chapter I compare human and zebrafish *DOCK6* and *EOGT* gene structures and describe zebrafish *dock6* and *eogt* gene expression throughout development. I detail the genome editing strategies I designed to create *dock6* and *eogt* zebrafish LOF mutant models and AOS disease-specific knock-in mutant models and present the models I recovered from these approaches.

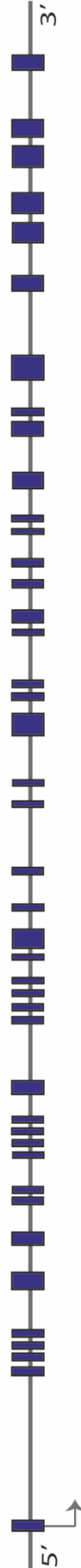
3.2 Humans and zebrafish share conserved *DOCK6* transcripts

To compare human *DOCK6* and zebrafish *dock6* gene structure, both sequences were identified in Ensembl (www.ensembl.org). The human *DOCK6* gene (GRCh38.p13, ENSG00000130158) has 16 transcripts comprising 6 protein-coding transcripts, 2 processed transcripts and 8 retained intron transcripts (Fig.3.1 A). The full-length protein coding transcript, *DOCK6-201*, is composed of 48 exons encoding 2,047 amino acids (Fig.3.1 B). The largest of the intron-retaining transcripts, *DOCK6-202*, is composed of 4 exons and 2 retained introns at the end of exon 3 and exon 4, and is 15,422bp long, with the exons spanning 3,152bp (Fig.3.1 C). Both *DOCK6-201* and *DOCK6-202* are conserved in zebrafish. The zebrafish *dock6* gene (GRCz11, ENSDARG00000035706) only has two transcripts annotated (Fig.3.2 A). *dock6-201* is the full-length protein coding transcript comprising 50 exons encoding 2,114 amino acids (Fig.3.2 B). The intron retaining *dock6-202* transcript, like humans, is composed

A Human *DOCK6* gene annotation on ensembl



B Human *DOCK6-201*



C Human *DOCK6-202*



3. Creating zebrafish models of AOS

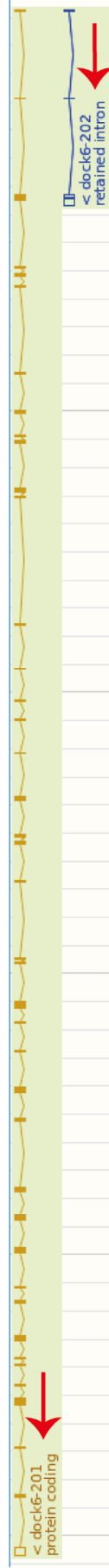
Figure 3.1. Human *DOCK6* gene structure. (A) Human *DOCK6* gene annotation from Ensembl (ENSG00000130158), showing multiple human *DOCK6* transcripts, with *DOCK6-201* and *DOCK6-202* highlighted with red arrows. (B) Human *DOCK6-201* full length protein coding transcript which is composed of 48 exons (dark blue). (C) Human *DOCK6-202* retained intron transcript which is composed of 4 exons (E1-E4, dark blue) and 2 retained introns at the end of exons 3 and 4 (RI3 and RI4, orange).

of 4 exons and has 1 retained intron at the end of exon 4, and is 13,926bp long, with the exons spanning 870bp (Fig.3.2 C). A further transcript, called *dock6-RI1*, has been identified in this thesis but is not yet annotated on Ensembl, and is believed to have intron 1 retained, however it is currently unknown how long this transcript is or how many exons it possesses (Fig.3.2 D). According to BLAST and UniProt, the human and zebrafish *DOCK6-201* coding sequences share 68% similarity, with the proteins sharing 71.6% identity. The human and zebrafish *DOCK6-202* genomic sequences share 47% similarity. It is currently unknown whether humans also possess a *DOCK6-RI1* transcript too. The similarity between both the protein coding transcript and the retained intron transcripts in humans and zebrafish suggests a potentially conserved functional role for these transcripts in both species, further supporting the use of zebrafish as a model to understand the role of *dock6* during cardiac development and the onset of CHDs in humans.

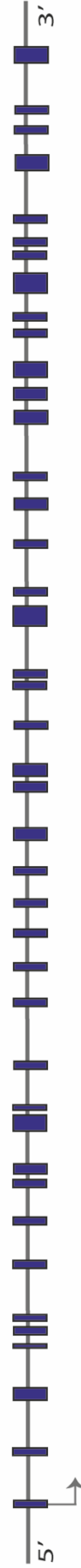
3.3 Zebrafish *dock6* transcripts are expressed in distinct tissues during cardiac development

To identify if *dock6* is important for the heart development process, I focused on investigating whether *dock6-201* and *dock6-RI1* are expressed in the zebrafish heart during cardiac development using mRNA *in situ* hybridisation. Zebrafish *dock6-201* full length protein coding transcript is expressed throughout early development, initially being maternally deposited with *dock6-201* mRNA visible at 3hpf (Fig.3.3 A), however zygotic gene expression is not detected until 20hpf, when *dock6-201* is observed throughout the head and in the dorsal aorta (DA) and posterior cardinal vein (PCV) of the tail (Fig.3.3 C). At 24hpf *dock6-201* is expressed throughout the head, with heightened expression in the midbrain-hindbrain boundary, and in the somite boundaries throughout the tail (Fig. 3.3 E). There is no clear expression of *dock6-201* in the heart at 24hpf although low levels of expression in the heart could be masked

A Zebrafish *dock6* gene annotation on ensembl



B Zebrafish *dock6-201*



C Zebrafish *dock6-202*



D Zebrafish *dock6-R11*



Figure 3.2. Zebrafish *dock6* gene structure. (A) Zebrafish *dock6* gene annotation on Ensembl (ENSDARG00000035706), showing *dock6-201* and *dock6-202* highlighted with red arrows. (B) Zebrafish *dock6-201* full length protein coding transcript which is composed of 50 exons (dark blue). (C) Zebrafish *dock6-202* retained intron transcript which is composed of 4 exons (E1-E4, dark blue) and 1 retained intron at the end of exon 4 (RI4, orange). (D) Zebrafish *dock6-RI1*, a new transcript identified in this thesis where intron 1 is retained (RI1, orange). It is currently unknown how long this transcript is, or how many exons it possesses.

by high *dock6-201* expression in the head (Fig.3.3 D). At 30hpf, *dock6-201* is still expressed in the head with heightened expression in the midbrain-hindbrain boundary and strong expression in the hindbrain (Fig.3.3 F), but from 50hpf onwards the expression in the head starts being downregulated (Fig.3.3 G) with very little expression seen at 72hpf (Fig.3.3 H).

In contrast, the zebrafish *dock6-RI1* retained intron transcript does not appear to be maternally deposited at 3hpf (Fig.3.3 I), and there is very little zygotic expression up to 24hpf (Fig.3.3 J,K). At 24hpf, *dock6-RI1* is expressed at low levels in the head (Fig.3.3 M), and slightly higher levels of expression are also observed in the heart tube myocardium (Fig.3.3 L). There are low levels of *dock6-RI1* expression in the head at 30hpf and 50hpf (Fig.3.3 N,O), but this has gone by 72hpf (Fig.3.3 P).

The specificity of both zebrafish *dock6-201* and *dock6-RI1* sense RNA expression patterns were confirmed by *in situ* hybridisation using a control sense probe, which should not bind to any RNA since no antisense RNA transcripts are annotated for *dock6*. For both genes there is no specific signal from the control sense probes (Fig.3.4 D-F,J-L) confirming that the sense RNA expression patterns for both transcripts represent true expression. The expression data for both *dock6* transcripts shows expression in distinct regions of the developing zebrafish embryo, with the protein coding transcript being expressed in regions where classical features of AOS arise, such as the top of the head and in limb extremities, whilst the retained intron transcript is expressed in the heart myocardium. This could suggest that different transcripts of the same gene regulate the development of different anatomical structures, and maybe mutations which target both transcripts could lead to more severe cases of AOS.

3. Creating zebrafish models of AOS

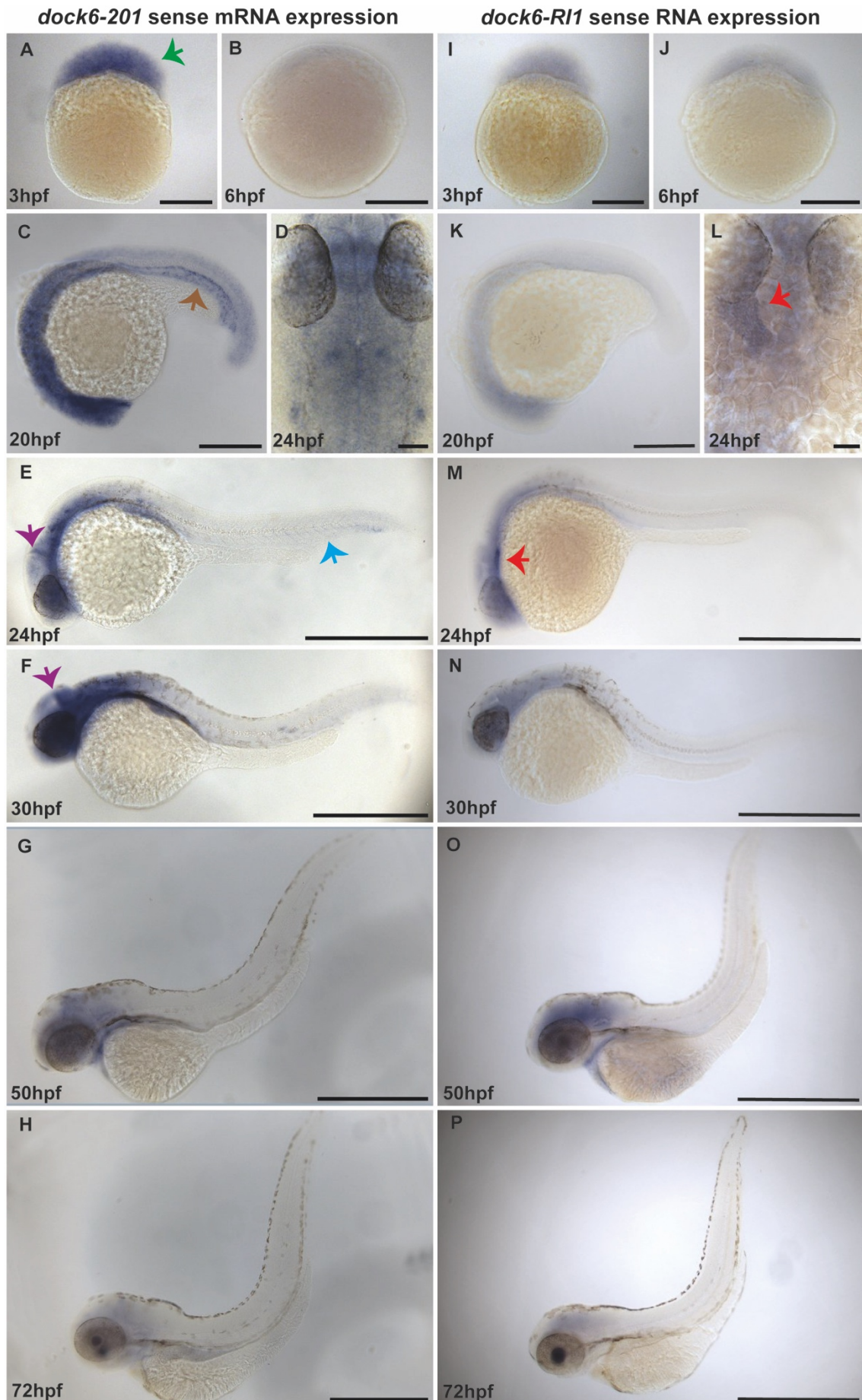


Figure 3.3. Zebrafish *dock6-201* and *dock6-R11* expression throughout zebrafish development. (A-P) *in situ* hybridisation analysis of *dock6-201* (A-H) and *dock6-R11* (I-P) expression in developing zebrafish embryos. (A) At 3hpf, *dock6-201* is expressed throughout the embryos, suggesting it is maternally deposited (green arrow). (B) At 6hpf there is little zygotic expression of *dock6-201*. (C) By 20hpf, *dock6-201* is expressed throughout the head and in the dorsal aorta and posterior cardinal vein of the tail (brown arrow), with expression becoming heightened in more distinct regions by 24hpf (E) where it can be seen in the midbrain-hindbrain boundary of the head (purple arrow) and in somite boundaries of the tail (blue arrow). (D) A dorsal view of the head at 24hpf reveals high levels of *dock6-201* expression throughout the head, with no distinct expression in the heart. (F) By 30hpf *dock6-201* expression is still strong in the head, with distinct expression in the midbrain-hindbrain boundary still visible (purple arrow). (G) At 50hpf, *dock6-201* is still expressed in the head, but from 72hpf onwards (H) there is little expression throughout the embryo. (I) *dock6-R11* appears not to be maternally deposited, with little expression visible at 3hpf. There is little zygotic expression at either 6hpf (J) or 20hpf (K), but expression is visible at 24hpf (M) in the head and heart myocardium (red arrow). (L) A dorsal view of the head at 24hpf reveals *dock6-R11* expression in the heart tube myocardium (red arrow). *dock6-R11* expression persists in the head at 30hpf (N) and 50hpf (O), with expression being reduced from 72hpf onwards (P). Scale bars: A, B, I, J: 200µm. C, K: 400µm. D, L: 50µm. E, F, G, H, M, N, O, P: 500µm.

3.4 Generating zebrafish *dock6* mutant models using CRISPR genome editing

To investigate the role that *dock6* is playing during cardiac development, and how mutations in *dock6* could be causative of CHDs in AOS patients, I created two zebrafish CRISPR *dock6* mutant models. Firstly, I aimed to create a *dock6* promoter-less mutant which prevents all transcription and translation of the *dock6* gene to understand what phenotypes a full loss of *dock6* function would result in. Secondly, I aimed to create a human disease-specific knock-in mutant model, in which a human mutation identified from an AOS patient was knocked into the zebrafish genome, to allow me to understand what the impact of this patient mutation is upon *dock6* function.

3. Creating zebrafish models of AOS

To create a LOF model, my original strategy was to create a promoter-less *dock6* mutant by deleting a region comprising the annotated promoter and translational start site, with the aim of preventing transcription and/or translation of the *dock6* gene. By deleting the promoter and preventing any transcription of this gene, this should avoid any confounding issues of genetic compensation via nonsense mediated decay of mutant mRNA transcripts (El-Brolosy et al., 2019). Additionally, I aimed to create an AOS disease-specific knock-in zebrafish mutant model, whereby I identified *dock6* variants in human AOS patients that were in conserved residues in zebrafish and were also causative of CHDs, and then introduced these variants into zebrafish genome. These models would allow me to understand how the mutated *dock6* gene found in human AOS patients was causing CHDs to arise and through comparison of the two models allows me to understand the pathology of the disease variant and whether it is causing loss of *dock6* function.

During the characterisation of *dock6* gene expression, I concluded that it may also be important to interrogate a potential functional role for the *dock6-R11* retained intron transcript, since this transcript is expressed in the myocardium at a key stage of zebrafish heart development. This would allow me to investigate the role of this transcript in more detail, and to see if it could be implicated in the onset of CHDs in AOS patients. Additionally, as the promoter-less mutant CRISPR strategy involved targeting the first intron of the *dock6* transcript (see details below), this meant it may be possible to recover a retained intron mutant founder where the first intron alone had been mutated without disrupting exon 1 of the coding sequence.

3.5 *dock6-201* promoter-less mutant CRISPR/Cas9-mediated genome editing strategy

To create *dock6-201* promoter-less mutants, the strategy encompassed using CRISPR/Cas9 genome editing technology to target the putative promoter region of the *dock6* gene annotated on the eukaryotic promoter database (<https://epd.epfl.ch//index.php>) thereby preventing RNA transcription and resulting in a full *dock6* LOF mutant. I designed guide RNAs (gRNAs) using CHOPCHOP (<https://chopchop.cbu.uib.no/>) (Labun et al., 2019) which target upstream of the annotated promoter region and downstream of the translational start site, with the aim of combining these gRNAs to fully excise this genomic region.

3. Creating zebrafish models of AOS

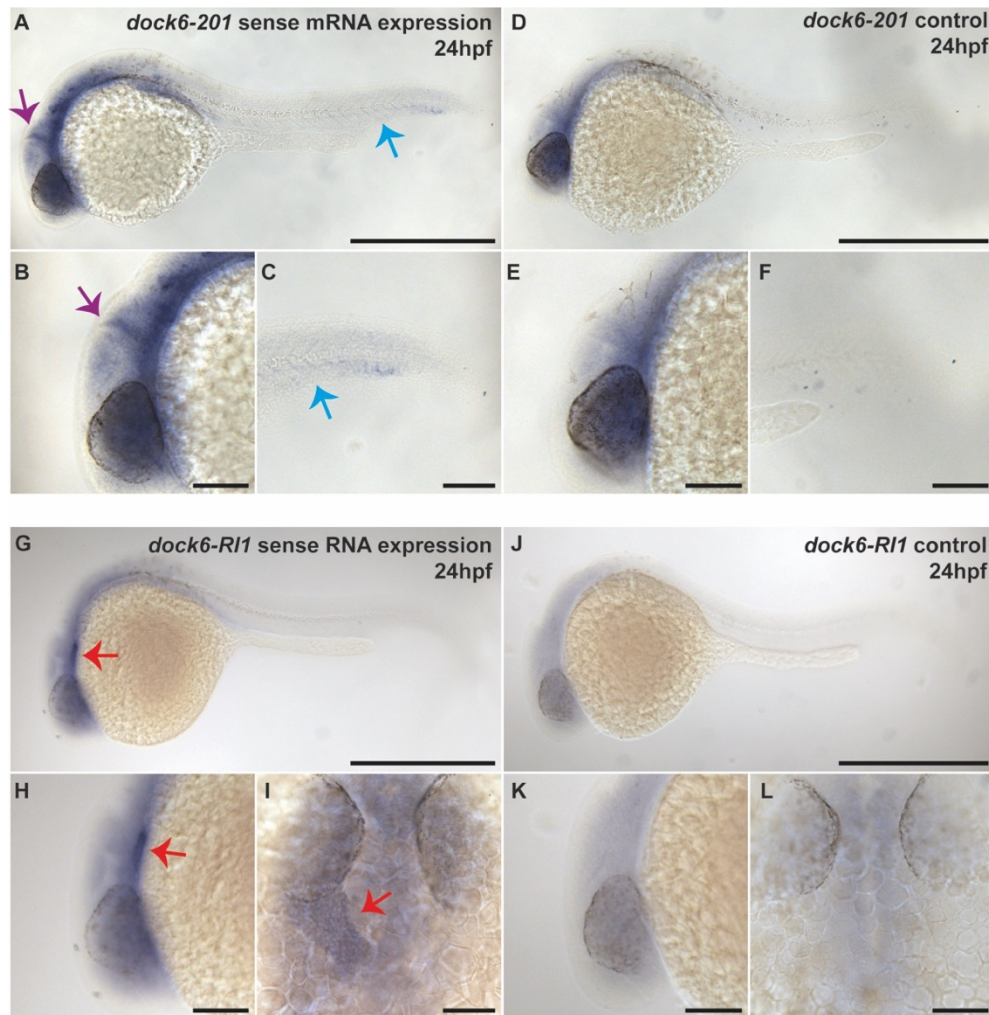


Figure 3.4. Zebrafish *dock6-201* and *dock6-R11* sense RNA expression and controls at 24hpf. A-L: *in situ* hybridisation analysis using antisense *dock6* probes (A-C, G-I) and control sense probes (D-F, J-L) (A) Zebrafish *dock6-201* sense mRNA expression at 24hpf with purple arrows highlighting specific expression in the midbrain-hindbrain boundary (B) and blue arrows highlighting expression in the somite boundaries of the tail (C). (D) Zebrafish *dock6-201* antisense RNA expression control probe at 24hpf highlighting a lack of specific expression in either the head (E) or tail region (F) therefore confirming *dock6-201* sense mRNA expression to be real. (G) Zebrafish *dock6-R11* sense RNA expression at 24hpf with a red arrow highlighting specific expression in the heart myocardium both laterally (H) and dorsally (I). (J) Zebrafish *dock6-R11* antisense RNA expression control probe at 24hpf showing a lack of any specific expression in the heart both laterally (K) and dorsally (L), therefore confirming the specific expression of *dock6-R11* sense RNA in the heart myocardium.

Scale bars: A, D, G, J: 500 μ m. B, C, E, F, H, I, K, L: 100 μ m.

3. Creating zebrafish models of AOS

I initially designed 2 gRNAs flanking the promoter and ATG, which are both located in exon 1 (Fig.3.5 A). Despite confirming that both gRNAs resulted in efficient cutting at the target site by Cas9 when injected into embryos individually, these gRNAs in combination did not result in efficient excision of the larger genomic region, with the gRNA downstream of exon 1 cutting much more efficiently. I therefore decided to inject this single gRNA alone and raise F0 founders to adulthood, with the goal of creating a large enough mutation to disrupt the translational start site located 98bp upstream and possibly the promoter region too. Unfortunately, I did not recover an F0 founder with germline transmission of a mutation big enough to disrupt this region, despite screening 30 F0 founders. I therefore aimed to instead identify a *dock6-201* truncation mutant founder from the AOS disease-specific knock-in mutant CRISPR strategy instead (see below), as this could still represent a *dock6-201* LOF mutant in which to perform further analyses.

Despite being unable to recover a *dock6-201* promoter-less mutant, I did identify several F0 founders with germline transmission of mutations in retained intron 1 of the *dock6-RI1* transcript. Interestingly, some of these F0 mutant founders displayed behavioural phenotypes such as exhaustion when netted, suggesting that a mutation in the retained intron transcript could impact cardiac function. Combined with my previous discovery that this retained-intron transcript is expressed in the zebrafish heart at a key stage of cardiac development (Fig.3.3 L&M), I decided to establish stable lines for two intronic mutations to investigate the role of this retained intron transcript in more detail. Of these two lines, one harbours a 41bp insertion in retained intron 1 of *dock6-RI1* (Fig.3.5 B) and the other contains a 28bp deletion, also in retained intron 1 (Fig.3.5 C). These founders were outcrossed to the *Tg(myl7:LifeACTGFP);Tg(flia:AC-TagRFP)* transgenic line (Derrick et al., 2019) in order to assess cardiac and vasculature morphogenesis in embryos with mutations in a retained intron of *dock6-RI1* (See Chapter 4).

3.6 *dock6-201* AOS disease-specific knock-in mutant CRISPR/Cas12a-mediated genome editing strategy

To create an AOS disease-specific knock-in mutant model for *dock6*, I wanted to identify a *DOCK6* mutation from an AOS patient in the literature which: 1) was associated with the most severe CHD; 2) affected an amino acid residue which was

3. Creating zebrafish models of AOS

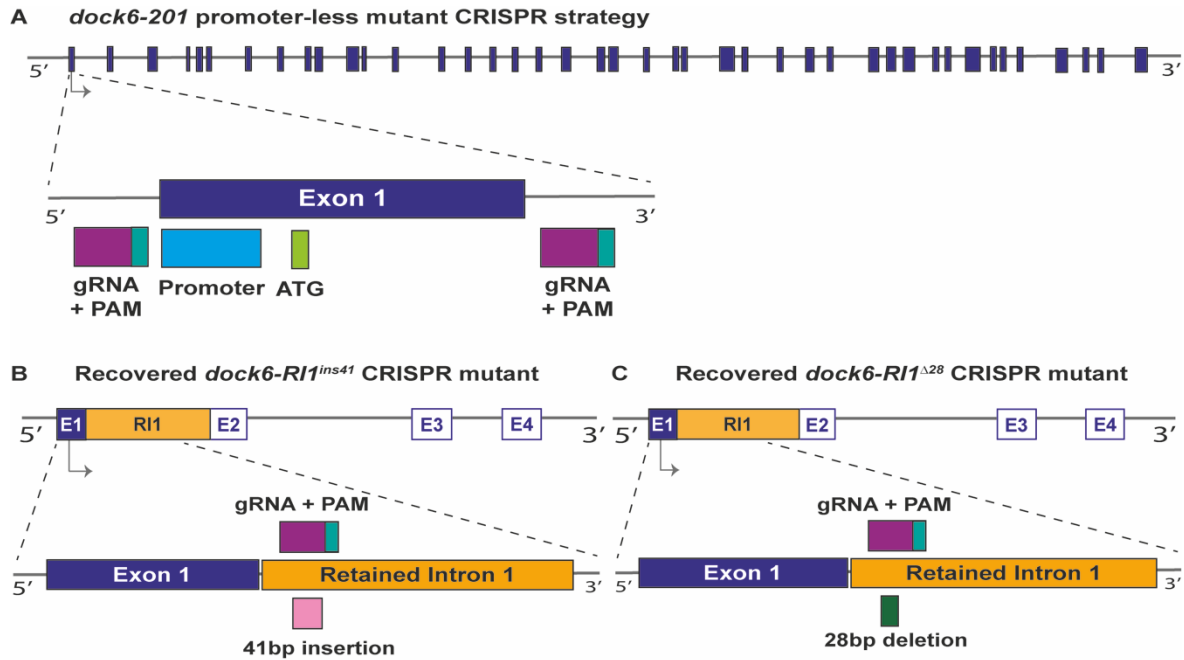


Figure 3.5. Zebrafish *dock6-201* LOF CRISPR/Cas9 gene editing strategy and the recovered *dock6-RI1* retained intron mutants. (A) Schematic showing the zebrafish *dock6-201* full length protein coding transcript with 50 exons annotated (dark blue). The highlighted region shows exon 1 (dark blue) with the annotated promoter region (light blue) and ATG translation start site (light green), along with 2 gRNAs flanking this region (purple, with the PAM in turquoise) designed to disrupt the promoter and ATG to create a *dock6-201* LOF mutant. (B) A schematic of the zebrafish *dock6-RI1* retained intron transcript with 4 exons (dark blue, E1-E4) and 1 retained intron (orange, RI1). The highlighted region depicts the *dock6-RI1^{ins41}* retained intron founder mutation, showing the 41bp insertion mutation (light pink) at the start of retained intron 1 (orange), overlapping with the target site of the downstream gRNA (purple, with the PAM in turquoise). (C) A schematic of the zebrafish *dock6-RI1* retained intron transcript with 4 exons (dark blue, E1-E4) and 1 retained introns (orange, RI1). The highlighted region depicts the *dock6-RI1^{Δ28}* retained intron founder mutation, showing the 28bp deletion mutation (dark green) at the start of retained intron 1 (orange), overlapping with target site of the downstream gRNA (purple, with the PAM in turquoise).

conserved between humans and zebrafish (Figure 3.6 A). CHDs are found in 31% of AOS patients with mutations in *DOCK6* (Hassed et al., 2017) and so it was important that the knock-in mutation I chose was also causative of CHDs in AOS patients. To

3. Creating zebrafish models of AOS

date there are 26 known mutations in *DOCK6* which have been linked to AOS, 9 of which are thought to be causative of CHDs. Interestingly, 5 of these mutations have also been identified in splice sites, suggesting that mis-splicing and potentially intron retention could be involved in the pathology of AOS (Fig.3.6 B).

The point mutation I chose to knock into the zebrafish genome to create a *DOCK6* AOS disease-specific mutant model is a G>T nonsense mutation in exon 29 of human *DOCK6* that leads to a premature termination codon before the GEF domain of *DOCK6*, which is required for its RAC1 activating function (Fig.3.6 B, black arrow). Patients with this mutation suffered from Tetralogy of Fallot and Persistent Left Superior Vena Cava (Lehman et al., 2014). To create knock-in mutations I utilised a different Cas enzyme called Cas12a, which had recently been identified as being a more efficient enzyme than Cas9 to facilitate knock-in mutations via homology-directed repair (HDR) in zebrafish (Bin Moon et al., 2018). This is thought to be due to differences in the location where the enzyme cuts the DNA: Cas9 cuts 3 nucleotides upstream of the PAM likely introducing indels into the gRNA target sequence which prevents re-cutting, while Cas12a cuts 18 nucleotides downstream of the PAM and does not produce indels in the crRNA target sequence, allowing re-cutting which likely increases the chance of HDR and knock-in of the desired mutation (Moreno-Mateos et al., 2017).

To create the knock-in mutant lines, I used the deep CRISPR design tool (<http://deepcrispr.info/>) (Kim et al., 2018) to design a CRISPR RNA (crRNA) which was targeted as close as possible to the site where I wanted to introduce the mutation. Once I had confirmed that the closest possible crRNA was targeting Cas12a to cut the DNA efficiently, I designed a single stranded oligonucleotide that contained the point mutation I wanted to introduce into *dock6*, along with homologous regions of DNA to be used as a template for HDR, thereby incorporating the point mutation into the genome (Fernandez et al., 2018). In the single stranded oligonucleotide, I also introduced a restriction site using silent mutations to facilitate identification of whether the oligo had been incorporated, along with silent mutations along the crRNA binding site and PAM to prevent re-cutting of the crRNA once the oligo had successfully been integrated (Fig.3.7 A).

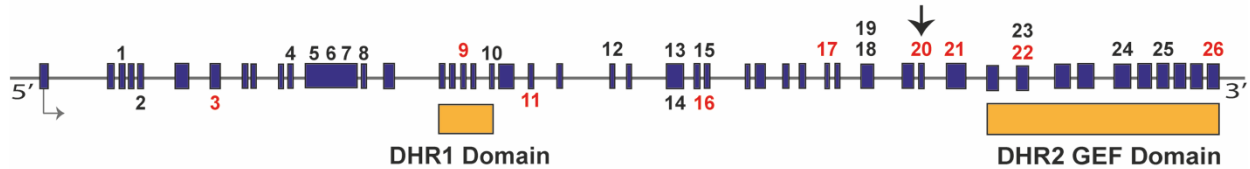
3. Creating zebrafish models of AOS

A Human *DOCK6-201* and zebrafish *dock6-201* sequence alignment

	NW Score	Identities	Gaps	Strand
	2579	4387/6407(68%)	325/6407(5%)	Plus/Plus
Human <i>DOCK6-201</i> → Query	4250	TGAAGGTTGTGCTGTACAGCCTGGGCAGTGCCAGAGTGCCTCTTCTTGCAGCATGGCC		4309
Zebrafish <i>dock6-201</i> → Sbjct	4439	TGAGGGTCCCTCCTCACAGTATGGCAGGAAACCAGAGCGCCTCTTCTTGCAGCACTGCT		4498
Query	4310	TGGCCACCCAGAGGGCCCTTGTGTCCAAGTTCCCGGAGCTGCTGTTTCGAGGAGGACACGG		4369
Sbjct	4499	TCAGTACACAGAGAGCTTTAGTCTACAAGTTTCCAGAGATGTTGTTTGAAGAGGACACTG		4558
Query	4370	AGCTGTGTGCCGACCTGTGCCTGAGGCTCCTACGACACTGTGGCAGCCGCATCAGCACCA		4429
Sbjct	4559	AGCTCTGTGCAGATCTGTGTTTGCGGTTACTGCGTCACTGCAGCAGCAGCGTGTAGCTCTG		4618
Query	4430	TCCGCACGCACGCCAGCGCCTCGCTGTACCTGCTCATGCCAGACAACCTTCGAGATCGGCC		4489
Sbjct	4619	TCCGCAGCCATGCCAGCGCCTCGCTCTACCTTCTCATGAGACAGAACCTTCGAGATCGGAA		4678

↑
Conserved G residue
where knock-in mutation
was to be created

B Human *DOCK6-201* reported mutations



Number	Exon	Mutation	Zygoty	Nature of Mutation	Causative of CHD	Reference
1	Exon 3	Arg63Gln	Compound heterozygous with no.25	Missense	None reported	Zhang et al., 2019
2	Exon 5	p.Glu162*	Homozygous	Nonsense	None reported	Sukalo et al., 2015
3	Exon 7	p.Val263Asp	Compound heterozygous with no.26	Missense	Yes – VSD ⁵	Sukalo et al., 2015
4	Exon 11	p.Asp416*	Homozygous	Nonsense	None reported	Shaheen et al., 2011
5	Exon 12	p.Arg429Glnfs*32	Homozygous	Frameshift	None reported	Alzahem et al., 2020
6	Exon 12	p.Gln434Argfs*21	Homozygous	Frameshift	None reported	Sukalo et al., 2015
7	Exon 12	p.Thr455Sfs*24	Homozygous	Frameshift	None reported	Shaheen et al., 2011
8	Exon 13	p.Arg466*	Compound heterozygous with no.23	Nonsense	None reported	Jin et al., 2022
9	Exon 17	p.Phe635Profs*32	Compound heterozygous with no.17	Frameshift	Yes – TAPVD ¹	Sukalo et al., 2015
10	Exon 19	p.Gly702Ser	Homozygous	Missense	None reported	Meester et al., 2018

3. Creating zebrafish models of AOS

11	Exon 21	p.Arg841Serfs* 6	Homozygous	Frameshift	Yes – Aortic Valve Dysplasia	Sukalo et al., 2015
12	Exon 23	p.Val923Ile	Homozygous	Missense	None reported	Meester et al., 2018
13	Exon 25	p.Leu1016Pro	Homozygous	Missense	None reported	Sukalo et al., 2015
14	Exon 25	p.Tyr1021*	Compound heterozygous with no.18	Nonsense	None reported	Wang et al., 2019
15	Exon 26	p.Glu1052Lys	Homozygous	Missense	None reported	Sukalo et al., 2015
16	Exon 26	p.Leu1064Valfs *60	Homozygous	Frameshift	Yes – TOF ² , PLSVC ³	Sukalo et al., 2019
17	Exon 32	c.4106+5G>T	Compound heterozygous with no.9	Splicing	Yes – TAPVD ¹	Sukalo et al., 2015
18	Exon 32	c.4106+2T > C	Compound heterozygous with no.14	Splicing	None reported	Wang et al., 2019
19	Exon 33	c.4107-1G>C	Homozygous	Splicing	None reported	Shaheen et al., 2013
20	Exon 35	p.Glu1494*	Homozygous	Nonsense	Yes – TOF ² , PLSCV ³	Lehman et al., 2014
21	Exon 36	c.4491+1G>A	Compound heterozygous with c.5939+2T>C	Splicing	Yes - Valvulopat hy	Sukalo et al., 2019
22	Exon 38	p.Arg1596Trp	Homozygous	Missense	Yes – PDA ⁴	Sukalo et al., 2015
23	Exon 38	p.Trp1599*	Compound heterozygous with no.8	Nonsense	None reported	Jin et al., 2022
24	Exon 41	c.5235+205_61 02-15delins10	Homozygous	4.3kb deletion	None reported	Sukalo et al., 2015
25	Exon 43	p.Glu1792Lys	Compound heterozygous with no.1	Missense	None reported	Zhang et al., 2019
26	Exon 46	c.5939+2T>C	Compound Heterozygous with no.3 and no.21	Splicing	Yes – VSD ⁵	Sukalo et al., 2015

TAPVD¹ = Total Anomalous Pulmonary Venous Connection

TOF² = Tetralogy of Fallot

PLSV³ = Persistent Left Superior Vena Cava

PDA⁴ = Patent Ductus Arteriosus

VSD⁵ = Ventricular Septal Defect

AVD⁶ = Aortic Valve Dysplasia

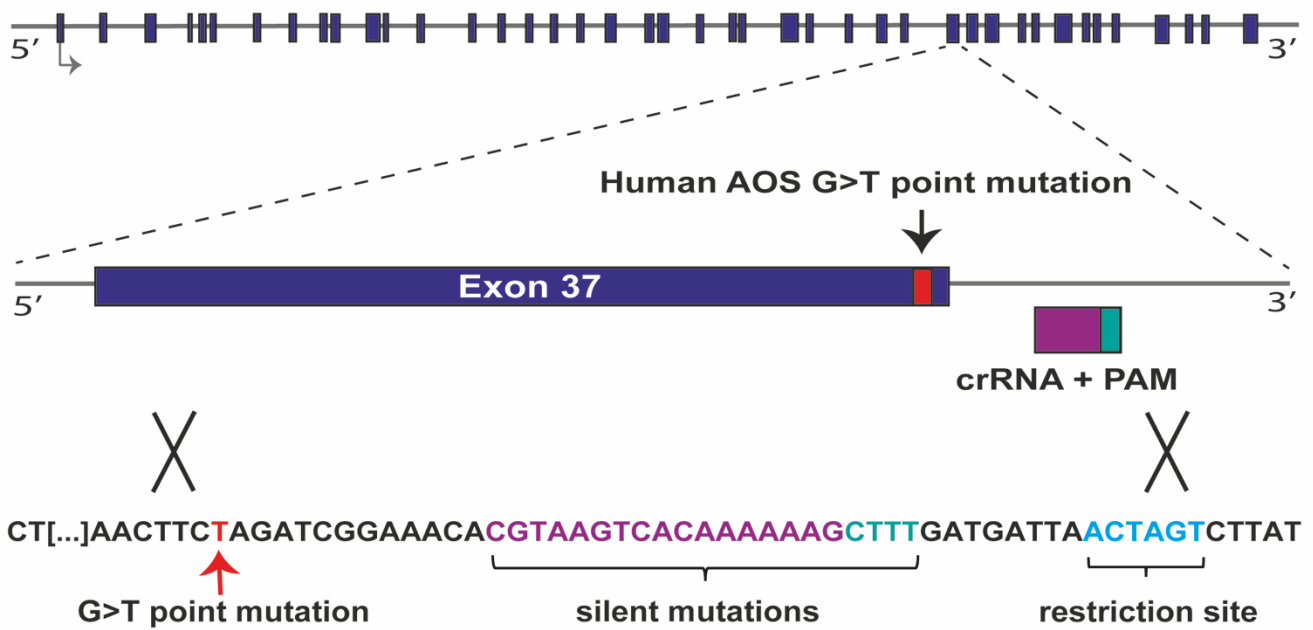
3. Creating zebrafish models of AOS

Figure 3.6. Location of AOS *DOCK6* mutations. (A) Alignment of the human and zebrafish *DOCK6-201* coding sequences on blast, showing 68% shared identity and the conserved G residue where the G>T knock-in mutation was to be created. (B) The human *DOCK6-201* gene with 48 exons (dark blue), and the DHR1 membrane localisation domain and DHR2 GEF domain annotated (orange). Numbers indicate the position of AOS mutations throughout the *DOCK6* gene and correspond to a mutation detailed in the table below. Numbers highlighted in red indicate mutations found in patients who also suffer from CHDs. The human mutation selected to knock-in to the zebrafish genome is shown by the black arrow. The table highlights all identified human *DOCK6* mutations found in AOS patients to date, indicating where in the *DOCK6* gene the mutation was found, the nature of the mutation and whether it is causative of CHDs.

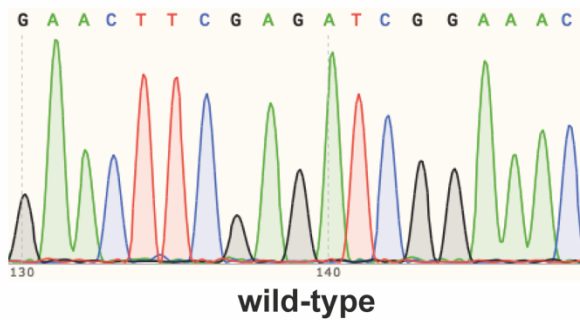
I first tested whether the knock-in strategy was working by injecting wild-type embryos with the crRNA, Cas12a enzyme and single stranded oligonucleotide, and genotyped these embryos for precise editing of the desired mutation. Following restriction digest and sequencing analysis, I confirmed the incorporation of the *dock6-201* G>T mutation into F0 injected embryos (Fig.3.7 C). Injected embryos were then raised to adulthood and outcrossed to wild-types to identify F0 founders transmitting the knock-in mutation through the germline. Despite screening 100 F0 founders I could not identify one with germline transmission of the knock-in mutation. Instead, I attempted to recover a *dock6-201* coding sequence mutant where the crRNA was targeting Cas12a to cut the genome, but the oligonucleotide hadn't been successfully incorporated. I hoped to recover a founder which had a coding sequence mutation which caused a frameshift to ensure I had a *dock6-201* mutant model to analyse. Out of the 100 F0 founders screened, I could identify only one which had a mutation disrupting an exon, which was a 36bp insertion and 65bp deletion at the end of exon 37 in *dock6-201*, close to where I had intended to create the knock-in mutation (Fig.3.7 D). Despite this mutation affecting splice donor sites, it did not seem to effect splicing, which was confirmed by designing primers which flanked exon intron boundaries. There is the possibility however of this mutation resulting in a cryptic splice site, which was not investigated in this study. This mutation substitutes 12 amino acids and deletes a further 18 amino acids encoded by the end of exon 37 in the *DOCK6* protein but does not cause a

3. Creating zebrafish models of AOS

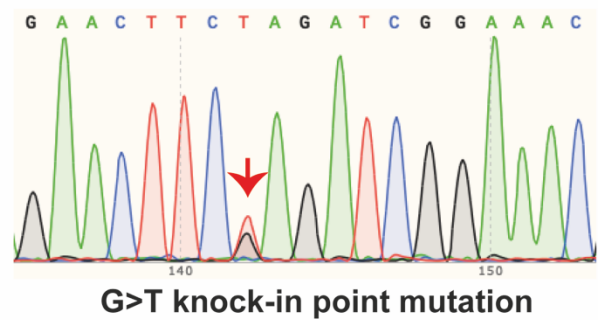
A *dock6-201* AOS disease specific knock-in CRISPR strategy



B Wild-type chromatogram



C Knock-in chromatogram



D Recovered *dock6-201*^{ins36Δ65} CRISPR mutant

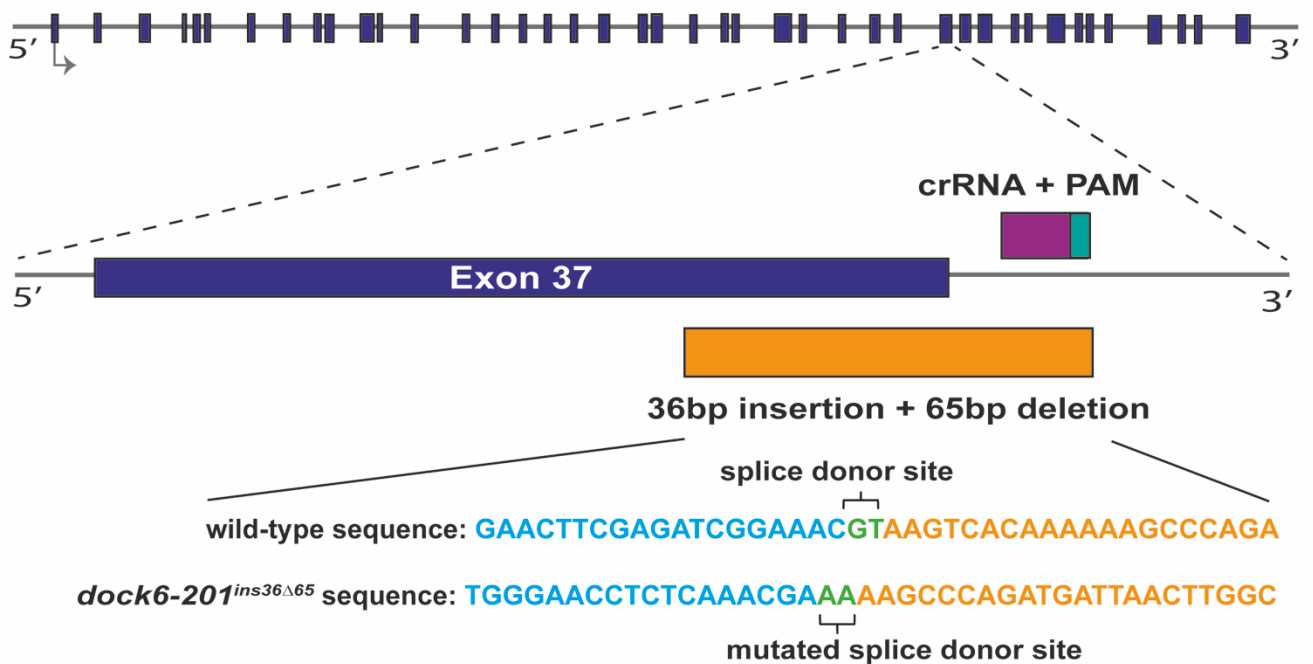


Figure 3.7. Zebrafish *dock6-201* AOS disease-specific knock-in CRISPR/Cas12a gene editing strategy and the recovered *dock6-201* coding sequence mutant. (A) Schematic showing the zebrafish *dock6-201* full length protein coding transcript with 50 exons annotated (dark blue). The highlighted region shows exon 37 (dark blue) with a conserved zebrafish residue which is mutated in AOS patients (G>T) (red) and a single crRNA (purple, with PAM in turquoise) designed to bind as close as possible to where the point mutation is going to be introduced. The sequence below shows a single-stranded oligonucleotide sequence used as a template to introduce the point mutation (red text) into the genome, flanked by homology regions to facilitate homology directed repair (black text). Silent mutations were introduced into the single stranded oligonucleotide where the crRNA binds (purple text) and PAM site (turquoise text), to prevent this region from being re-cut following incorporation. A restriction site (blue text) was also introduced using silent mutations to facilitate genotyping for successful incorporation of the oligo sequence into the genome. (B) Chromatogram of the wild-type zebrafish *dock6-201* gene sequence without the G>T point mutation incorporated. (C) Chromatogram of the same *dock6-201* gene sequence in an embryo where this G>T point mutation has been incorporated into the genome (red arrow highlights mixed G and T peak). (D) Schematic showing a *dock6-201* coding sequence mutant founder recovered from the knock-in strategy where the crRNA (purple, with the PAM in turquoise) has cut the gene but the single stranded oligo was not incorporated into the genome. This founder had germline transmission of a 36bp insertion and 65bp deletion (orange) at the end of exon 37 (dark blue) of the *dock6-201* gene. Despite this mutation affecting splice donor sites (green text), it did not seem to effect splicing.

frameshift. I outcrossed this F0 founder to the *Tg(myl7:LifeActGFP);Tg(fli1a:AC-TagRFP)* transgenic line, generating a stable line in which to assess cardiac and vascular morphology in homozygous mutants. Despite the difficulties faced in attempting to generate zebrafish *dock6* mutant CRISPR models, I managed to recover three novel models to carry out phenotypic analysis: *dock6-RI1^{ins41}* and *dock6-RI1^{Δ28}* retained intron mutant models, and the *dock6-201^{ins36Δ65}* coding sequence mutant model.

3.7 Humans and zebrafish share conserved *EOGT* transcripts

3. Creating zebrafish models of AOS

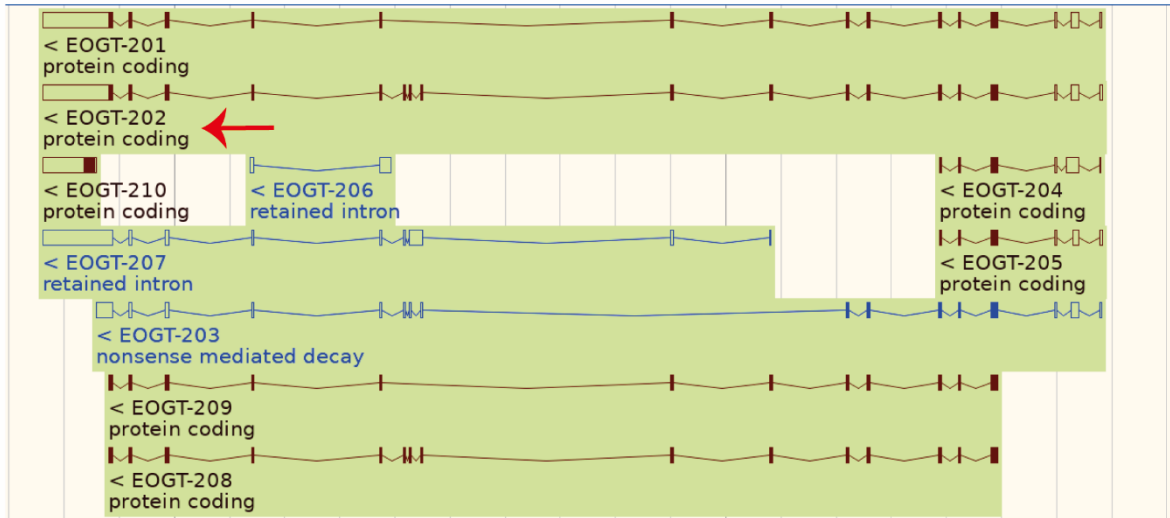
Similar to the approach taken with *DOCK6*, to compare human *EOGT* and zebrafish *eogt* gene structures, both sequences were identified in Ensembl. The human *EOGT* gene (GRCh38.p13, ENSG00000163378) has 10 transcripts annotated on Ensembl, 7 protein-coding transcripts, 1 nonsense-mediated decay transcript and 2 retained-intron transcripts (Fig.3.8 A), with several transcripts being alternatively spliced. The human *EOGT-202* transcript is the longest protein coding transcript for *EOGT* in humans and is composed of 18 exons and encodes 527 amino acids (Fig.3.8 C). There is also evidence of a human *EOGT* antisense RNA transcript named *CU687497* annotated on the UCSC genome browser from the hORFeome v1.1 collection (Rual et al., 2004) (Fig.3.8 B) which overlaps with the *EOGT-202* sense mRNA transcript from the 3' end of the gene and spans 7 exons, but skips exons 11-13 (Fig.3.8 D). The zebrafish *eogt* gene (GRCz11, ENSDARG0000022853) has only one transcript annotated on Ensembl (Fig.3.9 A), *eogt-201*, which is composed of 16 exons and encodes 519 amino acids (Fig.3.9 B). According to BLAST and UniProt, human *EOGT-202* and zebrafish *eogt-201* coding sequences share the highest level of similarity, with the coding sequences and proteins sharing 66% identity, suggesting a conserved function for *EOGT* in zebrafish which makes it a suitable model to study the roles of this gene in cardiac development.

3.8 Identification of a zebrafish *eogt* antisense transcript expressed in the heart during cardiac development

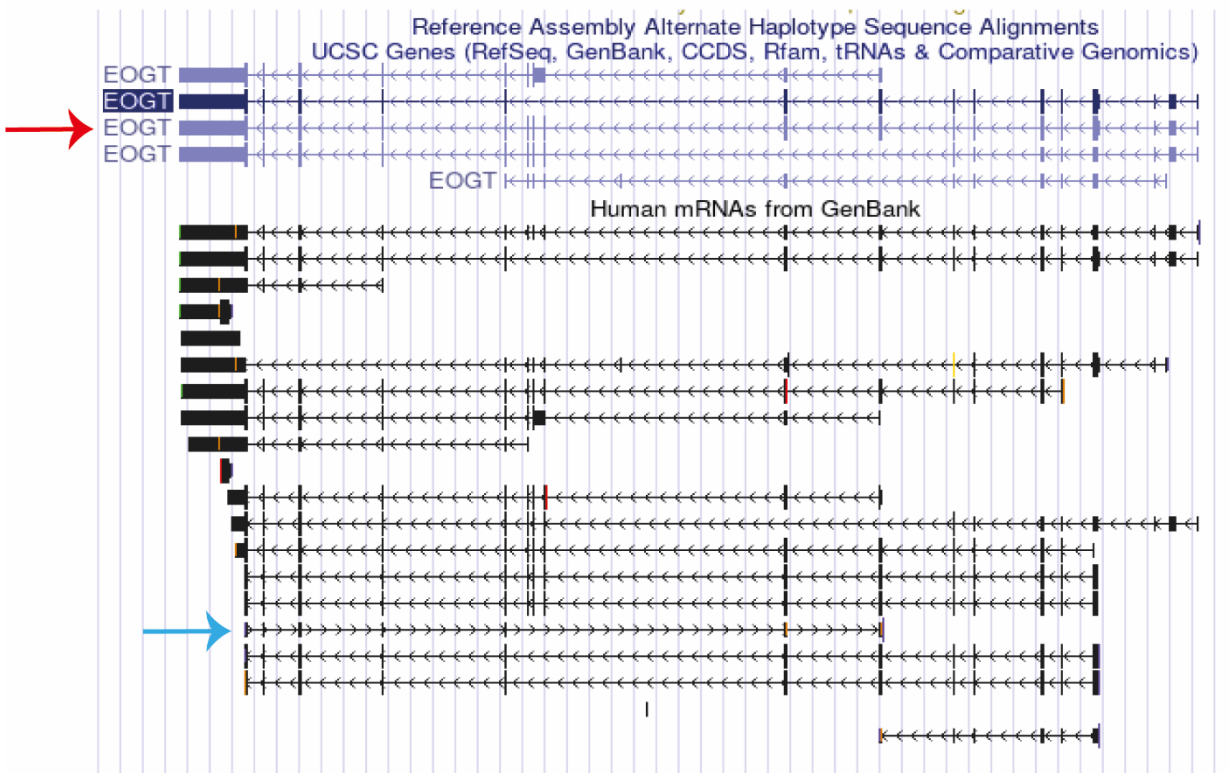
To investigate whether *eogt* is expressed in the zebrafish heart during cardiac development, I used *in situ* hybridisation to analyse *eogt* expression patterns throughout development. *eogt* mRNA is not maternally deposited (Fig.3.10 A), with expression first detected at 20hpf in the early zebrafish vasculature, in the DA, PCV and intersegmental vessels (ISVs) (Fig.3.10 C). By 24hpf *eogt* expression can still be seen in the DA and ISVs of the tail, along with expression in the mid cerebral vein (MCeV) which runs along the midbrain-hindbrain boundary in the head (Isogai et al., 2001) (Fig.3.10 E). *eogt* sense mRNA is downregulated in the vasculature from 30hpf onwards (Fig.3.10 F-H).

To confirm the *eogt* sense RNA expression pattern, I designed an *eogt* control sense probe, which should not bind to any RNA or produce any signal as there are no annotated zebrafish *eogt* antisense transcripts. Unexpectedly, I found from 20hpf *eogt*

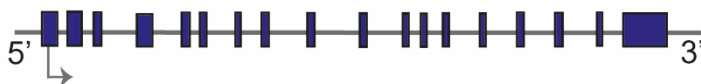
A Human *EOGT* gene annotation on ensembl



B Human *EOGT* gene annotation on UCSC genome browser



C Human *EOGT-202*



D Human *EOGT* antisense transcript (CU687497)

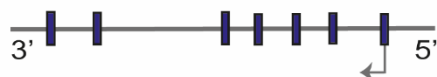


Figure 3.8. Human *EOGT* gene structure. (A) Human *EOGT* gene annotation on Ensembl (ENSG00000163378), showing multiple human *EOGT* transcripts, with *EOGT-202* highlighted with a red arrow. (B) Human *EOGT* gene annotation on the UCSC genome browser, showing multiple *EOGT* RNA transcripts, with *EOGT-202* highlighted with a red arrow. An annotated antisense transcript designated as *CU687497* runs in the opposite direction to the *EOGT-202* gene, spanning 7 exons from the 3' end of *EOGT-202* but skipping exons 11-13 (blue arrow). (C) Human *EOGT-202* full length protein coding transcript which is composed of 18 exons (dark blue). (D) Human *EOGT* antisense transcript *CU687497* which is composed of 7 exons (dark blue) overlapping with the 3' end of the *EOGT-202* protein coding transcript, skipping exons 11-13.

antisense RNA is expressed specifically in the heart disc (Fig.3.1 K) and at 24hpf, when the heart has formed a linear tube, *eogt* antisense RNA appears to be expressed in the myocardium (Fig.3.10 L,M). By 30hpf, expression of both sense and antisense RNA is reduced (Fig.3.10 F,N), with very little expression observed from 50hpf onwards (Fig.3.10 G,H,O,P). Although not annotated on any databases, this suggests that, similarly to humans, there is an *eogt* antisense transcript in zebrafish which overlaps with the protein-coding transcript.

Zebrafish *eogt* is expressed at similar stages of development to *dock6* (as described above), which is noteworthy as they are both implicated in AOS but are otherwise unrelated genes involved in the regulation of distinct signalling pathways. Additionally, both *dock6* and *eogt* are expressed in regions where the classical AOS features arise (ACC, TTLD), such as at the top of the head and in limb extremities. This provides further support for the use of zebrafish as a model to understand AOS, as expression of genes known to be mutated in human AOS are expressed in regions of the zebrafish embryo where defects commonly arise in humans. Furthermore, for both *dock6* and *eogt*, I have identified an alternative transcript which is expressed in the heart tube myocardium at 24hpf, a key stage of early zebrafish heart development when morphogenesis of the heart tube begins. This suggests that alternative non-coding transcripts for both genes could be involved in AOS pathogenesis and could be implicated in the onset of CHDs in AOS patients.

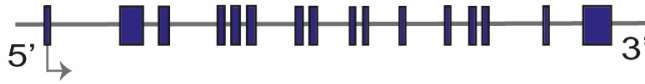
A Zebrafish *eogt* gene annotation on ensembl**B Zebrafish *eogt-201***

Figure 3.9. Zebrafish *eogt* gene structure. (A) Zebrafish *eogt* gene annotation on Ensembl (ENSDARG00000022853), showing only the single transcript *eogt-201* annotated. (B) Zebrafish *eogt-201* full length protein coding transcript which is composed of 16 exons (dark blue).

3.9 Generating zebrafish *eogt* mutant models using CRISPR genome editing

Similar to the *dock6* strategy described above, my original strategy for creating zebrafish *eogt* mutant models was to target the annotated promoter region and translational start site of the zebrafish *eogt* gene, with the aim of preventing transcription and/or translation to create a full *eogt* LOF mutant. This strategy was planned alongside the creation of an *eogt* AOS disease-specific knock-in mutant which would allow me to understand how specific mutations in *EOGT* leads to dysregulation of NOTCH signalling and causing CHDs in AOS patients.

For the *eogt* promoter-targeted mutant model, despite identifying gRNAs which targeted Cas9 to cut the target sites efficiently, I failed to recover a founder transmitting a mutation through the germline which was disrupting either the annotated promoter region or translational start site. Therefore, I instead attempted to recover an *eogt* coding sequence mutant from the disease-specific knock-in strategy, like the approach adopted to recover the *dock6-201* coding sequence mutant model described above.

3. Creating zebrafish models of AOS

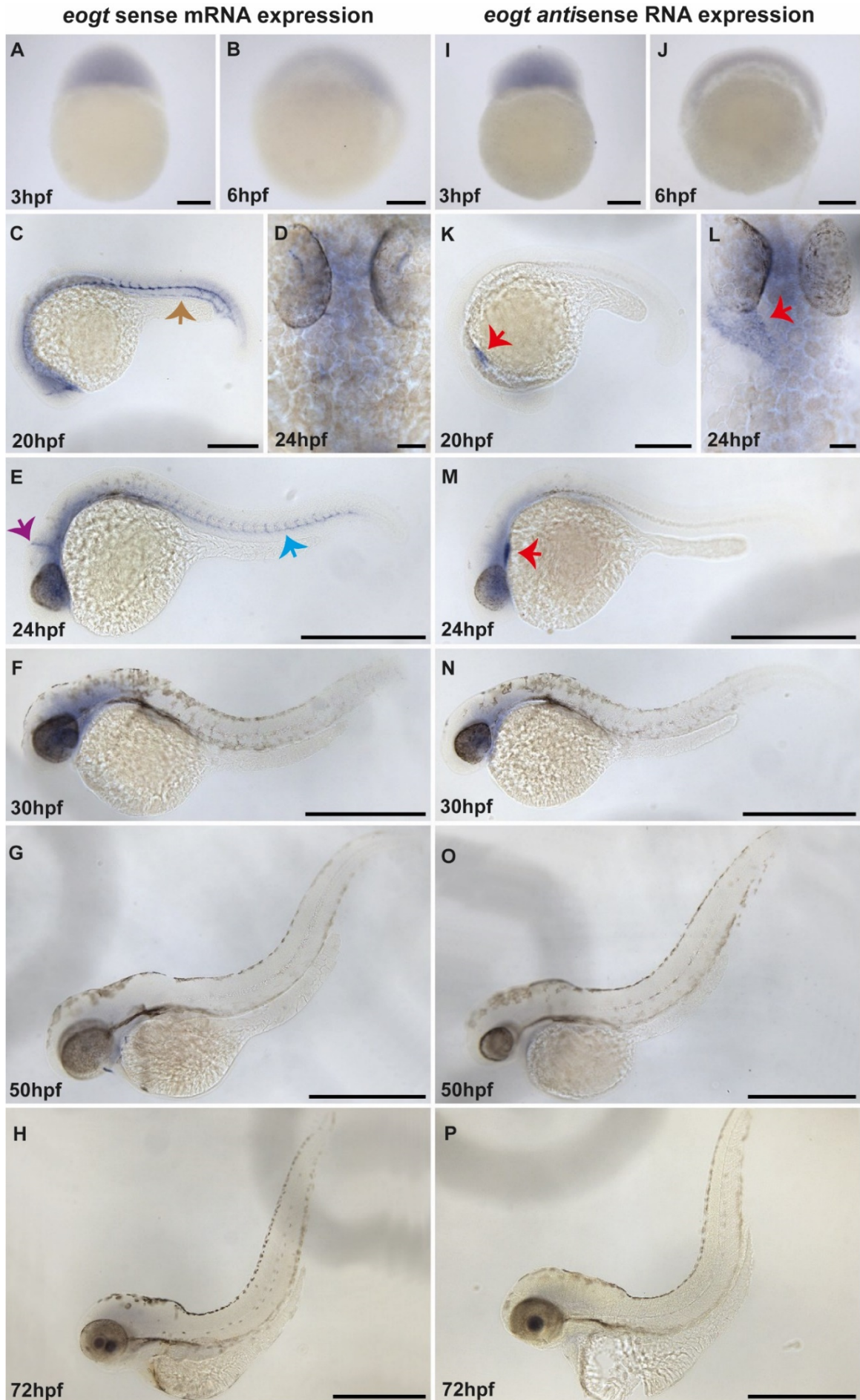


Figure 3.10. Zebrafish *eogt* sense and antisense RNA expression patterns throughout development. (A) *In situ* hybridisation analysis of *eogt* sense mRNA expression at 3hpf, showing *eogt-201* sense mRNA is not maternally deposited, or expressed zygotically at 6hpf (B). (C) By 20hpf, *eogt-201* sense mRNA is expressed throughout the zebrafish head and in the dorsal aorta and posterior cardinal vein in the tail (brown arrow), and at 24hpf (E) expression is observed in specific structures such as the mid-cerebral vein of the head (purple arrow) and in the dorsal aorta and developing intersegmental vessels of the tail (blue arrow). (D) A dorsal view of the head at 24hpf reveals little specific *eogt-201* sense mRNA expression in the head, with no distinct expression in the heart. (F) By 30hpf *eogt-201* sense mRNA expression is reduced, with expression throughout the vasculature no longer visible. From 50hpf onwards (G, H) there is no distinct *eogt-201* sense mRNA expression in the developing embryo. (I) *eogt* antisense RNA is not maternally deposited at 3hpf, and there is no zygotic expression at 6hpf (J). (K) By 20hpf there is very specific expression of *eogt* antisense RNA in the heart tube myocardium, which can also be seen clearly at 24hpf both laterally (M) and dorsally (L) (red arrows). (N) At 30hpf, *eogt* antisense RNA expression is reduced and can no longer be seen in the heart myocardium. At 50hpf (O) to 72hpf (P) there is no specific expression of *eogt* antisense RNA. Scale bars: A, B, I, J: 200µm. C, K: 400µm. D, L: 50µm. E, F, G, H, M, N, O, P: 500µm.

3.10 *eogt-201* AOS disease-specific knock-in mutant CRISPR/Cas12a-mediated genome editing strategy

I identified AOS patients from the literature with mutations in *EOGT* and selected a mutation in a residue conserved in zebrafish (Fig.3.11 A), and which was also causative of CHDs. To date there are 9 known *EOGT* mutations which have been identified in human AOS patients (Fig.3.11 B) and as only 16% of AOS patients with *EOGT* mutations suffer from CHDs (Hassed et al., 2017), it was important that I chose a mutation from a patient who also suffered from CHDs. The *EOGT* mutation chosen to be knocked-in to the zebrafish genome was a G>C missense mutation which causes misfolding of the *EOGT* protein and targets it for degradation (Shaheen et al., 2013) and the patient carrying this specific mutation suffered from an atrial septal defect (Shaheen et al., 2013).

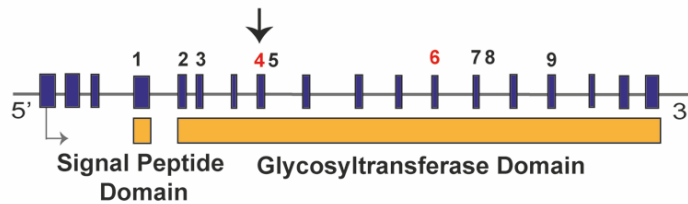
3. Creating zebrafish models of AOS

A Human *EOGT-202* and zebrafish *eogt-201* sequence alignment

	NW Score	Identities	Gaps	Strand
	407	1048/1594(66%)	44/1594(2%)	Plus/Plus
Human <i>EOGT-202</i> → Query	476	TCTATCTTGGATTAAAGAAACATCAAGAGAAATCATGACAGATTTAAGGAGGACTTTTTC		535
Zebrafish <i>eogt-201</i> → Sbjct	452	TGTATCTGGACCTGAGGAGTCCCCGAGAGGTCACGAGAGGTATAAAGAGGATTTCTGG		511
Query	536	AGAGTGGTAAAATTGGAGGGCACTGTAAACTTGACATCCGTACA--TTGAC-GTCTGAAG		592
Sbjct	512	AGCAGGGTGAGATCGGGGTCCTGCAGCCTTAACA---GTAAAGCTTTAGAGGCAGAAG		568
Query	593	GTCAGCGCAAAGCCCTCTGCAGTCATGGTTTGTCTGAGCTACAAAGCTATACTCAGCTCA		652
Sbjct	569	GGACACATAAGAGTCCCTACAGTCTTGGTTTCTGAATTGCAAACATATTCAGAGCTTG		628

↑
Conserved G residue
where knock-in mutation
was to be created

B Human *EOGT* reported mutations



Number	Exon/Intron	Mutation	Zygoty	Zygoty Nature of Mutation	Causative of CHD	Reference
1	Exon 4	p.His27Alafs*46	Compound Heterozygous with no.7	Frameshift	None reported	Meester et al., 2018
2	Exon 5	c.311+1G>T	Homozygous	Splicing	None reported	Meester et al., 2018
3	Exon 6	p.Cys135Tyr	Homozygous	Missense	None reported	Meester et al., 2018
4	Exon 8	p.Trp207Ser	Homozygous	Missense	ASD-II ¹	Shaheen et al., 2013
5	Exon 8	c.621-2A>T	Homozygous	Splicing	None reported	Dudoignon et al., 2019
6	Exon 12	p.Gly359Aspfs*28	Homozygous	Frameshift	Muscular VSD ² and PDA ³	Shaheen et al., 2013
7	Exon 13	p.Asn338Lysfs*24	Homozygous	Frameshift	None reported	Lukas et al., 2022
8	Exon 13	p.Arg377Gln	Homozygous	Missense	None Reported	Shaheen et al., 2013
9	Exon 15	c.1335-1G>A	Compound Heterozygous with no.1	Splicing	None reported	Meester et al., 2018

ASD-II¹ = Atrial Septal Defect Type II
Muscular VSD² = Muscular Septal Defect
PDA³ = Patent Ductus Arteriosus

3. Creating zebrafish models of AOS

Figure 3.11. Location of AOS *EOGT* mutations. (A) Alignment of the human and zebrafish *EOGT-202* coding sequences on blast, showing 66% shared identity and the conserved G residue where the G>C knock-in mutation was to be created. (B) The human *EOGT-202* gene with 18 exons (dark blue), and the functional signal peptide domain and glycosyltransferase domain annotated (orange). Numbers indicate the position of AOS mutations throughout the *EOGT* gene and correspond to a mutation detailed in the table below. Numbers highlighted in red indicate mutations in patients who also suffer from CHDs. The human mutation I identified to knock-in to the zebrafish genome is shown by the black arrow. The table highlights all identified human *EOGT* mutations found in AOS patients to date, indicating where in the *EOGT* gene the mutation was found, the nature of the mutation and whether it is causative of CHDs.

The knock-in strategy to generate a disease-specific *eogt* zebrafish mutant is the same as that described for *dock6*, with a crRNA designed as close as possible to the site where I wanted to knock-in the mutation and a single stranded oligo designed to incorporate the point mutation into the genome via HDR (Fernandez et al., 2018) (Fig.3.12 A). Unfortunately, I failed to successfully incorporate the human AOS *EOGT* point mutation into the zebrafish genome even in F0 embryos. Nevertheless, I raised F0 embryos to adulthood to attempt to recover an *eogt* frameshift or truncation mutant where the crRNA had successfully guided the Cas12a enzyme to cut the genome, but the oligo had not been incorporated, with the goal of generating an *eogt* LOF mutant model. After screening 40 founders, I only identified a single F0 founder with germline transmission of a mutation disrupting an exon, specifically a 28bp deletion mutation at the end of exon 6, close to where I wanted to create the AOS knock-in mutation (Fig.3.12 B). Despite this mutation disrupting a splice donor site at the end of exon 6, it does not appear to affect splicing, as confirmed using primers which flank intron-exon boundaries. This mutation removes 5 amino acids encoded by the end of exon 6 but does not result in a frameshift. As described above, I outcrossed this F0 mutant founder to the *Tg(myl7:LifeActGFP);Tg(fli1a:AC-TagRFP)* transgenic line so that I could visualise heart development and vascular morphology in this mutant model. Additionally, I outcrossed this F0 founder to the *Tg(myl7:LifeActGFP);Tg(Tp1bglob:hmgb1-mCherry)* global Notch reporter line (Parsons et al., 2009) so that I could interrogate the impact of the *eogt* mutation on

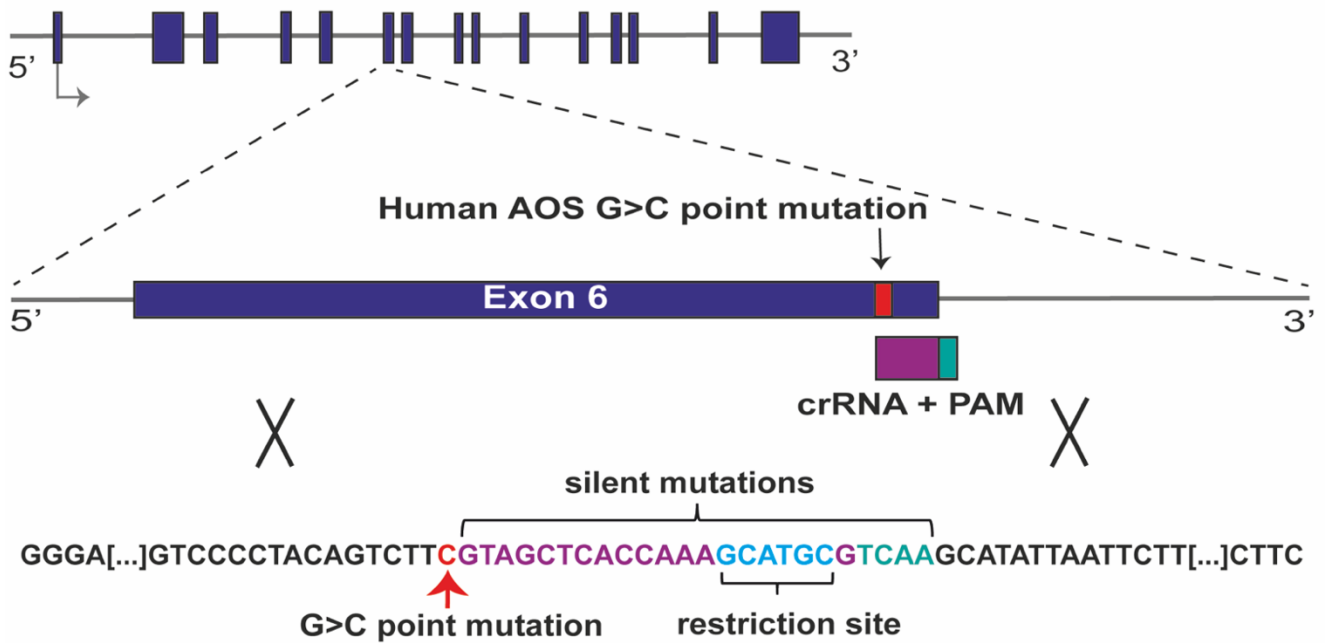
Notch signalling. Despite difficulties faced making *eogt* mutant zebrafish models, I did manage to create novel *eogt* mutant model for phenotypic analysis, *eogt-201*^{Δ28}.

3.11 Discussion

In chapter 3 I compare the gene structures of human and zebrafish *dock6* and *eogt*, and characterise expression dynamics of the zebrafish protein-coding transcripts during development. I further identify that both genes have a non-coding transcript which is expressed in the zebrafish myocardium at early stages of heart development. I also describe the approach taken and the challenges arising when attempting to create both *eogt* and *dock6* promoter-less zebrafish mutant models and human AOS disease-specific knock-in mutant models.

Since it is currently unknown how defects associated with AOS arise, such as ACC and TTLD, which affect 81% and 62% of AOS patients respectively (Dudoignon et al., 2020), a zebrafish disease model could provide mechanistic insights into the origins of these defects. In developing zebrafish embryos, I have shown that both *dock6-201* and *eogt-201* mRNA are expressed in similar regions, such as in the midbrain-hindbrain boundary and MCeV of the head and in somite boundaries and ISVs of the tail. It is noteworthy that both *dock6-201* and *eogt-201* are expressed in the zebrafish head, a region where ACC arises in human patients. At 24hpf, *dock6-201* is also expressed in a region of the cardinal vein at the tip of the zebrafish tail (Isogai et al., 2001), where TTLD arise in human patients. Additionally it has been suggested that these defects in humans could arise due to a lack of vascular growth to extremities, leading to ischemia in the head and digits (Pereira-Da-Silva et al., 2000, Okido et al., 2022). Both *dock6-201* and *eogt-201* are expressed in regions of developing vasculature in the zebrafish embryo at both 20hpf, in the DA and PCV, and at 24hpf in the midbrain-hindbrain boundary/mCeV and somite boundaries/ISVs respectively, suggesting that these genes are playing important roles in early vascular growth which could be disrupted in AOS. Another common AOS phenotype, cutis marmorata telangiectatica congenita (CMTC), which affects approximately 20% of AOS patients, and leads to dilated blood vessels and mottled skin (Hassed et al., 2017) could provide further evidence that AOS phenotypes arise from vascular defects.

A *eogt-201* AOS disease specific knock-in CRISPR strategy



B Recovered *eogt-201*^{Δ28} CRISPR mutant

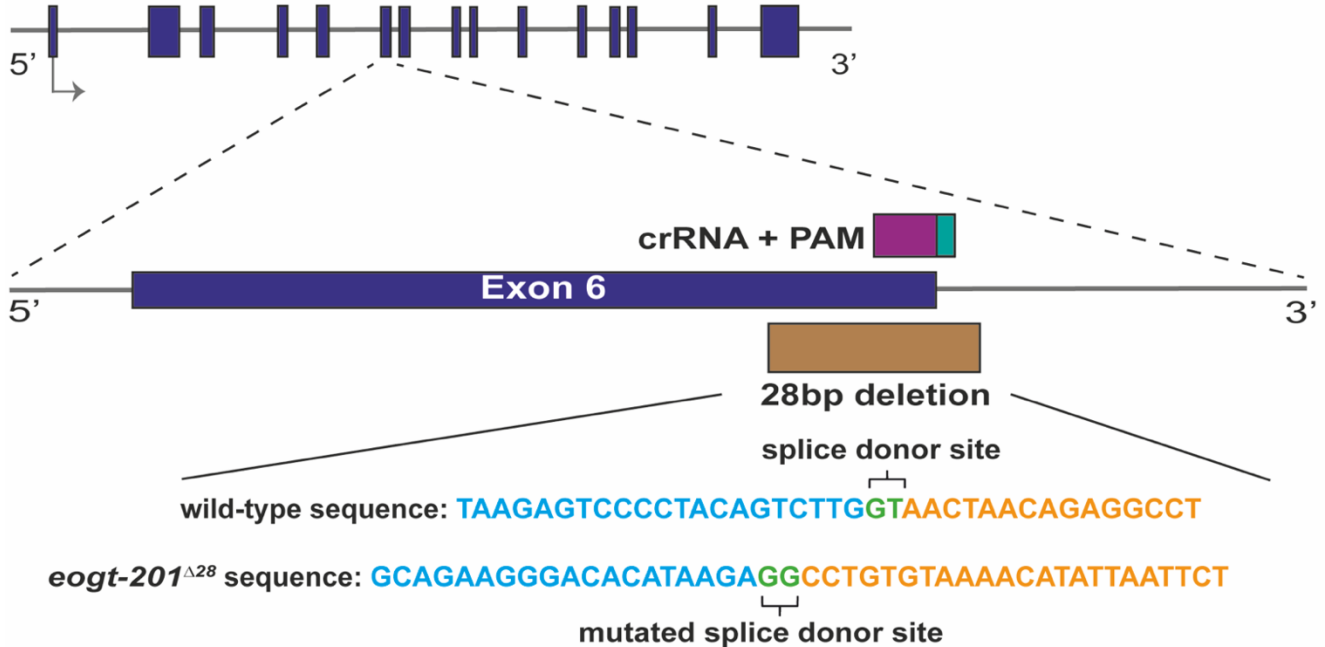


Figure 3.12. Zebrafish *eogt-201* AOS disease-specific knock-in CRISPR/Cas12a gene editing strategy and the recovered *eogt-201* coding sequence mutant. (A) Schematic showing the zebrafish *eogt-201* full length protein coding gene with 15 exons annotated (dark blue). The highlighted region shows exon 6 (dark blue) with a conserved zebrafish residue which is mutated in AOS patients (G>C) (red) and a single crRNA (purple, with PAM in turquoise) designed to bind as close as possible to where the point mutation is going to be introduced. The sequence below shows a single-stranded oligonucleotide sequence used as a template to introduce the point mutation (red text) into the genome, flanked by homology regions to facilitate homology directed repair (black text). Silent mutations were introduced into the single stranded oligonucleotide where the crRNA binds (purple text) and PAM site (turquoise text), to prevent this region from being re-cut following incorporation. A restriction site (blue text) was also introduced using silent mutations to facilitate genotyping successful incorporation into the genome. (B) Schematic showing an *eogt-201* coding sequence mutant founder recovered from the knock-in strategy where the crRNA (purple, with the PAM in turquoise) successfully targeted Cas12a to cut the gene but the single-stranded oligo was not incorporated into the genome. This founder is transmitting a 28bp deletion (brown) at the end of exon 6 (dark blue) through the germline. Despite this mutation affecting splice donor sites (green text), it did not seem to effect splicing.

It is well documented that Notch signalling is important for vasculogenesis where it has been shown to play a role in arterial differentiation during embryonic development in zebrafish (Lawson et al., 2001). Additionally there is evidence that the Notch ligand *dll4* (another AOS causative gene which is believed to be regulated by *eogt* (Sawaguchi et al., 2017)) is expressed in the same vascular structures as *eogt-201* at 24hpf, in the DA and ISVs of the zebrafish tail (Gore et al., 2012), and in the MCEV of the zebrafish head (Lawson et al., 2001). Although Rac1 hasn't been shown to be expressed/active specifically in the zebrafish embryo vasculature, a previous study reported that Rac1 is ubiquitously expressed in the zebrafish embryo at 20hpf, with heightened expression in epithelial cells at the somite boundaries (Srinivas et al., 2007, Henry et al., 2005), in a similar pattern to the *dock6-201* expression described here at 24hpf. It has also been shown from studies in mice that knock-out of Rac1 in

3. Creating zebrafish models of AOS

endothelial cells blocks cell migration and formation of cell-cell adhesions, resulting in vascular defects and embryonic lethality (Tan et al., 2008). Additionally, there is evidence to suggest that both Rac1 and DOCK proteins play important roles in zebrafish vasculogenesis as studies in zebrafish have shown that Rac1 is important for endothelial cell migration during the formation of ISVs (Epting et al., 2010), while 7 out of the 11 known DOCK proteins have been found to carry out functions during vasculogenesis, such as regulating vascular smooth muscle cell migration and proliferation (Benson and Southgate, 2021). This could indicate that both the RAC1 and NOTCH signalling pathways, which are both implicated in AOS, play important roles in vasculogenesis, where NOTCH signalling is required specifically in the developing vasculature (such as the ISVs and MCeV) while RAC1 is required in regions where the vasculature will form (such as the midbrain-hindbrain boundary and somite boundaries) to facilitate vascular growth. To investigate this, I could use two-colour fluorescent *in situ* hybridisation for both *dock6-201* and *eogt-201* alongside an *in situ* hybridisation probe for the zebrafish vascular marker *fli1a* to see whether *eogt-201* is expressed within the developing ISVs, and whether *dock6-201* is expressed in or around the developing ISVs. Additionally, I could use Rac1hu-Rac1 FRET sensors which indicate Rac1 activity (Kardash et al., 2011), in combination with the *Tg(fli1a:AC-TagRFP)* transgenic line to see whether Rac1 is active in the developing vasculature.

In addition to the first characterisation of the expression of zebrafish *dock6-201* and *eogt-201*, I identified that each gene has a putative non-coding transcript which is expressed in the heart myocardium at 24hpf, a key stage of early zebrafish heart development when the heart has formed a linear tube prior to looping morphogenesis and begins pumping blood around the body (Yalcin et al., 2017). Although the majority of the human genome is transcribed, only 2% of it is translated into functional proteins (Hobuß et al., 2019) and until fairly recently, non-coding transcripts have often been considered to be 'junk' RNA as they do not encode proteins and are often expressed at very low levels (Reicher et al., 2018). However, more recently they have been found to carry out important functional roles in gene regulation (Panni et al., 2020). There are different categories of non-coding RNAs, which are mainly classed into two groups based on their length: small non-coding RNAs are less than 200bp, while long non-coding RNAs (lncRNAs) are over 200bp in length (Dueñas et al., 2019).

3. Creating zebrafish models of AOS

As the human genome assembly contains an annotated *EOGT* antisense RNA transcript which overlaps with the *EOGT-201*, spanning from the 3' end of *EOGT-201* across 7 exons in the antisense direction, I wanted to identify whether a similar transcript existed in zebrafish. To attempt to identify the 5' and 3' ends of the non-coding transcript which overlaps with *eogt-201* in zebrafish, I used rapid amplification of cDNA ends (RACE) as this technique allows amplification of transcripts which are 5' capped and polyadenylated, a feature which lncRNAs also commonly possess (Kaushik et al., 2013), and which may have allowed me to identify if this transcript was likely to be a lncRNA. Additionally, knowing both the start and end of this transcript would better characterise it allowing me to design a tailored experimental approach to knock out or over-express the transcript to understand whether it plays a functional role in embryonic development. Despite the RACE experiment being unsuccessful, it is likely that this transcript is an antisense lncRNA due to several factors: I am unable to identify any open reading frames (ORFs) for this transcript, suggesting it is likely non-coding and not producing a protein. Additionally, the *in situ* hybridisation probe used to identify it was 800bp long, suggesting the transcript is likely well over 200bp in length (a parameter which is used to define lncRNAs from other shorter non-coding RNA transcripts), and short transcripts such as microRNAs are difficult to detect using conventional *in situ* hybridisation due to their small size (Nielsen, 2012). Other features associated with lncRNAs also relate to this *eogt* non-coding transcript, such as the finding that they are often expressed in a tissue specific manner (Clark and Blackshaw, 2014), which is in line with my observation that the *eogt* antisense transcript is expressed specifically in the heart myocardium (Fig.3.10 K,L&M). lncRNAs are also commonly spliced (Quinn and Chang, 2016), and as the *in situ* hybridisation probe used to identify this non-coding transcript was designed based on cDNA and spans several exon-exon boundaries, this would also suggest that the *eogt* antisense transcript is likely spliced too.

Although exact identification of the size and sequence of this antisense transcript could not be identified, *in situ* hybridisation analysis of *eogt* antisense RNA expression showed distinct expression specifically in the heart myocardium at early stages of cardiac development, suggesting it could play an important role in heart morphogenesis. In addition, the absence of *eogt-201* protein coding transcript expression in the heart suggests that different transcripts of this gene could be

3. Creating zebrafish models of AOS

important for development of different organs in zebrafish. Although there is no direct expression data to confirm this is the case, we can speculate that there are multiple *eogt* transcripts in humans which could carry out tissue specific roles during development. In addition, as only 16% of AOS patients with mutations in *eogt* suffer from CHDs (Hassed et al., 2017), we can also speculate that mutations may need to impact multiple transcripts for CHDs to be observed. However, countering this argument, if the human *EOGT* antisense transcript is the one shown in Figure 3.8 which spans 7 exons from the 3' end of the *EOGT-202* gene, then there is one human *EOGT* mutation which is causative of CHDs which does not overlap with this antisense transcript, so this might not be the case (see Figure 3.11).

Additional evidence to support a functional role for an *eogt* antisense RNA comes from reports in the literature that lncRNAs are involved in numerous processes associated with heart development (Alexanian and Ounzain, 2020), NOTCH signalling (Reicher et al., 2018) and cardiac disease pathology (Poller et al., 2018). One example of an antisense lncRNA required for cardiac development in mice is *sirt1*, which was found to overlap with the *sirt1* mRNA transcript, and plays an important role in upregulating *sirt1* mRNA and protein expression to induce and regulate cardiomyocyte proliferation during development (Li et al., 2018). Another example is *tie1AS* which in zebrafish negatively regulates *tie1* mRNA expression, a gene important for angiogenesis and vascular integrity during embryonic development. When the *tie1AS* lncRNA was knocked down, vascular defects were observed (Chowdhury et al., 2018) supporting its role as a regulator of vessel development. lncRNAs have also been found to be important in regulating NOTCH signalling during cardiac development. *CARMA*, an antisense lncRNA which plays a role in cardiomyocyte differentiation in human embryonic stem cells, was shown to be involved in the regulation of the NOTCH signalling pathway via the NOTCH effector *RBPJ*, as when *CARMA* is knocked down, NOTCH signalling is also inhibited (Kay et al., 2021). Additionally, 3 *DLL4* antisense lncRNA variants were identified by RACE initially in mouse endothelial cells, and these *DLL4* antisense transcripts were subsequently also identified in human endothelial cells (Chowdhury et al., 2019). The existence of lncRNAs involved in cardiac development, and the regulation of other genes in the NOTCH signalling pathway known to be mutated in AOS (*DLL4* and *RBPJ*), suggest that an *eogt* antisense RNA transcript could play an important role in cardiac development in humans, and we can

3. Creating zebrafish models of AOS

speculate that mutations in AOS patients might impact the function of either the sense or antisense transcripts (or both), thereby resulting in a range of observed phenotypes.

In addition to the antisense *eogt* transcript, I also found a putative *dock6* non-coding RNA which is expressed in the myocardium, although this is a retained intron transcript rather than an antisense lncRNA which I have called *dock6-RI1*. Similarly to lncRNAs, retained intron transcripts like *dock6-RI1* were considered to be junk RNA until fairly recently (Jacob and Smith, 2017). Intron retention is a form of alternative splicing whereby intronic sequence is retained within the mature mRNA transcript, and retained intron transcripts are thought to be generated from around 80% of protein coding genes (Grabski et al., 2021). Intron-retaining transcripts can have numerous different fates, including undergoing nonsense-mediated decay (Jaillon et al., 2008), being retained within the nucleus and undergoing stimulus-dependent splicing (Vanichkina et al., 2018) or even being translated into an alternative protein isoform (Gontijo et al., 2011), and these processes have been shown to be tightly regulated during development, for example to up- or down-regulate expression of specific genes which will allow cells to differentiate into the correct cell type (Vanichkina et al., 2018). A crucial role for intron retention during heart development has been found in pigs, where there are 4 alternatively spliced transcripts of the myocardial-expressed gene *ANKRD1*, three of which have retained introns. Under cardiac stress conditions *ANKRD1* positively regulates its intron retaining transcripts, suggesting that this could be a mechanism allowing cardiac cells to rapidly make more *ANKRD1* under stress conditions (Torrado et al., 2009). There is further evidence that mechanical stress can stimulate alternative splicing, for example different isoforms of the nonmuscle myosin-light chain kinase gene are expressed upon mechanical stress to the human lung endothelial cells (Mascarenhas et al., 2017) and mechanical strain can induce expression of different VEGF-A isoforms in osteoblast cells derived from rats and humans (Faure et al., 2008). These examples could provide insights into whether alternative splicing of *dock6* occurs due to mechanical stress, as expression of the *dock6-RI1* retained intron transcript can be observed in 24hpf cardiomyocytes at the time they start beating within the zebrafish embryo (Yalcin et al., 2017), raising the possibility that mechanical stress could trigger this alternative splicing event. To look at this in more detail I could use the *troponin t type 2a (tnnt2)* morpholino oligonucleotide (Sehnert et al., 2002), which blocks cardiac contractility, to see

3. Creating zebrafish models of AOS

whether expression of *dock6-R11* is prevented in the absence of heart contraction, or alternatively whether expression persists beyond 24hpf when contraction of the myocardium does not occur. Although *dock6-R11* has not yet been shown to be conserved in humans, the presence of other retained intron transcripts such as *dock6-202*, which is conserved between zebrafish and humans, suggests that more could exist but they haven't been characterised yet.

The finding that both *dock6* and *eogt* have non-coding transcripts which are conserved between humans and zebrafish, and that both are expressed in the myocardium at a key stage of cardiovascular development, provides an intriguing area of further exploration into whether these non-coding transcripts play a role in heart development and whether they could be implicated in the onset of CHDs. As discussed above, since non-coding transcripts have also been identified to be involved in the regulation of other AOS associated genes in human cells, for example *DLL4* (Chowdhury et al., 2019) and *RBPJ* (Kay et al., 2021) this could indicate that dysregulation of non-coding transcripts may be involved in the onset of AOS. In addition, several retained intron transcripts are annotated for both *DOCK6* and *EOGT*. Although dysregulated intron retention has not been directly linked to AOS, four of the mutations in the human *DOCK6* gene, and three of the mutations in the human *EOGT* gene in AOS patients affect splice sites, suggesting that disrupted intron retention could be implicated in the onset of AOS. Furthermore, although mutations in six genes have been identified to be causative of AOS, these mutations provide a genetic origin for approximately 50% of AOS patients (Mašek and Andersson, 2017). Depending on the method used to identify mutations there is a possibility that further causative mutations of AOS could be within intronic regions or alternative non-coding transcripts which aren't detected through whole exome or exon-targeted sequencing. The extent to which non-coding RNAs are involved in cardiac development, or the onset of CHDs is currently gaining interest, and it is an area which I explore in more detail in Chapters 4 and 5.

It is worth noting that a limitation of this study is that the *eogt* antisense transcript and the *dock6-R11* retained intron transcript identified in this study were not validated in further detail. Despite attempting to identify the exact sequences of these transcripts in more detail, for example using RACE, these attempts were unsuccessful. The *eogt* antisense RNA was identified using two separately designed *in situ* hybridisation

3. Creating zebrafish models of AOS

probes which bound to different regions of the transcript, while the *dock6-R11* retained intron transcript was identified using an *in situ* hybridisation probe and qPCR primers which bound to retained intron 1. It would have been preferable to independently validate these transcripts further using cDNA sequencing, transcript specific qPCR or additional targeted *in situ* hybridisation probes.

To try to interrogate the roles of *DOCK6* and *EOGT* during cardiac development, I used CRISPR/Cas9 genome editing to create zebrafish mutant models for both genes, with the intention of generating a promoter-less mutant model and an AOS disease-specific knock-in mutant model. To investigate the consequences of a complete loss of these genes during heart development, I wanted to target the promoter regions to ensure complete LOF and avoid any potential compensation via nonsense mediated decay which could confound analyses (El-Brolosy et al., 2019). However, when attempting to make promoter-less mutants for both *dock6-201* and *eogt-201* in zebrafish, it was not possible to recover mutant founders where the annotated promoter region and/or ATG had been successfully disrupted in either gene. Instead, I could only recover founders transmitting intronic mutations either side of the promoter and ATG region. This was surprising since I successfully identified and validated gRNAs that resulted in efficient cuts in the regions flanking the annotated promoter in F0 embryos. However, I could not identify any F0 adult founders transmitting exon-disrupting mutations through the germline. Furthermore, when attempting to make *eogt-201* LOF mutant zebrafish, approximately 75% of the embryos which had been injected with gRNAs had already died before 24hpf, suggesting that disrupting the *eogt* gene during early zebrafish development could be embryonic lethal. This could suggest that creating complete LOF zebrafish mutants for either *dock6-201* or *eogt-201* might not be possible, as the embryos may not be viable upon complete loss of either of these genes.

Analysis of zebrafish *dock6* expression at 3hpf shows that *dock6* is maternally deposited, suggesting that it is important at early stages to support the embryo through early development. Furthermore, this could explain why *dock6-201* LOF gRNA injected embryos were viable, while the majority of *eogt-201* LOF gRNA injected embryos were not, as *eogt* expression is not maternally deposited. The observation that there are numerous *DOCK6* transcripts in humans also raises the possibility that

3. Creating zebrafish models of AOS

these alternative *DOCK6* transcripts could compensate for a loss of *DOCK6*, if it is indeed essential for survival. Supporting this essential role for *DOCK6*, human fibroblast cells derived from AOS patients with *DOCK6* mutations use a compensation mechanism to adapt to a chronic loss of *DOCK6* gene expression. The AOS patient-derived *DOCK6* mutant fibroblasts upregulate a gene called *IQGAP1* which stabilises RAC1 and CDC42 in their active GTP bound states, allowing them to overcome the cytoskeletal defects observed when *DOCK6* expression is completely removed (Cerikan et al., 2016).

The only animal model to-date used try to understand the role of *Dock6* is a knock-down mouse model created to investigate the role of *Dock6* in axon extension, in which shRNA is used to create genetically modified mice with reduced *Dock6* expression. In this study the authors focus on the role of *Dock6* in axon extension in embryonic development and following injury in adults, but report very little on the general effects of a loss of *Dock6* on these mice (Miyamoto et al., 2013). The only other *Dock6* animal model reported is a CRISPR/Cas9 knock-out mutant mouse where regions throughout exon 12 and exon 13 of the *Dock6* gene were deleted. This mutation was reported to be pre-weaning lethal in homozygosity, with incomplete penetrance, suggesting that knock-out of *Dock6* is incompatible with survival in mice (Mallon et al., 2012). We can speculate that the incomplete penetrance could be due to the nature of this mutation, which disrupts the coding sequence but doesn't necessarily prevent transcription and translation of this gene, therefore compensation could be activated in these mutant mice. All other studies investigating the role of *DOCK6* to-date have been conducted on cell lines, mainly focusing on the role of *DOCK6* in neuronal growth (Miyamoto et al., 2013). The relative lack of animal models, combined with the difficulty in recovering exon-disrupting mutations in zebrafish suggests that a zebrafish *dock6* LOF model could be lethal, and the existence of multiple human *DOCK6* transcripts, along with known compensation mechanisms for a loss of *DOCK6* could imply this is an important gene for survival. This highlights the value of trying to establish a *dock6* mutant zebrafish model of AOS to understand the complexities associated with this gene such as genetic compensation, especially given the ease of genetic manipulation and live imaging of development that zebrafish models provide. Additionally, it will allow me to investigate further whether the *dock6-R11* retained intron transcript plays a role during cardiovascular development, similar to previous studies using zebrafish to investigate

3. Creating zebrafish models of AOS

other retained intron transcripts which show conservation between humans and zebrafish such as the *NFX1* gene, which encodes a conserved mRNA export receptor, and has intron 10 retained in both the human and zebrafish orthologues (Wang et al., 2015).

EOGT is conserved from *C.elegans* to humans, suggesting an evolutionarily important role for this gene (Ogawa et al., 2020). Knock-down of *eogt* in *Drosophila* causes lethality in most of these animals during second/third instar larval stages, and any larva surviving past this stage suffer wing and trachea defects similar to those observed in mutants affecting genes which play a role in epithelial-extracellular matrix interactions (Varshney and Stanley, 2017). RNAi targeted knock-down of *eogt* specifically in the *Drosophila* wing leads to wing blistering, another defect associated with epithelial-cellular matrix interactions (Sakaidani et al., 2011). Expression analysis in developing mouse embryos demonstrated that *Eogt* is expressed in the apical ectodermal ridge of embryonic mice at day E11.5, with localisation to digits by day E12.5, suggesting *Eogt* may be required for limb development (Shaheen et al., 2013). However, an *Eogt* LOF mutant mouse model did not exhibit the hallmark phenotypic characteristics associated with AOS (ACC, TTLD) but did however show shortened and more branched vasculature in the retina, which could support the hypothesis that defects in AOS patients could be due to vascular abnormalities (Sawaguchi et al., 2017). Together, the previous data from *EOGT* animal models does not give a clear reason why it was so challenging to make zebrafish *eogt* LOF mutants, but it is possible that zebrafish, like *Drosophila*, could suffer early lethality due to a complete loss of *eogt*, and maybe animals higher up the evolutionary scale are more able to adapt to/compensate for a loss of *EOGT*. The presence of numerous *EOGT* transcripts in humans, like *DOCK6*, could suggest a compensation mechanism for the loss of a full-length *EOGT* transcript, however, to date a compensation mechanism is yet to be shown for a loss of *EOGT*.

The difficulties recovering promoter-less mutant models for both *dock6* and *eogt* was unexpected, particularly as it is a technique which has been well characterised (Li et al., 2016) and adopted to successfully generate several mutants in-house (Derrick et al., 2021; Derrick et al., 2019). For *dock6*, testing the gRNAs in F0 embryos appeared to work well, and following genotyping I could identify embryos where the gRNAs had

3. Creating zebrafish models of AOS

made a large deletion of exon 1. Additionally, the embryos were phenotypically normal up to 5dpf, and appeared healthy when raised to adulthood, suggesting that disruption of the *dock6* gene in injected embryos was not lethal. However, the failure to recover any founders in which the region of exon 1 where the promoter and ATG resides was disrupted, could suggest that *dock6* is required for germline development and survival, and therefore no founders contained a mutant germline. The scenario appears slightly different for *eogt*, where approximately 75% of injected F0 embryos died within 24hpf following injection, suggesting that the gRNAs were likely very efficient and potentially causing biallelic mutations in which any cells or embryos where both copies of the *eogt* gene were mutated could not survive. Out of the embryos that were well enough to raise to adulthood I failed to recover any F0 founders transmitting a mutation through the germline that was disrupting the promoter or ATG, which suggests that embryos possessing such mutations were non-viable. Further supporting a hypothesis that disrupting the *eogt* gene was incompatible with zebrafish survival, when F0 embryos injected with the AOS disease-specific knock-in crRNA and oligo were raised to adulthood, although the embryos appeared phenotypically normal up to 5dpf, 50% of the F0 founders died during the first 3 months of being raised.

Despite these challenges in recovering promoter-less mutants for *dock6* and *eogt*, I did manage to recover coding sequence mutants for both genes. However, the incidence of F0 founder fish transmitting coding sequence mutations was rare in both cases, with only 1 founder out of 100 screened for *dock6* transmitting a germline mutation which disrupted exon sequence, and similarly only 1 founder out of 40 screened for *eogt*. As it is extremely unlikely out of that many founders screened for both genes to not find a mutation interrupting an exon, especially with germline transmission rates of CRISPR/Cas9 mutations being reported to be as high as 100% (Woong Y. Hwang et al., 2013), and the mutations that I did recover being in frame, it is possible to speculate that the mutant founders I recovered are hypomorphs and not complete LOF mutants, which I explore in more detail in Chapters 4 and 5.

This chapter has highlighted the importance of generating new models to elucidate the roles of both *DOCK6* and *EOGT* in cardiac development and the onset of CHDs, as there are currently few vertebrate animal models available which can shed light on the roles these genes are playing during heart development and specifically in the

3. Creating zebrafish models of AOS

pathology of AOS. I have generated novel genetic zebrafish models for both genes: two *dock6-R11* retained intron mutants, and *dock6-201* and *eogt-201* coding sequence mutants, and I explore the phenotypic impact of these mutations upon cardiac development in the following chapters.

4. Investigating the role of *dock6* in Cardiac Development and Congenital Heart Disease

4.1 Introduction

Dedicator of cytokinesis 6 (DOCK6) is an atypical guanine exchange factor (GEF) which activates RAC1 and CDC42 by cycling them from their inactive GDP bound states into their active GTP bound states (Gadea and Blangy, 2014), and plays important roles regulating the actin cytoskeleton during cell migration and cell adhesion (Miyamoto et al., 2007). DOCK6 belongs to the DOCK family of GEFs which has 11 members separated into four groups (Dock A-D) based on their sequence and the GTPase they activate (Nishikimi et al., 2013), with DOCK6 belonging to the DOCK-C subfamily (Gadea and Blangy, 2014). Unlike typical GEFs, which possess a dbl-homology (DH) domain which is responsible for catalysing the exchange of GDP for GTP, and a PH domain for membrane localisation (Benson and Southgate, 2021), DOCK GEFs are characterized by two DOCK homology regions: the DHR2 guanine nucleotide exchange factor domain, and the DHR1 membrane localisation domain (Kukimoto-Niino et al., 2021).

Mutations in *DOCK6* have been identified in autosomal recessive and compound heterozygous forms of Adams-Oliver Syndrome (AOS) (Shaheen et al., 2011b), and mutations in this gene account for approximately 4% of patients with AOS to date (Hassed et al., 2017). Of known AOS patients with mutations in *DOCK6*, alongside most patients suffering from the hallmark features of AOS – aplasia cutis congenita (ACC) and terminal transverse limb defects (TTLD) (94% and 100% of identified patients respectively), 12% suffered from cutis marmorata telangiectatica congenita (CMCT) and 31% suffered from congenital heart defects (CHDs), while 69% suffered from neurological defects (Hassed et al., 2017). *DOCK6* is one of two causative AOS genes which are involved in regulating the RAC1/CDC42 signalling pathways, with the other being *ARHGAP31*, a GTPase activating protein (GAP), mutations in which are linked with an autosomal dominant form of AOS (Sukalo et al., 2015). Mutations in *ARHGAP31* in AOS are gain-of-function, leading to a loss of active RAC1/CDC42 by keeping them in their inactive GDP bound forms (Southgate et al., 2011), indicating

that reduced RAC1/CDC42 signalling is behind the pathology of AOS in patients with mutations in either *DOCK6* or *ARHGAP31* (Shaheen et al., 2013).

Although mutations in *DOCK6* are known to be causative of AOS, the roles of *DOCK6* in embryogenesis are not well characterized, particularly in the context of heart development. It has been reported in mice that *DOCK6* is required to regulate RAC1/CDC42 activity during neurite outgrowth (Miyamoto et al., 2007) and the phosphorylation status of *DOCK6* is important to determine axonal growth or branching in dorsal root ganglion neurons (Miyamoto et al., 2013). *DOCK6* has also been shown to be upregulated in certain cancers and is linked to poor prognosis due to increased cell migration and invasion (Zhang et al., 2022). *DOCK6* activity is likely to be important for basic cellular function, as human fibroblast cells derived from AOS patients have adapted to be able to compensate for a chronic loss of *DOCK6* expression by upregulating expression of *IQGAP1* which can stabilise RAC1/CDC42 in their active GTP bound states in the absence of *DOCK6* (Cerikan et al., 2016).

Studies in mice have shown that RAC1 deficiency in cardiomyocytes leads to reduced myocardial growth in the embryo, resulting in CHDs consistent with those seen in AOS patients, such as ventricular septal defects and overriding aorta (Leung et al., 2021). It has also been reported that RAC1 is required in the second heart field (SHF) to facilitate SHF migration into the developing heart (Leung et al., 2014), and that deleting RAC1 in the precardiac mesoderm leads to disorganized, thin myocardial walls with defects in the alignment of the outflow tract (OFT) (Abu-Issa, 2015). Similarly, loss of CDC42 function in embryonic cardiomyocytes resulted in thin ventricular wall tissue and ventricular septal defects (Liu et al., 2017; Li et al., 2017).

While little is known about the exact role of *DOCK6* during cardiac development and the onset of CHDs, since *DOCK6* functions to modulate RAC1/CDC42 signalling we can speculate that *DOCK6* regulates similar processes in the developing heart to those regulated by RAC1 and CDC42. To investigate this further, a *DOCK6* mutant animal model would help improve our understanding of how mutations in *DOCK6* lead to dysregulation of RAC1/CDC42 during the onset of CHDs. In this chapter I characterize 3 novel *dock6* CRISPR mutant zebrafish lines: two *dock6-RI1* retained intron mutants (*dock6-RI1^{ins41}* and *dock6-RI1^{Δ28}*) and one *dock6-201* coding sequence mutant (*dock6-201^{ins36Δ65}*). I characterise the effects these mutations have on the

4. Investigating the role of *dock6*

expression of *dock6-201* and *dock6-R11* and perform an in-depth analysis of cardiac morphology during development. Additionally, I investigate the compensation pathway previously shown to be activated upon chronic loss of *dock6*, taking the first steps towards understanding whether this compensation pathway could be having protective effects in the onset of CHDs in AOS patients with mutations in *DOCK6*.

4.2 *dock6-R11* retained intron mutations overlap with active enhancer methylation marks

Zebrafish have 2 annotated *dock6* transcripts on *ensembl*, the full-length protein coding transcript, *dock6-201*, and a retained intron transcript, *dock6-202*, which has 4 exons and 1 retained intron at the end of exon 4. In chapter 3 I also identified a novel *dock6* retained intron transcript in zebrafish, *dock6-R11*, which has intron 1 retained. As the *dock6-202* retained intron transcript is conserved between humans and zebrafish, we can speculate that the *dock6-R11* transcript, which is expressed in the zebrafish heart at a key stage of cardiac development, could also be conserved between humans and zebrafish, and so I wanted to investigate the role of this retained intron transcript in more detail. To do this, I recovered 2 *dock6-R11* mutant founders: *dock6-R11^{ins41}* and *dock6-R11^{Δ28}*, both carrying mutations within retained intron 1 of the *dock6-R11* transcript, and each residing 102bp and 84bp downstream of the annotated promoter respectively (Fig.4.1 A). To analyse whether the region harbouring these mutations contained any features of interest, I used the zebrafish UCSC genome browser (GRCz11/danRer11) to determine whether the mutation sites overlap with any active enhancer sites, previously identified in published DANIO-CODE CHIP-seq data sets. I utilised a data set from the Skarmeta Lab who carried out CHIP-seq analysis of H3K4me3, H3k4me1 and H3k27ac histone modifications in whole zebrafish embryos at four different stages of development to identify stage specific enhancers that regulate embryonic development, including at 24hpf when *dock6* is expressed (Bogdanović et al., 2013). Using this data set, I found that both mutations overlap with H3K4me3 marks which are associated with transcriptional activation, and H3K27ac marks which are open chromatin marks indicating regulatory genome elements such as transcriptional enhancers (Fig. 4.1 B) This suggested that these mutations could be disrupting regulatory regions of the *dock6* gene.

4. Investigating the role of *dock6*

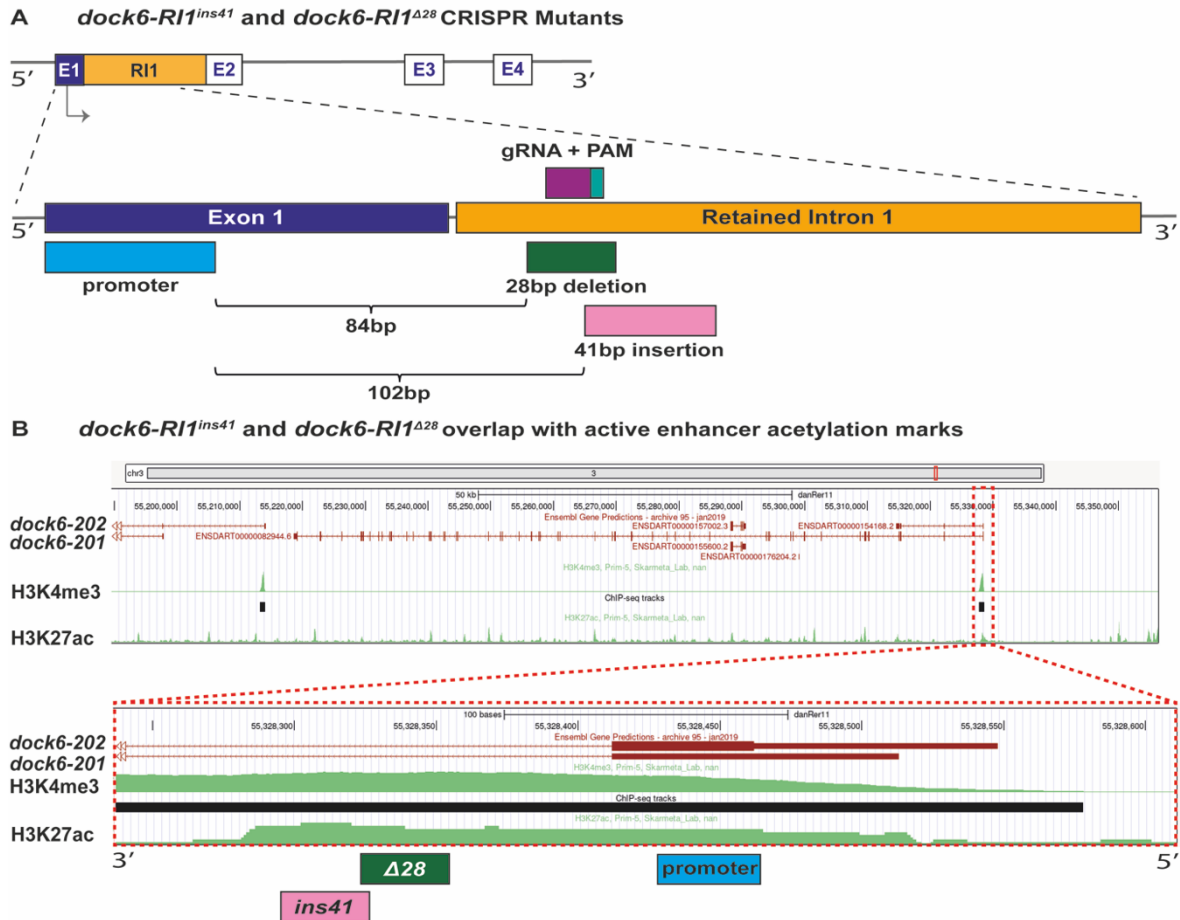


Figure 4.1. *dock6-R11* retained intron mutants overlap with active enhancer methylation marks. **(A)** Zebrafish *dock6-R11* retained intron transcript that has intron 1 retained (R11, orange). The *dock6-R11^{Δ28}* mutation (dark green) is located 84bp downstream of the annotated promoter (light blue) in retained intron 1 and is adjacent to and slightly overlapping the *dock6-R11^{ins41}* mutation (light pink) which is 102bp downstream of the annotated promoter. **(B)** Zebrafish *dock6* gene annotation on the UCSC genome browser with H3K4me3 and H3K27ac CHIP-Seq data derived from 24hpf zebrafish embryos. Both the *dock6-R11^{Δ28}* (dark green box) and *dock6-R11^{ins41}* (light pink box) mutations overlap with marks indicating transcriptional activation (H3K4me3) and regulatory elements (H3K27ac).

4.3 *dock6-R11^{ins41}* retained intron insertion mutation results in reduced expression of both *dock6* transcripts

According to CHIP-Seq data used to identify stage specific enhancers that regulate embryonic development, the *dock6-R11* retained intron mutants appeared to be disrupting regions of the *dock6* gene associated with active transcription and

4. Investigating the role of *dock6*

regulatory elements. I first wanted to analyse whether these mutations were having an impact on both *dock6-201* and *dock6-R11* gene expression during zebrafish development using *in situ* hybridisation and qPCR. In wild-type embryos the *dock6-R11* retained intron transcript is expressed at low levels in the head and higher levels in the linear heart tube at 24hpf (Fig. 4.2 A&B). However, in *dock6-R11^{ins41}* homozygous mutant embryos at the same stage, *dock6-R11* expression is reduced, with little expression visible throughout the head, and faint expression in the heart tube (Fig. 4.2 C&D). This significant reduction in gene expression was confirmed using qPCR analysis, which found a 50%-fold change reduction in *dock6-R11* expression in *dock6-R11^{ins41}* homozygous mutant embryos compared to wild-type embryos (Fig. 4.2 E). At 24hpf, *dock6-201* protein-coding transcript expression can be seen throughout the zebrafish head, with greater expression in the midbrain-hindbrain boundary, and in somite boundaries throughout the tail (Fig. 4.2 F&G). In *dock6-R11^{ins41}* homozygous mutant embryos *dock6-201* expression is also reduced throughout the head and tail, with expression in the midbrain-hindbrain boundary no longer visible (Fig. 4.2 H). While there is reduced *dock6-201* expression in the head, it appears in the *dock6-R11^{ins41}* homozygous mutant embryos that there might be increased expression of *dock6-201* in the heart (Fig. 4.2 I), although it is not clear whether there is expression in the heart in wild-type embryos which is normally masked by the expression in surrounding tissue, or whether there is an increase in *dock6-201* expression specifically in the heart in *dock6-R11^{ins41}* homozygous mutant embryos. The reduction in *dock6-201* expression in *dock6-R11^{ins41}* homozygous mutant embryos was also confirmed using qPCR analysis, and like *dock6-R11* expression, *dock6-201* expression is reduced by approximately 50% when compared to wild-type embryos (Fig. 4.2 J). As this mutation in the *dock6-R11* retained intron transcript results in a decreased expression of the *dock6-201* protein coding transcript, we can speculate that it either disrupts an intronic enhancer region which regulates expression of both transcripts, or that the *dock6-R11* retained intron transcript is regulating the expression of the *dock6-201* protein coding transcript.

4. Investigating the role of *dock6*

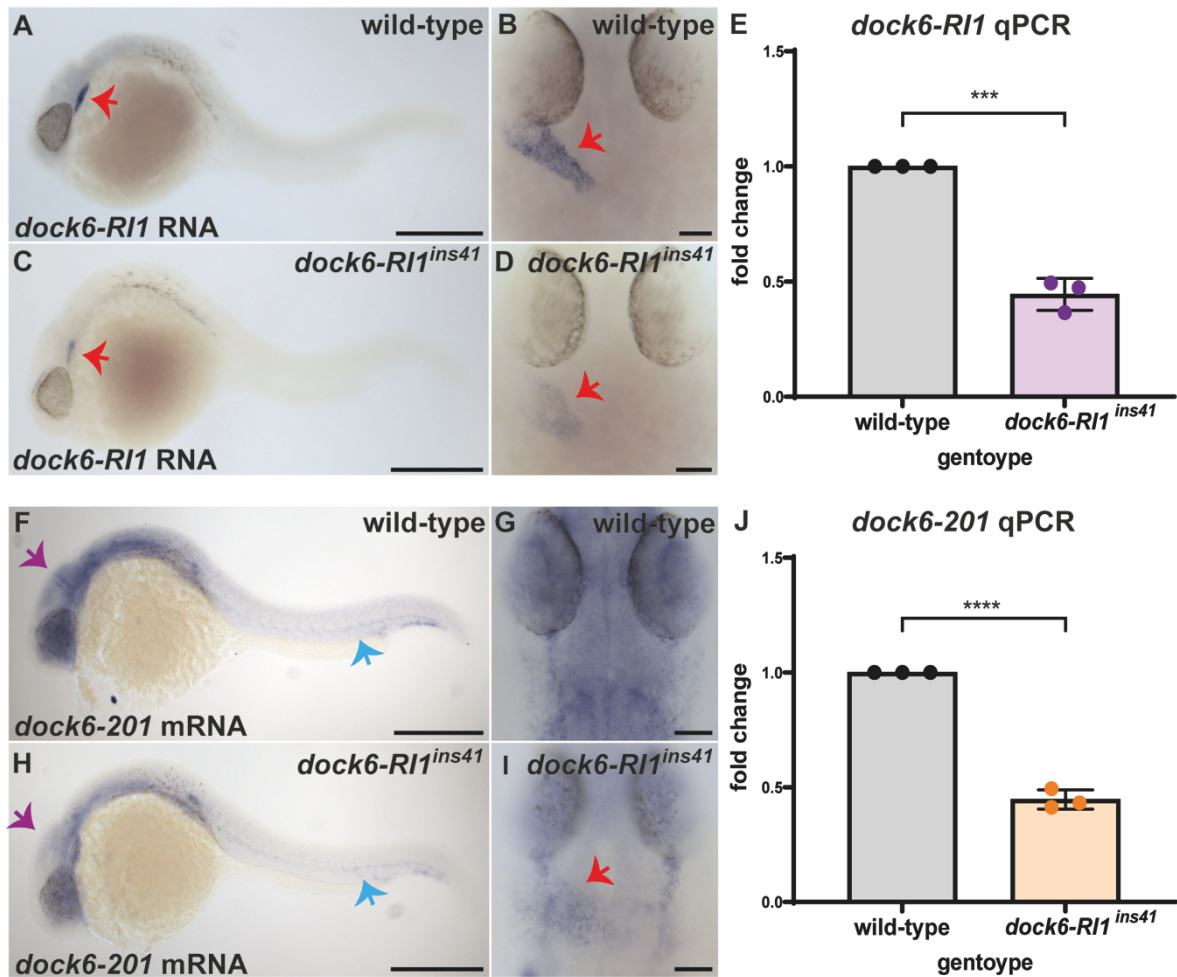


Figure 4.2. *dock6-RI1^{ins41}* mutation results in reduced expression of *dock6* transcripts. *in situ* hybridisation and qPCR analysis of *dock6-RI1* expression (A-E) and *dock6-201* expression (F-J) in *dock6-RI1^{ins41}* mutant embryos. (A) *dock6-RI1* is expressed in the head and heart myocardium (red arrow) at 24hpf in wild-type embryos. (B) A dorsal view of the head at 24hpf reveals *dock6-RI1* expression in the heart tube myocardium (red arrow) in a wild-type embryo. (C) *dock6-RI1* expression is reduced in the head and heart myocardium (red arrow) in *dock6-RI1^{ins41}* mutant embryos. (D) A dorsal view of a *dock6-RI1^{ins41}* mutant embryo head with reduced expression of *dock6-RI1* in the heart tube myocardium at 24hpf. (E) qPCR analysis of *dock6-RI1* RNA expression reveals a 50%-fold change reduction in *dock6-RI1* expression in *dock6-RI1^{ins41}* mutant embryos compared to wild-types at 24hpf. (F) *dock6-201* is expressed throughout the head and in the midbrain-hindbrain boundary (purple arrow) and in somite boundaries of the tail (blue arrow) in wild-type embryos at 24hpf. (G) A dorsal view of the head of a wild-type embryo

4. Investigating the role of *dock6*

at 24hpf reveals *dock6-201* expression throughout the head with no detectable expression in the heart tube myocardium. (H) *dock6-201* mRNA expression is reduced throughout the head and tail in *dock6-RI1^{ins41}* mutant embryos, with lower levels of expression in the midbrain-hindbrain boundary (purple arrow) and somite boundaries of the tail (blue arrow). (I) A dorsal view of a *dock6-RI1^{ins41}* mutant embryo with reduced *dock6-201* expression in the head, but increased expression in the heart tube myocardium (red arrow). (J) qPCR analysis of *dock6-201* mRNA expression reveals a 50%-fold change reduction in *dock6-201* expression in *dock6-RI1^{ins41}* mutant embryos compared to wild-types at 24hpf. E&J: mean \pm SD are plotted, unpaired t-test, ***: $p < 0.001$, ****: $p < 0.0001$. Scale bars: A, C, F & H = 500 μ m. B, D, G & I = 50 μ m. Mendelian ratios of *dock6-RI1* *in situ* hybridisation: wild-types = 6, heterozygotes = 11, homozygotes = 6. Mendelian ratios of *dock6-201* *in situ* hybridisation: wild-types = 3, heterozygotes = 6, homozygotes = 6.

4.4 *dock6-RI1 Δ 28* retained intron deletion mutation has no effect on *dock6-201* or *dock6-RI1* expression

As the *dock6-RI1^{ins41}* insertion mutation in the retained intron appears to regulate the expression of the *dock6-201* protein coding transcript, I next wanted to characterise the expression pattern of both *dock6* transcripts in *dock6-RI1 Δ 28* mutant embryos to see if this deletion mutation also led to downregulation of these transcripts. Despite the 28bp deletion mutation being in a similar region to the 41bp insertion mutation (within retained intron 1, 18bp upstream of the 41bp insertion) I found that this mutation appeared to have no effect on the expression of the *dock6-RI1* retained intron transcript when assayed using *in situ* hybridisation, with expression in the *dock6-RI1 Δ 28* mutant embryos still visible throughout the head and heart tube (Fig. 4.3 C&D). Similarly, there was no effect on expression of the *dock6-201* protein coding transcript in these mutant embryos either, with expression levels being comparable to wild-types, and clearly visible in the midbrain-hindbrain boundary and somite boundaries in the tail (Fig. 4.3 G) with no obvious expression in the heart (Fig. 4.3 H). It is noteworthy that despite these two mutations being created within the same region and within proximity to one another, they have differential effects on expression of *dock6-201* and *dock6-RI1* transcripts. We can therefore speculate that the region where the 41bp insertion mutation has been created might be important for regulating the expression

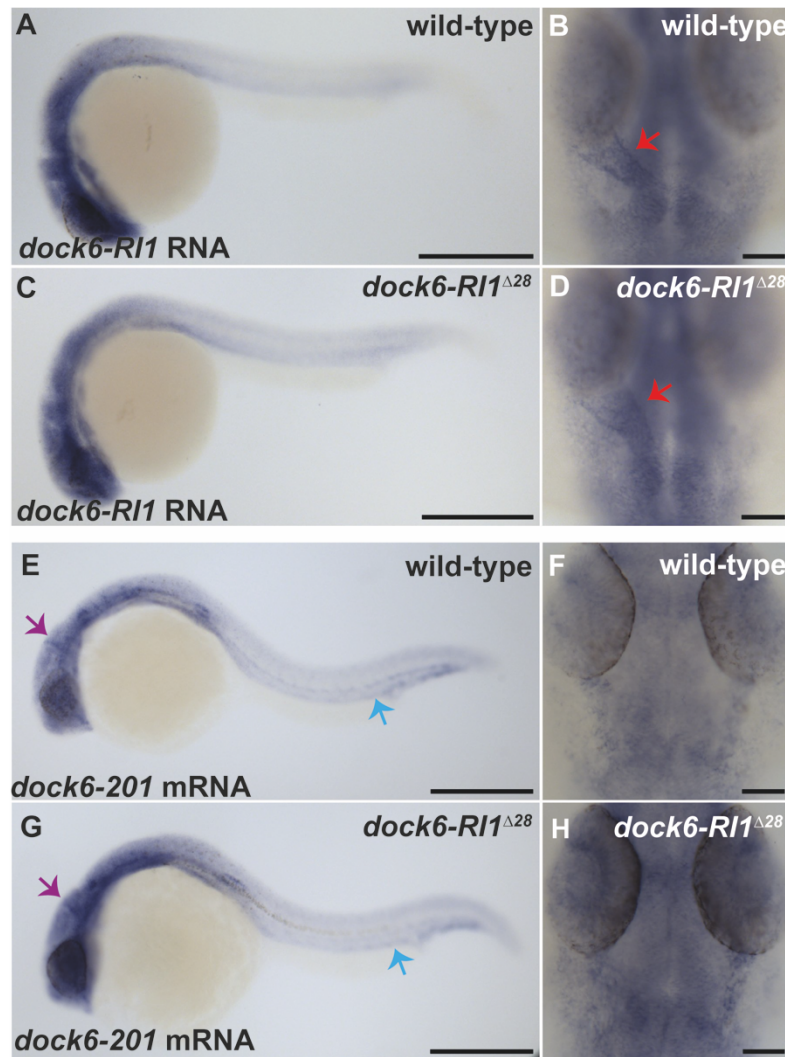


Figure 4.3. *dock6-R11*^{Δ28} mutation has no effect on *dock6* expression. *in situ* hybridisation analysis of *dock6-R11* (A-D) and *dock6-201* (E-H) expression in *dock6-R11*^{Δ28} mutant embryos. (A) *dock6-R11* is expressed throughout the head in wild-type embryos at 24hpf, and expression can be seen in the heart tube myocardium (red arrow) when imaging the head dorsally at 24hpf (B). (C) *dock6-R11* expression is comparable between *dock6-R11*^{Δ28} mutant embryos and wild-types at 24hpf, with expression seen throughout the head, and in the heart tube myocardium (red arrow) (D). (E) *dock6-201* is expressed throughout the head and in the midbrain-hindbrain boundary (purple arrow) and in somite boundaries of the tail (blue arrow) in wild-type embryos at 24hpf. (F) A dorsal view of the head of a wild-type embryo at 24hpf, showing *dock6-201* expression throughout the head, with no obvious expression in the heart tube myocardium. (G) *dock6-201*

4. Investigating the role of *dock6*

expression in *dock6-R11^{Δ28}* mutant embryos is comparable to wild-types with expression throughout the head and in the midbrain-hindbrain boundary (purple arrow) and somite boundaries of the tail (blue arrow). (H) A dorsal view of the head of a *dock6-R11^{Δ28}* mutant embryo shows comparable levels of *dock6-201* expression to wild-type embryos, with expression throughout the head but no obvious expression in the heart tube myocardium. Scale bars: A, C, E & G = 500μm. B, D, F, H: 50μm. Mendelian ratios of *dock6-R11 in situ* hybridisation: wild-types = 3, heterozygotes = 13, homozygotes = 4. Mendelian ratios of *dock6-201 in situ* hybridisation: wild-types = 8, heterozygotes = 8, homozygotes = 4.

of both *dock6* transcripts, and this provided me with a unique model to investigate the role of *dock6* during cardiac development as it resulted in decreased expression of both *dock6-201* and *dock6-R11* transcripts, and so we can also assume Dock6 activity is also reduced.

4.5 *dock6-R11* retained intron mutations have no effect on cardiac development

As the *dock6-R11^{ins41}* mutation results in decreased *dock6-R11* expression in the head and heart, and decreased *dock6-201* expression throughout the head and tail, with potential up-regulation of *dock6-201* expression in the heart, I wanted to investigate what impact this would have on cardiac development. To characterise heart morphology, I used an *in situ* hybridisation probe to visualise expression of the pan-myocardial gene *myl7*, revealing the morphology of the whole heart at both 24hpf when the heart is still a tube (Fig. 4.4 A&B) and 55hpf when the heart has undergone looping morphogenesis (Fig. 4.4 D&E). However, I found the hearts in *dock6-R11^{ins41}* mutant embryos to be comparable to wild-type embryos at both stages of development. To ensure there were no subtle differences in heart morphology at either of these stages, I measured heart area at both 24hpf and 55hpf but found there to be no significant difference between mutants and wild-type siblings (Fig. 4.4 C&F). Following formation of the linear heart tube at 24hpf, hearts undergo a complex looping and ballooning process to form the chambers of the adult heart. To assess the extent of cardiac looping, the looping ratio of the heart can be calculated by measuring both the linear length and looped length between both poles of the heart and dividing the looped length by the linear length (Fig. 4.4 G), giving a value greater than 1, where 1 means the heart is linear. After measuring the looping ratio of *dock6-R11^{ins41}* mutant

4. Investigating the role of *dock6*

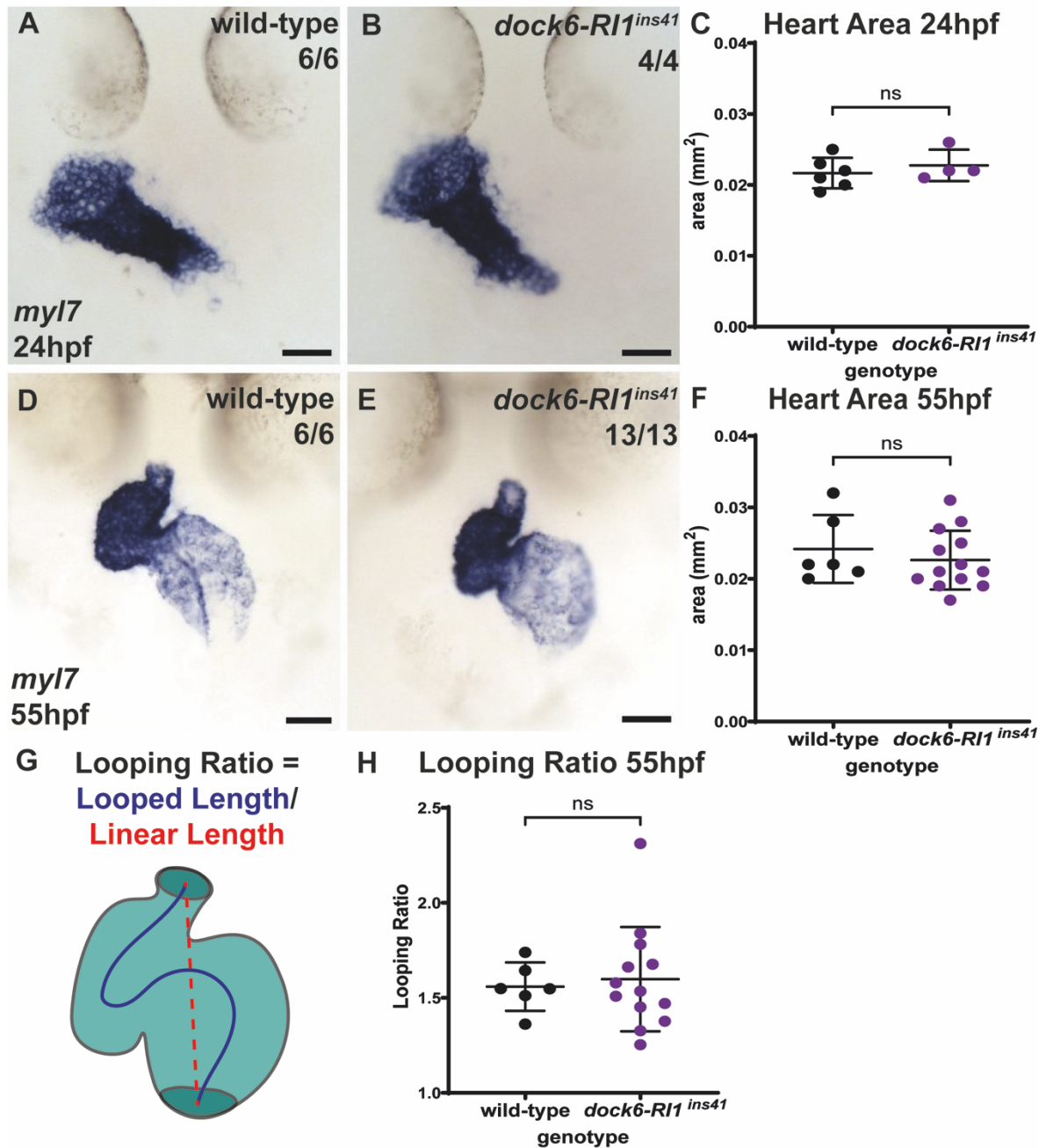


Figure 4.4. *dock6-RI1^{ins41}* mutation has no effect on cardiac morphology. mRNA *in situ* hybridisation analysis of a pan myocardial gene, *myl7*, to visualise heart morphology at both 24hpf (**A-B**) and 55hpf (**D-E**) in wild-type and *dock6-RI1^{ins41}* mutant embryos. Heart tube morphology at 24hpf in *dock6-RI1^{ins41}* mutant embryos (**B**) is comparable to that of wild-types (**A**), and there is no significant difference in heart tube area (**C**). (**D**) Analysis of heart morphology through *myl7* expression in 55hpf looped hearts of *dock6-RI1^{ins41}* mutant embryos (**E**) is comparable to wild-type morphology (**D**), with no significant difference in heart area (**F**). (**G**) Schematic illustrating how heart looping ratio is calculated, by dividing the

4. Investigating the role of *dock6*

looped length from either pole of the heart (dark blue line) by the linear length from either pole of the heart (red dotted line). (H) The looping ratio of *dock6-R11^{ins41}* mutant hearts at 55hpf is not significantly different from the looping ratio of wild-type hearts at 55hpf. C, F & H: mean \pm SD are plotted, unpaired t-test, ns: not significant. Scale bars: A, B, D & E = 50 μ m. Mendelian ratios of 24hpf *myl7 in situ* hybridisation: wild-types = 6, heterozygotes = 10, homozygotes = 4. Mendelian ratios of 55hpf *myl7 in situ* hybridisation: wild-types = 6, heterozygotes = 11, homozygotes = 13.

embryos I found there was no significant difference in the looping ratio compared to wild-type embryos (Fig. 4.4 H).

Although it appeared from the *in situ* hybridisation data that there is no significant difference in cardiac morphology between *dock6-R11^{ins41}* mutant hearts when compared to wild-type hearts, it can be difficult to identify subtle differences in 3D heart morphology using 2D *in situ* hybridisation images, particularly at later stages of development due to compaction of the tissues. To ensure I wasn't missing any subtle defects in cardiac morphology, I acquired live 3D images of the heart on the light-sheet microscope to ensure better preservation of tissue morphology and utilised a novel image analysis programme developed in-house called MorphoHeart (Sánchez-Posada, 2022) which creates 3D mesh reconstructions of the different tissue layers of the heart. MorphoHeart allows in depth analysis of heart morphology which is difficult to obtain from 2D *in situ* images, for example measuring the volume of chambers, the thickness of individual tissue layers and quantifying chamber geometry.

To further understand heart morphology in the *dock6* retained intron mutants I utilised the *Tg(myI7:LifeActGFP);Tg(fli1a:AC-TagRFP)* transgenic background to label the myocardium in green and the endocardium in magenta in the *dock6-R11^{ins41}* and *dock6-R11 ^{Δ 28}* mutant lines. I imaged the transgenic mutant hearts on the light-sheet microscope at 72hpf, a stage in which the adult structures of the heart are beginning to develop (e.g. chambers, valves, onset of trabeculation), providing insights into whether the hearts are developing normally. As there was no difference in either *dock6-201* or *dock6-R11* expression in *dock6-R11 ^{Δ 28}* mutant embryos, and no obvious gross morphological defects in the embryos up to 5dpf, it seemed unlikely that these mutants would suffer from cardiac abnormalities, however I imaged the hearts of these mutant embryos at 72hpf on the light-sheet microscope to rule this out. Analysis of

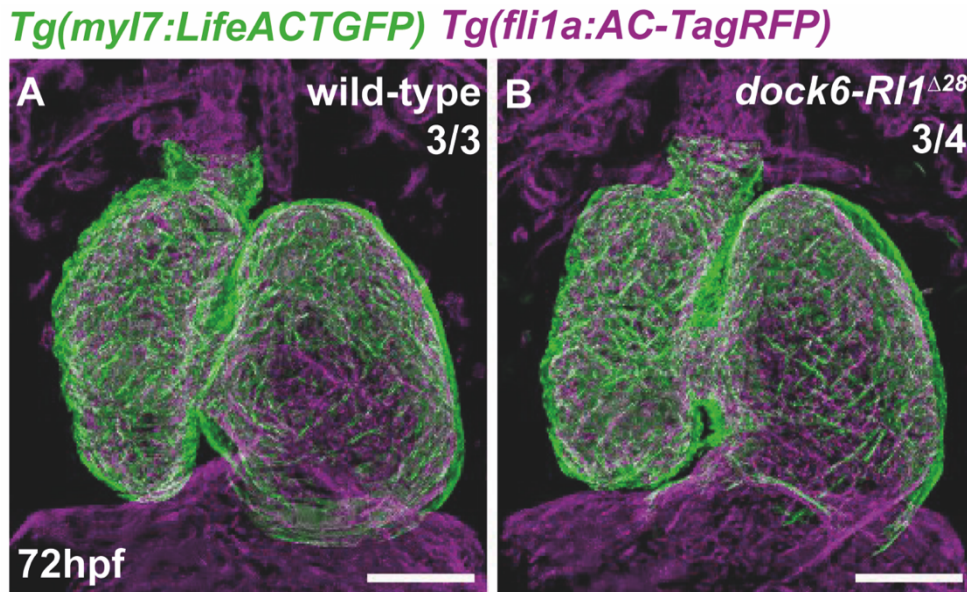


Figure 4.5. *dock6-RI1^{Δ28}* mutation has no effect on cardiac morphology. Maximum intensity projections of 72hpf hearts imaged on the light-sheet microscope with the *Tg(myI7:LifeActGFP)* transgene labelling the myocardium green and the *Tg(fli1a:AC-TagRFP)* transgene labelling the endocardium magenta (**A-B**). Morphology is comparable between a 72hpf wild-type heart (**A**) and a 72hpf *dock6-RI1^{Δ28}* mutant heart (**B**). Scale bars: 50μm. Mendelian ratio: wild-types = 3, heterozygotes = 13, homozygotes = 4.

maximum intensity projections of *dock6-RI1^{Δ28}* mutant hearts at 72hpf revealed heart morphology is comparable to wild-types (Fig. 4.5 A&B) and as *dock6-RI1^{Δ28}* embryos had no obvious effects on *dock6* expression, I decided not to carry out MorphoHeart analysis on these hearts.

As the *dock6-RI1^{ins41}* mutant embryos have down regulation of both *dock6* transcripts, I decided to focus on characterising the *dock6-RI1^{ins41}* mutant model in more detail as this model is more likely to represent reduced Dock6 function. Following light-sheet imaging of *dock6-RI1^{ins41}* mutant and wild-type sibling hearts (Fig. 4.6 A-C), I used MorphoHeart to generate 3D reconstructions of the heart and segment the different tissue layers to perform quantitative analysis of multiple parameters of heart morphogenesis. I found that most hearts in *dock6-RI1^{ins41}* mutant embryos have similar morphology to wild-type hearts (Fig. 4.6 B), however some hearts appeared to have mild morphological defects (Fig. 4.6 C). As the chambers grow they undergo ballooning, and analysis of myocardial ballooning which measures how ballooned the

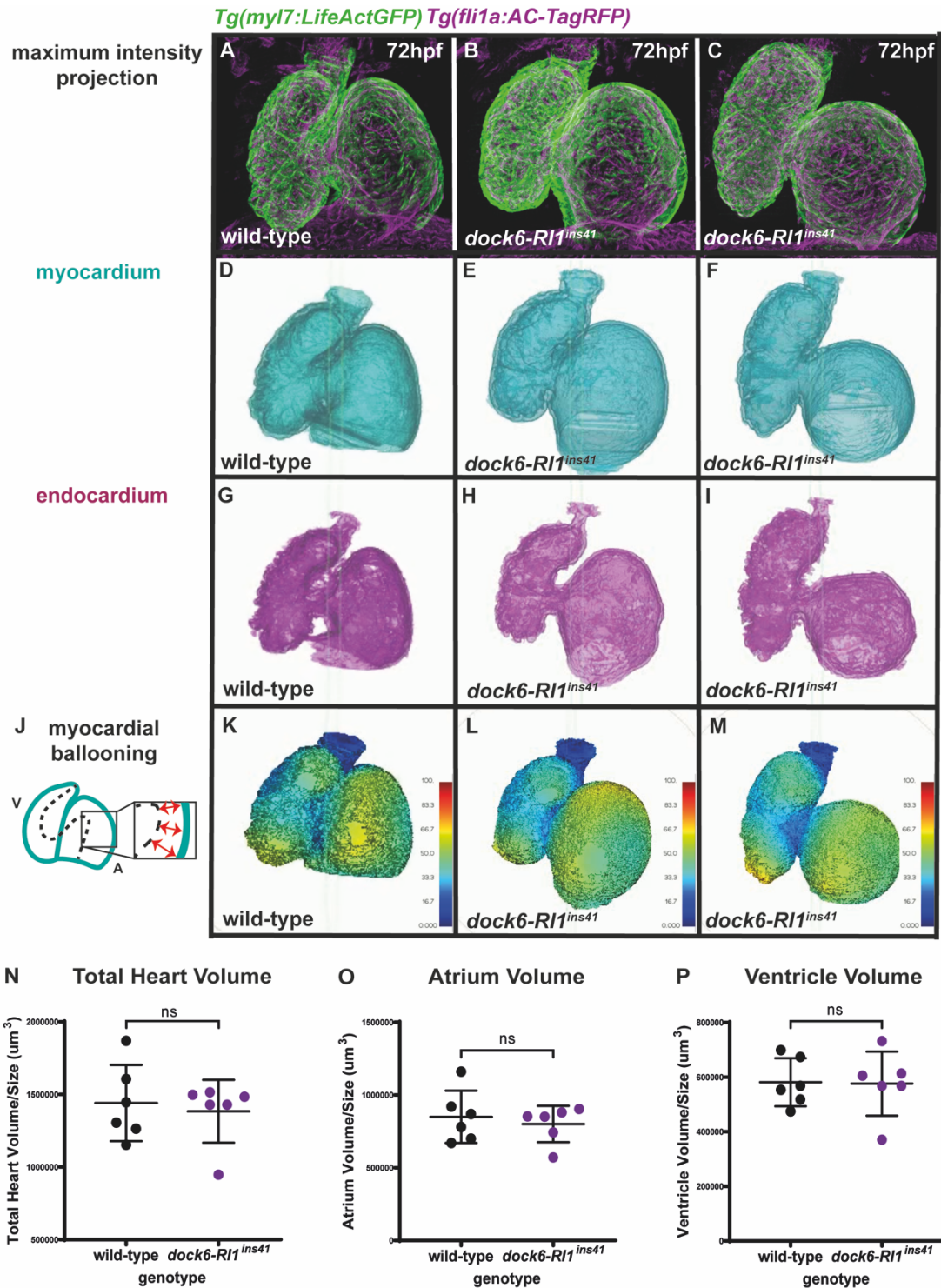


Figure 4.6. MorphoHeart analysis of cardiac morphology and size in *dock6-RI1^{ins41}* mutant embryos. MorphoHeart was used to create 3D reconstructions of *dock6-RI1^{ins41}* mutant and wild-type sibling heart tissue layers to carry out in depth tissue analysis on 72hpf hearts. Maximum intensity projections of 72hpf hearts imaged on the light-sheet microscope, with the *Tg(myl7:LifeActGFP)* transgene labelling the myocardium green and the *Tg(fli1a:AC-TagRFP)* transgene labelling

4. Investigating the role of *dock6*

the endocardium magenta in wild-type sibling hearts (**A**) and *dock6-R11^{ins41}* mutant hearts which have comparable morphology to wild-types (**B**) and *dock6-R11^{ins41}* mutant hearts which have mild morphological defects (**C**). MorphoHeart generated 3D reconstructions of the myocardium and endocardium for the wild-type heart in panel **A** (**D&G**) and the *dock6-R11^{ins41}* mutant hearts in panel **B** (**E&H**) and panel **C** (**F&I**). (**J**) Schematic showing how MorphoHeart analyses myocardial ballooning by measuring the distance the myocardial tissue has ballooned away from the midline of the heart. Myocardial ballooning heatmaps showing comparable ballooning for wild-type hearts (**K**), and *dock6-R11^{ins41}* mutant hearts (**L&M**). MorphoHeart quantitative analysis indicated there was no significant difference in heart size between wild-type and *dock6-R11^{ins41}* mutant hearts in terms of total heart volume (**N**), atrial volume (**O**) or ventricle volume (**P**). Mean \pm SD are plotted, N was analysed with the Mann-Whitney U test, O & P were analysed with the Unpaired t-test, ns: not significant. Scale bars: 50 μ m. Mendelian ratio: wild-types = 6, heterozygotes = 29, homozygotes = 8.

myocardial tissue is from the heart centreline (Fig. 4.6 J), reveals comparable chamber growth and morphology between *dock6-R11^{ins41}* mutant hearts and wild-type hearts (Fig. 4.6 K-M). After measuring parameters such as total heart volume (Fig. 4.6 N) and volume of both the atrium (Fig. 4.6 O) and ventricle (Fig. 4.6 P), no significant difference was found between wild-type and *dock6-R11^{ins41}* mutant hearts, indicating that the size of the hearts are comparable between wild-types and *dock6-R11^{ins41}* mutants.

MorphoHeart can also measure the thickness of individual tissue layers of the heart, and as mutations in *Rac1* in mice have been linked to decreased myocardial tissue thickness, I wanted to see whether there was any difference in myocardial thickness between wild-type and *dock6-R11^{ins41}* mutant hearts. Using MorphoHeart, I created 3D heatmaps indicating myocardial thickness for both *dock6-R11^{ins41}* mutant and wild-type sibling hearts and found that most *dock6-R11^{ins41}* mutant hearts appeared to display similar myocardial tissue thickness (Fig. 4.7 C) compared to wild-type hearts (Fig. 4.7 B), with some hearts appearing to have reduced myocardial thickness, particularly in the ventricle (Fig.4.7 D). However, following MorphoHeart quantitative analysis, I found there was no significant difference in the volume of myocardial tissue in the

4. Investigating the role of *dock6*

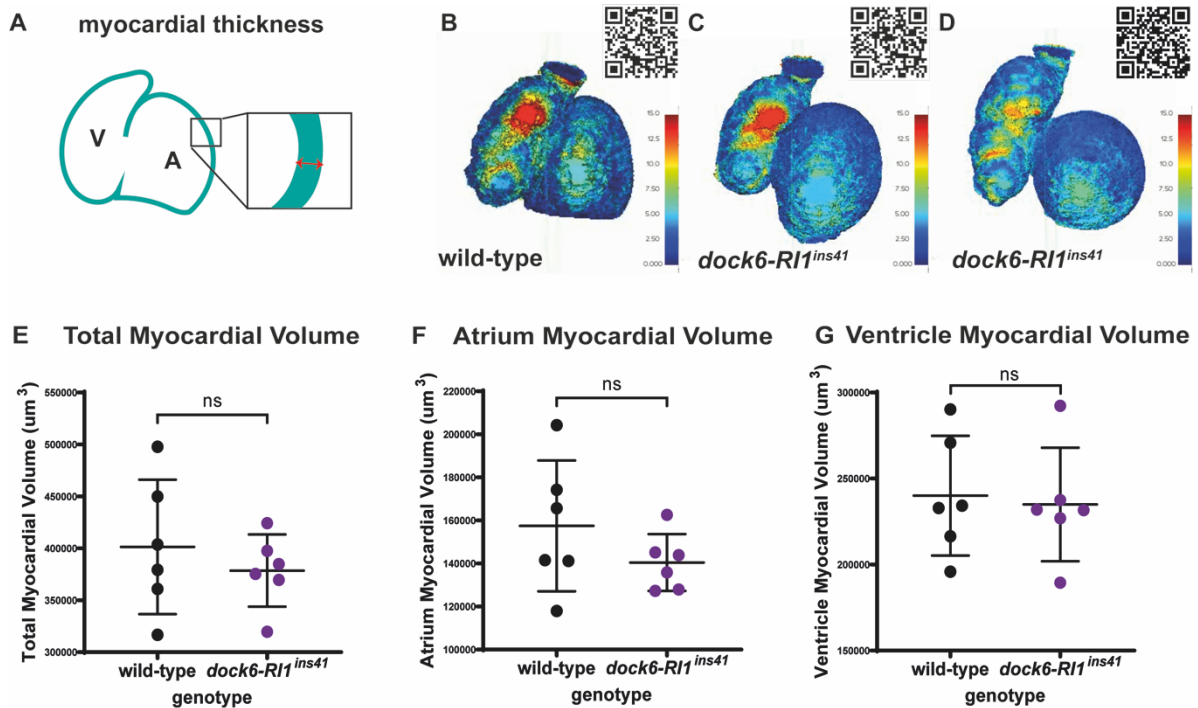


Figure 4.7. MorphoHeart analysis of myocardial thickness in *dock6-RI1^{ins41}* mutant embryos. MorphoHeart was used to create 3D myocardial thickness heatmaps of *dock6-RI1^{ins41}* mutant and wild-type sibling hearts and conduct quantitative analysis of myocardial tissue volume. **(A)** Schematic showing how MorphoHeart measures myocardial tissue thickness. **(B-D)** Myocardial thickness heatmaps indicate thicker myocardial tissue with reds/yellows, and thinner myocardial tissue with greens/ blues. Myocardial thickness heatmaps from a wild-type heart **(B)**, a *dock6-RI1^{ins41}* mutant heart with morphology comparable to wild-type **(C)**, and a *dock6-RI1^{ins41}* mutant heart with mild morphological defects **(D)**. 3D rotating movies of the myocardial thickness heatmaps can be found by scanning QR codes next to the images. MorphoHeart quantitative analysis indicated there was no significant difference in myocardial tissue volume in either in the whole heart **(E)**, the atrium **(F)** or the ventricle **(G)** of *dock6-RI1^{ins41}* mutant hearts compared to wild-type hearts. Mean \pm SD are plotted, E, F & G were analysed with the Unpaired t-test, ns: not significant.

whole heart (Fig. 4.7 E) or in the atrium (Fig. 4.7 F) or ventricle (Fig. 4.7 G) of *dock6-RI1^{ins41}* mutant hearts compared to wild-types. This suggests that the *dock6-RI1^{ins41}* mutation, despite causing a reduction in expression of both *dock6* transcripts, is having no effect on cardiac development. It also suggests that a loss of *dock6* expression in

these mutants is not resulting in reduced myocardial thickness, like seen in mice *Rac1* mutant models, suggesting that a loss of *dock6* in these mutants is not having an impact on *Rac1* function, or alternatively *Rac1* is not carrying out similar processes during zebrafish heart development as it does in mice.

4.6 *dock6-R11^{ins41}* retained intron insertion mutation has no effect on adult behaviour

I previously showed that *dock6-R11^{ins41}* mutant embryos exhibit a reduction in *dock6-201* and *dock6-R11* expression throughout the head. As previous studies have shown that 69% of AOS patients with mutations in *dock6* also suffer from neurological abnormalities (Hassed et al., 2017), and as it is known that DOCK6 is required to regulate RAC1 and CDC42 activities during neurite outgrowth in mouse neuroblastoma cells (Miyamoto et al., 2007) I wanted to investigate whether there were any neurological abnormalities that may manifest in behavioural phenotypes in these retained intron mutant fish. I raised *dock6-R11^{ins41}* homozygous mutant embryos and wild-type siblings to adulthood, and although there were no obvious defects in these fish at 3 months of age, *dock6-R11^{ins41}* homozygous mutant adult fish appeared to become hyperactive following stress, for example after netting. Studies in mice with conditional knock-out of *Rac1* in developing neurons have provided evidence that loss of RAC1 in the developing brain results in hyperactivity (Pennucci et al., 2015), therefore I wanted to investigate whether hyperactivity was overserved in *dock6-R11^{ins41}* mutant fish, which had reduced levels of *dock6* expression in the brain during development. Additionally, zebrafish have been shown to be a useful model for studying human neurological conditions, for example ADHD, of which hyperactivity is one of the symptoms (Fontana et al., 2019). Therefore, I conducted behavioural analysis experiments on *dock6-R11^{ins41}* mutant and wild-type sibling adult fish by recording their movements over an eight-hour period and quantifying time spent either inactive or hyperactive, to see whether these fish displayed hyperactivity. However, I found that there was no significant difference in inactivity (Fig. 4.8 A&B) or hyperactivity (Fig. 4.8 C&D) between the mutants and wild-types, suggesting that these fish do not exhibit behavioural defects due to a reduction of *dock6* expression in the head during embryonic development.

4. Investigating the role of *dock6*

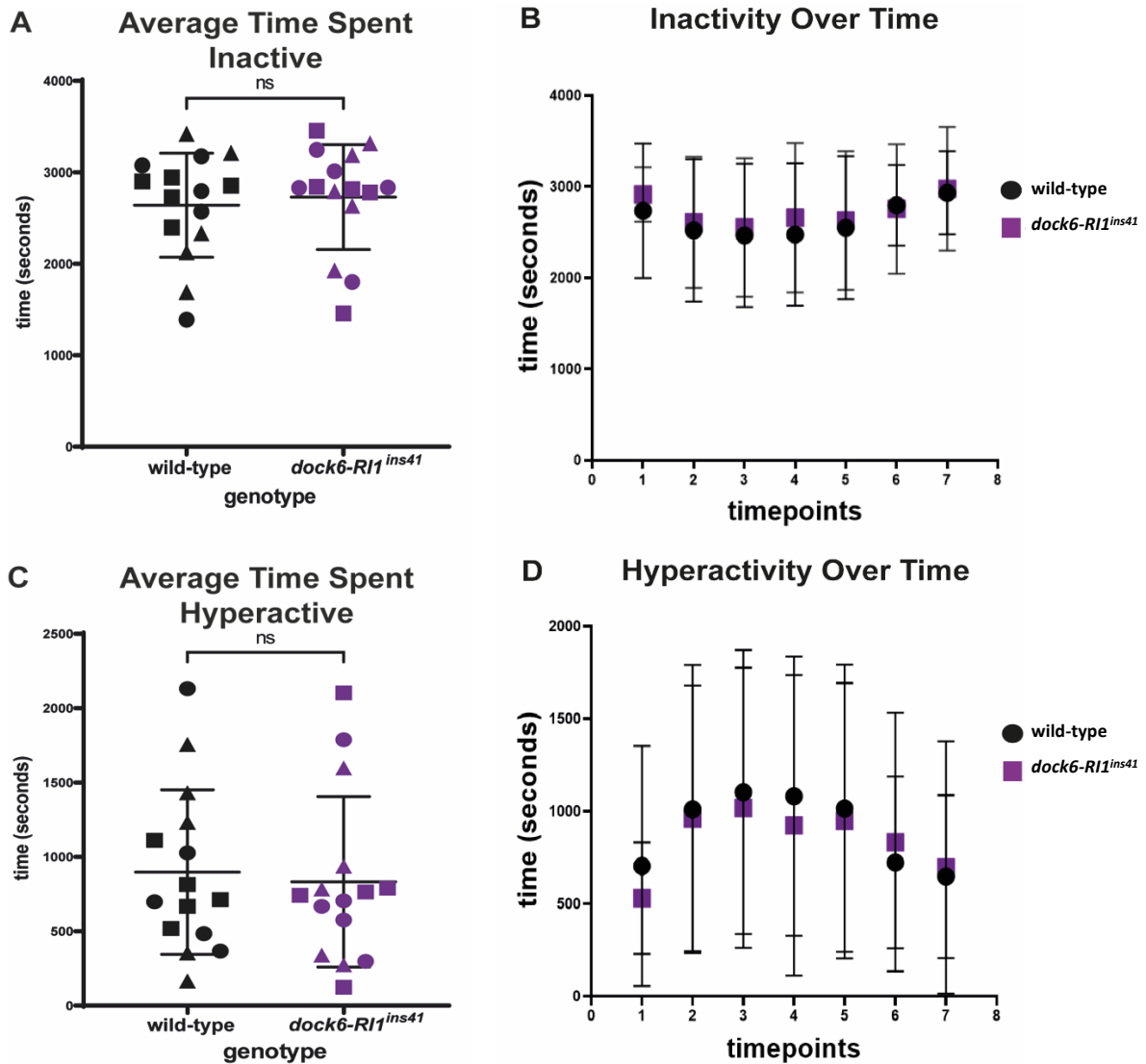


Figure 4.8. *dock6-R11^{ins41}* mutation has no effect on adult behaviour. Behavioural analysis experiments conducted over an 8-hour period in wild-type sibling and *dock6-R11^{ins41}* homozygous mutant adult fish. There is no significant difference in the average time spent inactive between *dock6-R11^{ins41}* mutant adults and wild-type siblings (A), or at each individual time point over the 8-hour period in which they were observed (B). There is no significant difference in the average amount of time spent hyperactive between *dock6-R11^{ins41}* mutant adults and wild-type siblings (C), or at each individual time point over the 8-hour period in which they were observed (D). Mean \pm SD are plotted, A&C are analysed with the Mann-Whitney U test, ns: not significant. Different icons in A&C indicate 3 technical repeats.

4.7 Investigating potential compensation mechanisms in *dock6* mutants – *isg15* expression is heterogeneous during early development

Despite there being a reduction in *dock6-201* and *dock6-R11* expression in *dock6-R11^{ins41}* mutant embryos, this appeared to have no phenotypic consequence. This was surprising since in wild-type embryos, *dock6-R11* is expressed in both the head and the heart and *dock6-201* throughout the head and midbrain-hindbrain boundary, and both are reduced in the *dock6-R11^{ins41}* mutant embryos with no apparent consequence on cardiac development or adult behaviour. However, a previous study has shown that in fibroblast cells isolated from AOS patients with mutations in *DOCK6*, these cells have an intrinsic adaptation mechanism allowing them to adapt to a chronic loss of *DOCK6* expression (Cerikan et al., 2016). Under wild-type conditions, *DOCK6* activates *RAC1* and *CDC42* by promoting the exchange of a GDP molecule for a GTP, however under acute *DOCK6* knock-down *RAC1* and *CDC42* levels are reduced as they remain in their inactive GDP bound states. Surprisingly, under a chronic loss of *DOCK6* expression, an increase in globular actin levels triggers a compensation mechanism to become activated, leading to downregulation of a small ubiquitin-like modifier called *ISG15*, which normally targets another gene called *IQGAP1* for degradation. Upon downregulation of *ISG15*, *IQGAP1* levels increase, and *IQGAP1* can stabilise *RAC1* and *CDC42* in their active GTP bound states in the absence of *DOCK6* by preventing GTP hydrolysis. Cells that activate this compensation mechanism can then overcome defects observed in an acute *DOCK6* knock-down condition, such as collapse of the actin cytoskeleton and membrane blebbing (Cerikan and Schiebel, 2019).

As *dock6-R11^{ins41}* mutant embryos had a loss of *dock6* expression, but otherwise appeared phenotypically normal, I wanted to investigate whether a similar compensation mechanism could be occurring in these mutant embryos, activated by a chronic loss of *dock6* expression. If this is the case, there would be reduced expression of *isg15* in *dock6-R11^{ins41}* mutant embryos. To investigate this, I designed an *in situ* hybridisation probe spanning the full length of the zebrafish *isg15* gene (GrcZ11, ENSDARG00000086374) to analyse expression of *isg15* in *dock6-R11^{ins41}* mutant embryos and wild-type siblings. Unexpectedly, *isg15* mRNA expression within zebrafish embryos at 3 and 6hpf in both wild-type and *dock6-R11^{ins41}* mutants is

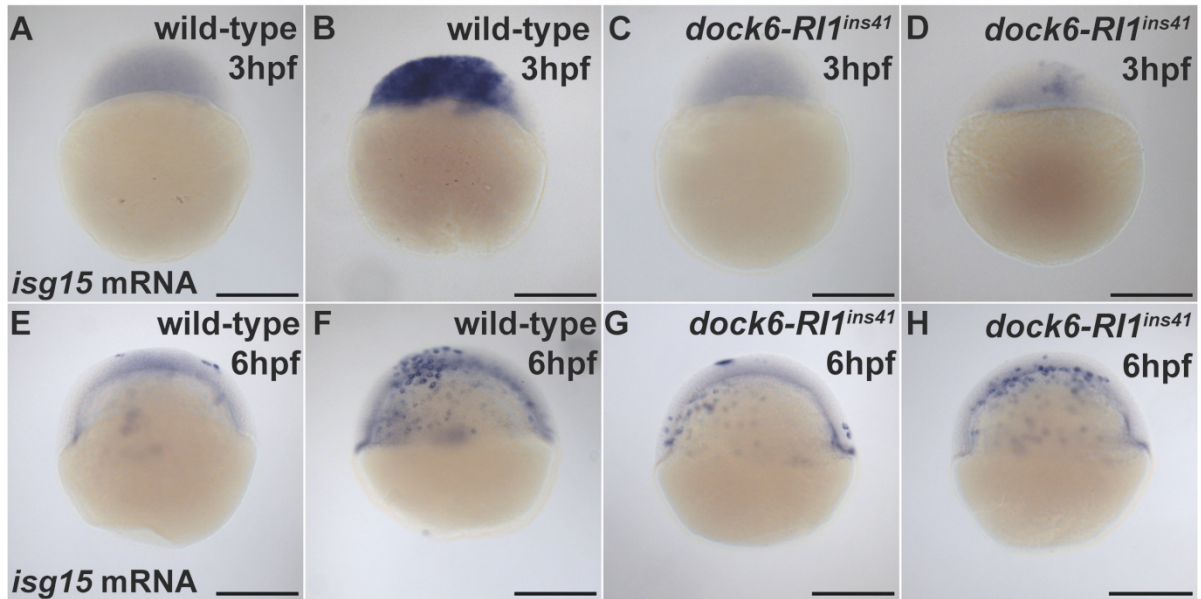


Figure 4.9. *isg15* expression is heterogeneous during zebrafish development. *in situ* hybridisation analysis of *isg15* mRNA expression in wild-type and *dock6-RI1^{ins41}* mutant embryos at 3hpf (A-D) and 6hpf (E-H). (A) A wild-type embryo at 3hpf with low levels of *isg15* expression, compared to another wild-type embryo at 3hpf displaying high levels of *isg15* expression (B). *isg15* expression is also variable among *dock6-RI1^{ins41}* mutant embryos at 3hpf, with some embryos expressing low levels (C) and some embryos expressing higher amounts of *isg15* mRNA (D). Heterogeneous expression of *isg15* persists at 6hpf with some wild-type embryos displaying low levels of expression (E) and others displaying higher levels of expression (F). Expression is also variable within the embryo, where subsets of cells exhibit higher levels of expression (E-F). Heterogeneous expression of *isg15* also occurs in *dock6-RI1^{ins41}* mutant embryos at 6hpf, with some embryos displaying lower expression (G) and some displaying higher levels of expression (H), and like wild-type embryos there are also differences in *isg15* expression at a cellular level (G-H). Scale bars: 200 μ m.

heterogeneous from embryo to embryo, with some embryos exhibiting almost no *isg15* expression and others with high levels of expression (Fig. 4.9 A-H). In addition, *isg15* expression at 6hpf is also heterogeneous within individual embryos at a cellular level, where some cells have high levels of expression and some cells have apparently no *isg15* expression (Fig. 4.9 E-H). This heterogeneity made it difficult to identify whether there was an overall reduction in *isg15* levels in *dock6-RI1^{ins41}* mutant embryos

compared to wild-types, however it led me to question whether the individual level of *isg15* within an embryo can be protective as to how well an embryo can adapt to mutations in *dock6*, and therefore be a predictor of whether an individual embryo will develop more severe phenotypes if they have mutations in *dock6*.

Although it is difficult to directly test whether this compensation mechanism is occurring only in some *dock6-RI1^{ins41}* mutant embryos due to the heterogeneous expression of *isg15*, previous studies have demonstrated that if compensation is occurring, this can be prevented by over-expressing *isg15* mRNA (Cerikan et al., 2016). Therefore, I cloned the zebrafish *isg15* open reading frame into the PCS2+ vector containing a 5' SP6 promoter and a 3' SV40 Poly(A) signal, allowing me to transcribe *isg15* mRNA for over-expression (Fig. 4.10 A). I first injected *isg15* mRNA into 1 cell stage wild-type embryos and confirmed the over-expression was working via *in situ* hybridisation at 6hpf which showed clearly elevated levels of *isg15* (Fig. 4.10 B&C), although this over-expression was mostly cleared by 24hpf (Fig. 4.10 D&E). Once I had confirmed that the over-expression worked, I investigated whether over-expressing *isg15* mRNA had any effect on cardiac morphology in *dock6-RI1^{ins41}* mutant embryos, since if the phenotypes between *isg15* injected and un-injected *dock6-RI1^{ins41}* mutant embryos differ, this would suggest that *dock6-RI1^{ins41}* mutant embryos are adapting to a loss of *dock6*, and it may reveal what roles Dock6 is playing during cardiac development.

4.8 Over-expressing *isg15* mRNA in *dock6-RI1^{ins41}* retained intron insertion mutant embryos leads to cardiac abnormalities

To investigate whether there is compensation due to a reduction in *dock6* expression in *dock6-RI1^{ins41}* mutant embryos, this compensation mechanism may be blocked via over-expressing *isg15* mRNA and presence of cardiac defects assessed, which may reveal insights into the roles Dock6 plays during cardiac development. Following *isg15* mRNA or water control injection in 1 cell stage embryos derived from an in-cross of *dock6-RI1^{ins41}* heterozygous adults, I raised embryos to 72hpf to assess cardiac morphology using light-sheet microscopy and MorphoHeart, analysing similar parameters to those previously described in *dock6-RI1^{ins41}* mutants, including chamber volumes, myocardial thickness, and chamber geometry. Alongside this, embryos were fixed at 6hpf to confirm the over-expression of *isg15* was successful.

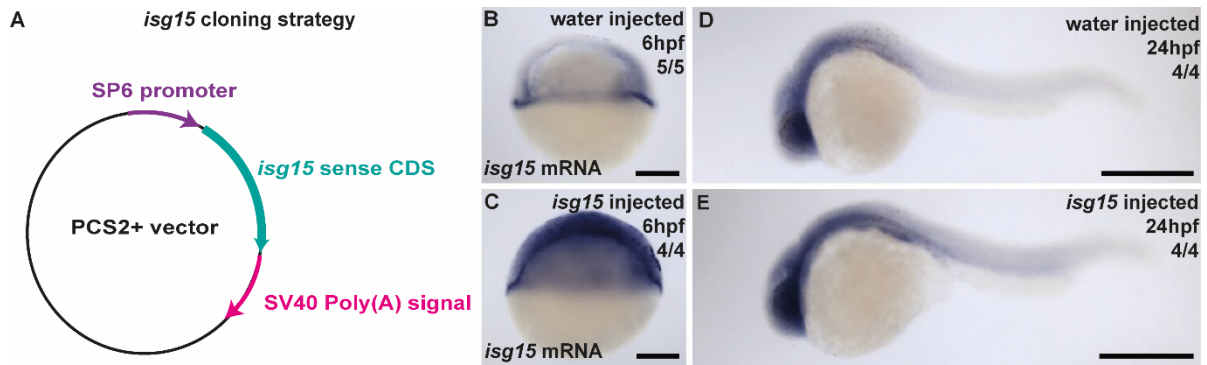


Figure 4.10. *isg15* coding sequence cloning strategy and RNA over-expression in zebrafish embryos. Cloning the *isg15* coding sequence to over-express *isg15* mRNA in zebrafish embryos to block potential compensation in *dock6-R11^{ins41}* mutants. (A) The full length *isg15* coding sequence (turquoise) was cloned into the PCS2+ vector containing a 5' SP6 RNA polymerase promoter (purple) and a 3' SV40 Poly(A) signal (pink) to allow transcription of *isg15* mRNA for over-expression experiments. *isg15* mRNA or water was injected into 1 cell stage zebrafish embryos and *isg15* expression was analysed at 6hpf and 24hpf by *in situ* hybridisation to test whether over-expression had worked (B-E). (B) A 6hpf water injected embryo showing wild-type expression of *isg15*, compared to an *isg15* mRNA injected embryo showing increased expression of *isg15* (C). (D) A 24hpf water injected zebrafish embryo showing wild-type *isg15* expression, with comparable expression in a 24hpf *isg15* mRNA injected zebrafish embryo (E), indicating that from 24hpf *isg15* mRNA over-expression is not maintained. Scale bars: B & C: 200µm, D & E: 500µm.

Following initial image processing of the wild-type and *dock6-R11^{ins41}* mutant hearts on Arivis image analysis software, which removes background and enhances the contours of the image (Fig. 4.11 A-D), I noticed that the morphology of the *dock6-R11^{ins41}* mutant hearts injected with *isg15* mRNA looked different compared to all control groups (wild-type embryos injected with either *isg15* mRNA or water and *dock6-R11^{ins41}* mutant embryos injected with water), particularly that the ventricles appeared to have an unusual shape and/or orientation (Fig. 4.11 D). As it was difficult to understand how the morphology was different in these mutant embryos from a 2D image, I created 3D rotating movies of the original light-sheet microscope image stacks using Imaris software, allowing me to analyse the morphology of these hearts

4. Investigating the role of *dock6*

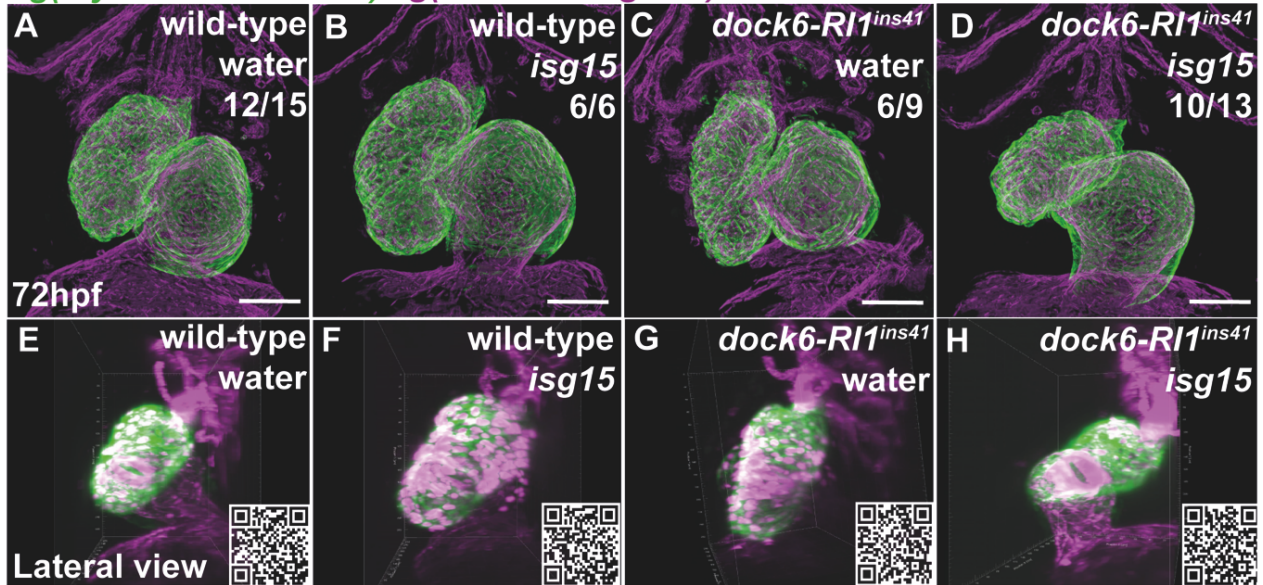
in more detail (Fig. 4.11 E-H). Visualisation of these hearts from a lateral view revealed that the *dock6-Rl1^{ins41}* mutant embryos injected with *isg15* mRNA had defects in chamber orientation, with the ventricles appearing to be tilted at a 90° angle in relation to the atrium (Fig. 4.11 H), rather than the two chambers being more aligned as seen in the wild-type controls and *dock6-Rl1^{ins41}* mutant embryos injected with water (Fig. 4.11 E-G). It is possible that the misplaced ventricle in *dock6-Rl1^{ins41}* mutant embryos injected with *isg15* mRNA could be due to misplacement of the whole heart, or from specific mispositioning of the ventricle, but it is difficult to determine exactly what the defect is from the light-sheet images. However, MorphoHeart can quantify chamber geometry and orientation to assess the relationship between the two chambers in more detail, by measuring both the ventral angle between the chambers (Fig. 4.11 I) and the sagittal angle between chambers (Fig. 4.11 J).

MorphoHeart analysis revealed that the ventral angle between chambers is not significantly different in *dock6-Rl1^{ins41}* mutant embryos injected with *isg15* mRNA compared to any of the controls (Fig. 4.11 K). However, the sagittal angle measured between the atrium and ventricle was significantly reduced in *dock6-Rl1^{ins41}* mutant embryos injected with *isg15* mRNA compared to both wild-types controls, but not significantly different from *dock6-Rl1^{ins41}* mutant embryos injected with water (Fig. 4.11 L). Differences in these phenotypes suggest that compensation could be occurring in these *dock6-Rl1^{ins41}* mutant embryos and that blocking compensation by over-expressing *isg15* mRNA leads to defects in chamber orientation.

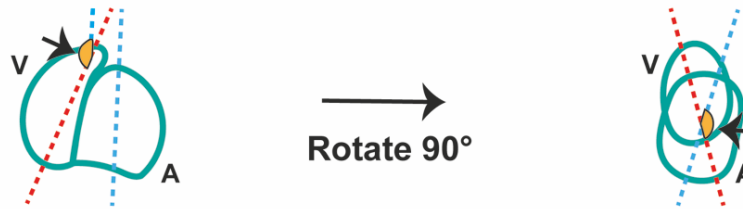
After observing defects in chamber orientation in *dock6-Rl1^{ins41}* mutant embryos injected with *isg15* mRNA, I wanted to see if there were any defects in OFT morphology, as chamber orientation is required to ensure correct connection to the vasculature at both poles of the heart (Bajolle et al., 2006), and it has been reported that mutations in *Rac1* in mice result in OFT defects (Leung et al., 2016). To assess OFT morphology, I injected embryos derived from a *dock6-Rl1^{ins41}* heterozygous mutant in-cross with either *isg15* mRNA or water at the 1 cell stage and imaged the OFT at 5dpf on the light-sheet microscope. In the single technical repeat of this experiment, the OFT in the *dock6-Rl1^{ins41}* mutant embryos injected with *isg15* mRNA (Fig. 4.12 D) did not seem to be morphologically different compared to the wild-type embryos (Fig. 4.12 A&B) or the homozygous mutants injected with water (Fig. 4.12

4. Investigating the role of *dock6*

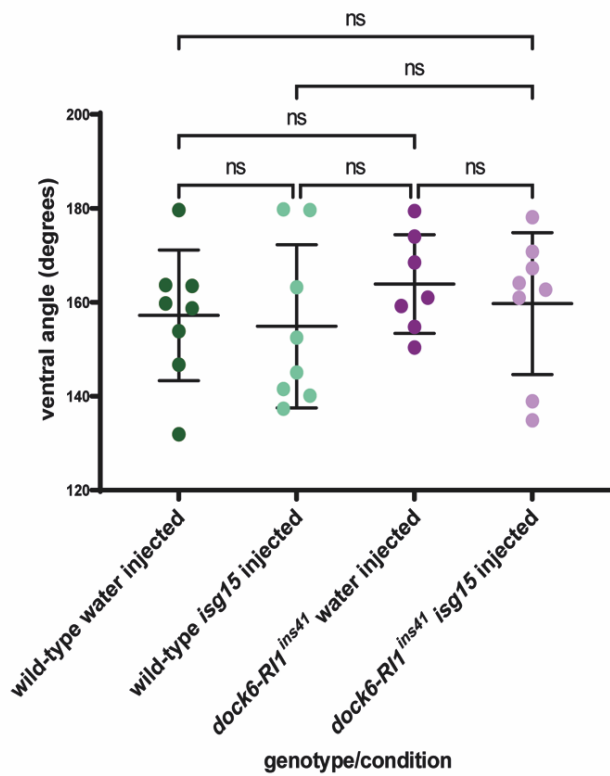
Tg(myI7:LifeACTGFP) *Tg(fli1a:AC-TagRFP)*



I Ventral Angle (Ventral View) J Sagittal Angle (Lateral View)



K Ventral Angle Between Chambers



L Sagittal Angle Between Chambers

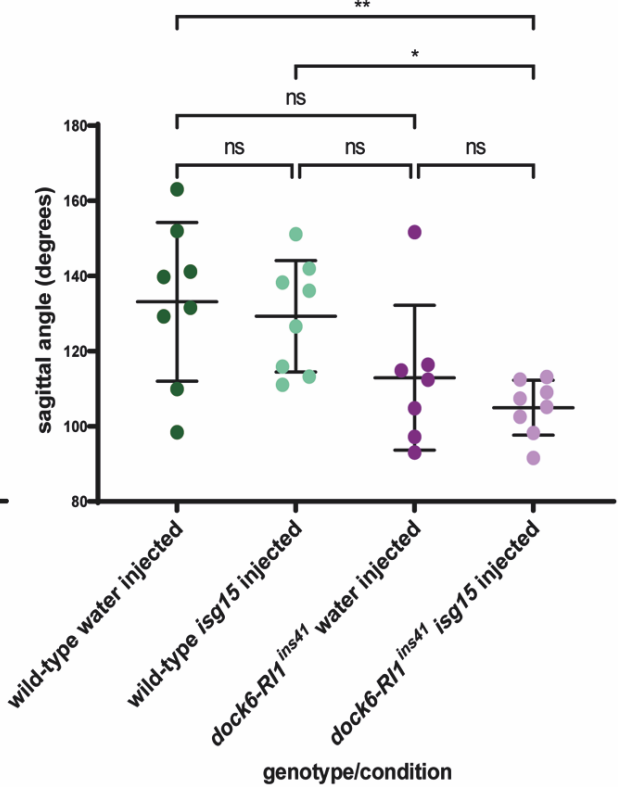


Figure 4.11. Over-expressing *isg15* mRNA in *dock6-R11^{ins41}* mutant embryos leads to chamber orientation defects. Light-sheet microscopy (A-H) and MorphoHeart image analysis (I-L) to quantify chamber orientation in *dock6-R11^{ins41}* mutant embryos. (A-D) Maximum intensity projections of light-sheet images of a heart at 72hpf with the *Tg(myI7:LifeActGFP)* transgene labelling the myocardium in green and the *Tg(fli1a:AC-TagRFP)* transgene labelling the endocardium in magenta, from a wild-type embryo injected with water (A), a wild-type embryo injected with *isg15* mRNA (B), a *dock6-R11^{ins41}* mutant embryo injected with water (C) and a *dock6-R11^{ins41}* mutant embryo injected with *isg15* mRNA (D). (E-H) Lateral views of these light-sheet images from the right side of the embryo with the ventricle in the foreground and the atrium in the background. 3D rotating movies of these hearts can be found by scanning QR codes next to the images. (I-J) Schematics showing how MorphoHeart quantifies the ventral angle between chambers (I) and the sagittal angle between chambers (J). (K) MorphoHeart analysis of the ventral angle between chambers in hearts from *dock6-R11^{ins41}* mutant embryos injected with *isg15* mRNA compared to wild-type controls or *dock6-R11^{ins41}* mutant embryos injected with water, revealing no significant differences. (L) MorphoHeart analysis shows in *dock6-R11^{ins41}* mutant embryos injected with *isg15* mRNA the sagittal angle between heart chambers is significantly reduced compared to wild-type control embryos, but not significantly different from the hearts of *dock6-R11^{ins41}* mutant embryos injected with water. K & L: mean \pm SD are plotted and analysed using One-Way ANOVA with Tukey's Multiple Comparisons test, ns: not significant, *: $P < 0.05$, **: $P < 0.01$. Mendelian ratio: wild-types = 13, heterozygotes = 25, homozygotes = 11.

C). Although no obvious morphological defects can be observed in these mutants injected with *isg15* mRNA, further quantitative analysis would be required to confirm this.

While using MorphoHeart to segment the different tissue layers of the heart, I wanted to assess whether cardiac defects associated with mutations in *Rac1/Cdc42* in mice (such as decreased chamber size and thinner ventricular myocardium) (Leung et al., 2014, Liu et al., 2017) were also present in *dock6-R11^{ins41}* mutants injected with *isg15* mRNA, to assess whether defects arising due to a loss of *dock6* could be due to

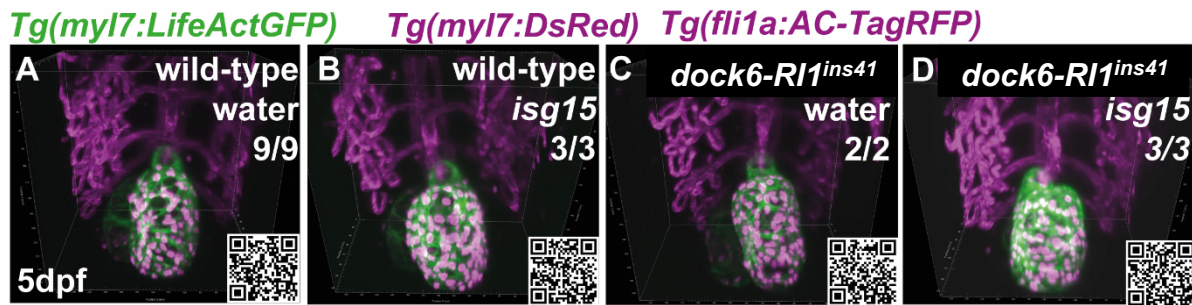


Figure 4.12. Over-expressing *isg15* mRNA in *dock6-RI1^{ins41}* mutant embryos has no effect on OFT morphology. (A-D) Maximum intensity projections of light-sheet ventral images of hearts at 5dpf with the *Tg(myI7:LifeActGFP)* transgene labelling the myocardium in green, the *Tg(fli1a:AC-TagRFP)* transgene labelling the endocardium in magenta, and the *Tg(myI7:DsRed)* transgene labelling the myocardial cell nuclei also in magenta. Images show comparable OFT morphology in hearts from wild-type embryos injected with either water (A) or *isg15* mRNA (B) and *dock6-RI1^{ins41}* mutant embryos injected with either water (C) or *isg15* mRNA (D). 3D rotating movies of these hearts can be found by scanning QR codes next to the images. Mendelian ratio: wild-types = 12, heterozygotes = 17, homozygotes = 5.

impaired RAC1/CDC42 activity. I first analysed myocardial volume and thickness in *dock6-RI1^{ins41}* mutant embryos injected with *isg15* mRNA, as reduced myocardial thickness is seen in mice with mutations in *Rac1* and *Cdc42*, and so similar defects could indicate that Dock6 is regulating Rac1/Cdc42 during cardiac development. Using MorphoHeart analysis I created 3D myocardial thickness heatmaps of hearts from wild-type and *dock6-RI1^{ins41}* mutant embryos injected with either *isg15* mRNA or water (Fig. 4.13 B-E). Despite it appearing from the heatmaps that the heart from the *dock6-RI1^{ins41}* mutant injected with *isg15* mRNA might have thinner myocardium, particularly in the ventricle (Fig. 4.13 E) compared to the *dock6-RI1^{ins41}* mutant injected with water (Fig. 4.13 D) or both wild-type controls (Fig. 4.13 B&C), following analysis of whole heart myocardium I found there was no significant difference in total myocardial tissue volume (Fig. 4.13 F). To see whether there was a reduction in myocardial tissue volume specifically in the ventricle, similar to what is described in *Rac1* mutant mice models, I separated out the atrium and ventricle myocardium thickness data, but I found there was no significant difference in the ventricle myocardium thickness in *dock6-RI1^{ins41}* mutants injected with *isg15* mRNA compared to controls (Fig. 4.13 H).

4. Investigating the role of *dock6*

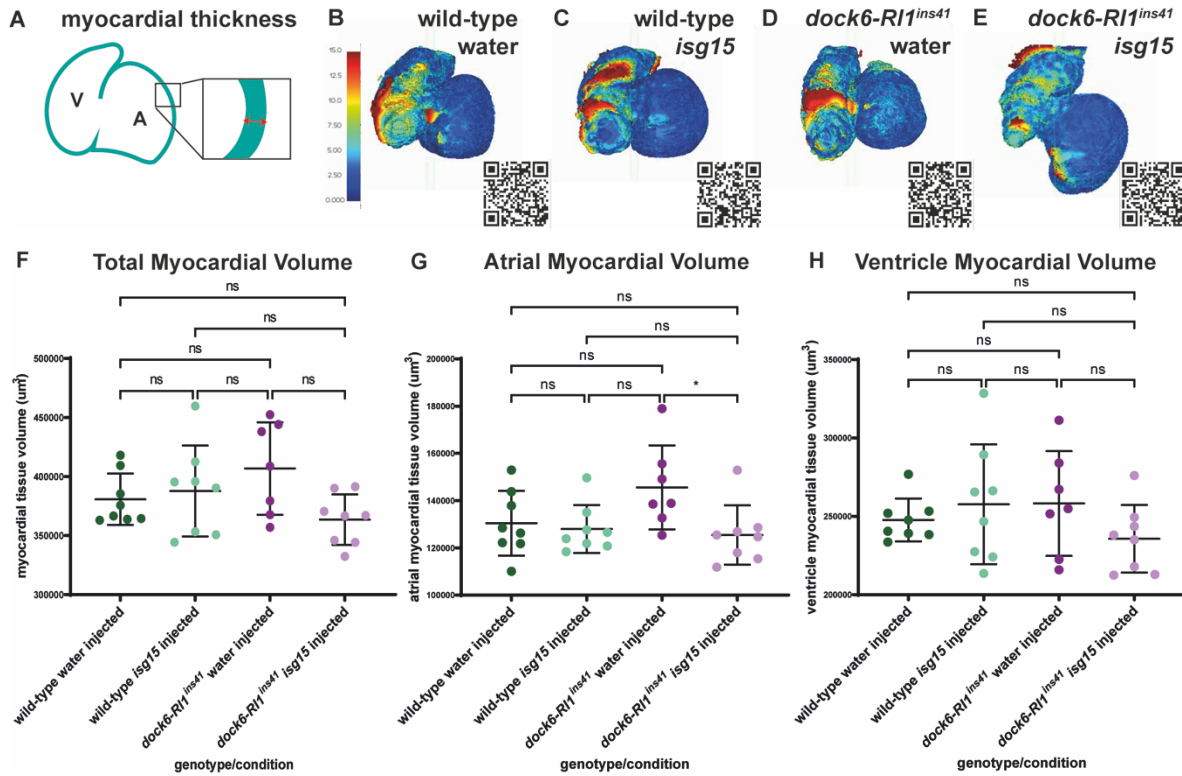


Figure 4.13. Over-expressing *isg15* mRNA in *dock6-R11^{ins41}* mutant embryos has no effect on myocardial tissue thickness. MorphoHeart myocardial thickness heatmaps (B-E) and quantitative analysis of myocardial tissue thickness (F-H). (A) Schematic showing how MorphoHeart measures myocardial tissue thickness. (B-E) Myocardial thickness heatmaps indicate thicker myocardial tissue with reds/yellows, and thinner myocardial tissue with greens/blues. Myocardial thickness 3D heatmaps from a wild-type embryo injected with water (B), a wild-type embryo injected with *isg15* mRNA (C), a *dock6-R11^{ins41}* mutant embryo injected with water (D) and a *dock6-R11^{ins41}* mutant embryo injected with *isg15* mRNA (E). 3D rotating movies of the myocardial thickness heatmaps can be found by scanning QR codes next to the images. MorphoHeart quantitative analysis indicated there was no significant difference in myocardial tissue thickness between wild-type and *dock6-R11^{ins41}* mutant hearts injected with either water or *isg15* mRNA for total myocardium volume (F) or ventricle myocardial volume (H). (G) There is no significant difference in atrial myocardial thickness between *dock6-R11^{ins41}* mutant embryos injected with *isg15* mRNA and either of the wild-type control conditions, however there is a significant difference in atrial myocardial thickness in *dock6-R11^{ins41}* mutant embryos injected with *isg15* mRNA compared to mutants injected with water, which appear to have

4. Investigating the role of *dock6*

thicker atrial myocardium. F: mean \pm SD are plotted and analysed using Kruskal-Wallis test with Dunn's Multiple Comparisons test, G&H: mean \pm SD are plotted and analysed with one-way ANOVA with Tukey's Multiple Comparisons test, *: $P < 0.05$, ns: not significant.

When analysing the atrium myocardium thickness, I did find this was significantly reduced in *dock6-RI1^{ins41}* mutants injected with *isg15* mRNA compared to mutants injected with water, which appeared to have thicker myocardial tissue. However, neither of the mutants injected with either *isg15* mRNA or water had significantly different atrial myocardial thickness when compared to the control conditions (Fig. 4.13 G).

I next analysed heart size and growth using MorphoHeart to quantify myocardial ballooning, measuring growth of the heart chamber walls away from the central midline of the heart. Heatmaps of myocardial ballooning indicate greater ballooning in red and yellow, with less ballooning being shown in green and blue (Fig. 4.14 B-E). At 72hpf, *dock6-RI1^{ins41}* mutant embryos injected with *isg15* mRNA showed reduced myocardial ballooning compared to wild-types injected with either *isg15* mRNA or water, and *dock6-RI1^{ins41}* mutant embryos injected with water, particularly in the ventricle and around the ventricular apex, as indicated by less red and yellow on the heatmap (Fig. 4.14 E). This suggests that these hearts are failing to grow to the same extent as the control hearts, however the total heart volume is not significantly different in *dock6-RI1^{ins41}* mutant embryos injected with *isg15* mRNA compared to controls, indicating that heart growth is not restricted in these mutants, or that geometry of the ballooning is not the same (Fig. 4.14 F). Additionally, the volume of the atrium or the ventricle is not significantly different in *dock6-RI1^{ins41}* mutant embryos injected with *isg15* compared to controls (Fig. 4.14 G&H) suggesting no defects in individual chamber growth. Together this data suggests that blocking compensation in *dock6-RI1^{ins41}* mutant embryos leads to decreased heart myocardial ballooning, however the overall size of the hearts in these mutants is not significantly different compared to controls, which could suggest altered heart geometry. Overall, it appears that loss/reduction of *dock6* expression in *dock6-RI1^{ins41}* mutant embryos appears to be compensated for in some mutants, as over-expressing *isg15* mRNA in an attempt to prevent activation of a compensating pathways leads to cardiac defects which are not observed in the

4. Investigating the role of *dock6*

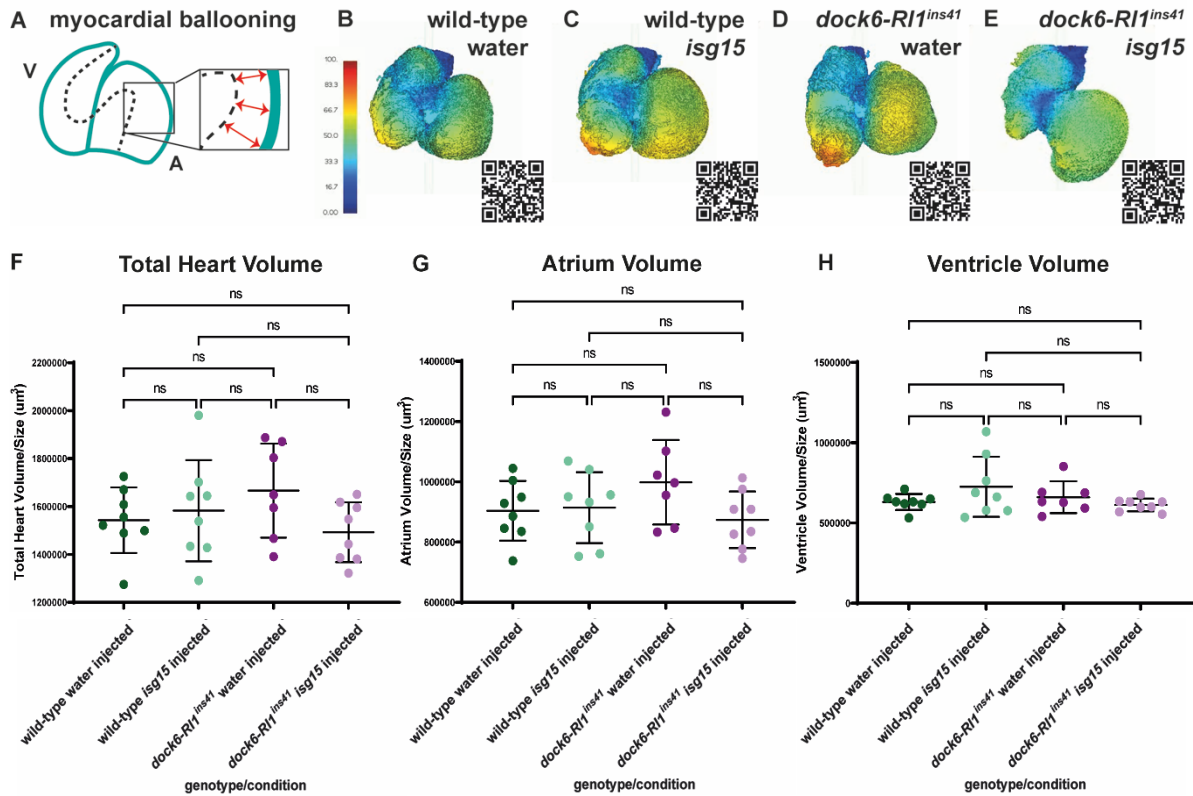


Figure 4.14. Over-expressing *isg15* mRNA in *dock6-R11^{ins41}* mutant embryos has no effect on heart size but does cause reduced myocardial ballooning. MorphoHeart myocardial ballooning heatmaps (**B-E**) and quantitative analysis of heart volume (**F-H**). (**A**) Schematic showing how MorphoHeart quantifies myocardial ballooning by measuring the distance that myocardial tissue balloons away from the central midline of the heart. (**B-E**) Myocardial ballooning heatmaps indicate greater chamber ballooning with reds/yellows, and less chamber ballooning with greens/blues. Myocardial ballooning heatmaps from a wild-type embryo injected with water (**B**), a wild-type embryo injected with *isg15* mRNA (**C**), a *dock6-R11^{ins41}* mutant embryo injected with water (**D**) and a *dock6-R11^{ins41}* mutant embryo injected with *isg15* mRNA, showing reduced myocardial ballooning (**E**). 3D rotating movies of the myocardial ballooning heatmaps can be found by scanning QR codes next to the images. MorphoHeart quantitative analysis indicated there was no significant difference between wild-type and *dock6-R11^{ins41}* mutant hearts injected with either water or *isg15* mRNA for total heart volume (**F**), atrial volume (**G**) or ventricle volume (**H**). **F, G & H**: mean \pm SD are plotted and analysed with one-way ANOVA with Tukey's Multiple Comparisons test, ns: not significant.

control *dock6-RI1^{ins41}* mutant embryos injected with water, such as decreased myocardial ballooning and chamber orientation defects.

4.9 *dock6-201^{ins36Δ65}* coding sequence mutation has no effect on *dock6-201* expression or cardiac development

In addition to characterising the *dock6-RI1* retained intron mutant lines, I also investigated what effect a mutation in the *dock6-201* protein-coding transcript would have on heart morphology. As I failed to recover a founder through the *dock6-201* promoter-less mutant strategy, I recovered a *dock6-201* coding sequence mutant from my attempts to generate a *dock6* disease-specific knock-in mutant, identifying an F0 founder transmitting a 36bp insertion and 65bp deletion at the end of exon 37 (Fig. 4.15 A). This mutation substitutes 12 amino acids and deletes a further 18 amino acids, 23 of which are conserved between humans and zebrafish. These mutated amino acids are located before the DHR2 domain which is required for GEF activity in the Dock6 protein (Fig. 4.15 B), but this mutation does not cause a frameshift. Despite mutating many conserved amino acids in the Dock6 protein, this mutation appears to have no effect on *dock6-201* expression, which is comparable to wild-types with clear expression throughout the head and midbrain-hindbrain boundary in *dock6-201^{ins36Δ65}* embryos (Fig. 4.15 D&E).

Although there does not seem to be any difference in *dock6-201* expression in these mutant embryos, the loss of conserved amino acids could still compromise Dock6 function, and I therefore investigated heart morphology in *dock6-201^{ins36Δ65}* mutant embryos. I imaged these hearts on the light-sheet microscope at 72hpf to assess cardiac morphology in 3D, however I found no obvious defects in heart development in mutant hearts compared to wild-type siblings (Fig. 4.15 F&G). To ensure that there were no other phenotypic defects in these mutants I also raised *dock6-201^{ins36Δ65}* homozygous mutant embryos and wild-type siblings to adulthood, but these fish appeared healthy with no obvious gross morphological defects at 3 months old, suggesting that the *dock6-201^{ins36Δ65}* is not having any effects of Dock6 protein function which would result in lethality or defects in adulthood.

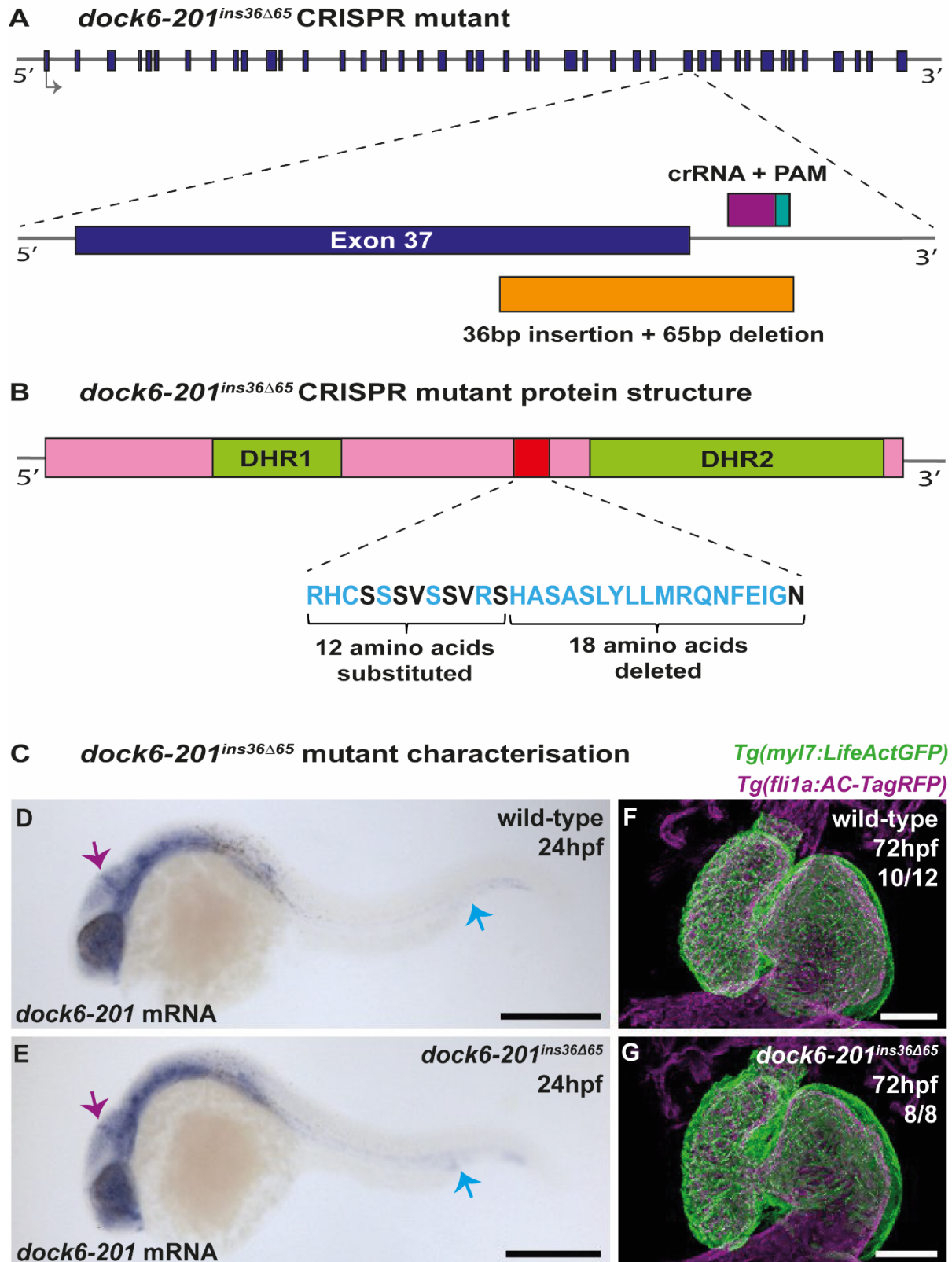


Figure 4.15. *dock6-201^{ins36Δ65}* mutation has no effect on *dock6-201* expression or heart morphology. (A) Zebrafish *dock6-201* transcript composed of 50 exons,

4. Investigating the role of *dock6*

highlighting exon 37 (dark blue) where the *dock6-201^{ins36Δ65}* mutation was created (orange). (B) Dock6 protein structure (pink) with the DHR1 and DHR2 domains annotated (light green) and the *dock6-201^{ins36Δ65}* mutation (red) upstream of the DHR2 domain. This mutation substitutes 12 amino acids and deletes a further 18 from the Dock6 protein, 23 of which are conserved between humans and zebrafish (light blue text). (C) Characterisation of *dock6-201^{ins36Δ65}* mutants through analysis of *dock6-201* mRNA expression at 24hpf using *in situ* hybridisation (D-E) and heart morphology at 72hpf using light-sheet microscopy (F-G). (D) *dock6-201* is expressed throughout the head and in the midbrain-hindbrain boundary (purple arrow), along with the somite boundaries of the tail (blue arrow) in wild-type embryos at 24hpf. (E) *dock6-201* expression appears comparable to wild-types in *dock6-201^{ins36Δ65}* mutant embryos with expression visible throughout the head and in the midbrain-hindbrain boundary (purple arrow) and in the somite boundaries of the tail (blue arrow). (F) Maximum intensity projections of light-sheet images showing a ventral view of a 72hpf heart from a wild-type embryo with the *Tg(myl7:LifeActGFP)* transgene labelling the myocardium in green and the *Tg(fli1a:AC-TagRFP)* transgene labelling the endocardium in magenta. (G) Heart morphology in *dock6-201^{ins36Δ65}* mutant embryos is comparable to wild-type siblings at 72hpf. Scale bars: D & E: 500µm. F & G: 50µm. Mendelian ratio *dock6-201 in situ* hybridisation: wild-types = 3, heterozygotes = 6, homozygotes = 5; mendelian ratio light-sheet imaging: wild-types = 12, heterozygotes = 25, homozygotes = 8.

4.10 Discussion

In Chapter 4 I investigate the role of *dock6* during cardiac development, with the aim of understanding how it could be involved in the onset of CHDs in AOS patients. I characterise two *dock6-R11* retained intron transcript mutant zebrafish lines, showing that the two mutations have different effects on *dock6-201* and *dock6-R11* expression, and in addition characterise heart morphology in these mutants. I investigate a compensation mechanism in *dock6-R11^{ins41}* homozygous mutant embryos which allows them to adapt to a loss of *dock6-201* expression, and show that when this compensation mechanism is blocked, cardiac defects are observed in these mutants. Finally, I characterize a *dock6-201* coding sequence mutant, but show that this mutation has minimal effects on *dock6-201* expression or cardiac development.

4. Investigating the role of *dock6*

Despite having a reduction in *dock6* expression, *dock6-R11^{ins41}* mutant embryos did not display cardiac defects. As it is known that chronic loss of DOCK6 function triggers a cell intrinsic adaptation mechanism in human fibroblast cells derived from AOS patients with mutations in *DOCK6* (Cerikan and Schiebel, 2019), I wanted to investigate if the same was true in *dock6-R11^{ins41}* mutant embryos which also have a reduction in *dock6* expression. As described in Cerikan et al., under acute *DOCK6* depletion, for example siRNA targeting of *DOCK6*, there is a reduction in RAC1 and CDC42 activity leading to cytoskeletal defects such as cell rounding and membrane blebbing. However, under chronic depletion of *DOCK6*, such as CRIPSR/Cas9 knock-out, cells can adapt to this loss of *DOCK6* and recover cytoskeletal defects within 120 hours following depletion. This adaptation mechanism is due to a compensation pathway triggered by an increase in globular actin levels within the cell. Actin polymerisation states within a cell can regulate gene expression through serum response factors (SRF) and myocardin related transcription factors (MRTF), and increased globular actin binds to MRTF/SRF and sequesters it in the cytoplasm preventing it from translocating to the nucleus. As MRTF/SRF regulates expression of the small ubiquitin like modifier interferon stimulated gene 15 (*ISG15*), this sequestration of MRTF/SRF in the cytoplasm leads to a reduction in *ISG15* expression levels. The main target of *ISG15* in this compensation pathway is a protein called IQ motif containing GTPase activating protein 1 (IQGAP1), which is involved in actin cytoskeleton regulation and can stabilise RAC1 and CDC42 in their active GTP bound states by preventing GTP hydrolysis. As *ISG15* expression is reduced, this leads to increased levels of IQGAP1, which is normally targeted for degradation by *ISG15*, leading to IQGAP1 dependent stabilisation of RAC1 and CDC42 in the absence of *DOCK6*, and recovery of actin cytoskeletal defects observed when *DOCK6* is acutely knocked down (Cerikan et al., 2016).

Human fibroblast cells derived from AOS patients with mutations in *DOCK6* showed a 4-fold decrease in *ISG15* mRNA levels, and a double knock-out of both *ISG15* and *DOCK6* leads to an increased adaptation to *DOCK6* loss indicated by higher levels of active RAC1 and CDC42 (Cerikan and Schiebel, 2019). Similarly, this compensation mechanism can be blocked by over-expressing *ISG15* mRNA, leading to actin cytoskeletal defects in *DOCK6* knock-out cells but having no effect on actin cytoskeletal dynamics in wild-type cells (Cerikan et al., 2016). This could provide

4. Investigating the role of *dock6*

insights into the pathology and varied penetrance of AOS in patients with *DOCK6* mutations, as higher levels of *ISG15* expression could worsen phenotypes, while lower levels of *ISG15* expression could enhance adaptation to a loss of *DOCK6*.

While testing whether this compensation mechanism was occurring in *dock6-RI1^{ins41}* mutant embryos which have a reduction in *dock6* expression, I found that *isg15* mRNA expression at 3 and 6hpf was heterogeneous from embryo to embryo, and even from cell to cell within one embryo. Despite this variability in *isg15* expression making it difficult to identify whether this compensation pathway is occurring, it did raise the question as to whether the level of *isg15* expression within individual embryos can make them able to adapt to a loss of *dock6* expression if they possess mutations in the *dock6* gene, especially since patients with AOS suffer from a spectrum of feature severity (Dudoignon et al., 2019). It would be interesting to investigate phenotypic variability in a larger number of *dock6-RI1^{ins41}* mutant embryos using MorphoHeart to see whether there are some embryos with disrupted cardiac morphology, as seen in Figure 4.6, and whether this correlates with baseline levels of *isg15* expression. One way this could be investigated is to clone the *isg15* promoter upstream of a GFP construct to select embryos with higher levels of *isg15* expression at 6hpf and investigate heart morphology in these embryos at later stages. It would also be interesting to acquire cell data from AOS patients with mutations in *DOCK6* and see if there is any correlation between *ISG15* expression levels and severity of phenotype, however this might be difficult to analyse as variability in *ISG15* levels might be at very early developmental stages, like in zebrafish, making it difficult to access this data. Transcriptional heterogeneity during development is not uncommon, and variation in levels of gene expression known as transcriptional noise is thought to occur in undifferentiated cells prior to cell differentiation to trigger commitment to certain cell fates (Mohammed et al., 2017). Cell differentiation begins as early as 4hpf in zebrafish, at which point germ-layer specific markers can be detected (Xiao et al., 2016). As this is just after the time I begin observing heterogeneity in *isg15* expression in 3hpf embryos, we can speculate that the *isg15* heterogeneity at 6hpf in zebrafish could be transcriptional noise occurring prior to cell differentiation, like that observed in mice embryos (Mohammed et al., 2017). It would therefore be interesting to assess whether this heterogeneity in *isg15* expression has any consequences for the embryo, particularly in the ability to compensate for a loss of *dock6*.

4. Investigating the role of *dock6*

Although the heterogeneity of *isg15* expression made it difficult to assess whether there is compensation occurring in *dock6-Rl1^{ins41}* mutant embryos, I could examine expression levels of other compensation pathway components, for example assessing whether expression of *iqgap1* increases, or alternatively whether there is increased globular actin levels within cells derived from these embryos using fluorescently labelled DNaseI which binds to globular actin (Cramer et al., 2002). I could also attempt to look at protein levels, however there is currently no available antibody which is predicted/shown to recognise Isg15 in zebrafish. Additionally, it is unknown whether other components of the compensation pathway, like *isg15*, are also expressed heterogeneously, and so it might not be as clear as global up/down regulation of these genes to indicate whether the compensation pathway is active. To overcome this, I could modulate components of the compensation pathway to see if I can phenocopy *isg15* over-expression. For example, if attempting to knock-out *iqgap1* in *dock6-Rl1^{ins41}* mutant embryos, which would prevent adaptation to a loss of *dock6*, results in the same phenotypes as over-expression of *isg15* in *dock6-Rl1^{ins41}* mutant embryos it would confirm that the compensation pathway is active in these mutants.

Following over-expression of *isg15* mRNA in *dock6-Rl1^{ins41}* mutant embryos, I found this led to chamber orientation defects and decreased myocardial ballooning in hearts at 72hpf, suggesting that compensation is occurring in these embryos to restore Rac1 activity in the absence of Dock6, and preventing cardiac abnormalities from arising. Although it has not yet been shown that there is a reduction in Rac1/Cdc42 activity in *dock6-Rl1^{ins41}* mutant embryos injected with *isg15*, similar defects can be observed in other animal models with *Rac1/Cdc42* mutations. In mice, mutations in *Rac1* in the pre-cardiac mesoderm led to thin, disorganised myocardial walls and defects in OFT alignment, despite the hearts initially forming a heart tube which looped correctly. *Rac1* mutant mice then suffer from oedema and haemorrhage which leads to lethality, and as no significant difference was found in cell death or cell proliferation in these hearts, it is thought that RAC1 is required within cardiomyocytes to facilitate cell-cell and cell-extracellular matrix adhesions (Abu-Issa, 2015). In another study also conducted in mice, myocardial specific deletion of *Rac1* produced similar phenotypes, such as thin and disorganised myocardial tissue, with reduced expression of the planar cell polarity gene *Scrib* in the myocardium (Leung et al., 2021). These mice also suffered from a range of CHDs similar to those identified in patients with mutations in *DOCK6*, such

as double outlet right ventricle, ventricular septal defects and overriding aorta (Sukalo et al., 2015). Unlike the previous study, this study found that *Rac1* mutations in myocardial cells led to a reduction in myocardial cell proliferation in these hearts, suggesting that RAC1 is required in the myocardium for both cell organisation and proliferation (Leung et al., 2021). Defects described in *Rac1* mutant mice, such as thin disorganised myocardial walls, overlap with defects seen in *dock6-R11^{ins41}* mutant zebrafish embryos injected with *isg15*, for example decreased myocardial ballooning, and we can therefore speculate that disrupted *Rac1* activity is also responsible for these defects arising.

Further studies in mice investigated the effects of *Rac1* mutations in the SHF and found similar cardiac defects, such as disrupted cellular organisation and proliferation, and reduced SHF migration into the OFT, resulting in OFT and valve defects. This study also found that there was reduced expression of the cardiac neural crest (CNC) chemoattractant Semaphorin3c, likely resulting in a reduction in CNC cells to the heart and worsening the OFT defects observed (Leung et al., 2016). Another study found that mutating *Rac1* in the SHF led to a disruption in cell polarity, along with defects in lamellipodia formation and cell elongation, resulting in decreased cell migration (Leung et al., 2014). Together this data suggests that RAC1 is required in both the primary myocardial cells and SHF cell population to ensure correct cell polarity and cell migration into the heart for development to occur correctly. As SHF and CNC cells contribute to OFT and ventricle myocardial tissue in the developing zebrafish heart (Li et al., 2003), it is possible that defects such as chamber orientation and decreased ventricle myocardial ballooning in *dock6-R11^{ins41}* mutant embryos could arise due to similar defects in SHF and CNC migration.

Mutations in *Cdc42* within mice embryonic cardiomyocytes produced similar phenotypes to mutations in *Rac1*. Knock-out of *Cdc42* in mice cardiomyocytes resulted in thin ventricular myocardial tissue and ventricular septal defects, eventually resulting in lethality (Liu et al., 2017). Another study in mice also found *Cdc42* mutations in cardiomyocytes caused reduced cell proliferation and cell-cell adhesions, resulting in thin ventricular walls and ventricular septal defects (Jieli Li et al., 2017). It has also been shown that CDC42 is required in CNC cells to facilitate their migration into the OFT, and when CDC42 fails to localise correctly within these cells it leads to

restricted cell migration resulting in OFT defects (Fritz et al., 2019). In *Drosophila* embryos, *Cdc42* is required in a specific subset of Cardioblast cells which migrate together to form the embryonic heart tube, and when *Cdc42* is mutated in these cells they fail to migrate or form cell-cell contacts with neighbouring Cardioblasts (Swope et al., 2014). Additionally, *Drosophila Cdc42* mutant Cardioblasts fail to polarize and form cell-cell adhesions with neighbouring cells, resulting in defects in cardiac lumen formation (Vogler et al., 2014). Together this data suggests, alike RAC1, CDC42 is required in developing cardiomyocytes to regulate their proliferation, polarisation, and cell migration, along with being important for the formation of cell-cell adhesions. Again, similarities between defects seen in mice with mutations in *Cdc42*, such as thin ventricular walls, and defects in *dock6-RI1^{ins41}* mutant zebrafish embryos injected with *isg15*, such as reduced myocardial ballooning, could indicate that these defects are arising via *Cdc42* inactivity in the absence of *Dock6*.

These studies investigating the roles of RAC1 and CDC42 in cardiomyocytes could provide insights into the defects observed in *dock6-RI1^{ins41}* mutant embryos injected with *isg15* mRNA, where I suggest that compensation due to a loss of *dock6* expression is blocked. Loss of both *Dock6* function and the compensating pathway could therefore lead to decreased activity of the downstream targets of *dock6*, *Rac1* and *Cdc42*, however I have yet to show this is the case in the models presented in this thesis. I could test whether there is a reduction in *Rac1* and *Cdc42* activities in cardiomyocytes using Raichu-*Rac* and Raichu-*Cdc42* fluorescent resonance energy transfer (FRET) based sensors which consist of the *Rac1/Cdc42* binding domain of PAK, along with *Rac1* or *Cdc42*, and two fluorescent proteins (e.g. CFP and YFP). FRET biosensors work via a conformational change upon activation, resulting in altered distance between the two fluorophores and thereby changing the amount of energy transfer between the two fluorophores, allowing indication of whether the biosensor is active or not (Kardash et al., 2011). For example, when *Rac1/Cdc42* are in their inactive GDP bound states they do not bind to the PAK binding domain resulting in increased energy transfer between the two fluorophores which are close together in proximity, however upon *Rac1/Cdc42* activation they then bind to the PAK binding domain, leading to a conformational change in the biosensor and separating the fluorophores further away from each other resulting in reduced energy transfer. Therefore, by calculating the ratio of fluorophore emission it is possible to determine

4. Investigating the role of *dock6*

whether Rac1/Cdc42 are in their active or inactive states. As these FRET biosensors work in both live and fixed tissue (Kardash et al., 2011), I could inject them into one-cell stage *dock6-R11^{ins41}* mutant embryos along with *isg15* mRNA, and investigate Rac1 and Cdc42 activities in *myl7*-RFP-tagged myocardial cells to determine whether Rac1 and Cdc42 activities are reduced in the developing heart myocardium.

Despite not knowing whether defects arising in *dock6-R11^{ins41}* mutant embryos injected with *isg15* are due to reduced activity of Rac1/Cdc42, similar defects have been observed in mice models with *Rac1/Cdc42* mutations, for example numerous studies report thinner myocardial tissue and I observed a reduction in myocardial tissue ballooning in *dock6* mutants with *isg15* over-expression (see Figure 4.14). Although currently unproven, it is possible that chamber orientation defects could arise due to a lack of myocardial ballooning which could be required to orientate the chambers correctly. CHDs were commonly observed in other animal models with mutations in *Rac1* and *Cdc42*, and it would be interesting to investigate whether further structural malformations arise in later stage *dock6-R11^{ins41}* mutant embryos with blocked compensation, as it is known that looping and ballooning in developing hearts is required to properly align the chambers and cardiac vasculature to ensure the heart can establish a double circulatory system (Garrec et al., 2017). If this process fails to occur correctly, this increases the likelihood of developing CHDs similar to those found in AOS patients with mutations in *DOCK6*, such as ventricular septal defects (Alkhateeb et al., 2021) and Tetralogy of Fallot (Männer, 2009). It has also been shown that actin cytoskeletal dynamics are involved in orchestrating myocardial ballooning as analysis of a *myo5b* mutant zebrafish model which has failed myocardial ballooning demonstrated that cardiomyocytes had actin cytoskeletal defects and a lack of correctly localized N-cadherin (Grassini et al., 2019). These processes are Rac1/Cdc42 dependent, so we can speculate that similar defects in actin cytoskeletal dynamics and N-Cadherin localisation could be contributing to the ballooning defects observed in *dock6-R11^{ins41}* mutant embryos injected with *isg15*. To test whether this is the case, I could utilise an N-cadherin antibody along with high resolution microscopy to investigate localisation of N-cadherin to adherens junctions in the *dock6-R11^{ins41}* mutant hearts. To investigate whether cytoskeletal dynamics are disrupted, I could utilise the *Tg(myl7:LifeActGFP);Tg(fli1a:AC-TagRFP)* double transgenic line which labels myocardial and endocardial actin, along with high resolution microscopy to

4. Investigating the role of *dock6*

assess whether actin organisation appears disrupted in the myocardium and endocardium of *dock6-R11^{ins41}* mutant embryos injected with *isg15*.

The decreased myocardial ballooning in the hearts of *dock6-R11^{ins41}* mutant embryos injected with *isg15* could also be linked to growth defects in the heart. Studies in mice have shown that RAC1 and CDC42 have been found to be important for myocardial cell proliferation and migration of the SHF, and mutations in *Rac1/Cdc42* in the SHF results in thinner myocardium (Leung et al., 2014). To investigate whether similar defects in SHF migration are occurring in *dock6-R11^{ins41}* mutants injected with *isg15*, I could utilise the *Tg(myI7:DsRed)* transgenic line which labels myocardial cell nuclei to look at myocardial cell number between 24 and 72hpf when SHF addition occurs (Liu and Stainier, 2012). Reduced myocardial cell numbers indicating potential defects in SHF addition could then be investigated further by visualising SHF addition using the *Tg(myI7:eGFP);Tg(myI7:DsRed)* double transgenic line, whereby myocardial cells which make up the original heart tube express both green and red fluorophores, and any cells added to the heart tube more recently from the SHF will only express GFP due to the longer maturation time of dsRed, allowing quantification of cells added to the heart from the SHF (Pater et al., 2009). If there appears to be a reduction in cell number at later stages of development, when the heart grows mainly due to cell proliferation (Günthel et al., 2018), I could utilise BrdU incorporation assays to assess the rate of cell proliferation at these stages in *dock6-R11^{ins41}* mutant embryos injected with *isg15*. Additionally, by labelling the nuclei of the hearts, for example using the *Tg(myI7:DsRed)* transgenic line, I can investigate whether a reduction in myocardial cell size in *dock6-R11^{ins41}* mutant embryos injected with *isg15* contributes to reduced chamber ballooning by measuring internuclear distance between cells as a proxy for cell size.

As mouse models with mutations in *Rac1* and *Cdc42* showed defects in cell polarity, resulting in cardiac defects similar to the ones I observe in *dock6-R11^{ins41}* mutant embryos injected with *isg15*, such as reduced myocardial growth (Leung et al., 2014), it would be interesting to investigate cell polarity in *dock6-R11^{ins41}* mutants injected with *isg15*. To do this, I could utilise *in situ* hybridisation probes and antibodies for *Scrib*, a cell polarity gene which is downregulated in mice with mutations in *Rac1* in the SHF (Leung et al., 2014), and determine whether *Scrib* localisation is disrupted in the

4. Investigating the role of *dock6*

myocardium of *dock6-R11^{ins41}* mutants injected with *isg15*, indicating defects in cell polarity. Additionally, as mice models with mutated *Rac1* in the myocardium suffer from hypertrabeculation (Leung et al., 2021), it would be interesting to investigate whether any defects arise in ventricular trabeculation in *dock6-R11^{ins41}* mutant embryos injected with *isg15*, as reduced ventricle ballooning could indicate defects in trabeculation due to the ventricle not developing correctly.

Raising *dock6-R11^{ins41}* mutant embryos injected with *isg15* mRNA to adulthood, along with the mutant siblings injected with water and wild-type siblings injected with both *isg15* mRNA and water, would give insights into whether these fish are viable, but also allow investigation into whether they suffer from heart defects, or any other defects like those found in AOS patients (such as ACC/TTLD or neurological defects) later in juvenile stages or early adulthood. It would also be interesting to repeat the behavioural analysis experiments on *dock6-R11^{ins41}* mutant embryos injected with *isg15* mRNA, as it could be possible that behavioural phenotypes are also being masked by the same compensation mechanism, perhaps explaining why no behavioural phenotypes were seen in the *dock6-R11^{ins41}* mutant embryos despite a reduction in *dock6* expression throughout the head (see Figure. 4.8). I could also utilise other behavioural assays which have been designed to study zebrafish behavioural disorders to investigate whether these mutants have elevated anxiety following exposure to certain stresses, whether they show normal social interactions with other fish, or whether they display defects in learning abilities, all of which could give insights into whether these mutants display defects in cognitive development (Kalueff et al., 2014).

Despite creating 3 different *dock6* mutant zebrafish lines, only the *dock6-R11^{ins41}* mutant seemed to have any effect on *dock6* expression, despite the mutation being created in a similar region to the *dock6-R11^{Δ28}* mutation which appeared to have no effect on expression of either of the *dock6* transcripts. The only *dock6-201* mutant line I managed to recover with disrupted exonic sequence was the *dock6-201^{ins36Δ65}* mutant, which substitutes 12 amino acids and removes a further 18 amino acids at the end of exon 37 of the *dock6-201* gene. Despite 23 of these mutated amino acids being conserved between humans and zebrafish, this mutation appears to have no effect on zebrafish viability or lead to cardiac defects. We can speculate that this is due to the

fact that this mutation does not disrupt either of the DHR domains in the Dock6 protein required for membrane localisation or GEF activity, and as the mutation is in frame and does not encode a premature stop codon prior to the DHR2 GEF domain (like the human AOS patient mutation I aimed to knock-in) it is likely that this mutation is not preventing Dock6 from being able to activate Rac1 and Cdc42. Additionally, it has been shown that mutant mRNA transcripts which undergo nonsense mediated decay can trigger genetic compensation via upregulation of related genes which can then mask mutant phenotypes (El-Brolosy et al., 2019), so it is also possible that if this *dock6-201^{ins36Δ65}* mutation causes degradation of *dock6-201* mRNA, it could trigger compensation by upregulating expression of another *dock6* transcript or related gene which is carrying out a similar function. However, as I do not observe a reduction in *dock6-201* expression in *dock6-201^{ins36Δ65}* mutant embryos it is unlikely that compensation due to nonsense mediated decay is occurring in these mutants, making it more likely that this mutation does not affect Dock6 protein function.

After identifying a cardiac specific retained intron transcript, *dock6-RI1*, I found that a 41bp insertion mutation into retained intron 1 of this transcript reduced both *dock6-201* and *dock6-RI1* expression and led to cardiac defects upon blocking compensation. How this *dock6-RI1^{ins41}* mutation is resulting in these phenotypes is still unknown, but there are two possibilities: either mutating the retained intron transcript reduces/alters the functions of this transcript itself, or the mutation is impacting the regulatory landscape, for example disrupting an enhancer region which is required to regulate both *dock6-201* and *dock6-RI1* expression.

Although aberrant splicing can lead to intron retention which can contribute to the pathology of certain diseases (Wong et al., 2016), intron retention has also been found to be important for normal biological functions (Vanichkina et al., 2018) and alongside being highly tissue specific, it is tightly regulated during development, differentiation and stress conditions (Rekosh and Hammarskjold, 2018). An example of intron retention regulating gene expression during cell differentiation is in haematopoiesis, where intron retention is lower in B cell precursors which are undergoing proliferation, but increases when these cells reach dormant phases associated with low levels of proliferation (Ullrich and Guigó, 2020). A further example is in quiescent stem cells, which have been found to have higher levels of expression of intron retaining

4. Investigating the role of *dock6*

transcripts which keep them in a quiescent state, and then splicing of these intron retaining transcripts occurs upon exit from quiescence (Yue et al., 2020). Whether this *dock6-RI1* intron retaining transcript is carrying out a similar role during heart development, for example preventing cardiomyocytes from proliferating at 24hpf, would be interesting to investigate further.

Further examples of intron retention regulating gene expression during development are found in *Drosophila*, where alternate splicing leads to two isoforms of the *Robo3* gene: *Robo3.1* which is fully spliced, and *Robo3.2* which has an intron retained within the mature mRNA and encodes a protein which is also conserved in humans. These two *Robo3* isoforms carry out opposing roles during axonal guidance during development, alongside being tightly spatially regulated during axonal midline crossing (Chen et al., 2008). Although it is unknown whether *dock6-202* encodes a protein, there is an annotated open reading frame which spans the full length of the *dock6-RI1* coding sequence which would encode a protein composed of 128 amino acids. Therefore, it would be interesting to investigate whether *dock6-201* and *dock6-202* could be producing individual protein isoforms, alike the *Robo3* gene in *Drosophila*, which carry out distinct functions during development.

Although it is still unknown what exactly the function of the *dock6-RI1* retained intron transcript is, it's very tight spatiotemporal expression dynamics can lead us to speculate that it is required in the heart myocardium around 24hpf to carry out a specific function. Whether it is spliced in response to stress or translated into an alternative *dock6* protein isoform remains to be found. However, I have shown that the *dock6-RI1^{ins41}* mutation in retained intron 1 of *dock6-RI1* results in downregulation of the *dock6-201* protein coding transcript. It would therefore be interesting to investigate whether the *dock6-RI1* transcript itself is required to activate or regulate *dock6-201* expression, as the intronic mutation causes down regulation of both *dock6-RI1* and *dock6-201* expression, or whether the *dock6-RI1^{ins41}* mutation is disrupting an intronic enhancer region which is required to promote expression of both *dock6-201* and *dock6-RI1* independently. I have not been able to identify any examples in the literature of an intronic mutation in a retained intron transcript resulting in downregulation of the neighbouring protein coding gene, and so it is less likely that the *dock6-RI1* retained intron transcript itself is regulating *dock6-201* expression,

4. Investigating the role of *dock6*

particularly as intron retaining transcripts generally regulate their own expression rather than that of neighbouring protein coding genes (Grabski et al., 2021). Additionally, if *dock6-RI1* is regulating *dock6-201* expression, I would expect both the *dock6-RI1^{ins41}* and *dock6-RI1^{Δ28}* mutations to have similar effects on *dock6-201* expression, but this is not what was observed. Therefore, it is more likely that an intronic enhancer has been disrupted by the *dock6-RI1^{ins41}* mutation, resulting in downregulation of both *dock6-201* and *dock6-RI1* expression.

Intronic enhancers are commonly found in genes with tissue specific expression, rather than genes which are ubiquitously expressed, and it has been found that the majority of aorta- and muscle-specific enhancer-like signatures reside within introns in humans (Borsari et al., 2021). Intronic enhancers have been found to regulate gene expression during heart development, for example in mice, an intronic enhancer has been identified in intron 4 of the *Gata2* gene which controls *Gata2* expression in the endothelium during development (Khandekar et al., 2007). Additionally, an intronic enhancer within the human *DOCK5* gene has been identified which regulates *DOCK5* expression, providing evidence that the same could occur in *DOCK6* (Borsari et al., 2021). A mutation disrupting an intronic enhancer would also explain why the *dock6-RI1^{ins41}* mutation causes downregulation of both *dock6* transcripts, while the *dock6-RI1^{Δ28}* has no effect on *dock6* expression, because the intronic enhancer region only overlaps with the *dock6-RI1^{ins41}* mutation site. As these intronic mutations overlap with active enhancer methylation marks as shown in Figure 4.1 B, it is possible to speculate that a disrupted intronic enhancer region is responsible for the reduced expression of both *dock6* transcripts in the *dock6-RI1^{ins41}* mutant embryos, but it is still unclear why reduction in gene expression is only observed in the *dock6-RI1^{ins41}* mutants, and not *dock6-RI1^{Δ28}* mutants. We can speculate that the *dock6-RI1^{ins41}* mutation must overlap with an enhancer which regulates *dock6-201* and *dock6-RI1* expression, while the *dock6-RI1^{Δ28}* mutation does not, and this could be investigated by cloning the enhancer sequences which overlap with these mutations into a GFP reporter plasmid, and inject them into 1 cell-stage embryos to observe where the enhancer is driving GFP expression (Taminato et al., 2016). If the enhancer region overlapping with the *dock6-RI1^{ins41}* mutation drives GFP expression in the same expression domains as *dock6-201* and *dock6-RI1*, while the enhancer region overlapping with the *dock6-*

4. Investigating the role of *dock6*

R11^{Δ28} mutation does not, we can speculate that only the *dock6-R11^{ins41}* mutation disrupts an enhancer region required for *dock6-201* and *dock6-R11* expression.

To summarise, in this chapter I analyse three of the first reported zebrafish *dock6* mutant models: *dock6-R11^{ins41}*, *dock6-R11^{Δ28}* and *dock6-201^{ins36Δ65}*. I show that these mutations have different effects on the expression of two *dock6* transcripts in zebrafish, *dock6-201* and *dock6-R11*, and predict that the *dock6-R11^{ins41}* mutation could be disrupting an intronic enhancer region which regulates expression of both *dock6* transcripts. I show that a reduction of *dock6* expression in *dock6-R11^{ins41}* mutant embryos does not seem to influence heart morphology, adult behaviour, or viability. I investigated the expression of one of the genes involved in a pathway previously shown to compensate for loss of *dock6*, *isg15*, which is expressed heterogeneously across zebrafish embryos. Over-expressing *isg15* mRNA in *dock6-R11^{ins41}* mutant embryos results in cardiac abnormalities including decreased myocardial ballooning and defects in chamber orientation, suggesting that this compensation pathway is occurring in *dock6-R11^{ins41}* mutants. This data provides evidence that this compensation pathway due to a loss of *dock6* expression can be protective in AOS patients with mutations in *DOCK6* and could explain the variability in phenotypes seen in these patients. Further analysis of heart morphology could provide insights into how exactly these defects arise in *dock6-R11^{ins41}* mutant embryos injected with *isg15*, and it would be interesting to acquire data from patients with mutations in *DOCK6* to see whether *ISG15* levels also vary in patients similar to my observations in zebrafish, and whether this could be an indicator of AOS disease severity.

5. Investigating the role of *eogt* in Cardiac Development and Congenital Heart Disease

5.1 Introduction

EGF domain-specific O-GlcNAc transferase (EOGT) is a post translational modification enzyme that transfers an O-GlcNAc (N-acetylglucosamine) to Serine or Threonine residues in proteins with epidermal growth factor-like (EGF) repeats (Varshney and Stanley, 2017). EOGT plays important roles in vascular development (Sawaguchi et al., 2017) and epithelial-cell matrix interactions during development (Müller et al., 2013) and has been found to O-GlcNAcylate several proteins, including NOTCH receptors and ligands which interact via their EGF repeats (Ogawa and Okajima, 2019). This interaction between NOTCH receptors and ligands is important to activate the NOTCH signalling pathway, triggering several cleavages of the NOTCH receptor, leading to translocation of the NOTCH intracellular domain to the nucleus and activating expression of NOTCH target genes (Tashima and Okajima, 2018). EOGT has been found to be particularly important for NOTCH1 receptor interactions with DLL1 and DLL4 ligands, and mutations in O-GlcNAc domains in the NOTCH1 receptor led to reductions in DLL4 binding (Sawaguchi et al., 2017).

Mutations in *EOGT* have been found in autosomal recessive and compound heterozygous forms of Adams-Oliver syndrome (AOS) (Meester et al., 2019), accounting for approximately 5% of AOS patients known to date (Hassed et al., 2017). Of known AOS patients with mutations in *EOGT*, 95% suffer from aplasia cutis congenita (ACC) 26% suffer from terminal transverse limb defects (TTLD), 6% suffering from cutis marmorata telangiectatica congenita (CMTC) and 16% suffer from congenital heart defects (CHDs) (Hassed et al., 2017).

EOGT has mainly been studied in the context of vascular development, as it is known to be highly expressed in endothelial cells (Ogawa and Okajima, 2019). It has been shown in mice that *Eogt* is required for retinal angiogenesis and vascular integrity, but *Eogt* loss of function (LOF) did not show similar phenotypes to those observed in AOS patients (ACC & TTLD) (Sawaguchi et al., 2017). In *Drosophila*, *eogt* LOF is lethal by second-instar larval stage, showing defects similar to *Drosophila* mutants lacking proteins required for epithelial-cell matrix interactions (Varshney and Stanley, 2017).

This suggests specific roles for *EOGT* during vascular development and epithelial-cell matrix interactions, but it is unknown what roles *EOGT* plays during cardiac development, or why some AOS patients with mutations in *EOGT* are born with CHDs.

As *EOGT* has been shown to activate the NOTCH signalling pathway (Sawaguchi et al., 2017) and as NOTCH signalling is known to be important for numerous aspects of cardiovascular development, such as regulating SHF cell proliferation (Lescroart et al., 2018), valve development (Timmerman et al., 2004), and trabeculation (D'Amato et al., 2016), we can speculate that *EOGT* is playing a role in similar processes during heart development. As it is still unknown how *EOGT* is causing CHDs to arise in AOS patients, an animal model to understand this process in more detail would prove invaluable to understand if mutations in *EOGT* lead to dysregulation of the NOTCH signalling pathway during the onset of CHDs. In this chapter I investigate the role of *eogt* during zebrafish cardiovascular development by over-expressing *eogt* RNA and by characterising the first reported zebrafish *eogt* coding sequence mutant, *eogt-201^{Δ28}*, to understand whether *eogt* regulates Notch signalling in the heart and to identify the role it plays during cardiovascular development. Additionally, I characterise a novel *eogt* antisense RNA which is expressed in the zebrafish heart myocardium at a key early stage of cardiac development and assess whether this antisense transcript has a functional role in regulating Notch signalling or cardiovascular development.

5.2 Strategy to over-express *eogt* sense and antisense RNA to investigate their effects on heart development and Notch signalling

Zebrafish have 1 annotated *eogt* transcript on Ensembl, the full-length protein coding transcript *eogt-201*. However, in Chapter 3 I described an *eogt* antisense transcript which I discovered whilst performing a control experiment using a sense RNA probe which was not predicted to bind any RNA as no *eogt* antisense transcripts are annotated in zebrafish. This *eogt* antisense RNA overlaps with the *eogt* sense RNA transcript from the 3' end of the gene and is expressed in the heart myocardium during early heart development. Additionally, there is a human *EOGT* antisense RNA transcript annotated on the UCSC genome browser which also overlaps with human *EOGT-202* sense RNA from the 3' end of the gene spanning 7 exons. The existence of *EOGT* antisense transcripts in both humans and zebrafish suggests a potential role

5. Investigating the role of *eogt*

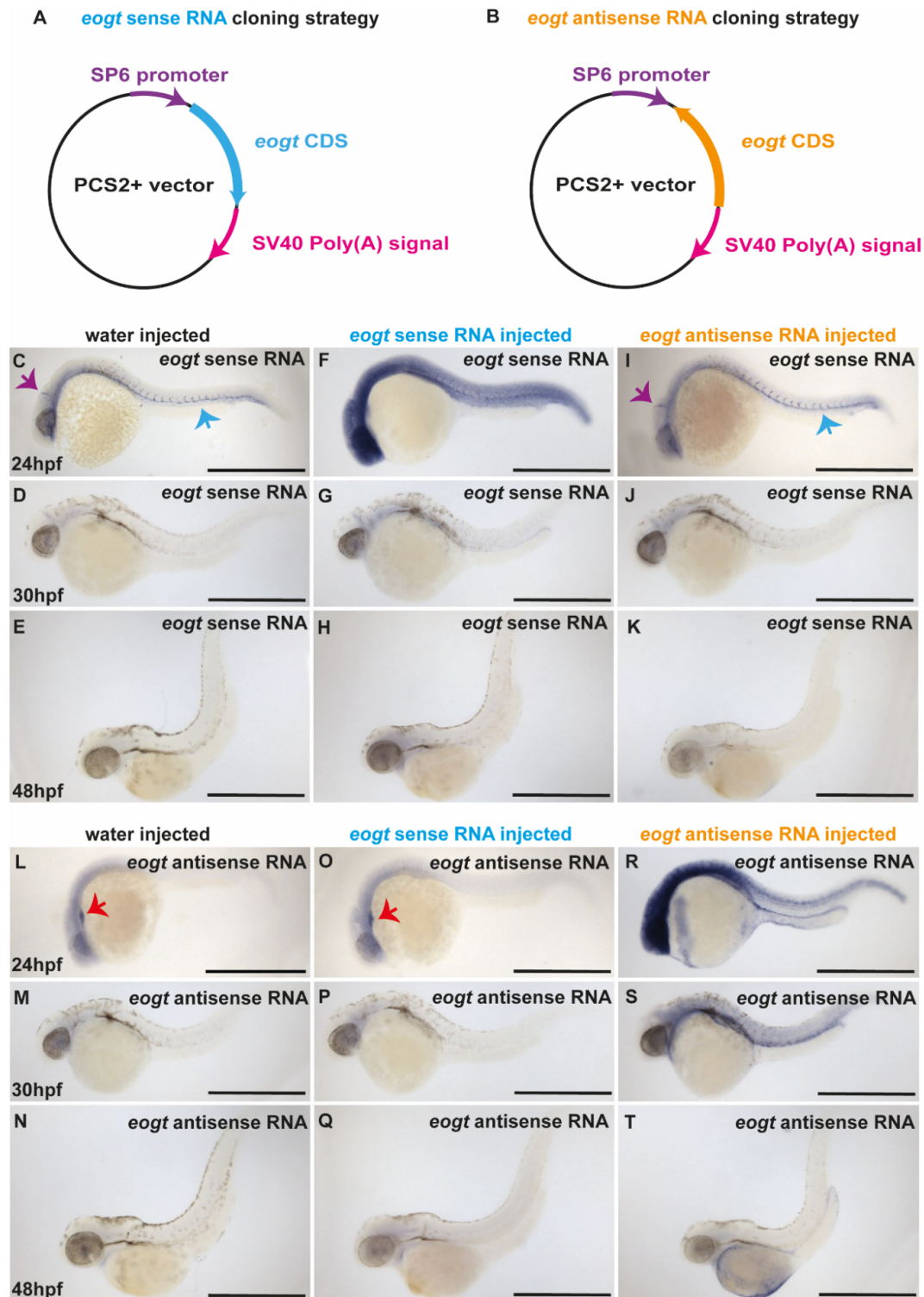


Figure 5.1. *eogt* sense and antisense coding sequence cloning strategy and RNA over-expression in zebrafish embryos. Cloning the *eogt* coding sequence to over-express *eogt* sense and antisense RNA in zebrafish embryos. (A) The full length *eogt* coding sequence (blue) was cloned into the PCS2+ vector containing a 5' SP6 RNA polymerase promoter (purple) and a 3' SV40 Poly(A) signal (pink) in a

5. Investigating the role of *eogt*

forward orientation to allow transcription of *eogt* sense RNA for over-expression experiments. **(B)** The full length *eogt* coding sequence (orange) was cloned into the PCS2+ vector containing a 5' SP6 RNA polymerase promoter (purple) and a 3' SV40 Poly(A) signal (pink) in an antisense orientation to allow transcription of *eogt* antisense RNA for over-expression experiments. Either *eogt* sense RNA, antisense RNA or water was injected into 1 cell stage zebrafish embryos and *eogt* sense or antisense RNA expression was analysed at 24hpf, 30hpf and 48hpf by *in situ* hybridisation to confirm successful over-expression and investigate cross-regulation of the two transcripts **(C-T)**. **(C)** A 24hpf water injected embryo showing wild-type expression of *eogt* sense RNA with expression in the MCEV (purple arrow) and in the DA and ISVs of the tail (blue arrow). **(D-E)** At 30hpf **(D)** and 48hpf **(E)** water injected embryos show no expression of *eogt* sense RNA. **(F)** At 24hpf *eogt* sense RNA injected embryos show elevated ubiquitous expression of *eogt* sense RNA, indicating that over-expression of *eogt* sense RNA was successful. **(G)** At 30hpf *eogt* sense RNA injected embryos show minimal *eogt* sense RNA expression, which is comparable to wild-type expression at this stage. **(H)** At 48hpf *eogt* sense RNA injected embryos show no expression of *eogt* sense RNA which is comparable to wild-type expression at this stage. **(I)** An *eogt* antisense RNA injected embryo at 24hpf showing wild-type expression of *eogt* sense RNA with expression in the MCEV (purple arrow) and in the DA and ISVs of the tail (blue arrow), indicating that over-expression of *eogt* antisense RNA does not affect *eogt* sense RNA expression. **(J-K)** At 30hpf **(J)** and 48hpf **(K)** *eogt* antisense RNA injected embryos show no expression of *eogt* sense RNA, comparable to wild-type expression. **(L)** At 24hpf water injected embryos show wild-type expression of *eogt* antisense RNA with expression in the heart tube myocardium (red arrow). **(M-N)** At 30hpf **(M)** and 48hpf **(N)** water injected embryos show no expression of *eogt* antisense RNA. **(O)** At 24hpf *eogt* sense RNA injected embryos show wild-type expression of *eogt* antisense RNA in the heart tube myocardium, indicating that over-expression of *eogt* sense RNA does not affect *eogt* antisense RNA expression. **(P-Q)** At 30hpf **(P)** and 48hpf **(Q)** *eogt* sense RNA injected embryos show no expression of *eogt* antisense RNA, comparable to wild-type expression. **(R)** At 24hpf *eogt* antisense RNA injected embryos show elevated ubiquitous expression of *eogt* antisense RNA, indicating that over-expression of *eogt* antisense RNA was successful. **(S)** At 30hpf *eogt*

antisense RNA injected embryos show heightened ubiquitous expression of *eogt* antisense RNA, which is elevated compared to wild-type expression of *eogt* antisense RNA at this stage. (T) At 48hpf *eogt* antisense RNA injected embryos show slightly elevated *eogt* antisense RNA expression around the yolk, but otherwise no expression of *eogt* antisense RNA throughout the rest of the embryo, which is comparable to wild-type expression of *eogt* antisense RNA at this stage. Scale bars: 500µm.

for this conserved antisense transcript which I propose could be a long non-coding RNA (lncRNA) (see Chapter 3). To investigate this potential lncRNA further, I initially used RACE to try to identify the 5' and 3' ends of the antisense *eogt* transcript in zebrafish, as this would allow me to design a tailored strategy to knock-out and/or over-express it to understand whether it has a functional role during cardiac development, but these experiments were unsuccessful. Despite not identifying the 5' or 3' ends of this transcript, I hypothesised that the *eogt* antisense transcript spans a large region of the *eogt* gene, as I had detected it using two different *in situ* hybridisation probes which overlapped to cover the full length of the *eogt* gene, with both detecting antisense RNA expression in the heart. As this antisense transcript likely spans a large proportion of the *eogt* gene, I decided to clone the full open reading frame for *eogt-201* in both the sense and antisense direction into a PCS2+ vector containing a 5' SP6 RNA Polymerase promoter and a 3' SV40 Poly(A) signal (Fig. 5.1 A&B). This would allow me to transcribe both *eogt* antisense and sense RNA for over-expression experiments to investigate whether over-expressing *eogt* antisense RNA has any effect on *eogt* sense RNA expression, as it has been shown for other genes that antisense transcripts can regulate the expression of their sense counterparts (Li et al., 2015; Li et al., 2018).

To first confirm successful over-expression of *eogt* sense and antisense RNA I injected wild-type embryos at the 1 cell stage with either RNA or water as a control, and fixed embryos at 24hpf, 30hpf and 48hpf to detect *eogt* sense or antisense over-expression via *in situ* hybridisation, using antisense and sense probes respectively. In the water injected control embryos, *eogt* sense RNA is expressed in the mid-cerebral vein (MCeV) and in the dorsal aorta (DA) and intersegmental vessels (ISVs) throughout the tail at 24hpf (Fig. 5.1 C) with very little expression at 30hpf and 48hpf (Fig. 5.1 D&E).

as previously described in Chapter 3. Embryos injected with *eogt* sense RNA showed global over-expression of *eogt* sense RNA throughout the embryo at 24hpf (Fig. 5.1 F), however this over-expression was mostly gone at 30hpf and 48hpf (Fig. 5.1 G&H). Over-expressing *eogt* antisense RNA appeared to have no effect on *eogt* sense RNA expression, which was comparable to water injected embryos with expression visible in the MCEV and the DA and ISVs of the tail at 24hpf (Fig. 5.1 I), and no visible expression of *eogt* sense RNA at 30hpf and 48hpf (Fig. 5.1 J&K).

In water injected embryos, *eogt* antisense RNA is expressed in the heart myocardium at 24hpf (Fig. 5.1 L), with little expression at 30hpf and 48hpf (Figure 5.1 M&N). Over-expressing *eogt* antisense RNA resulted in global upregulation of *eogt* antisense RNA expression throughout the embryo at 24hpf (Fig. 5.1 R), with heightened expression still observed at 30hpf (Fig. 5.1 S) but over-expression mostly gone by 48hpf (Fig. 5.1 T). However, over-expressing *eogt* sense RNA has little effect on *eogt* antisense RNA expression, with expression being comparable to the water injected embryos from 24hpf to 48hpf (Fig. 5.1 O-Q). This confirmed successful over-expression of *eogt* sense and antisense RNA but suggests that over-expression of these transcripts is not easily tolerated by zebrafish embryos which rapidly degrade them, particularly in the case of *eogt* sense RNA where expression is gone by 30hpf. To check whether this early temporary over-expression of *eogt* sense or antisense RNA had any effect on zebrafish embryo viability, I raised injected embryos to 5dpf, however they exhibited no obvious gross morphological phenotypes. Together this data shows that I can successfully over-express both *eogt* sense and antisense RNA in the zebrafish embryo at the timepoint when these genes are normally expressed, but expression is rapidly degraded from 24hpf onwards. This also suggests that over-expressing *eogt* sense or antisense RNA has no effect on the expression of the other *eogt* transcript, as in both over-expression conditions expression of the other transcript appeared comparable to that in water injected embryos.

5.3 Over-expressing *eogt* sense or antisense RNA has no effect on cardiac development

To assess whether over-expressing *eogt* sense or antisense RNA has any impact on cardiac development, I injected both RNAs into 1 cell stage embryos, and fixed the injected embryos at 24hpf and 55hpf to characterise heart morphology via *in situ*

5. Investigating the role of *eogt*

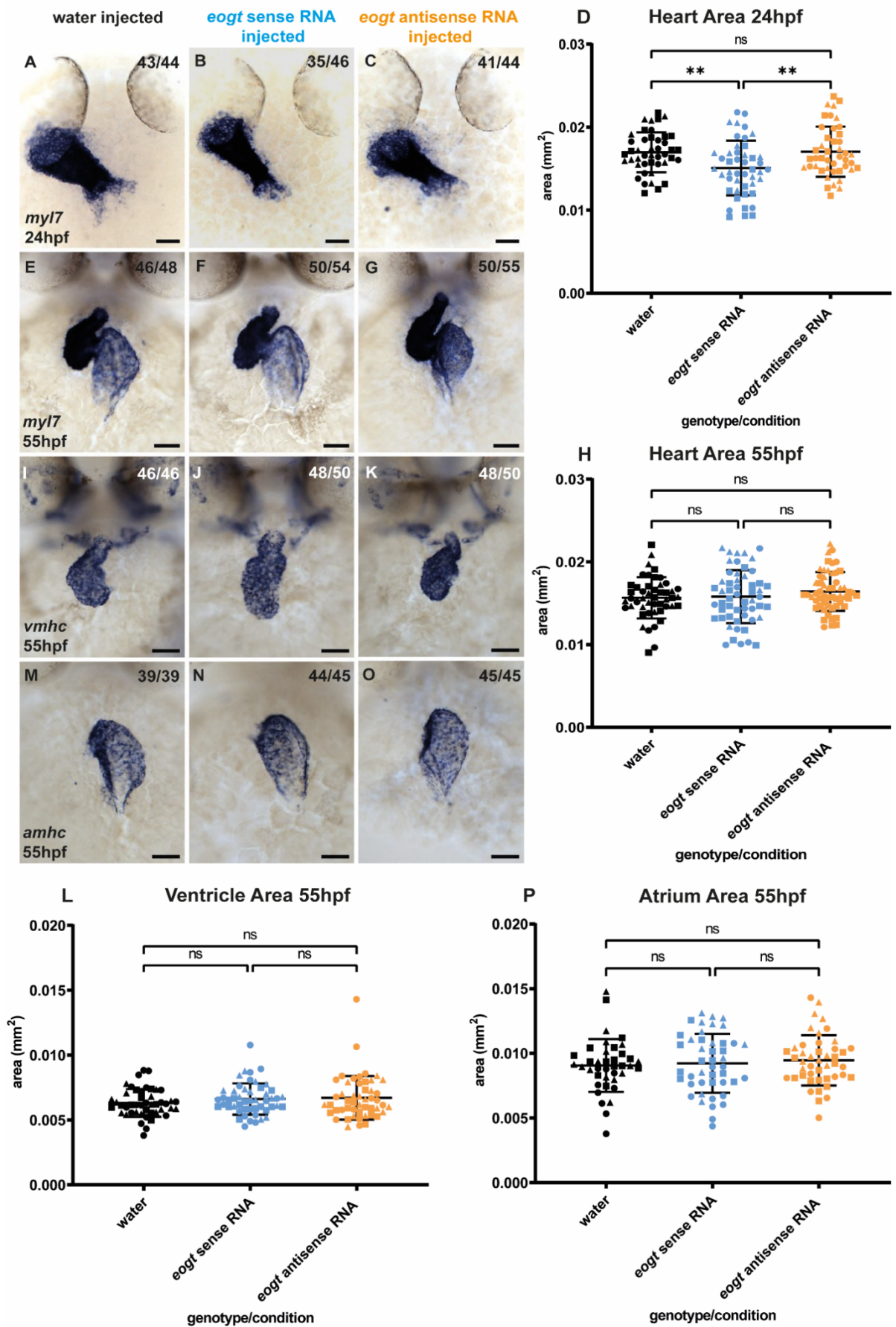


Figure 5.2. Over-expressing *eogt* sense or antisense RNA has no effect on cardiac size. mRNA *in situ* hybridisation analysis of a pan myocardial gene, *myl7*, to visualise heart morphology at 24hpf (**A-C**) and 55hpf (**E-G**), and mRNA *in situ* hybridisation analysis of chamber specific genes, *vmhc* (**I-K**) and *amhc* (**M-O**), to visualise ventricle and atria morphology respectively at 55hpf. Analysis of heart tube size at 24hpf in embryos injected with either water (**A**) *eogt* sense RNA (**B**), or *eogt* antisense RNA (**C**) reveals over-expressing *eogt* sense RNA results in smaller hearts at 24hpf compared to the hearts in water injected embryos or embryos injected with *eogt* antisense RNA (**D**). Analysis of looped heart size at 55hpf in embryos injected with either water (**E**), *eogt* sense RNA (**F**) or *eogt* antisense RNA (**G**) reveals no significant difference in heart area for any of the injection conditions (**H**). Analysis of ventricle morphology through *vmhc* expression at 55hpf in embryos injected with either water (**I**), *eogt* sense RNA (**J**) or *eogt* antisense RNA (**K**), shows no significant difference in ventricle area between any of the injection conditions (**L**). Analysis of atrial morphology through expression of *amhc* at 55hpf shows no significant differences (**P**) between embryos injected with either water (**M**), *eogt* sense RNA (**N**) or *eogt* antisense RNA (**O**). D, H & P: mean \pm SD are plotted and analysed using One-Way ANOVA with Tukey's Multiple Comparisons test. L: mean \pm SD are plotted and analysed using Kruskal-Wallis test with Dunn's Multiple Comparisons test, ns: not significant, **: $P < 0.01$. Scale bars: 50 μ m.

hybridisation. To visualise heart morphology I performed *in situ* hybridisation using the pan myocardial *myl7* probe at both 24hpf (Fig. 5.2 A-C) and 55hpf (Fig. 5.2 E-G), and although there were no obvious defects in heart morphology, after measuring the area of the heart tube at 24hpf I found it was significantly reduced in embryos injected with *eogt* sense RNA compared to embryos injected with water or *eogt* antisense RNA (Fig. 5.2 D). However, any defects in heart size had recovered by 55hpf, at which point there was no significant difference in heart area between embryos injected with water and either *eogt* sense or antisense RNA (Fig. 5.2 H). To assess the individual heart chambers in more detail, I used chamber specific *in situ* hybridisation probes to label either the ventricle or atrium individually, using the *ventricular myosin heavy chain* (*vmhc*) or *atrial myosin heavy chain* (*amhc*) probes respectively. Ventricle morphology between the different injection conditions appeared comparable (Fig. 5.2 I-K) with no

significant difference detected in ventricle area (Fig. 5.2 L). Similarly, there was no difference in atrial morphology between embryos injected with water or *eogt* sense or antisense RNA (Fig. 5.2 M-O), and no difference in atrium area between the different conditions (Fig. 5.2 P). Together this data suggests that overexpressing *eogt* sense or antisense RNA appears to have little impact on whole heart morphology at either 24hpf or 55hpf, or chamber morphology at 55hpf.

5.4 Notch signalling pathway components are expressed in the ventricle and OFT during early cardiac development

As EOGT is thought to be regulating NOTCH signalling (Sawaguchi et al., 2017) and as NOTCH signalling is known to be important for correct cardiac development (MacGrogan et al., 2018), I investigated expression of Notch signalling pathway components in the heart at 26hpf when *eogt* sense and antisense RNA are normally expressed, and when the transcripts were still strongly upregulated in the over-expression models (Fig. 5.1). I focused in particular on the expression of *notch1* and *dll4* which are known to require EOGT O-GlcNAcylation to be able to interact in mice (Sawaguchi et al., 2017). I performed *in situ* hybridisation expression analysis of the Notch receptors *notch1a* and *notch1b* and found that both genes are expressed broadly throughout the zebrafish embryo at 26hpf (Fig. 5.3 A&C). *notch1a* is strongly expressed in the head at 26hpf with no obvious expression in the heart (Fig. 5.3 B), however despite *notch1b* also being expressed in the head at 26hpf, there is heightened expression in the endocardium and OFT of the heart (Fig. 5.3 D). To investigate whether the Notch ligand *dll4* is expressed at 26hpf in the zebrafish heart, I utilised the *Tg(dll4in3:GFP)* transgenic zebrafish line (Sacilotto et al., 2013) to visualise *dll4* expression, in combination with the *Tg(flk1:ras-cherry)* transgenic line which labels endocardial cell membranes red (Chi et al., 2008). I found that *dll4* is expressed throughout the endocardium and OFT at 26hpf, with expression also heightened in the left side of the heart myocardium (Fig. 5.3 F). This shows that *notch1* and *dll4*, which have been shown to require *eogt* O-GlcNAcylation to interact and activate the Notch signalling pathway (Sawaguchi et al., 2017) are expressed in the heart ventricle and OFT at 26hpf, the same time that *eogt* is expressed in the developing embryo. As I found only *eogt* antisense RNA to be expressed in the heart at this stage of development, and *eogt* sense RNA expression in the MCEV and ISVs

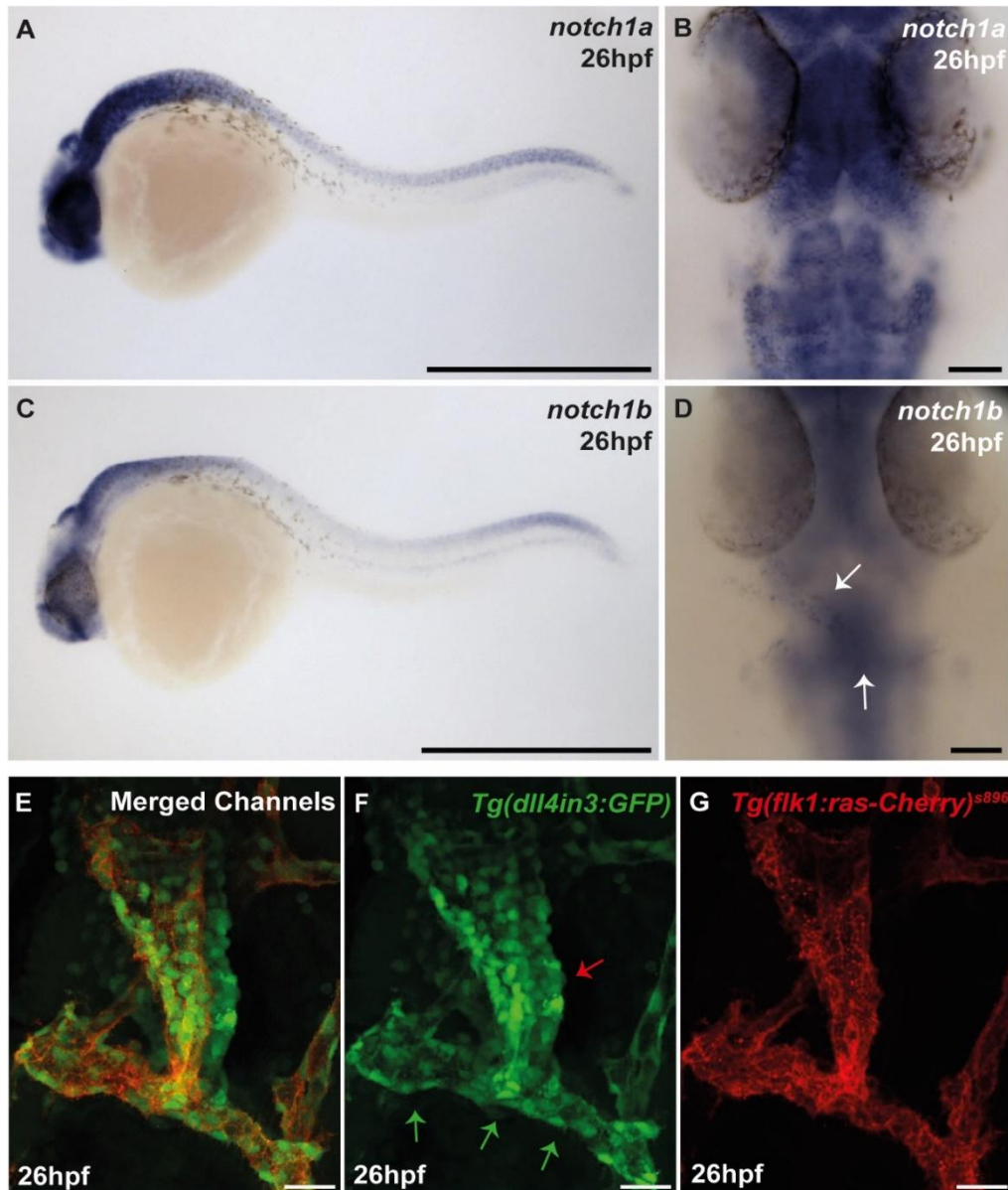


Figure 5.3. Components of the Notch signalling pathway are expressed in the primitive ventricle and OFT of the developing heart. mRNA *in situ* hybridisation analysis of *notch1a* (A-B) and *notch1b* (C-D) expression in the zebrafish embryo at 26hpf, and expression of *dll4* using the transgenic line *Tg(dll4in3:GFP)* in combination with the *Tg(flk1:ras:mCherry)* endocardial cell membrane marker (E-G). Lateral view reveals expression of *notch1a* is expressed broadly throughout the embryo at 26hpf (A) and a dorsal view shows ubiquitous *notch1a* expression throughout the head with no obvious expression in the heart (B). *notch1b* is also expressed broadly throughout the embryo at 26hpf (C) and a dorsal view shows ubiquitous expression throughout the head, with heightened expression in the heart tube endocardium and OFT endocardium (white arrows) (D). (E) Maximum intensity

projections of confocal image z-stacks in a 26hpf *Tg(dll4in3:GFP);Tg(flk1:ras-cherry)* double transgenic embryo labelling *dll4* expression in green and endocardial cell membranes in red. (F) At 26hpf *dll4* is expressed in both the myocardium and endocardium, with heightened expression on the left side of the myocardium (red arrow), and in the OFT endocardium (green arrows), which overlaps with transgenic expression of the endocardial cell membrane marker *Tg(flk1:ras-cherry)* (G). Scale bars: A&C: 500µm; B, D, E, F & G: 50µm.

of the tail (See Chapter 3), I wanted to investigate whether either *eogt* transcript can regulate Notch activity in the heart, OFT or arterial pole endothelium during heart development.

5.5 Over-expressing *eogt* sense or antisense RNA has no effect on OFT development

As EOGT is implicated in NOTCH signalling, which is known to be important for OFT development (Jain et al., 2010), I investigated OFT development at different stages of cardiac development in embryos over-expressing either *eogt* sense or antisense RNA. Since it is difficult to visualise OFT morphology using the pan myocardial and chamber specific *in situ* hybridisation probes used in Figure 5.2, I performed *in situ* hybridisation analysis of different OFT markers, including the flow responsive gene *krüppel-like factor 2a* (*klf2a*). *klf2a* is expressed in the OFT at 26hpf following the onset of blood flow, and could indicate whether there are patterning/flow defects in the over-expression models which could also suggest defects in OFT morphology (Vermot et al., 2009). Another OFT marker I investigated is *latent transforming growth factor beta binding protein 3* (*ltbp3*), an extracellular matrix gene which at 26hpf is expressed in the SHF cell population which will contribute to the arterial pole of the heart and formation of the OFT (Zhou et al., 2011), and disruption to this cell population could result in OFT defects. To visualise OFT morphology at later stages of heart development when the bulbous arteriosus is beginning to develop, I investigated *ltbp3* and *aggrecan a* (*acana*) expression at 50hpf and 72hpf respectively (Zhou et al., 2011 ;Rambeau et al., 2017). When characterising *klf2a* expression by *in situ* hybridisation in the *eogt* over-expression models at 26hpf (Fig. 5.4 A-C), there appeared to be a mild increase in *klf2a* expression in the OFT of *eogt* antisense RNA injected embryos (Fig. 5.4 C) compared to water injected controls or *eogt* sense RNA injected embryos (Fig. 5.4 A,B). To quantify whether *klf2a* expression was significantly altered upon *eogt*

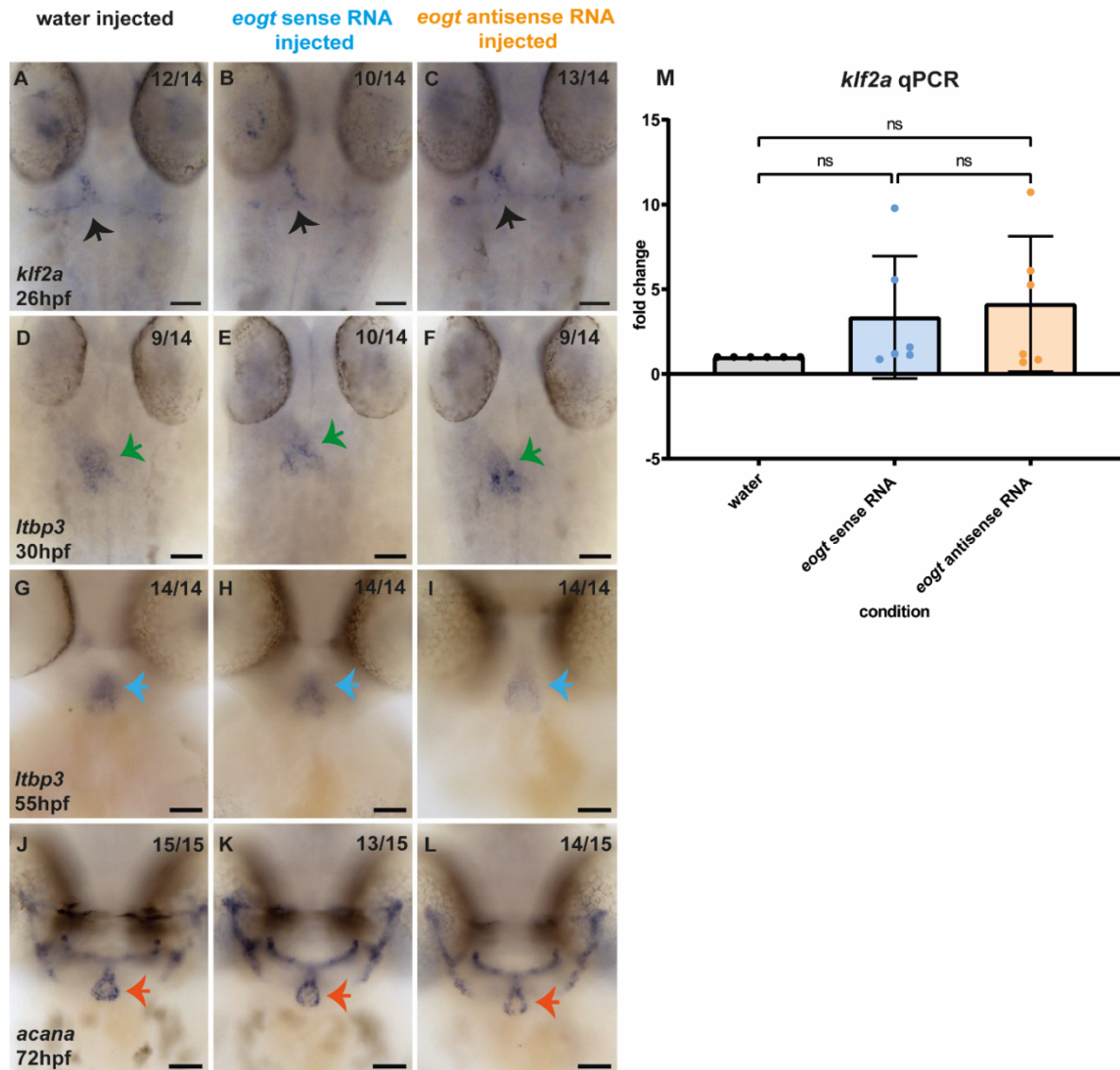


Figure 5.4. Over-expressing *eogt* sense or antisense RNA has no effect on OFT morphology. mRNA *in situ* hybridisation analysis of the expression of OFT genes *klf2a* at 26hpf (A-C), *Itbp3* at 30hpf (D-F) and 55hpf (G-I), and *acana* at 72hpf (J-L), and qPCR analysis of *klf2a* expression in all injection conditions (M). *klf2a* is expressed throughout the OFT endocardium at 26hpf (black arrows) in embryos injected with either water (A), *eogt* sense RNA (B) or *eogt* antisense RNA (C). *Itbp3* is expressed in the OFT at 30hpf (green arrows) and bulbous arteriosus 55hpf (blue arrows) in embryos injected with either water (D&G), *eogt* sense RNA (E&H) or *eogt* antisense RNA (F&I). *acana* expression in the bulbous arteriosus at 72hpf (red arrows) is comparable in embryos injected with either water (J), *eogt* sense RNA (K) or *eogt* antisense RNA (L). (M) qPCR analysis of *klf2a* mRNA expression at 26hpf shows no significant difference in *klf2a* expression in embryos injected with either

water, *eogt* sense RNA or *eogt* antisense RNA. M: mean \pm SD are plotted and analysed using Kruskal-Wallis test with Dunn's Multiple Comparison test, ns: not significant. Scale bars: 50 μ m.

antisense RNA over-expression, I conducted qPCR on cDNA generated from water injected embryos and *eogt* sense or antisense RNA injected embryos at 26hpf. However, qPCR analysis confirmed that *klf2a* expression levels were not significantly different in *eogt* antisense RNA injected embryos compared to water injected embryos or embryos injected with *eogt* sense RNA (Fig. 5.4 M). I also investigated *Itbp3* expression at both 30hpf (Fig. 5.4 D-F) and 55hpf (Fig. 5.4 G-I) but found expression levels and domains to be comparable across all injection conditions. Similarly, I carried out *in situ* hybridisation for *acana* at 72hpf, but again found expression to be comparable between all injection conditions (Fig. 5.4 J-L). This data suggests that over-expression of *eogt* sense or antisense RNA is having no impact on OFT development, as OFT morphology appeared comparable between all experimental conditions. It also suggests that *eogt* sense or antisense RNA over-expression is having no impact on Notch dependent processes during OFT development, however investigation of Notch signalling activity during OFT development would be required to support this conclusion.

Additionally, as I have shown *eogt* sense RNA is expressed in the developing vasculature (see Chapter 3) and previous studies have shown that *eogt* is involved in retinal angiogenesis in mice (Sawaguchi et al., 2017), I investigated early vascular development in embryos with over-expression of either *eogt* sense or antisense RNA. I performed *in situ* hybridisation analysis of *fli1a* which is expressed throughout the zebrafish vasculature (Lawson and Weinstein, 2002), and although early vascular morphology appeared normal in embryos injected with either water or *eogt* sense or antisense RNA (Fig. 5.5 A-C), there appeared to be a mild reduction in *fli1a* expression in embryos injected with *eogt* antisense RNA (Fig. 5.5 C). Notch signalling is required in zebrafish to control *fli+* haemo-vascular progenitor cell proliferation (Chun et al., 2011), and so to confirm whether over-expression of *eogt* antisense RNA has an effect on *fli1a* expression I carried out qPCR analysis of *fli1a* in embryos injected with water or *eogt* sense or antisense RNA. However, I found that there was no significant difference in *fli1a* expression across all injection conditions (Fig. 5.5 D). This suggests

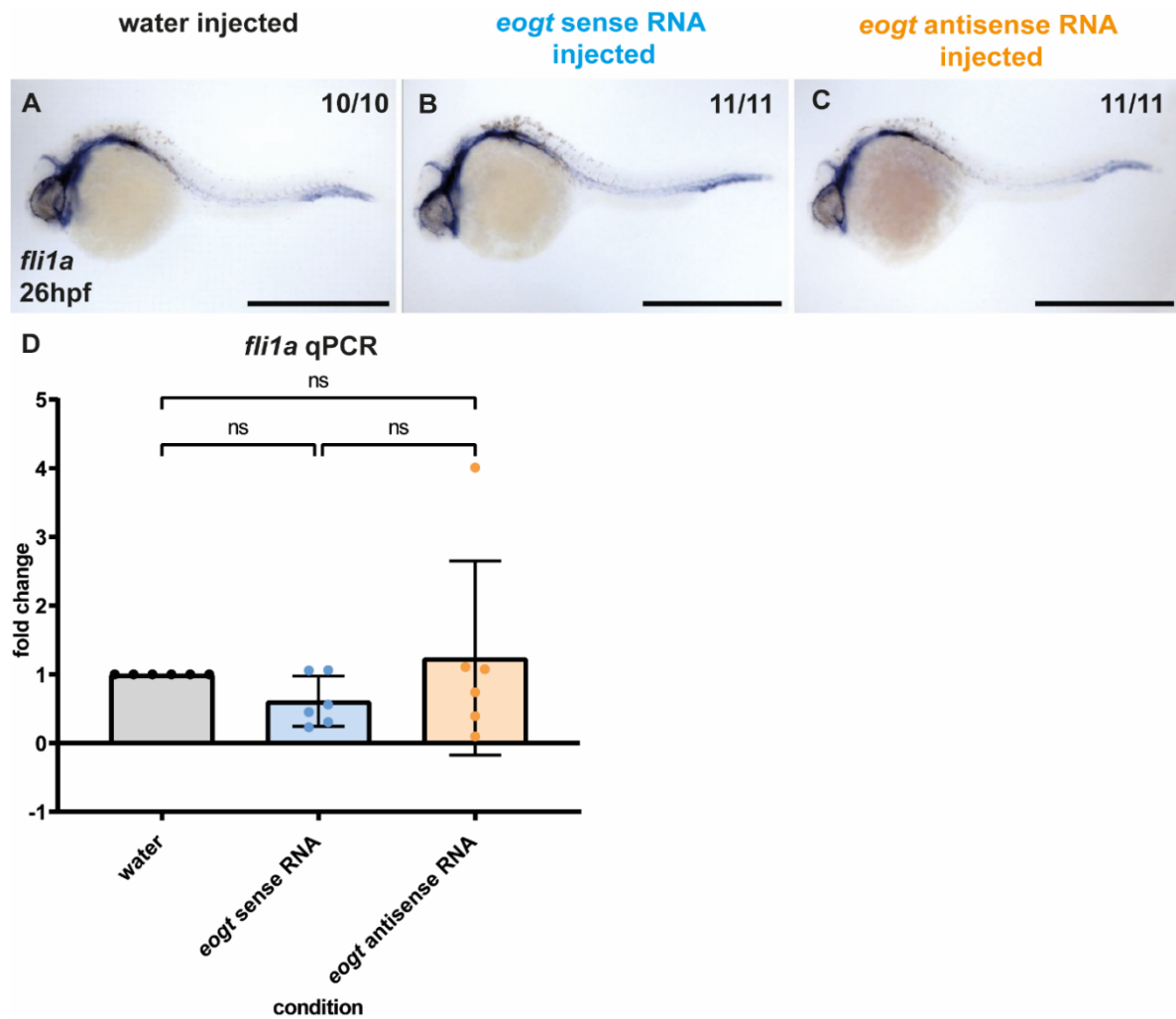


Figure 5.5. Over-expressing *eogt* sense or antisense RNA has no effect on early vascular development. mRNA *in situ* hybridisation analysis of the expression of vascular marker *fli1a* (A-C) and qPCR analysis of *fli1a* expression in all injection conditions (D). *fli1a* expression at 26hpf in embryos injected with either water (A), *eogt* sense RNA (B) or *eogt* antisense RNA (C) reveals no differences in early vascular development between groups. (D) qPCR analysis of *fli1a* mRNA expression at 26hpf shows no significant difference in *fli1a* expression in embryos injected with either water, *eogt* sense RNA or *eogt* antisense RNA. D: mean \pm SD are plotted and analysed using Kruskal-Wallis test with Dunn's Multiple Comparison test, ns: not significant. Scale bars: 500 μm.

that over-expression of *eogt* sense or antisense RNA has no effect on early vascular development or *fli1a* expression. As both of these processes are Notch signalling dependent, further investigation of Notch activity during vascular development would

be interesting to investigate whether *eogt* sense or antisense RNA over-expression is having any impact on vasculogenesis.

5.6 Over-expressing *eogt* sense or antisense RNA has no effect on Notch signalling in the developing heart

Despite over-expression of either *eogt* sense or antisense RNA having little impact on heart morphology, I wanted to investigate whether over-expressing either transcript impacted Notch signalling in the developing heart, particularly in the OFT where *notch1* and *dll4* are both expressed (Fig. 5.3), as over-expression of *EOGT* cDNA, along with *NOTCH1* cDNA, in HEK293T cells increased NOTCH1-DLL4 binding (Sawaguchi et al., 2017). To do this I out-crossed the *Tg(fli1a:EGFP)* transgenic line which labels endothelial cells green (Roman et al., 2002), to the global Notch reporter line *Tg(Tp1bglob:hmgb1-mCherry)* (Parsons et al., 2009) and injected the 1 cell stage embryos with either water or *eogt* sense or antisense RNA. Injected embryos were fixed at 26hpf followed by immunohistochemistry using the anti-DM-Grasp antibody which labels the myocardium (Trevarrow et al., 1990), together allowing visualisation of both tissue layers of the heart along with the Notch reporter (Fig. 5.6 A-L). Notch signalling appeared to be mainly active in the endocardial tissue of the heart in all injected embryos (Fig. 5.6 J-L), and there appeared to be a mild increase in Notch-positive endocardial cells in the *eogt* antisense RNA injected embryos (Fig. 5.6 L). However, quantification of the number of Notch positive cells throughout the whole endocardium in each injection group revealed no significant difference between water injected control embryos or embryos injected with either *eogt* sense or antisense RNA (Fig. 5.6 M). As *notch1b* and *dll4* appeared to be expressed at higher levels in the OFT (Fig. 5.3), and as previous studies have shown that Notch signalling is important for OFT development (Jain et al., 2010), I analysed more closely the number of Notch positive cells specifically in the OFT endocardium, as it appeared there might be an increase in Notch positive endocardial cells in the OFT of *eogt* antisense RNA injected embryos (Fig. 5.6 L). However, the number of Notch positive endocardial cells in the OFT of *eogt* antisense RNA injected embryos was not significantly different compared to the hearts of water injected embryos or embryos injected with *eogt* sense RNA (Fig. 5.6 N). Overall, this data suggests that over-expressing *eogt* sense or antisense RNA

5. Investigating the role of *eogt*

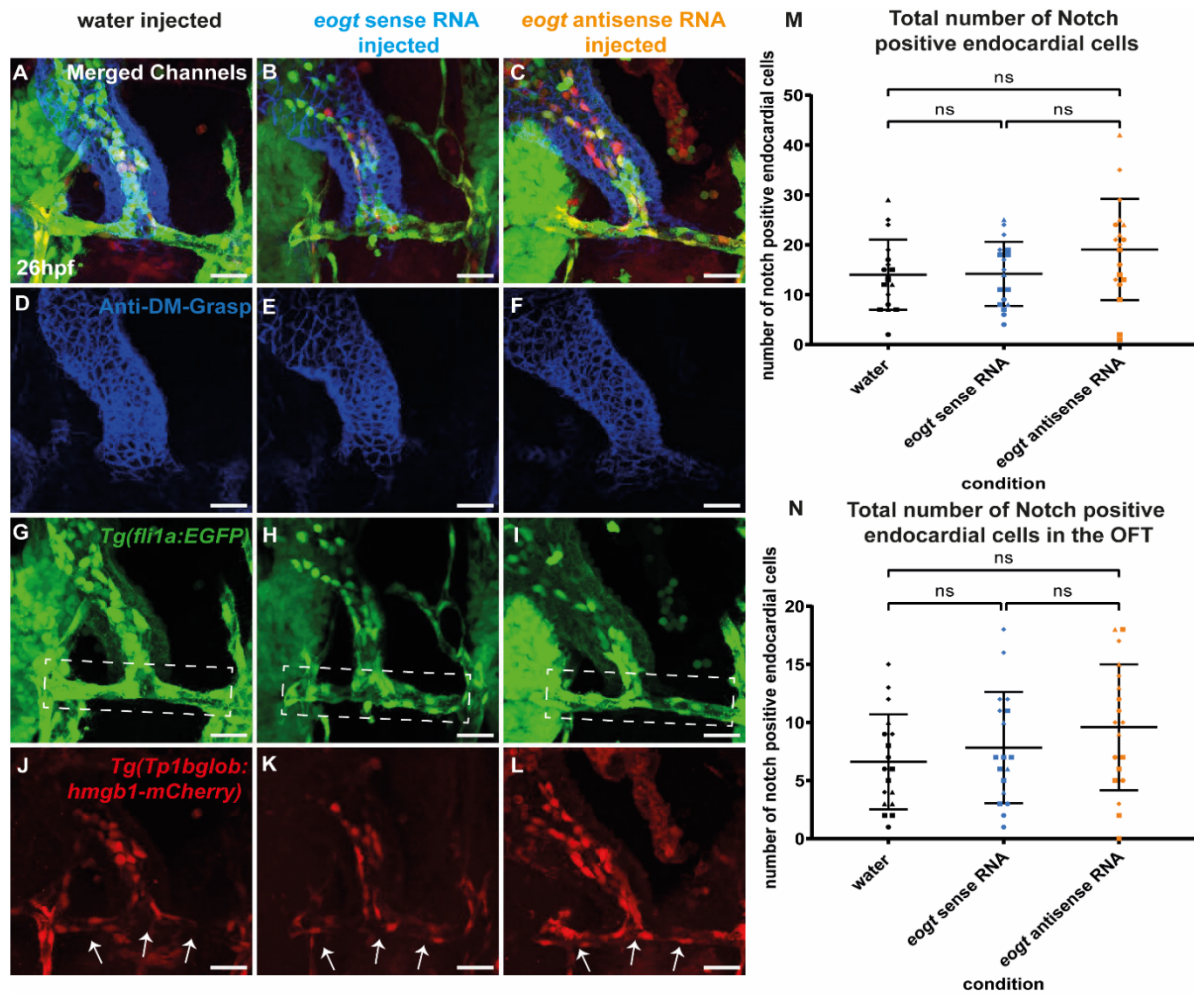


Figure 5.6. Over-expression of *eogt* sense or antisense RNA has no effect on Notch signalling in the developing heart. Merged maximum intensity projections of confocal image z-stacks of the heart at 26hpf in *Tg(fli1a:EGFP); Tg(Tp1bglob:hmg1-mCherry)* double transgenic embryos labelling endocardial cells green and cells with active Notch signalling red, in combination with anti-DM-Grasp immunostaining to label heart tube myocardium. Anti-DM-Grasp immunostaining shows comparable heart tube morphology in embryos either injected with water (D), *eogt* sense RNA (E) or *eogt* antisense RNA (F). *Tg(fli1a:EGFP)* transgenic expression in the endocardium and surrounding vasculature at 26hpf in embryos injected with either water (G), *eogt* sense RNA (H) or *eogt* antisense RNA (I), with the OFT endocardium region highlighted by the white dotted box. *Tg(Tp1bglob:hmg1-mCherry)* global Notch signalling is active in the endocardium of embryos injected with either water (J), *eogt* sense RNA (K) or *eogt* antisense RNA (L) with white arrows indicating OFT endocardial cells with active

Notch signalling. (M) Quantitative analysis revealed there was no significant difference between the number of Notch positive endocardial cells in the hearts of embryos injected with either water, *eogt* sense RNA or *eogt* antisense RNA (M). Similarly, there was no significant difference in the number of Notch positive cells in the OFT endocardium (region indicated by white dotted box in panels G-I) of hearts from embryos injected with either water or *eogt* sense or antisense RNA (N). M&N: mean \pm SD are plotted and analysed using One-Way ANOVA with Tukey's Multiple Comparisons test, ns: not significant. Scale bars: 50 μ m.

has no significant effect on Notch signalling in the developing heart of zebrafish embryos at 26hpf.

5.7 *eogt-201 Δ 28* coding sequence mutant has no effect on *eogt* sense or antisense expression

Although it appears that over-expression of *eogt* sense or antisense RNA is having no impact on heart morphology or Notch signalling in the developing heart, these experiments do not conclusively show that *eogt* is not playing a role in heart development, and therefore I also wanted to investigate what happens to these processes in an *eogt* mutant model. I characterised an *eogt* coding sequence mutant which I recovered from the unsuccessful AOS disease-specific knock-in strategy described in Chapter 3. This *eogt* mutation encompasses a 28bp deletion at the end of exon 6 (Fig. 5.7 A), and despite being an out-of-frame mutation spanning an intron-exon border, this mutation does not impact splicing and results in an in-frame deletion of 5 amino acids in the glycosyltransferase domain, all of which are conserved between zebrafish and humans (Fig. 5.7 B).

I initially wanted to see what the impact of this mutation was on *eogt* sense and antisense RNA expression using *in situ* hybridisation. In *eogt-201 Δ 28* homozygous mutant embryos *eogt* sense RNA expression appears unaffected as it is clearly visible in the MCEV and the DA and ISVs in the tail (Fig. 5.7 D), and comparable to *eogt* sense RNA expression in wild-type siblings (Fig. 5.6 C). Similarly, *eogt* antisense RNA expression also appears unaffected in *eogt-201 Δ 28* mutant embryos, with expression visible in the heart tube myocardium at 24hpf (Fig. 5.7 G&H) which is comparable to *eogt* antisense RNA expression in wild-type embryos (Fig. 5.7 E&F). This suggests

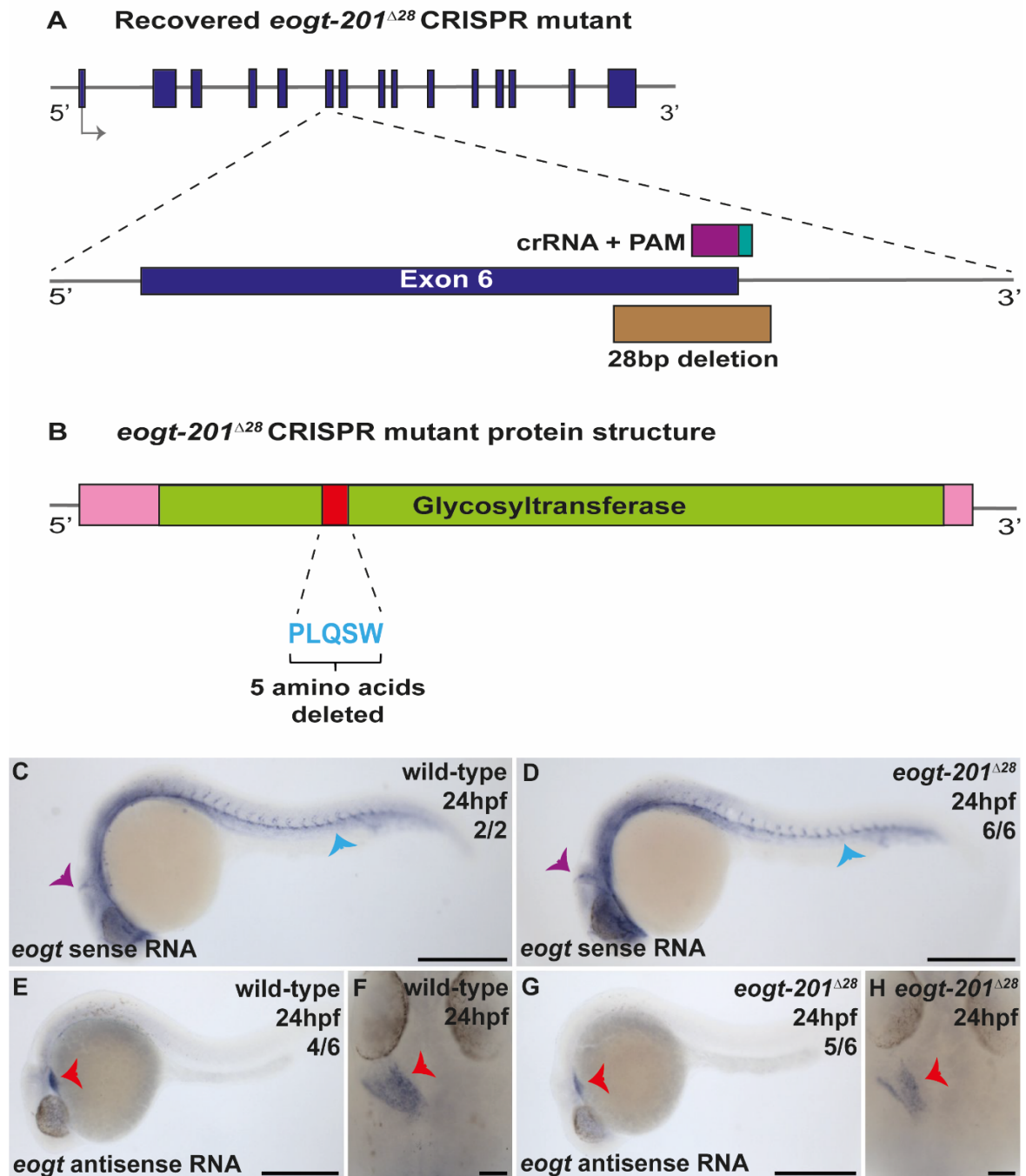


Figure 5.7. *eogt-201*^{Δ28} mutation has no effect on *eogt* sense or antisense RNA expression. (A) Zebrafish *eogt-201* transcript composed of 15 exons, highlighting exon 6 (dark blue) where the *eogt-201*^{Δ28} mutation was created (brown). (B) Eogt protein structure (pink) highlighting the glycosyltransferase domain (light green) and the *eogt-201*^{Δ28} mutation (red) within the glycosyltransferase domain. This mutation deletes 5 amino acids, all of which are conserved between humans and zebrafish (light blue text). (C) *in situ* hybridisation analysis of *eogt-201* mRNA expression in

wild-type embryos and *eogt-201^{Δ28}* mutants, showing *eogt* mRNA expression in the MCEV (purple arrow) and in the DA and ISVs in the tail (blue arrow) in a wild-type sibling, and comparable expression to wild-type in an *eogt-201^{Δ28}* mutant (**D**). (**E**) *in situ* hybridisation analysis of *eogt* antisense RNA expression in wild-type embryos at 24hpf, showing *eogt* antisense RNA expression in the heart myocardium (red arrow), which can be seen in more detail dorsally (**F**, red arrow). *eogt* antisense RNA expression in *eogt-201^{Δ28}* mutants is comparable to wild-type expression which can be seen in the heart myocardium (**G&H**, red arrows). Scale bars: C, D, E & G: 500μm. F&H: 50μm. Mendelian ratio of *eogt* sense *in situ* hybridisation: wild-types = 2, heterozygotes = 13, homozygotes = 6; Mendelian ratio of *eogt* antisense *in situ* hybridisation: wild-types = 6, heterozygotes = 10, homozygotes = 6.

that the *eogt-201^{Δ28}* coding sequence mutation does not have an effect on *eogt* sense or antisense RNA expression.

5.8 *eogt-201^{Δ28}* coding sequence mutant has no effect on cardiac development

Despite the *eogt-201^{Δ28}* mutation having no effect on *eogt* sense or antisense RNA expression, it does remove 5 conserved amino acids from the Eogt glycosyltransferase domain. Since it is unknown whether these mutations have an impact on protein function and/or heart development, I characterised heart development in *eogt-201^{Δ28}* homozygous mutant embryos. Firstly, I analysed whether the *eogt-201^{Δ28}* coding sequence mutation had an effect on OFT morphology using similar approaches to those described above in the *eogt* over-expression experiments. I performed mRNA *in situ* hybridisation analysis of the flow responsive gene *klf2a*, and extracellular matrix genes *ltbp3* and *acana* which are expressed in the OFT at different stages of cardiac development. However, I found no obvious differences in gene expression in *eogt-201^{Δ28}* homozygous mutant embryos when compared to wild-type siblings for *klf2a* at 26hpf (Fig. 5.8 A&B), *ltbp3* at 30hpf (Fig. 5.8 C&D) or *acana* at 72hpf (Fig. 5.8 E&F), suggesting that the *eogt-201^{Δ28}* mutation has no effect on OFT morphology.

To analyse overall heart morphology in greater detail than is possible using 2D *in situ* hybridisation images, I analysed *eogt-201^{Δ28}* mutant hearts using the MorphoHeart image analysis programme, allowing segmentation of the different tissue layers of the

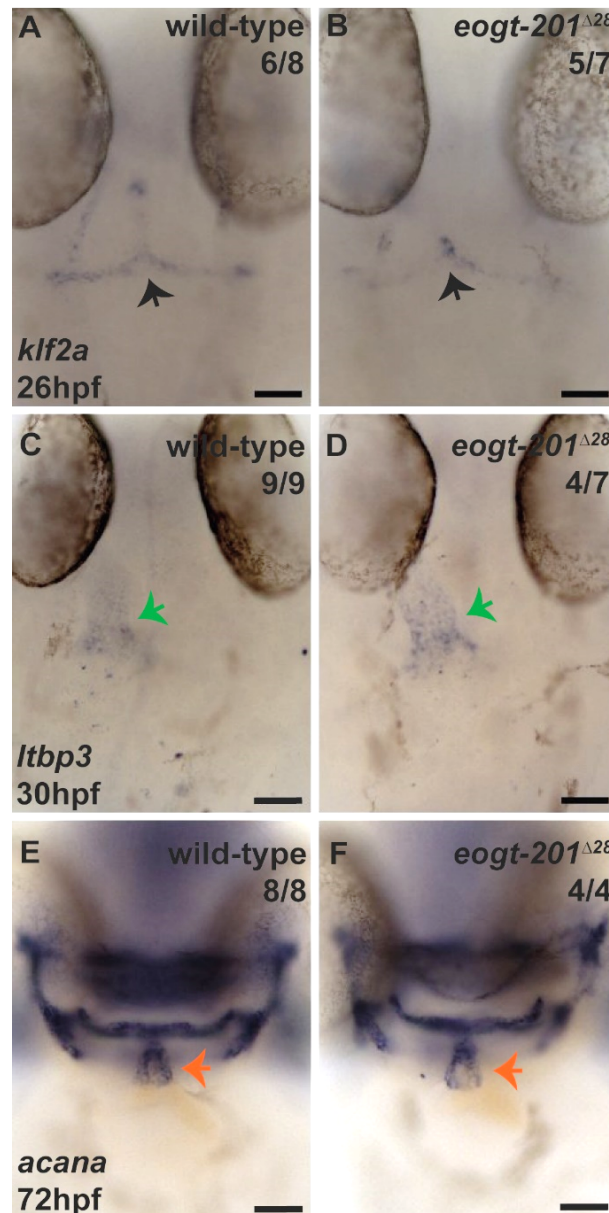


Figure 5.8. *eogt-201*^{Δ28} mutation has no effect on OFT morphology. mRNA *in situ* hybridisation analysis of genes expressed in the OFT to visualise OFT morphology throughout development, such as *klf2a* at 26hpf (**A**&**B**), *Itbp3* at 30hpf (**C**&**D**) and *acana* at 72hpf (**E**&**F**). Expression of *klf2a* throughout the OFT endocardium at 26hpf (black arrows) is comparable between wild-type siblings (**A**) and *eogt-201*^{Δ28} mutant embryos (**B**). *Itbp3* expression at 30hpf can be seen in the OFT (green arrows) and expression is comparable between wild-type siblings (**C**) and *eogt-201*^{Δ28} mutant embryos (**D**). *acana* is expressed in the bulbous arteriosus at 72hpf (red arrows) with expression comparable between wild-type siblings (**E**) and *eogt-201*^{Δ28} mutant embryos (**F**). Scale bars: 50µm. Mendelian ratio of *klf2a* in

situ hybridisation: wild-types = 8, heterozygotes = 7, homozygotes = 7; mendelian ratio of *Itbp3* *in situ* hybridisation: wild-types = 9, heterozygotes = 12, homozygotes = 7; mendelian ratio of *acana* *in situ* hybridisation: wild-types = 8, heterozygotes = 13, homozygotes = 4.

heart and subsequent in-depth quantitative tissue analysis. Embryos derived from an incross of *eogt-201^{Δ28}* heterozygous mutant fish in the *Tg(myl7:LifeActGFP);Tg(fli1a:AC-TagRFP)* transgenic background (labelling the myocardium green and the endocardium red) were raised to 72hpf and the hearts imaged on the light-sheet microscope (Fig. 5.9 A&D). MorphoHeart was then used to create 3D reconstructions of the myocardium (Fig. 5.9 C&D) and the endocardium (Fig. 5.9 H&I). Using MorphoHeart, I also analysed myocardial ballooning, which calculates the distance myocardial tissue balloons away from the midline of the heart (Fig. 5.9 E), and I found that the ventricle in *eogt-201^{Δ28}* homozygous mutants appears to balloon less (Fig. 5.9 G) compared to the ventricle in wild-type sibling hearts (Fig. 5.9 F). Furthermore, as Notch activity appeared to be mainly in the heart endocardium, I analysed endocardial tissue thickness (Fig. 5.9 J) to assess whether endocardial tissue is thinner in *eogt-201^{Δ28}* homozygous mutants, potentially as a result of dysregulated Notch signalling and found that there is a mild reduction in endocardial tissue thickness in the ventricle of *eogt-201^{Δ28}* mutant hearts (Fig. 5.9 L) compared to wild-type hearts (Fig. 5.9 K). To investigate heart development further, I measured parameters such as total heart volume (Fig. 5.10 A) and volume of both the atrium (Fig. 5.10 B) and ventricle (Fig. 5.10 C) but found there to be no significant difference in heart size between wild-types and *eogt-201^{Δ28}* homozygous mutants. To further assess whether there are differences in endocardial thickness I measured the total volume of endocardial tissue in the heart (Fig. 5.10 D), alongside volume of endocardial tissue in both the atrium (Fig. 5.10 E) and ventricle (Fig. 5.10 F), however there was no significant difference in endocardial volume in either the whole heart or in individual chambers between wild-type siblings or *eogt-201^{Δ28}* mutants. This data suggests that the *eogt-201^{Δ28}* mutation could be resulting in reduced myocardial ballooning in the ventricle during heart development, however this would require further investigation into why this could be occurring. Furthermore, the *eogt-201^{Δ28}* mutation appears to not affect embryo viability in general as these embryos were raised to adulthood and appeared phenotypically normal at 3 months of age.

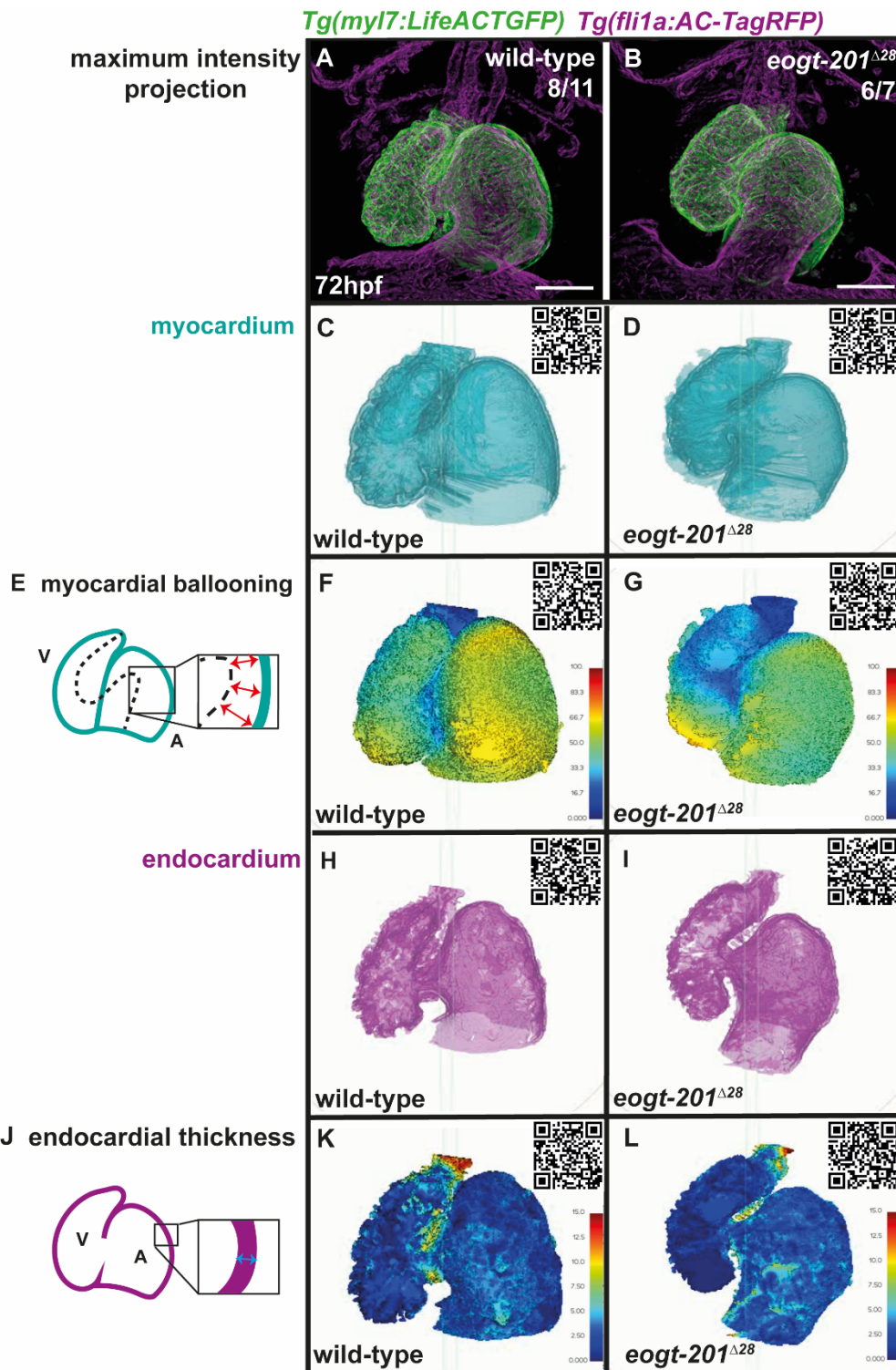


Figure 5.9. MorphoHeart analysis of cardiac morphology in *eogt-201^{Δ28}* mutant embryos. MorphoHeart image analysis was used to create 3D reconstructions of *eogt-201^{Δ28}* mutant and wild-type sibling heart tissue layers to carry out in depth quantitative analysis of heart morphology at 72hpf. Maximum intensity projections of a *Tg(myI7:LifeActGFP);Tg(fli1a:AC-TagRFP)* wild-type sibling heart (**A**) and an *eogt-201^{Δ28}* mutant heart (**B**) imaged on the light-sheet microscope at 72hpf,

labelling the myocardial tissue green and the endocardial tissue magenta. MorphoHeart-generated 3D reconstructions of the myocardial (C&D) and endocardial (H&I) tissue layers of the wild-type heart imaged in (A) and the *eogt-201^{Δ28}* mutant heart imaged in (B) to carry out morphological analysis of the individual tissue layers. MorphoHeart visualisation of myocardial ballooning, which calculates the distance the myocardial tissue has ballooned away from the midline of the heart (E) revealed a mild reduction in myocardial ballooning in the ventricle of the *eogt-201^{Δ28}* mutant heart (G) compared to the wild-type heart (F). Analysis of endocardial tissue thickness (J), with endocardial thickness heatmaps showing mildly reduced thickness for the *eogt-201^{Δ28}* mutant heart (L) compared to the wild-type heart (K). Scale bars: 50μm. Mendelian ratio: wild-types = 11, heterozygotes = 15, homozygotes = 7.

5.9 *eogt-201^{Δ28}* coding sequence mutant has no effect on Notch signalling in the developing heart

Finally, I wanted to assess whether Notch signalling is disrupted in the hearts of *eogt-201^{Δ28}* mutant embryos, taking a similar experimental approach to that described above in the *eogt* over-expression experiments by counting Notch positive endocardial cells. I crossed the *eogt-201^{Δ28}* heterozygous adults carrying the *Tg(myl7:LifeActGFP)* transgene which labels the heart myocardium green to *eogt-201^{Δ28}* heterozygotes carrying the *Tg(Tp1bglob:hmgbl-mCherry)* Notch reporter, obtaining *eogt-201^{Δ28}* homozygous mutant embryos with both green myocardial cells and red cells positive for Notch activity. These embryos were fixed at 26hpf and immunostaining was carried out to label the endocardial cells using the anti-Fli1b antibody (Moore et al., 2013) (Fig. 5.11 A&B). Similar to the *eogt* over-expression experiments, I counted the total number of Notch positive cells throughout the whole endocardium (Fig. 5.11 G&H), and although there appeared to be a reduced number of Notch positive endocardial cells in *eogt-201^{Δ28}* mutant embryos this was not significantly different compared to wild-type siblings (Fig. 5.11 I). I then counted the number of Notch positive cells in the OFT endocardium, but again found there was no significant difference between *eogt-201^{Δ28}* mutant or wild-type embryos (Fig. 5.11 J). This data suggests that there is no significant difference in Notch signalling in the endocardium of *eogt^{Δ28}* mutant embryos compared to wild-type siblings, suggesting that either this mutation has no effect on

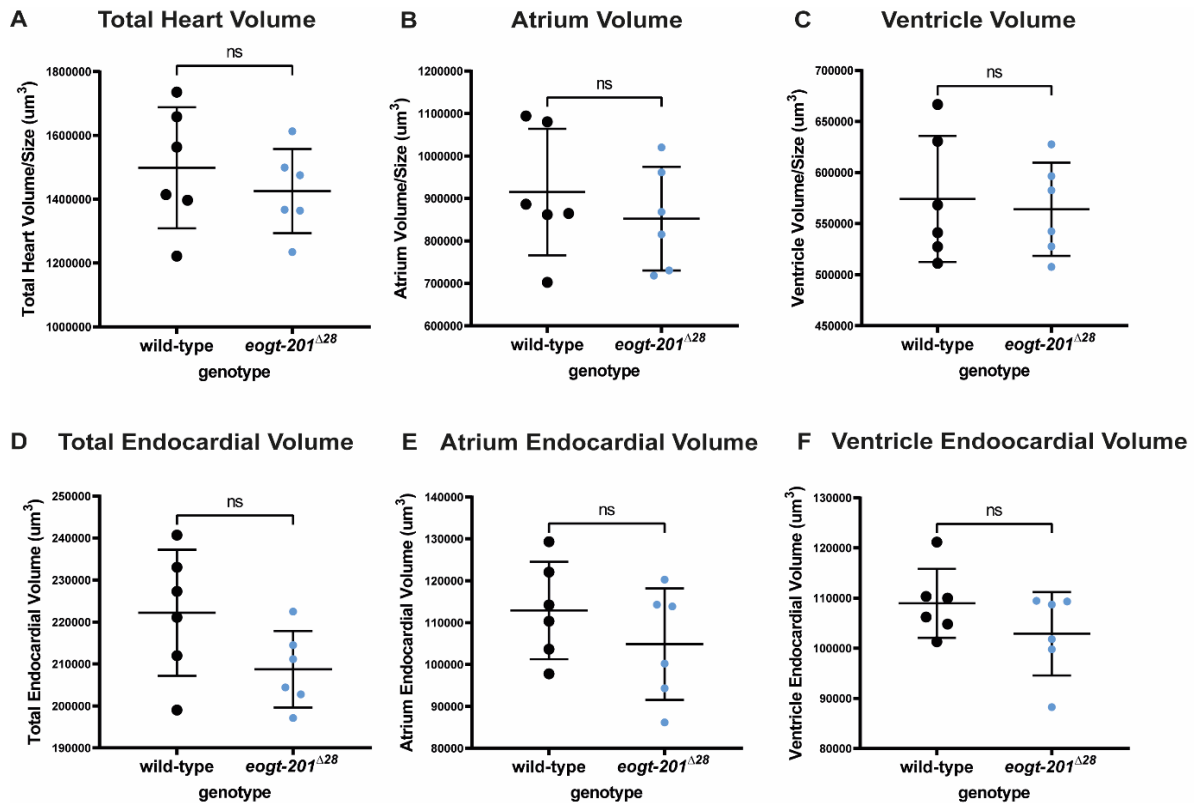


Figure 5.10. *eogt-201*^{Δ28} mutation has no effect on cardiac development. MorphoHeart quantitative analysis indicated there was no significant difference in heart size between wild-type and *eogt-201*^{Δ28} mutant hearts in terms of total heart volume (A), atrial volume (B) or ventricle volume (C). Similarly, there was no significant difference in endocardial tissue volume in either in the whole heart (D) or in the atrium (E) or ventricle (F). Mean ± SD are plotted and analysed with the Unpaired t-test, ns: not significant.

the ability of the Eogt protein to O-GlcNAcylate Notch receptors and ligands to activate Notch signalling in the heart endocardium at 26hpf, or that Eogt is not required to activate Notch signalling in the heart endocardium at this stage of development.

Together this data suggests that the *eogt-201*^{Δ28} coding sequence mutation, despite removing 5 conserved amino acids from the Eogt protein, has minimal effects on heart morphology and Notch signalling in the heart at 26hpf. Given the difficulties recovering an *eogt* mutant zebrafish line, it is possible that any mutation in *eogt* which causes a LOF phenotype could be lethal, and that I was able to recover a stable line because this specific mutation appears to have no consequence on Eogt function or embryo viability.

5. Investigating the role of *eogt*

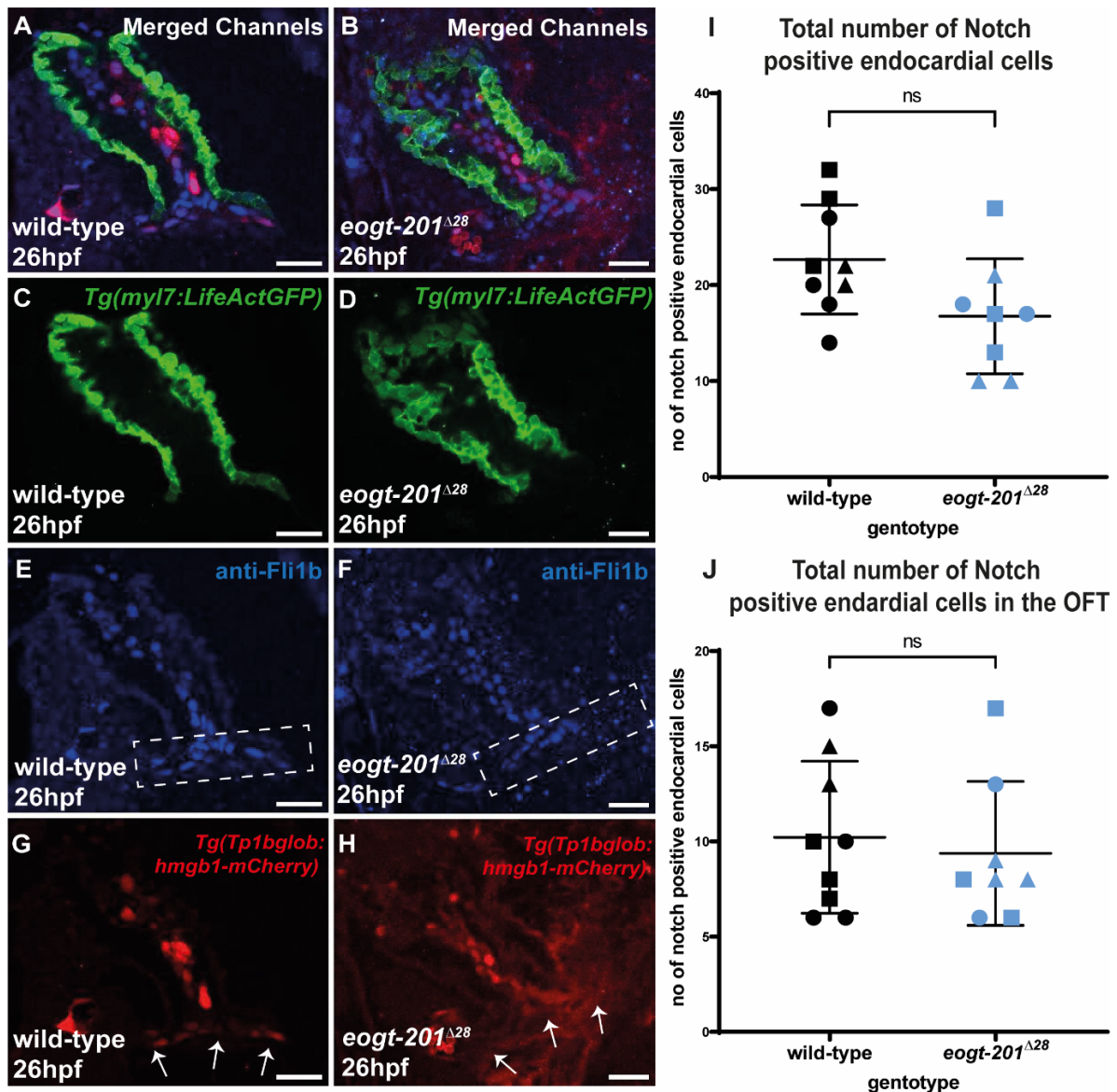


Figure 5.11. *eogt-201^{Δ28}* mutation has no effect on Notch signalling in the developing heart. Single slice confocal images of the heart at 26hpf from *Tg(myI7:LifeActGFP);Tg(Tp1bglob:hmgbl-mCherry)* double transgenic embryos (A&B) labelling the myocardium green (C&D) and cells with active Notch signalling red (G&H) in combination with the anti-Fli1b antibody to label endocardial cell nuclei blue (E&F). Single slice confocal images of 26hpf hearts with transgene expression labelling the myocardium green, Notch positive cells red and endocardial cells blue in wild-type sibling embryos (A) or *eogt-201^{Δ28}* mutant embryos (B). *Tg(myI7:LifeActGFP)* transgenic expression labels myocardial tissue green in wild-type siblings (C) or *eogt-201^{Δ28}* mutant embryos (D). Anti-Fli1b immunostaining shows endocardial cell nuclei in wild-type sibling hearts (E) and *eogt-201^{Δ28}* mutant

hearts (**F**), with the OFT endocardium region highlighted by the white dotted box. *Tg(Tp1bglob:hmgb1-mCherry)* global Notch signalling shown throughout the 26hpf heart endocardium in both wild-type siblings (**G**) and *eogt-201^{Δ28}* mutant hearts (**H**). Quantitative analysis revealed no significant difference between the number of Notch positive endocardial cells in the hearts of *eogt-201^{Δ28}* mutant embryos compared to wild-type siblings (**I**). Similarly, there was no significant difference in the number of Notch positive cells in the OFT endocardium (region indicated by white dotted box in panel **E&F**) of hearts from *eogt-201^{Δ28}* mutants compared to wild-type siblings (**J**). I&J: mean ± SD are plotted. I was analysed using the Unpaired t-test, J was analysed using the Mann-Whitney U test, ns: not significant. Scale bars: 50µm. Mendelian ratio: wild-types = 9, heterozygotes = 21, homozygotes = 7.

5.10 Discussion

In chapter 5 I investigate the role of *eogt* during cardiac development and regulation of Notch signalling in the developing zebrafish heart to understand how mutations in *eogt* lead to the onset of CHDs in AOS patients. I over-express *eogt* sense RNA in zebrafish embryos to investigate whether an abundance of *eogt* RNA has an effect on cardiovascular development or Notch signalling, and I also over-express *eogt* antisense RNA to investigate potential functional roles of this novel *eogt* antisense RNA transcript which is expressed in the heart myocardium at 24hpf. Finally, I characterise an *eogt-201^{Δ28}* coding sequence mutant, which removes 5 conserved amino acid residues from the Eogt protein, but again show that this mutation has minimal effects on *eogt* sense or antisense RNA expression, Notch signalling or heart development.

EOGT is highly conserved from *C.elegans* to humans, with substrate specificity being so similar that the mouse homolog of *Eogt* is able to rescue defects in *eogt* null *Drosophila*, suggesting an important evolutionary role for this gene among numerous organisms (Sakaidani et al., 2012). The difficulties in trying to make an *eogt* mutant line in zebrafish, where the majority of F0 gRNA injected embryos died whilst attempting to make *eogt* LOF mutant models (see Chapter 3), combined with the mutant line I managed to recover having minimal effects on Eogt protein function, suggest that LOF mutations in the *eogt* gene might be incompatible with survival in

zebrafish embryos. This would be similar to *Drosophila*, where *eogt* LOF animals fail to survive past larval stages (Varshney and Stanley, 2017). However, in mice, despite *eogt* being expressed at the apical ectodermal ridge of developing limb buds in the embryo (Shaheen et al., 2013) and being expressed ubiquitously in adults (Sakaidani et al., 2012), *Eogt* null mice were viable and fertile, with the only observed phenotype being retinal vascular defects (Sawaguchi et al., 2017).

The *eogt-201^{Δ28}* coding sequence mutant, despite disrupting a splice site, does not appear to cause aberrant splicing and despite mutating 5 conserved amino acids in the glycosyltransferase domain it does not appear to impact *eogt* function or Notch activity in the developing heart. This raises the question as to whether *eogt* carries out similar roles in regulating Notch signalling in fish as it has been shown to do in mice (Sawaguchi et al., 2017), or alternatively whether this mutation in *eogt* is having an impact on *Eogt* function. At present there is no antibody which is predicted/shown to recognise *Eogt* in zebrafish, making it difficult to assess whether the *eogt-201^{Δ28}* mutation is having an impact on protein expression. However, there is an O-GlcNAc antibody shown to work on tissue sections of the zebrafish brain (Lee et al., 2020), and using this antibody in combination with a zebrafish *notch1* transgenic line such as *Tg(notch1b-15:GFP)* (Chiang et al., 2017) could show co-localisation of O-GlcNAcylation with *notch1b* expression in the developing heart. Using both the O-GlcNAc antibody and the *Tg(notch1b-15:GFP)* transgene together in the *eogt-201^{Δ28}* mutant could show whether there is reduced O-GlcNAcylation associated with expression of the *notch1b* receptor in the developing heart, and this could indicate whether this mutant is affecting *Eogt* function and also suggest whether Notch1 appears to be a target of *Eogt* in zebrafish.

In humans, all known *EOGT* mutations identified to-date in AOS patients disrupt *EOGT* enzyme function either by introducing a premature stop codon resulting in a truncated form of the *EOGT* enzyme which lacks the catalytic domain making it non-functional, or resulting in misfolding of the *EOGT* protein and targeting it for degradation, with one mutation preventing *EOGT* from being able to bind to the O-GlcNAc substrate (Varshney and Stanley, 2017). This shows that defective O-GlcNAcylation by *EOGT* is behind the pathology of AOS in patients with *EOGT* mutations, however it has not yet been shown that human mutations in *EOGT* specifically result in defective NOTCH

signalling in AOS. It is known that in AOS patients with mutated *NOTCH1*, some of the mutations identified reside in the EGF repeats which could be targets of EOGT O-GlcNAcylation, but a direct link between *EOGT* mutations and loss of NOTCH signalling is yet to be shown (Stittrich et al., 2014). Furthermore, the *eogt-201^{Δ28}* mutation described in this study appears to have no effect on Notch signalling in the developing zebrafish heart, however whether this is due to the mutation having no effect on Eogt function or whether Eogt acts on other proteins during zebrafish heart development is still to be investigated. Despite not being shown directly in AOS, it has been shown in cell lines derived from patients suffering from pancreatic cancer that EOGT O-GlcNAcylates NOTCH1 to promote NOTCH intra-cellular domain localisation to the nucleus to activate the NOTCH signalling pathway, indicating that NOTCH1 is a direct target of EOGT O-GlcNAcylation in humans (Yang et al., 2012). This data, together with studies demonstrating that other NOTCH signalling pathway components are commonly mutated in AOS, provide evidence suggesting that mutations in *EOGT* are resulting in defective NOTCH signalling in AOS, but further analysis is required to understand exactly how *EOGT* mutations are resulting in the onset of this disease (Ogawa et al., 2015).

Further support that mutations in *EOGT* are resulting in defective NOTCH signalling in AOS patients comes from investigating other glycosyltransferases, which have also been shown to be important for NOTCH receptor and ligand interactions and are associated with diseases with similar phenotypes to AOS (Matsumoto et al., 2020). There are four known O-linked glycan modifications identified at specific sites on NOTCH EGF repeats mediated by the following glycosyltransferases: protein O-glycosyltransferase 1 (POGLUT1), protein O-fucosyltransferase 1 (POFUT1), protein O-glycosyltransferase 2/3 (POGLUT2/3) and EOGT (Pandey et al., 2020). LOF of either *Poglut1* and *Pofut1* is embryonic lethal in mice, and these embryos failed to correctly form a heart and displayed vascular defects (Fernandez-Valdivia et al., 2011; Shi and Stanley, 2003). Heterozygous mutations in both *POGLUT1* and *POFLUT1* in humans are associated with an autosomal dominant disorder called Dowling-Degos Disease (DDD) which is characterised by hyperpigmented skin (Buket Basmanav et al., 2015), however like mouse *Eogt* mutant models, mouse models with heterozygous mutations in either *Poflut1* or *Poglut1* are healthy and viable and do not show the hyperpigmentation feature associated with DDD (Matsumoto et al., 2020).

Additionally, mutations which reduce the activity of *POGLUT* have been identified in patients with limb-girdle muscular dystrophy, which is characterised by reduced NOTCH signalling in satellite cells resulting in impaired muscular development (Servián-Morilla et al., 2016). Autosomal recessive mutations in Lunatic Fringe (LFNG), an enzyme which elongates O-fucose modifications (Kakuda and Haltiwanger, 2017), have been found in patients with Spondylocostal Dysostoses, a skeletal disorder which arises during development and is caused by defects in somitogenesis (Matsumoto et al., 2020). Together this data suggests that glycosyltransferases play important roles in regulating the NOTCH signalling pathway, and it shows that mutations in genes carrying out similar roles to *EOGT* result in dysregulated NOTCH signalling and lead to diseases with similar phenotypes to AOS.

Despite evidence suggesting *EOGT* regulates NOTCH signalling, previous studies have shown that *EOGT* O-GlcNAcylates other proteins with EGF repeats (Ogawa and Okajima, 2019), so it could be possible that *eogt* has other targets which could be dysregulated and resulting in the phenotypes observed in AOS. In *Drosophila*, knock-down of *eogt* in the wing results in wing blistering, which is exacerbated by simultaneously removing either one copy of the *dumpy* gene, which is involved in maintaining the integrity of the apical extracellular matrix, or the *wingblister* gene, which encodes a laminin α chain, suggesting potential genetic interactions between *eogt* and these genes, which both have extracellular EGF domains (Müller et al., 2013). Additionally, it was shown that Dumpy is a direct target for Eogt O-GlcNAcylation in the wings and trachea, and therefore loss of Dumpy O-GlcNAcylation in *eogt* null *Drosophila* is thought to be responsible for the epithelial-cell matrix interaction defects which cause lethality (Sakaidani et al., 2012). Furthermore, although components of the Notch signalling pathway are shown to be O-GlcNAcylated by *eogt* in *Drosophila* (Harvey et al., 2016), *eogt* null animals did not display phenotypes associated with disrupted Notch signalling, such as neurogenesis or defects in wing vein formation (Varshney and Stanley, 2017) and removal of Notch signalling pathway components in *eogt* null *Drosophila* actually suppressed the wing blistering phenotype (Müller et al., 2013). This data suggests that defects in *Drosophila* *eogt* mutants arise mainly due to disrupted epithelial-cell matrix interactions, which are caused by a lack of O-GlcNAcylation of Dumpy rather than Notch signalling pathway components (Varshney and Stanley, 2017), highlighting that Eogt targets other than

the Notch signalling pathway could be important to investigate in the onset of AOS. Furthermore, other EOGT targets identified in mammals have been found to be implicated in cardiovascular development, for example heparin sulfate proteoglycan 2 (HSPG2) (Varshney and Stanley, 2017) is known to be important for vascular and cardiac development, with *Hspg2* null mice being embryonic lethal and displaying vascular defects (Costell et al., 2002). Additionally, laminin subunit alpha 5 (LAMA5) has also been found to be an EOGT target in mammals (Varshney and Stanley, 2017) and has also been found to be implicated in the onset of a multisystemic syndrome which presents with similar phenotypes to AOS, such as skin anomalies and cardiovascular defects (Sampaolo et al., 2017). This suggests that other EOGT targets alongside NOTCH signalling pathway components could be disrupted in AOS patients with EOGT mutations, and that dysregulation of these other EOGT target genes could be resulting in the phenotypes observed in AOS.

As over-expressing *eogt* sense or antisense RNA appears to have no effect on cardiac Notch signalling, it is possible to speculate that over-expression of *eogt* does not affect Notch signalling during cardiac development. Discrepancies in the literature indicate that it is currently unknown what effect over-expressing *eogt* has on Notch signalling, as over-expression of *eogt* in *Drosophila* had no impact on Notch signalling in the wing or eye tissues (Müller et al., 2013). However, in HEK293T cells, over-expression of both *Eogt* cDNA along with *Notch1* cDNA enhanced NOTCH1-DLL4 binding, but it is worth noting that over-expression of Notch1 cDNA alone also significantly increases NOTCH1-DLL4 binding, although at a lower level compared to over-expression of both *Notch1* and *Eogt* cDNA (Sawaguchi et al., 2017). Similarly, despite showing increased NOTCH1-DLL4 interactions when both *Eogt* and *Notch1* cDNA are over-expressed, they do not show increased NOTCH signalling, indicating that over-expression of *Eogt* might not result in higher levels of NOTCH activity (Sawaguchi et al., 2017). In line with these findings, I found that over-expressing either the *eogt* sense or antisense RNA has no effect on Notch signalling in the developing heart in zebrafish embryos. Like described above for the *eogt-201^{Δ28}* mutant, it would be useful to test whether over-expression of *eogt* sense RNA is resulting in an increase in Eogt protein expression and activity in the zebrafish embryo. As there is no antibody predicted/shown to recognise Eogt in zebrafish, I could utilise the O-GlcNAc antibody described above to see whether there is an increase in O-GlcNAcylation when *eogt*

sense RNA is over-expressed, which would suggest increased Eogt protein activity. As these *eogt* transcripts are degraded after 24hpf, a similar timing to when these genes are normally downregulated, this suggests that they are subject to the same regulation/degradation as endogenous transcripts, making it difficult to investigate the impact of long-term over-expression. Therefore, it would be interesting to investigate the impact of persistent over-expression of these genes at later stages of development and this could perhaps be investigated by creating transgenic zebrafish lines carrying a construct where either *eogt* sense or antisense RNA is expressed under the control of the heat shock promoter Hsp70. Exposing these animals to heat shock after 24hpf will trigger ubiquitous over-expression (Shoji and Sato-Maeda, 2008) of *eogt* sense or antisense RNA at later stages of development, allowing me to see whether prolonged over-expression has an effect on Notch dependent processes later in heart development.

NOTCH signalling is involved in multiple aspects of cardiac development, including later in development when *eogt* sense or antisense RNA are no longer expressed in the zebrafish embryo. As *eogt* sense and antisense RNA are rapidly degraded after 24hpf, it would be interesting to investigate these other Notch dependent processes in prolonged *eogt* over-expression experiments to see whether excessive *eogt* sense or antisense RNA expression has any impact on later heart development. For example, Notch signalling is required for valve development, which occurs around 55hpf in zebrafish embryos (Timmerman et al., 2004), so it would be interesting to investigate in more detail whether *eogt* over-expression at this stage affects valve development by investigating Notch signalling in the valves, and using endocardial and myocardial markers to visualise atrioventricular and OFT valve morphology. Similarly, NOTCH signalling is also required for trabeculation, which begins around 72hpf in the developing zebrafish heart (Grego-Bessa et al., 2007), and it would be interesting to investigate trabeculation in the ventricle in *eogt* sense or antisense RNA over-expression models using light-sheet imaging to count the trabeculating cells and understand whether this process occurs normally when either *eogt* is over-expressed later in development.

Furthermore, since it is unclear what specific roles the *eogt* antisense RNA might play during heart development, it would be interesting to knock-out the *eogt* antisense

transcript to assess whether this results in defects in heart development or Notch signalling. As this *eogt* antisense RNA is not annotated in zebrafish, and as the 5' and 3' ends are not known, it is difficult to design a knock-out strategy to investigate potential functional roles it could have during cardiac development. At present it is unknown whether this *eogt* antisense transcript regulates *eogt* expression, and although there are examples of cis-regulating lncRNAs, the majority of reported lncRNAs are trans-acting (Beermann et al., 2016). Additionally, as over-expression of either *eogt* sense or antisense RNA does not result in increased or decreased expression of the other transcript, this could suggest that the *eogt* antisense transcript is acting on a completely different gene and process that is currently unknown. Knocking-out the antisense transcript and identifying whether this results in a cardiac phenotype could direct towards processes/signalling pathways this antisense transcript could be regulating, or alternatively I could assess other known mammalian EOGT target proteins other than NOTCH signalling pathway components, such as HSPG2 or LAMA5 (Varshney and Stanley, 2017) and see whether expression or function of these genes is disrupted in *eogt* antisense over-expression conditions.

The difficulties posed by not knowing the 5' and 3' end of the *eogt* antisense transcript, and the fact that it overlaps with a large proportion of the *eogt* sense transcript, makes it difficult to mutate this antisense transcript specifically to investigate whether it has a functional role without also mutating the *eogt* sense RNA. While it is unknown whether the *eogt-201^{Δ28}* mutation is also mutating the *eogt* antisense transcript, it does not appear to be influencing either *eogt* sense or antisense expression. As 5% of AOS patients with mutations in *EOGT* also suffer from CHDs (Hassed et al., 2017), it is possible to speculate that mutations affecting both the sense and antisense transcripts might be required to result in CHDs arising. However, mapping AOS mutations that are associated with CHDs onto the human *EOGT* gene (Fig. 3.11) reveals that at least one known mutation which is causative of CHDs does not overlap with the human *EOGT* antisense transcript annotated on the UCSC genome browser, suggesting that mutations which only affect the *eogt* sense transcript are sufficient to result in CHDs in AOS patients.

Despite the *eogt-201^{Δ28}* mutation appearing to have minimal effects on heart morphology or Notch signalling, there did appear to be reduced ventricle myocardial

ballooning in *eogt-201^{Δ28}* mutant hearts compared to wild-type sibling hearts. It is known in mice that NOTCH signalling is required in the CNC cell population for smooth muscle cell differentiation, resulting in OFT and ventricular septal defects (High et al., 2007). As zebrafish do not have a separated OFT, it is thought that CNC cells contribute to myocardial tissue in the ventricle and OFT (Li et al., 2003), so it is possible that Notch signalling could be required in zebrafish CNC cells to encourage differentiation into myocardial cells upon migration to the ventricle. However, further investigation of whether Notch signalling is required in CNC cells would be needed to confirm this, which could be achieved by labelling CNC cells with the *sox10* promoter driving eGFP expression (George et al., 2020) and combining this with a Notch reporter to see whether Notch signalling is disrupted in CNC cells in the *eogt-201^{Δ28}* mutant. Furthermore, by labelling CNC cells it would be possible to see whether fewer CNC cells contribute to ventricle myocardial tissue in *eogt-201^{Δ28}* mutant hearts compared to wild-types, indicating that decreased ventricular ballooning is due to defects in CNC cell addition to the heart in this mutant model.

In this chapter, I analyse over-expression of *eogt* sense RNA, and over-expression of a novel *eogt* antisense RNA which is expressed in the zebrafish myocardium during early cardiac development. After assessing the impact of over-expressing these RNAs on cardiac development and Notch signalling in the developing heart, I conclude that over-expression of both *eogt* sense and antisense RNA appears to have no effect on expression of the reciprocal transcript, Notch signalling in the heart endocardium at 26hpf or cardiac development. Similarly, I characterise the first reported *eogt-201^{Δ28}* mutant and again show that this mutation appears to have minimal effects on *eogt* sense or antisense RNA expression or Notch signalling in the heart endocardium at 26hpf, but results in decreased ventricle myocardial ballooning at 72hpf. Despite over-expressing and mutating *eogt*, there is no impact in Notch signalling in the heart in either model, indicating two possibilities: 1) *eogt* over-expression/the *eogt-201^{Δ28}* mutant model has no effect on Notch signalling in the developing heart; or 2) *eogt* sense or antisense RNA does not regulate Notch signalling in the heart at this stage of development. As there are other protein targets of *EOGT* O-GlcNAcylation (Varshney and Stanley, 2017), exploring further *EOGT* targets other than NOTCH signalling pathway components could provide insights into how mutations in *EOGT* result in defects observed in AOS patients. This data suggests that generating suitable

5. Investigating the role of *eogt*

animal models with which to interrogate function of the *eogt* gene in the context of cardiac development is challenging and complex, particularly with the difficulties in recovering an *eogt* LOF mutant and achieving sustained over-expression of *eogt* after 24hpf. Therefore, it is possible that disrupting the function of *Eogt* is incompatible with survival in zebrafish, making it a difficult loss-of-function to model using zebrafish embryos, and could potentially explain why no zebrafish mutant models for *eogt* LOF have previously been described.

6. Discussion

Despite Adams-Oliver syndrome (AOS) being first described in 1945 (Adams and Oliver, 1945), the mechanisms behind several features of this disease still elude scientists: why only 50% of cases are linked to 6 known genes; how mutations in these genes result in the defects observed in AOS; and why there is such variability in phenotypes, even within the same family possessing the same genetic mutation (Zepeda-Romero et al., 2022). Here I create the first reported *dock6* and *eogt* zebrafish disease models to investigate the pathology behind AOS, with particular focus on cardiac development with the aim to understand why a proportion of AOS patients are born with congenital heart defects (CHDs). Additionally, for both *dock6* and *eogt* I identify associated non-coding transcripts which are expressed specifically in the heart during an early stage of zebrafish heart development and investigate what role these non-coding transcripts could be playing during cardiac development and the onset of CHDs. Finally, I investigate a compensation pathway which is responsible for adapting to a chronic loss of *dock6* expression in human cells and provide evidence that this compensation pathway could be playing a role in preventing CHDs in AOS patients with *DOCK6* mutations. In this chapter I discuss why only 50% of cases have a known genetic cause, possible ways mutations in known causative genes result in the phenotypes observed in AOS and why there is such variability in phenotypes seen in this disease, all in light of my thesis work.

6.1 Why is AOS associated with such varied feature severity?

AOS is a highly variable disorder with both phenotypic and genetic heterogeneity (Dudoignon et al., 2019), as some patients present with severe phenotypes which are incompatible with survival, while others display mild phenotypes which can often evade diagnosis (Hassed et al., 2017). This is also the case within families possessing the same genetic mutations, for example two siblings with the same inherited *DOCK6* mutation displayed different phenotypes, with one patient almost evading AOS diagnosis due to presenting only subtle defects of the hands and feet, alongside neurological and retinal vascular defects upon closer inspection, while their sibling who inherited the same mutation displayed the hallmark features of AOS: aplasia cutis

congenita (ACC) and terminal transverse limb defects (TTLD), alongside more severe neurological and retinal vascular defects (Zepeda-Romero et al., 2022). Furthermore this is not unusual in familial cases of AOS, with other studies identifying siblings with the same AOS mutation displaying varying severity of phenotypes (Amor et al., 2000; Balasubramanian and Collins, 2009).

AOS can be both inherited and sporadic, and it was found that sporadic cases of AOS commonly possess a wider range of phenotypes compared to cases linked to inherited genetic mutations, however why the phenotypes observed in AOS vary so much across patients is still unknown (Hassed et al., 2017). Linking specific genetic mutations to the onset of certain AOS phenotypes has been investigated, with CHDs being more common in AOS patients with mutations in *NOTCH1*, *DLL4* and *RBPJ*, while neurological abnormalities exist more frequently in AOS patients with mutations in *DOCK6* (Meester et al., 2018). However, it is thought incomplete penetrance and genetic heterogeneity could play a role in the varied phenotypes observed in AOS, a phenomenon which occurs in other inherited syndromes such as Alagille syndrome (Meester et al., 2019) and Joubert syndrome (Bachmann-Gagescu et al., 2015).

The idea that genetic heterogeneity in patients with AOS could result in varied phenotypes provides an interesting area of further exploration. In chapter 4 I characterise zebrafish heart morphology in *dock6-R11^{ins41}* homozygous mutants, and while the majority of these embryos had comparable heart morphology to wild-type embryos, a subset of embryos displayed abnormal cardiac morphology (see Fig. 4.6). One limitation of this experiment could be whether it was powered correctly to take into account heterogeneity, and maybe analysing more mutant embryos could help identify heterogeneous phenotypes. Additionally, while characterising zebrafish *dock6-R11^{ins41}* mutants, I identified that a gene involved in a compensation pathway required to adapt to a loss of *dock6*, *isg15* (Cerikan et al., 2016) showed genetic heterogeneity between embryos and even heterogeneity at a cellular level in 6hpf zebrafish embryos (See Fig. 4.9). Reduction in *ISG15* is required to activate the compensation pathway that allows cells derived from AOS patients to adapt to a chronic loss of *DOCK6*, and therefore if patients have different baseline levels of *ISG15*, this could make them more or less able to adapt to a loss of *DOCK6*, potentially indicating how severe features will be in AOS patients with *DOCK6* mutations.

Intriguingly, other animal models with mutations in genes associated with AOS found varying phenotypes linked to genetic heterogeneity and incomplete penetrance. One example is in mice with heterozygous mutations for *Dll4*, where most mice died by embryonic day E10.5, while a small proportion survived and were indistinguishable from their wild-type siblings (Gale et al., 2004). Interestingly, this study suggests that the differences in genetic backgrounds of these mice indicate whether they will develop features which are incompatible with survival or whether they will be healthy and viable, as an increased number of heterozygous *Dll4* mutant mice survived in one background strain compared to another (Gale et al., 2004). Furthermore, in *Drosophila*, the genetic background of individual animals could predict how severe phenotypes would be in *Drosophila RBPJ/Su(H)* mutants. This study found that the levels of expression of the *Drosophila Notch* receptor or the co-repressor gene *Hairless* in the genetic backgrounds in individual flies could enhance the severity of tissue specific phenotypes in combination with *RBPJ/Su(H)* mutations (Gagliani et al., 2022), indicating that genetic backgrounds can influence feature severity in animal models of AOS genes, and that individual genetic background in humans could explain why AOS phenotypes vary so widely in patients with the same genetic mutation.

Although it does not explain why related AOS patients with the same inherited mutation suffer from different phenotypes, it is possible to speculate that some of the variability in phenotypic severity across AOS patients arises from the nature of the mutation they possess. In *Drosophila* it was found that the specific *RBPJ/Su(H)* mutations resulted in more severe phenotypes, particularly if the specific mutation disrupted DNA binding resulting in disruption to Notch target gene expression (Gagliani et al., 2022). Furthermore, it has been shown that if a mutation results in a truncated RNA transcript, this transcript can undergo nonsense mediated decay and trigger genetic compensation via upregulation of related genes which can mask phenotypes (El-Brolosy et al., 2019). This was found to occur in patients with mutations in the *FBN1* gene with Marfan syndrome, where patients with the mildest form of the disease had the lowest amount of the mutant transcript due to mutations which resulted in a premature stop codon in *FBN1* resulting in nonsense mediated decay, compared to patients who had missense mutations in *FBN1* who suffered greater disease severity (El-Brolosy et al., 2019). While this doesn't explain why AOS patients with the same genetic mutation can present with different phenotypes, it does

suggest that the nature of the genetic mutation could contribute to the variability. In this study I characterise coding sequence mutations for both *dock6* and *eogt* (see chapter 3), neither of which are truncation mutations causing nonsense mediated decay, but also do not present with a phenotype. As it was so difficult to recover loss of function (LOF) mutant founders for both *dock6* and *eogt*, I hypothesise that the coding sequence mutations must be having no effect on protein function, allowing me to recover stable lines possessing these mutations. It would be interesting to investigate whether the nature of specific AOS patient mutations, such as truncation mutations, result in varied phenotypes by attempting to create a range of AOS mutations in *dock6* and *eogt* in zebrafish and assessing the severity of phenotype.

It is also possible that a combination of genetic mutations and environmental factors could influence the severity of phenotypes in AOS patients, and this could potentially explain why related patients with the same inherited mutation have differing severity of the disease. Studies in mice have shown that a combination of *Notch1* heterozygous mutations and hypoxia during gestation is linked to an increased likelihood of CHDs commonly observed in AOS such as ventricular septal defects and double outlet right ventricle (Chapman et al., 2020). Furthermore, it was suggested that two identical twins with Alagille syndrome had differing phenotypes because one twin had experienced hypoxia during development. The twins inherited heterozygous *JAG1* mutations, however twin B experienced hypoxia due to problems with blood flow through the umbilical artery, and this is believed to have caused more severe phenotypes than occurred in twin A, such as restricted growth and liver abnormalities (Izumi et al., 2016). Additionally, heterozygous *Dll4* mutations in the SHF of mice in combination with prenatal alcohol exposure led to increased outflow tract (OFT) defects, suggesting that early exposure to alcohol can increase the likelihood of developing a CHD if you have a genetic predisposition (Harvey et al., 2022). It has also been found that a combination of a high lipid diet and heterozygous *Rbpj* mutations in mice was found to worsen the haemodynamic parameters associated with calcific aortic disease (Nus et al., 2011), and hyperglycaemia in mice during gestation in combination with heterozygous *Notch1* mutations increased the risk of ventricular septal defects (Basu et al., 2017). This data suggests that a variety of environmental factors in combination with genetic predisposition can influence disease

severity and could explain the variation of phenotypes observed in AOS patients, in particular the variation of CHD severity.

Together this data indicates that many factors likely contribute to the variability of phenotypes in patients with AOS, considering the specific mutation, genetic background of the individual, and environmental influences. Heterogeneity can make it difficult to create and assess disease models, however it is important models represent heterogeneity in order to accurately model how the disease presents in humans. While models which completely disrupt gene function might be easier to assess, this would also prove challenging in the case of *dock6* and *eogt*, as creating complete LOF mutants proved challenging, and I suspect could be incompatible with survival (see chapter 3). Therefore, as this disease is difficult to model due to the extreme variation on an individual basis, further investigation of how these factors interplay is important to understand the occurrence of severe cases of this disease in more detail.

6.2 How do phenotypes in AOS arise?

Although it is currently unknown how mutations in the 6 genes linked to AOS result in phenotypes observed in this disease, all known causative genes are involved with regulation of either the RAC1/CDC42 or NOTCH signalling pathways, suggesting dysregulation of these pathways is involved (Hassed et al., 2017). However, as these two signalling pathways are distinct, it is unsure how dysregulation of two individual signalling pathways are linked to the same disease, and whether there is overlap or crosstalk between the functions of the two pathways (Cohen et al., 2014). As both RAC1/CDC42 and NOTCH signalling have been found to be important for vascular development (Gridley, 2007; De Smet et al., 2009) and as vascular anomalies are commonly found in patients with AOS (Lehman et al., 2014) it is thought that defects in vasculogenesis could be behind the various phenotypes which arise in AOS patients (Stittrich et al., 2014). One of the main diagnostic phenotypes of AOS, alongside ACC and TTLD, is cutis marmorata telangiectatica congenita (CMTC), which results in dilated blood vessels and mottled skin and occurs in around 26% of reported AOS patients (Hassed et al., 2017). Numerous CHDs affecting the main vessels of the heart have also been reported in AOS patients including patent ductus arteriosus and pulmonary stenosis (Hassed et al., 2017). Furthermore, diffuse angiopathy and retinal

vascular defects have also been reported in AOS patients (Lehman et al., 2014) providing further evidence that defective vasculogenesis could be behind the phenotypes arising in this disease. Additionally, in chapter 3 I show that both *dock6* and *eogt* are expressed in the early vasculature in zebrafish (see Fig. 3.3 & Fig. 3.10), providing additional support that phenotypes which arise in AOS are due to defects in vasculature development.

It has previously been suggested that AOS phenotypes are a result of defects in small vessel development resulting in loss of blood flow to locations where defects arise (Swartz et al., 1999). One study proposes that ACC and TTLD could arise in AOS patients due to rapid growth of the brain and limbs, resulting in stretching of the skin, which in combination with defective vascular growth results in ischaemia and necrosis in the scalp and at limb extremities (Pereira-Da-Silva et al., 2000b). This was supported in mice models which showed that inhibition of NOTCH signalling in vascular smooth muscle cell precursors during a specific window of embryonic development resulted in necrosis in the scalp and limb extremities (Chang et al., 2012). Furthermore, endothelial-specific deletion of RAC1 in mice results in lethality and defects in vascular development, including a complete lack of small branched vessels (Tan et al., 2008), and knock-out of either RAC1 or CDC42 in the limb bud mesenchyme of mice embryos results in TTLD similar to those in AOS patients such as short limbs and syndactyly (Suzuki et al., 2013). Together this data could suggest that RAC1 and NOTCH are required in developing vasculature to ensure adequate blood flow to limb extremities to ensure correct development. It would be interesting to investigate whether there are defects in vascular development in the *dock6-R11^{ins41}* homozygous mutants with blocked compensation that I describe in chapter 4, as although this mutant model displays cardiac defects I did not look in detail at developing vasculature. However, it is known that disruption to other genes associated with Notch and Rac1/Cdc42 signalling in zebrafish commonly result in vascular defects, for example knock-down of *dll4* results in excessive vasculature branching (Leslie et al., 2007), and knock-down of another Dock GEF, *dock180/elmo1*, results in impaired vascular development (Epting et al., 2010). This provides further evidence that disruption to the NOTCH and RAC1/CDC42 signalling pathways result in vascular defects which could be implicated in the phenotypes observed in AOS patients.

Although NOTCH and RAC1/CDC42 are both known to be involved in vascular development, these two pathways regulate separate processes, for example RAC1/CDC42 are mainly involved in processes such as endothelial cell migration and regulation of cell adhesions and polarity (De Smet et al., 2009; Norden et al., 2016; Barry et al., 2015) while NOTCH signalling is required more for cell differentiation and cell fate decisions (Gridley, 2007). Therefore, how mutations in genes regulating these two signalling pathways that drive different cellular processes result in the same disease is still unknown. A study by Polacheck et al., has suggested a link between both the NOTCH and RAC1 signalling pathways in the development of cell junctions and barrier formation during vascular development, whereby NOTCH1-DLL4 mediated signalling triggered cleavage of the NOTCH intracellular domain, releasing the NOTCH transmembrane domain (NTD). The NTD was previously not known to have a biological function, but has been shown to activate a non-canonical NOTCH signalling pathway, whereby it interacts with partner proteins, including a GEF called TRIO, which can form a complex with VE-cadherin and activate RAC1 in order to form vascular adherens junctions and maintain barrier integrity (Polacheck et al., 2017). This data could explain why in *Eogt* mutant mice, which have reduced NOTCH1-DLL4 mediated signalling, there is a reduction in vascular integrity in the retina (Sawaguchi et al., 2017), which could be due to reduced non-canonical NOTCH signalling resulting in a decrease in vascular adherens junction formation. However, reduced vascular integrity was also observed in *Rbpj* heterozygous mutant mice (Sawaguchi et al., 2017), which isn't involved in this non-canonical NOTCH signalling pathway, so it could be the case that a combination of both canonical and non-canonical NOTCH pathway disruption could be contributing to vascular defects observed in AOS. As this study links both the NOTCH and RAC1 signalling pathways together, along with vascular development, all of which are thought to be implicated in AOS, investigating this non-canonical NOTCH signalling pathway in more detail could provide insights into how defects in AOS arise.

Another study found that in breast cancer cells, inhibition of the canonical NOTCH signalling pathway results in upregulation of a non-canonical NOTCH signalling pathway which increases CDC42 activity and the formation of filopodia, but decreases RAC1 activity and the formation of lamellipodia, thereby reducing cancer cell migration (Liu et al., 2019). This data could explain why in *Eogt* mutant mice, increased filopodia

extension was observed in vascular retina (Sawaguchi et al., 2017), as loss of canonical NOTCH signalling in these cells could trigger this non-canonical signalling pathway which leads to increased activation of CDC42, resulting in increased filopodia formation during vessel branching. This provides further evidence of NOTCH and RAC1 signalling pathway interactions which could be involved in the pathogenesis of AOS and could provide evidence that both canonical and non-canonical NOTCH signalling pathways could be implicated in the onset of this disease. It would be interesting to investigate whether interactions between the non-canonical NOTCH signalling pathway and RAC1 signalling occurs in zebrafish, and this could be achieved by investigating Rac1 activity using Rac1 FRET sensors in zebrafish *notch1* and *dll4* mutants, as a reduction in Rac1 activity could indicate Rac1 is downstream Notch signalling. In chapter 5 I investigated disruption to Notch signalling in *eogt-201* coding sequence mutants, however it would also be interesting whether Rac1 signalling is disrupted in these mutants too, as this if *eogt* is mediating Notch signalling, this could suggest interaction between both the Notch and Rac1 signalling pathways.

Despite it still being unknown exactly how defects in AOS arise, most data highlight the importance of correct vascular development, and the involvement of both RAC1/CDC42 and NOTCH signalling pathways in this process indicate that defective vasculogenesis could be the main driver of phenotypes arising in AOS. It is possible that the main defects which arise in AOS, such as ACC, TTLD and CMTc, are a result of decreased vasculature branching and reduced vasculature integrity causing lack of blood flow to the developing scalp and limb extremities and causing necrosis of the developing tissues (Swartz et al., 1999; Pereira-Da-Silva et al., 2000). Other defects such as CHDs could arise for numerous reasons, such as due to faulty vasculature development, particularly for CHDs which affect the main heart arteries, and it is known that endothelial cells are important for correct cardiovascular development, as zebrafish *cloche* mutants which lack the endothelial layer of the heart display cardiac defects (Stainier et al., 1995). Additionally, CHDs could arise as a result of defects in SHF and CNC contributions to the heart, as it has been shown that both RAC1/CDC42 and NOTCH signalling are required in these cell populations to facilitate cardiac development (Leung et al., 2016) (Varadkar et al., 2008) (Lescroart et al., 2018). Furthermore, it is likely that mutations in specific genes are also accompanied by further defects depending on gene specific processes, for example the observation

that mutations in *DOCK6* are more closely related to neurological defects is in line with studies showing that *DOCK6* plays a role in neurite outgrowth in mice (Miyamoto et al., 2007). Therefore, I think AOS phenotypes likely arise due to a combination of processes being dysregulated, with the underlying cause of the hallmark features (ACC&TTL) relating to defective vascular development, however the specific additional phenotypes observed in AOS likely depend on the genetic mutation the patient has.

6.3 Are non-coding mutations involved in the pathogenesis of AOS?

To date, the 6 known genes identified to be causative of AOS, only account for approximately 50% of patients, with the other 50% of AOS patients having no identified genetic cause (Dudoignon et al., 2019). As all known genes are involved in regulating either the NOTCH or RAC1/CDC42 signalling pathways, it is likely that more genes will be identified in future which are related to these signalling pathways. In chapter 3 I identify non-coding transcripts associated with both zebrafish *dock6* and *eogt*, which are expressed specifically in the heart myocardium at an early stage of heart development. Interestingly, there is evidence that these non-coding transcripts are also conserved between zebrafish and humans, indicating they could have an evolutionarily conserved functional role. Therefore, further mutations in non-coding transcripts associated with the 6 identified causative genes could be identified in AOS patients. Most studies identify AOS patient mutations using whole exome sequencing, therefore missing potential mutations in non-coding regions which could impact expression of these 6 known genes. Several studies acknowledge this as a limitation, for example one study shows that in a subset of AOS patients they identified *DOCK6* heterozygous mutations and as *DOCK6* mutations are associated with the autosomal recessive form of AOS, they suggest that these patients could have further mutations in non-coding regions, cryptic splice sites or in enhancer regions which could cause compound heterozygous *DOCK6* mutations resulting in AOS (Meester et al., 2018). Other developmental diseases where the genetic cause remains unidentified for a subset of patients, such as Joubert Syndrome in which 38% of patients have no identified genetic mutation, also acknowledge that it is likely other variants are being missed which might reside in non-coding regions involved in regulating gene expression, splicing or translation (Bachmann-Gagescu et al., 2015). Furthermore, an

intronic deletion mutation in *NOTCH3* was identified in a patient with CADASIL syndrome, resulting in splicing abnormalities and whole intron retention, and as no genetic cause is identified in around 10% of CADASIL patients, they suggest sequencing introns could identify further variants resulting in this disease (Bianchi et al., 2013). This data suggests that mutations within non-coding regions could be important for the diagnosis of AOS, and that further investigation into non-coding regions could identify mutations involved in regulatory elements of these known causative genes.

Investigation into the existence of non-coding transcripts in the form of retained intron transcripts and lncRNAs for the 6 known genes associated with AOS in humans reveals the complexity of these genes. Numerous splice variants are annotated on Ensembl for *DOCK6*, *EOGT*, *RBPJ*, *NOTCH1* and *ARHGAP31*, retained intron transcripts exist for *DOCK6*, *EOGT*, *RBPJ*, *NOTCH1* and *DLL4*, and a lncRNA for *ARHGAP31*, called *ARHGAP31-AS* is annotated which overlaps in the antisense direction with part of the *ARHGAP31* protein coding transcript (Kimura et al., 2006). Further exploration of non-coding transcripts in the literature indicate that retained intron transcripts and lncRNAs also play important roles in cardiovascular development, and regulation of both the NOTCH and RAC1/CDC42 signalling pathways.

In Chapter 4 I investigate a mutation in a retained intron within the *dock6-R11* retained intron transcript and show that this mutation results in decreased expression of both *dock6-R11*, and the *dock6-201* protein coding transcript. Furthermore, I show that this reduction in *dock6* expression in *dock6-R11* retained intron mutant embryos could be being compensated for by a cell intrinsic adaptation mechanism, and when this compensation pathway is blocked cardiac defects such as disorganised chamber geometry and decreased myocardial ballooning are observed. Alternate splicing and intron retention have been found to be involved in numerous developmental processes, for example intron retention has been found to be important for cell differentiation during haematopoiesis (Rekosh and Hammarskjold, 2018) and during heart development, where multiple transcripts of the *ANKRD1* gene exist in the developing pig heart, and alternate splicing and intron retention is triggered as a stress response (Torrado et al., 2009). Further examples of alternate splicing regulating the actin

cytoskeleton involve the GEF TRIO, which as described above has been found to be involved in formation of vascular adherens junctions (Polacheck et al., 2017), but additionally, alternatively spliced isoforms of TRIO have been found to be involved in neurite outgrowth during brain development, with some isoforms exhibiting two GEF domains rather than one (Portales-Casamar et al., 2006). Additionally, alternate splicing has been found to occur for other DOCK GEFs, such as *DOCK10* where alternate splicing of the first exon results in different *DOCK10* isoforms which are expressed in different types of lymphocytes (Alcaraz-García et al., 2011). The presence of numerous intron retaining transcripts and splice variants for each of the genes implicated in AOS could suggest important functional roles for these transcripts, and it would be interesting to determine whether mutations in retained introns could be involved in the onset of AOS. As AOS patient mutations in both *DOCK6* and *EOGT* have been identified in splice sites, it would also be interesting to investigate whether disruption to alternate splicing could also be involved in AOS pathogenesis.

In addition to intron retention, non-coding transcripts such as lncRNAs have also been found to be involved in cardiovascular development and regulation of the NOTCH and RAC1/CDC42 signalling pathways. In Chapter 5 I investigate the role of an *eogt* antisense RNA, which I propose could be a lncRNA, however over-expressing this lncRNA appeared to have no impact on heart development, Notch signalling in the developing heart or embryo viability. lncRNAs associated with some of the other genes involved in AOS have been identified, including 3 *Dll4* antisense (*Dll4-AS*) lncRNAs which regulate the expression of *Dll4* during angiogenesis in mice (Li et al., 2015), and these *Dll4* antisense transcripts have also been found to be conserved in humans (Chowdhury et al., 2019). Several lncRNAs have been found to interact with *NOTCH1*, such as the lncRNA *H19* which in humans, negatively regulates expression of the *NOTCH1* receptor, and over-expression of *H19* led to disrupted *NOTCH1* expression in calcific aortic valve disease (Hadji et al., 2016). Furthermore, the lncRNA *Meg3* is thought to negatively regulate NOTCH signalling during angiogenesis, with loss of *Meg3* resulting in increased expression of NOTCH signalling pathway genes such as *Dll4* and *Hes1* in the brains of rats (Gordon et al., 2010). Commonly, lncRNAs can work in association with microRNAs (miRNAs) which are small non-coding RNAs that regulate genes at a post-transcriptional level (Flores-Huerta et al., 2021). Emerging evidence has indicated cross-talk between lncRNAs and miRNAs, particularly during

cardiac development and disease (Huang, 2018), for example in the interactions between the lncRNA *CARMA* and the miRNA *MIR-133a2* during cardiomyocyte differentiation in human embryonic stem cells. Following inhibition of *CARMA*, this leads to downregulation of *MIR-133a2*, and expression of *MIR-133a2* target genes, one of which is *RBPJ*. This leads to downregulation of NOTCH signalling in cardiomyocytes, resulting in disrupted cardiomyocyte differentiation (Kay et al., 2021). Together this data highlights the important of lncRNAs in regulating NOTCH signalling during cardiovascular development.

LncRNAs regulating the RAC1/CDC42 signalling pathways have mainly been implicated in cancer biology, for example, over-expression of a lncRNA called *EBLN3P* leads to increased DOCK4 activity by inhibiting a microRNA which normally binds and inhibits DOCK4 from activating RAC1, and increased DOCK4 activity aids cell migration during liver cancer progression (Li et al., 2020). Additionally, the lncRNA *H19*, which was reported above to be involved in the regulation of *NOTCH1* expression (Hadji et al., 2016), is also involved in activating CDC42 to promote cell migration in hepatocellular carcinoma (Zhou et al., 2019). Like *EBLN3P*-dependent regulation of RAC1, *H19* over-expression inhibits a microRNA which normally prevents *CDC42* expression, leading to an increase in *CDC42* expression and activity which then increases tumour cell migration (Zhou et al., 2019). A lncRNA is annotated on Ensembl for *ARHGAP31*, one of the genes commonly mutated in AOS, called *ARHGAP31-AS* and it overlaps with part of the *ARHGAP31* sense transcript, but the expression pattern and function of *ARHGAP31-AS* has not been investigated (Kimura et al., 2006). However, a lncRNA associated with another GAP, *ARHGAP5-AS* has been shown to be involved in increasing translation of *RAC1* mRNA and promoting motility of hepatocellular carcinoma cells. This data shows that in addition to NOTCH signalling regulation, lncRNAs are also commonly involved in regulating the RAC1/CDC42 signalling pathways and due to the existence of lncRNAs associated with genes and regulating processes commonly dysregulated in AOS, it would be interesting to further investigate whether lncRNAs play a role in AOS pathology.

Overall, this data highlights the importance of non-coding RNAs and how they are involved in the regulation of heart development and RAC1/CDC42 and NOTCH signalling. Therefore, it could be possible that mutations in non-coding transcripts

associated with the 6 known genes identified to be causative of AOS could also be implicated in the onset of the disease and therefore conducting whole genome sequencing rather than exome sequencing might be beneficial in AOS patients where no exonic mutation has been identified.

6.4 Future perspectives

The original aims of this study were to assess how mutations in *DOCK6* and *EOGT* lead to dysregulation of RAC1/CDC42 and NOTCH signalling respectively in the onset of AOS in humans, using zebrafish as a model organism. Due to the difficulties I faced when making zebrafish LOF mutant models, or knocking in human AOS mutations into the zebrafish genome, it has been difficult to understand exactly the roles these genes are playing in regulating RAC1/CDC42 and NOTCH signalling in AOS patients possessing mutations in these genes. As the *dock6-RI1^{ins41}* mutant leads to a reduction in *dock6-201* expression in the zebrafish embryo during development, and when compensation in these embryos is blocked this leads to heart defects consistent with mice mutants of *Rac1* and *Cdc42*, such as thinner ventricular myocardium and OFT defects (Leung et al., 2016), it is possible to speculate that mutations in *dock6* are resulting in dysregulated RAC1 and CDC42. However, to draw this conclusion would require further investigation to confirm this is the case, for example by using RAC1/CDC42 FRET sensors to show disrupted RAC1/CDC42 activity in the developing hearts in *dock6-RI1^{ins41}* mutant embryos with blocked compensation. Understanding whether *eogt* regulates NOTCH signalling during cardiac development has been more complicated, due to the fact that I failed to recover an *eogt* mutant which was resulting in down-regulation of *eogt* expression. In the *eogt-201* mutant I did manage to recover there appeared to be no difference in NOTCH signalling in the developing heart at 26hpf. Whether this is because *eogt* is regulating another protein during heart development (Varshney and Stanley, 2017) or whether this is because the *eogt-201* mutant was having no effect on NOTCH signalling remains to be investigated.

In hindsight, knowing how difficult it would be to create *dock6* and *eogt* LOF mutants, alternative methods could have been taken to try to create these mutant zebrafish models. For example, I could have targeted the ATG directly, rather than designing guide RNAs which flank the promoter region and ATG, by designing a guide RNA

which overlaps with the ATG and therefore directly disrupts the ATG to prevent any translation. Furthermore, I could have tried to directly target functional domains of the protein, for example when making the *dock6* LOF mutant I could have attempted to target the DHR2 GEF domain, therefore making the protein unable to activate RAC1 and CDC42. Additionally, once I had established that *dock6* and *eogt* LOF mutations might not be compatible with survival in zebrafish, I could have attempted to make crispants to investigate the effect of these mutations in G0 mutant embryos when embryos are able to survive up to 5dpf without a fully functional cardiovascular system. This would have allowed me to investigate the effects of *dock6* and *eogt* LOF on the developing heart without the issues I faced when trying to raise stable LOF mutants to adulthood.

Although it is still unknown exactly how mutations in AOS lead to dysregulation of the NOTCH and RAC1/CDC42 signalling pathways and cause defects such as ACC, TTLD and CHDs, this work has shed light onto potential areas of further exploration which could help improve the understanding of this disease. As there is evidence both from this thesis and other studies suggesting that individual background levels of gene expression in combination with AOS mutations can potentially contribute to feature severity (Gale et al., 2004; Gagliani et al., 2022), further research into the genetic backgrounds of patients with AOS could provide insights into levels of gene expression that could lead to more severe cases of the disease, and this could be used for genetic counselling to advise parents on the likelihood of disease severity. Furthermore, in depth correlation of genotype to phenotype could provide insights into whether the nature of the specific mutation a patient has could lead to severe cases of the disease, like in Marfan syndrome where mutations in *FBN1* resulting in nonsense mediated decay of mutated mRNA transcripts result in less severe cases of the disease (El-Brolosy et al., 2019). It would also be useful to conduct further investigations into whether genetic mutations along with environmental factors such as alcohol exposure and a higher lipid diet lead to more severe cases of AOS, as mutations in AOS causative genes in combination with these environmental factors resulted in an increased risk of developing CHDs (Nus et al., 2011; Harvey et al., 2022). Therefore, genetic counselling could be provided to pregnant mothers of children at risk of developing AOS to reduce risk factors which could cause increased disease severity.

As defective vascular development is thought to be the main driver behind the onset of AOS features, further investigation into how dysregulation of RAC1/CDC42 and NOTCH signalling leads to vascular abnormalities in AOS would be beneficial to improve the understanding of how severe defects arise and how they can be treated/prevented. A particular focus on the non-canonical NOTCH signalling pathway could also provide insights into how interactions between both the NOTCH and RAC1/CDC42 signalling pathways result in vascular defects in AOS (Polacheck et al., 2017). Finally, the investigation of non-coding transcripts in the 50% of AOS patients with no underlying genetic mutation could provide further mutations which are causative of AOS. Following whole exome sequencing of the 6 known causative genes of AOS, patients with no identified causative mutation could then undergo whole genome sequencing with particular focus on annotated retained introns or antisense lncRNA transcripts to attempt to identify further causative mutations of this disease.

Together, these proposed future experiments will significantly enhance the understanding of AOS origins, and provide better ways of understanding the genetic causes of the disease and how the most severe defects in AOS arise.

7. Bibliography

- Abu-Issa, R., 2015. Rac1 modulates cardiomyocyte adhesion during mouse embryonic development. *Biochem. Biophys. Res. Commun.* 456, 847–852. <https://doi.org/10.1016/j.bbrc.2014.12.042>
- Adams, F.H., Oliver, C.P., 1945. HEREDITARY DEFORMITIES IN MAN. *J. Hered.* 36, 3–7. <https://doi.org/10.1093/oxfordjournals.jhered.a105415>
- Alankarage, D., Ip, E., Szot, J.O., Munro, J., Blue, G.M., Harrison, K., Cuny, H., Enriquez, A., Troup, M., Humphreys, D.T., Wilson, M., Harvey, R.P., Sholler, G.F., Graham, R.M., Ho, J.W.K., Kirk, E.P., Pachter, N., Chapman, G., Winlaw, D.S., Giannoulatou, E., Dunwoodie, S.L., 2019. Identification of clinically actionable variants from genome sequencing of families with congenital heart disease. *Genet. Med.* 21, 1111–1120. <https://doi.org/10.1038/s41436-018-0296-x>
- Alcaraz-García, M.J., Ruiz-Lafuente, N., Sebastián-Ruiz, S., Majado, M.J., González-García, C., Bernardo, M.V., Álvarez-López, M.R., Parrado, A., 2011. Human and mouse DOCK10 splicing isoforms with alternative first coding exon usage are differentially expressed in T and B lymphocytes. *Hum. Immunol.* 72, 531–537. <https://doi.org/10.1016/j.humimm.2011.03.024>
- Alexanian, M., Ounzain, S., 2020. Long Noncoding RNAs in Cardiac Development. *Cold Spring Harb. Perspect. Biol.* a037374. <https://doi.org/10.1101/cshperspect.a037374>
- Algaze, C., Esplin, E.D., Lowenthal, A., Hudgins, L., Tacy, T.A., Tierney, E.S.S., 2013. Expanding the phenotype of cardiovascular malformations in Adams–Oliver syndrome. *Am. J. Med. Genet. A.* 161, 1386–1389. <https://doi.org/10.1002/ajmg.a.35864>
- Alkhateeb, A., Mansour, A., Tanidir, I.C., 2021. Topsy-turvy heart: A first recorded case report with intracardiac anomaly. *Echocardiography* 38, 114–117. <https://doi.org/10.1111/echo.14950>
- Amor, D.J., Leventer, R.J., Hayllar, S., Bankier, A., 2000. Polymicrogyria associated with scalp and limb defects: variant of Adams–Oliver syndrome. *Am. J. Med. Genet.* 93, 328–334. [https://doi.org/10.1002/1096-8628\(20000814\)93:4<328::aid-ajmg13>3.0.co;2-0](https://doi.org/10.1002/1096-8628(20000814)93:4<328::aid-ajmg13>3.0.co;2-0)
- Ayoub, M.D., Kamath, B.M., 2020. Alagille Syndrome: Diagnostic Challenges and Advances in Management. *Diagnostics* 10, 907. <https://doi.org/10.3390/diagnostics10110907>
- Bachmann-Gagescu, R., Dempsey, J.C., Phelps, I.G., O’Roak, B.J., Knutzen, D.M., Rue, T.C., Ishak, G.E., Isabella, C.R., Gorden, N., Adkins, J., Boyle, E.A., de Lacy, N., O’Day, D., Alswaid, A., Ramadevi A, R., Lingappa, L., Lourenço, C., Martorell, L., Garcia-Cazorla, À., Ozyürek, H., Haliloğlu, G., Tuysuz, B., Topçu, M., University of Washington Center for Mendelian Genomics, Chance, P., Parisi, M.A., Glass, I.A., Shendure, J., Doherty, D., 2015. Joubert syndrome: a model for untangling recessive disorders with extreme genetic heterogeneity. *J. Med. Genet.* 52, 514–522. <https://doi.org/10.1136/jmedgenet-2015-103087>
- Bagatto, B., Francl, J., Liu, B., Liu, Q., 2006. Cadherin2 (N-cadherin) plays an essential role in zebrafish cardiovascular development. *BMC Dev. Biol.* 6, 23. <https://doi.org/10.1186/1471-213X-6-23>
- Bajolle, F., Zaffran, S., Kelly, R.G., Hadchouel, J., Bonnet, D., Brown, N.A., Buckingham, M.E., 2006. Rotation of the Myocardial Wall of the Outflow Tract

- Is Implicated in the Normal Positioning of the Great Arteries. *Circ. Res.* 98, 421–428. <https://doi.org/10.1161/01.RES.0000202800.85341.6e>
- Bakkers, J., 2011. Zebrafish as a model to study cardiac development and human cardiac disease. *Cardiovasc. Res.* 91, 279–288. <https://doi.org/10.1093/cvr/cvr098>
- Balasubramanian, M., Collins, A.L., 2009. Aplasia cutis congenita, terminal limb defects and periventricular leukomalacia in one sibling with minor findings in the other-probable autosomal recessive Adams-Oliver Syndrome. *Eur. J. Med. Genet.* 52, 234–238. <https://doi.org/10.1016/j.ejmg.2009.04.005>
- Barry, D.M., Xu, K., Meadows, S.M., Zheng, Y., Norden, P.R., Davis, G.E., Cleaver, O., 2015. Cdc42 is required for cytoskeletal support of endothelial cell adhesion during blood vessel formation. *Development* dev.125260. <https://doi.org/10.1242/dev.125260>
- Basu, M., Zhu, J.-Y., LaHaye, S., Majumdar, U., Jiao, K., Han, Z., Garg, V., 2017. Epigenetic mechanisms underlying maternal diabetes-associated risk of congenital heart disease. *JCI Insight* 2, e95085. <https://doi.org/10.1172/jci.insight.95085>
- Beermann, J., Piccoli, M.-T., Viereck, J., Thum, T., 2016. Non-coding RNAs in Development and Disease: Background, Mechanisms, and Therapeutic Approaches. *Physiol. Rev.* 96, 1297–1325. <https://doi.org/10.1152/physrev.00041.2015>
- Benson, C.E., Southgate, L., 2021. The DOCK protein family in vascular development and disease. *Angiogenesis* 24, 417–433. <https://doi.org/10.1007/s10456-021-09768-8>
- Bianchi, S., Dotti, M.T., Gallus, G.N., D'Eramo, C., Di Donato, I., Bernardi, L., Maletta, R., Puccio, G., Bruni, A.C., Federico, A., 2013. The first deep intronic mutation in the NOTCH3 gene in a family with late-onset CADASIL. *Neurobiol. Aging* 34, 2234.e9–2234.e12. <https://doi.org/10.1016/j.neurobiolaging.2013.03.005>
- Bin Moon, S., Lee, J.M., Kang, J.G., Lee, N.-E., Ha, D.-I., Kim, D.Y., Kim, S.H., Yoo, K., Kim, D., Ko, J.-H., Kim, Y.-S., 2018. Highly efficient genome editing by CRISPR-Cpf1 using CRISPR RNA with a uridinylate-rich 3'-overhang. *Nat. Commun.* 9, 3651. <https://doi.org/10.1038/s41467-018-06129-w>
- Bogdanović, O., Fernández-Miñán, A., Tena, J.J., de la Calle-Mustienes, E., Gómez-Skarmeta, J.L., 2013. The developmental epigenomics toolbox: CHIP-seq and MethylCap-seq profiling of early zebrafish embryos. *Methods San Diego Calif* 62, 207–215. <https://doi.org/10.1016/j.ymeth.2013.04.011>
- Boland, A., Côté, J., Barford, D., 2022. Structural biology of DOCK-FAMILY guanine nucleotide exchange factors. *FEBS Lett.* 1873-3468.14523. <https://doi.org/10.1002/1873-3468.14523>
- Borsari, B., Villegas-Mirón, P., Pérez-Lluch, S., Turpin, I., Laayouni, H., Segarra-Casas, A., Bertranpetit, J., Guigó, R., Acosta, S., 2021. Enhancers with tissue-specific activity are enriched in intronic regions. *Genome Res.* 31, 1325–1336. <https://doi.org/10.1101/gr.270371.120>
- Bos, J.L., Rehmann, H., Wittinghofer, A., 2007. GEFs and GAPs: Critical Elements in the Control of Small G Proteins. *Cell* 129, 865–877. <https://doi.org/10.1016/j.cell.2007.05.018>
- Bouma, B.J., Mulder, B.J.M., 2017. Changing Landscape of Congenital Heart Disease. *Circ. Res.* 120, 908–922. <https://doi.org/10.1161/CIRCRESAHA.116.309302>
- Bowley, G., Kugler, E., Wilkinson, R., Lawrie, A., Eeden, F., Chico, T.J.A., Evans, P.C., Noël, E.S., Serbanovic-Canic, J., 2021. Zebrafish as a tractable model of

- human cardiovascular disease. *Br. J. Pharmacol.* bph.15473. <https://doi.org/10.1111/bph.15473>
- Bray, S.J., 2006. Notch signalling: a simple pathway becomes complex. *Nat. Rev. Mol. Cell Biol.* 7, 678–689. <https://doi.org/10.1038/nrm2009>
- Brown, L.A., Rodaway, A.R.F., Schilling, T.F., Jowett, T., Ingham, P.W., Patient, R.K., Sharrocks, A.D., 2000. Insights into early vasculogenesis revealed by expression of the ETS-domain transcription factor Fli-1 in wild-type and mutant zebrafish embryos. *Mech. Dev.* 90, 237–252. [https://doi.org/10.1016/S0925-4773\(99\)00256-7](https://doi.org/10.1016/S0925-4773(99)00256-7)
- Buckingham, M., Meilhac, S., Zaffran, S., 2005. Building the mammalian heart from two sources of myocardial cells. *Nat. Rev. Genet.* 6, nrg1710. <https://doi.org/10.1038/nrg1710>
- Buijttendijk, M.F.J., Barnett, P., Hoff, M.J.B., 2020. Development of the human heart. *Am. J. Med. Genet. C Semin. Med. Genet.* 184, 7–22. <https://doi.org/10.1002/ajmg.c.31778>
- Buket Basmanav, F., Fritz, G., Lestringant, G.G., Pachat, D., Hoffjan, S., Fischer, J., Wehner, M., Wolf, S., Thiele, H., Altmüller, J., Pulimood, S.A., Rütten, A., Kruse, R., Hanneken, S., Frank, J., Danda, S., Bygum, A., Betz, R.C., 2015. Pathogenicity of POFUT1 in Dowling-Degos Disease: Additional Mutations and Clinical Overlap with Reticulate Acropigmentation of Kitamura. *J. Invest. Dermatol.* 135, 615–618. <https://doi.org/10.1038/jid.2014.406>
- Canalis, E., Zanotti, S., 2014. Hajdu-Cheney syndrome: a review. *Orphanet J. Rare Dis.* 9, 200. <https://doi.org/10.1186/s13023-014-0200-y>
- Caron, C., DeGeer, J., Fournier, P., Duquette, P.M., Luangrath, V., Ishii, H., Karimzadeh, F., Lamarche-Vane, N., Royal, I., 2016. CdGAP/ARHGAP31, a Cdc42/Rac1 GTPase regulator, is critical for vascular development and VEGF-mediated angiogenesis. *Sci. Rep.* 6, 27485. <https://doi.org/10.1038/srep27485>
- Cerikan, B., Schiebel, E., 2019. Mechanism of cell-intrinsic adaptation to Adams-Oliver Syndrome gene DOCK6 disruption highlights ubiquitin-like modifier ISG15 as a regulator of RHO GTPases. *Small GTPases* 10, 210–217. <https://doi.org/10.1080/21541248.2017.1297882>
- Cerikan, B., Shaheen, R., Colo, G.P., Gläßer, C., Hata, S., Knobloch, K.-P., Alkuraya, F.S., Fässler, R., Schiebel, E., 2016. Cell-Intrinsic Adaptation Arising from Chronic Ablation of a Key Rho GTPase Regulator. *Dev. Cell* 39, 28–43. <https://doi.org/10.1016/j.devcel.2016.08.020>
- Chang, L., Nosedá, M., Higginson, M., Ly, M., Patenaude, A., Fuller, M., Kyle, A.H., Minchinton, A.I., Puri, M.C., Dumont, D.J., Karsan, A., 2012. Differentiation of vascular smooth muscle cells from local precursors during embryonic and adult arteriogenesis requires Notch signaling. *Proc. Natl. Acad. Sci.* 109, 6993–6998. <https://doi.org/10.1073/pnas.1118512109>
- Chapman, G., Moreau, J.L.M., I P, E., Szot, J.O., Iyer, K.R., Shi, H., Yam, M.X., O'Reilly, V.C., Enriquez, A., Greasby, J.A., Alankarage, D., Martin, E.M.M.A., Hanna, B.C., Edwards, M., Monger, S., Blue, G.M., Winlaw, D.S., Ritchie, H.E., Grieve, S.M., Giannoulatou, E., Sparrow, D.B., Dunwoodie, S.L., 2020. Functional genomics and gene-environment interaction highlight the complexity of congenital heart disease caused by Notch pathway variants. *Hum. Mol. Genet.* 29, 566–579. <https://doi.org/10.1093/hmg/ddz270>
- Chen, Z., Gore, B.B., Long, H., Ma, L., Tessier-Lavigne, M., 2008. Alternative Splicing of the Robo3 Axon Guidance Receptor Governs the Midline Switch from

- Attraction to Repulsion. *Neuron* 58, 325–332. <https://doi.org/10.1016/j.neuron.2008.02.016>
- Chi, N.C., Shaw, R.M., De Val, S., Kang, G., Jan, L.Y., Black, B.L., Stainier, D.Y.R., 2008. *Foxn4* directly regulates *tbx2b* expression and atrioventricular canal formation. *Genes Dev.* 22, 734–739. <https://doi.org/10.1101/gad.1629408>
- Chiang, I.K.-N., Fritzsche, M., Pichol-Thievend, C., Neal, A., Holmes, K., Lagendijk, A., Overman, J., D'Angelo, D., Omini, A., Hermkens, D., Lesieur, E., Liu, K., Ratnayaka, I., Corada, M., Bou-Gharios, G., Carroll, J., Dejana, E., Schulte-Merker, S., Hogan, B., Beltrame, M., De Val, S., Francois, M., 2017. SoxF factors induce Notch1 expression via direct transcriptional regulation during early arterial development. *Development* dev.146241. <https://doi.org/10.1242/dev.146241>
- Chowdhury, T.A., Koceja, C., Eisa-Beygi, S., Kleinstiver, B.P., Kumar, S.N., Lin, C.-W., Li, K., Prabhudesai, S., Joung, J.K., Ramchandran, R., 2018. Temporal and Spatial Post-Transcriptional Regulation of Zebrafish *tie1* mRNA by Long Noncoding RNA During Brain Vascular Assembly. *Arterioscler. Thromb. Vasc. Biol.* 38, 1562–1575. <https://doi.org/10.1161/ATVBAHA.118.310848>
- Chowdhury, T.A., Li, K., Ramchandran, R., 2019. Lessons learned from a lncRNA odyssey for two genes with vascular functions, *DLL4* and *TIE1*. *Vascul. Pharmacol.* 114, 103–109. <https://doi.org/10.1016/j.vph.2018.06.010>
- Chun, C.Z., Remadevi, I., Schupp, M.-O., Samant, G.V., Pramanik, K., Wilkinson, G.A., Ramchandran, R., 2011. Fli+ etsrp+ Hemato-Vascular Progenitor Cells Proliferate at the Lateral Plate Mesoderm during Vasculogenesis in Zebrafish. *PLoS ONE* 6, e14732. <https://doi.org/10.1371/journal.pone.0014732>
- Clark, B.S., Blackshaw, S., 2014. Long non-coding RNA-dependent transcriptional regulation in neuronal development and disease. *Front. Genet.* 5, 164. <https://doi.org/10.3389/fgene.2014.00164>
- Cohen, I., Silberstein, E., Perez, Y., Landau, D., Elbedour, K., Langer, Y., Kadir, R., Volodarsky, M., Sivan, S., Narkis, G., Birk, O.S., 2014. Autosomal recessive Adams–Oliver syndrome caused by homozygous mutation in *EOGT*, encoding an EGF domain-specific O-GlcNAc transferase. *Eur. J. Hum. Genet.* 22, 374–378. <https://doi.org/10.1038/ejhg.2013.159>
- Costell, M., Carmona, R., Gustafsson, E., González-Iriarte, M., Fässler, R., Muñoz-Chápuli, R., 2002. Hyperplastic Conotruncal Endocardial Cushions and Transposition of Great Arteries in Perlecan-Null Mice. *Circ. Res.* 91, 158–164. <https://doi.org/10.1161/01.RES.0000026056.81424.DA>
- Cramer, L.P., Briggs, L.J., Dawe, H.R., 2002. Use of fluorescently labelled deoxyribonuclease I to spatially measure G-actin levels in migrating and non-migrating cells. *Cell Motil. Cytoskeleton* 51, 27–38. <https://doi.org/10.1002/cm.10013>
- D'Amato, G., Luxán, G., del Monte-Nieto, G., Martínez-Poveda, B., Torroja, C., Walter, W., Bochter, M.S., Benedito, R., Cole, S., Martinez, F., Hadjantonakis, A.-K., Uemura, A., Jiménez-Borreguero, L.J., de la Pompa, J.L., 2016. Sequential Notch activation regulates ventricular chamber development. *Nat. Cell Biol.* 18, 7–20. <https://doi.org/10.1038/ncb3280>
- De Smet, F., Segura, I., De Bock, K., Hohensinner, P.J., Carmeliet, P., 2009. Mechanisms of Vessel Branching: Filopodia on Endothelial Tip Cells Lead the Way. *Arterioscler. Thromb. Vasc. Biol.* 29, 639–649. <https://doi.org/10.1161/ATVBAHA.109.185165>

- De Zoysa, P., Toubat, O., Harvey, D., Choi, J., Kumar, S.R., 2021. Murine Model of Cardiac Defects Observed in Adams-Oliver Syndrome Driven by Delta-Like Ligand-4 Haploinsufficiency. *Stem Cells Dev.* 30, 611–621. <https://doi.org/10.1089/scd.2021.0058>
- Denk-Lobnig, M., Martin, A.C., 2019. Modular regulation of Rho family GTPases in development. *Small GTPases* 10, 122–129. <https://doi.org/10.1080/21541248.2017.1294234>
- Derrick, C.J., Pollitt, E.J.G., Sanchez Sevilla Uruchurtu, A., Hussein, F., Grierson, A.J., Noël, E.S., 2021a. Lamb1a regulates atrial growth by limiting second heart field addition during zebrafish heart development. *Development* 148, dev199691. <https://doi.org/10.1242/dev.199691>
- Derrick, C.J., Sánchez-Posada, J., Hussein, F., Tessadori, F., Pollitt, E.J., Savage, A.M., Wilkinson, R.N., Chico, T.J., Eeden, F.J. van, Bakkers, J., Noël, E.S., 2019. Asymmetric Hapln1a drives regionalised cardiac ECM expansion and promotes heart morphogenesis during zebrafish development. *bioRxiv* 838128. <https://doi.org/10.1101/838128>
- Desgrange, A., Garrec, J.-F.L., Meilhac, S.M., 2018. Left-right asymmetry in heart development and disease: forming the right loop. *Development* 145, dev162776. <https://doi.org/10.1242/dev.162776>
- Di Felice, V., Zummo, G., 2009. Tetralogy of Fallot as a Model to Study Cardiac Progenitor Cell Migration and Differentiation During Heart Development. *Trends Cardiovasc. Med.* 19, 130–135. <https://doi.org/10.1016/j.tcm.2009.07.004>
- Dietrich, A.-C., Lombardo, V.A., Veerkamp, J., Priller, F., Abdelilah-Seyfried, S., 2014. Blood Flow and Bmp Signaling Control Endocardial Chamber Morphogenesis. *Dev. Cell* 30, 367–377. <https://doi.org/10.1016/j.devcel.2014.06.020>
- D'Souza, B., Miyamoto, A., Weinmaster, G., 2008. The many facets of Notch ligands. *Oncogene* 27, 5148–5167. <https://doi.org/10.1038/onc.2008.229>
- Dudoignon, B., Huber, C., Michot, C., Di Rocco, F., Girard, M., Lyonnet, S., Rio, M., Rabia, S.H., Daire, V.C., Baujat, G., 2020. Expanding the phenotype in Adams–Oliver syndrome correlating with the genotype. *Am. J. Med. Genet. A.* 182, 29–37. <https://doi.org/10.1002/ajmg.a.61364>
- Dueñas, A., Expósito, A., Aranega, A., Franco, D., 2019. The Role of Non-Coding RNA in Congenital Heart Diseases. *J. Cardiovasc. Dev. Dis.* 6, 15. <https://doi.org/10.3390/jcdd6020015>
- Duquette, P.M., Lamarche-Vane, N., 2014. Rho GTPases in embryonic development. *Small GTPases* 5, e972857. <https://doi.org/10.4161/sgtp.29716>
- El-Brolsy, M.A., Kontarakis, Z., Rossi, A., Kuenne, C., Günther, S., Fukuda, N., Kikhi, K., Boezio, G.L.M., Takacs, C.M., Lai, S.-L., Fukuda, R., Gerri, C., Giraldez, A.J., Stainier, D.Y.R., 2019. Genetic compensation triggered by mutant mRNA degradation. *Nature* 568, 193–197. <https://doi.org/10.1038/s41586-019-1064-z>
- Epting, D., Wendik, B., Bennewitz, K., Dietz, C.T., Driever, W., Kroll, J., 2010. The Rac1 Regulator ELMO1 Controls Vascular Morphogenesis in Zebrafish. *Circ. Res.* 107, 45–55. <https://doi.org/10.1161/CIRCRESAHA.109.213983>
- Erhardt, S., Zheng, M., Zhao, X., Le, T.P., Findley, T.O., Wang, J., 2021. The Cardiac Neural Crest Cells in Heart Development and Congenital Heart Defects. *J. Cardiovasc. Dev. Dis.* 8, 89. <https://doi.org/10.3390/jcdd8080089>
- Faure, C., Linossier, M.-T., Malaval, L., Lafage-Proust, M.-H., Peyroche, S., Vico, L., Guignandon, A., 2008. Mechanical signals modulated vascular endothelial growth factor-A (VEGF-A) alternative splicing in osteoblastic cells through actin

- polymerisation. *Bone* 42, 1092–1101.
<https://doi.org/10.1016/j.bone.2008.02.011>
- Fernandez, J.P., Vejnar, C.E., Giraldez, A.J., Rouet, R., Moreno-Mateos, M.A., 2018. Optimized CRISPR-Cpf1 system for genome editing in zebrafish. *Methods* 150, 11–18. <https://doi.org/10.1016/j.ymeth.2018.06.014>
- Fernandez-Valdivia, R., Takeuchi, H., Samarghandi, A., Lopez, M., Leonardi, J., Haltiwanger, R.S., Jafar-Nejad, H., 2011. Regulation of mammalian Notch signaling and embryonic development by the protein O -glucosyltransferase Rumi. *Development* 138, 1925–1934. <https://doi.org/10.1242/dev.060020>
- Flores-Huerta, N., Silva-Cázares, M.B., Arriaga-Pizano, L.A., Prieto-Chávez, J.L., López-Camarillo, C., 2021. LncRNAs and microRNAs as Essential Regulators of Stemness in Breast Cancer Stem Cells. *Biomolecules* 11, 380. <https://doi.org/10.3390/biom11030380>
- Fontana, B.D., Franscescon, F., Rosemberg, D.B., Norton, W.H.J., Kalueff, A.V., Parker, M.O., 2019. Zebrafish models for attention deficit hyperactivity disorder (ADHD). *Neurosci. Biobehav. Rev.* 100, 9–18. <https://doi.org/10.1016/j.neubiorev.2019.02.009>
- Fritz, K.R., Zhang, Y., Ruest, L.B., 2019. Cdc42 activation by endothelin regulates neural crest cell migration in the cardiac outflow tract. *Dev. Dyn.* 248, 795–812. <https://doi.org/10.1002/dvdy.75>
- Fukata, M., Nakagawa, M., Kuroda, S., Kaibuchi, K., 1999. Cell adhesion and Rho small GTPases. *J. Cell Sci.* 112, 4491–4500. <https://doi.org/10.1242/jcs.112.24.4491>
- Gadea, G., Blangy, A., 2014. Dock-family exchange factors in cell migration and disease. *Eur. J. Cell Biol.* 93, 466–477. <https://doi.org/10.1016/j.ejcb.2014.06.003>
- Gagliani, E.K., Gutzwiller, L.M., Kuang, Y., Odaka, Y., Hoffmeister, P., Hauff, S., Turkiewicz, A., Harding-Theobald, E., Dolph, P.J., Borggreffe, T., Oswald, F., Gebelein, B., Kovall, R.A., 2022. A Drosophila Su(H) model of Adams-Oliver Syndrome reveals cofactor titration as a mechanism underlying developmental defects. *PLOS Genet.* 18, e1010335. <https://doi.org/10.1371/journal.pgen.1010335>
- Gale, N.W., Dominguez, M.G., Noguera, I., Pan, L., Hughes, V., Valenzuela, D.M., Murphy, A.J., Adams, N.C., Lin, H.C., Holash, J., Thurston, G., Yancopoulos, G.D., 2004. Haploinsufficiency of delta-like 4 ligand results in embryonic lethality due to major defects in arterial and vascular development. *Proc. Natl. Acad. Sci.* 101, 15949–15954. <https://doi.org/10.1073/pnas.0407290101>
- Garrec, J.-F.L., Domínguez, J.N., Desgrange, A., Ivanovitch, K.D., Raphaël, E., Bangham, J.A., Torres, M., Coen, E., Mohun, T.J., Meilhac, S.M., 2017. A predictive model of asymmetric morphogenesis from 3D reconstructions of mouse heart looping dynamics. *eLife* 6, e28951. <https://doi.org/10.7554/elife.28951>
- George, R.M., Maldonado-Velez, G., Firulli, A.B., 2020. The heart of the neural crest: cardiac neural crest cells in development and regeneration. *Development* 147, dev188706. <https://doi.org/10.1242/dev.188706>
- Giardoglou, P., Beis, D., 2019. On Zebrafish Disease Models and Matters of the Heart. *Biomedicines* 7, 15. <https://doi.org/10.3390/biomedicines7010015>
- Goicoechea, S.M., Awadia, S., Garcia-Mata, R., 2014. I'm coming to GEF you: Regulation of RhoGEFs during cell migration. *Cell Adhes. Migr.* 8, 535–549. <https://doi.org/10.4161/cam.28721>

- Gontijo, A.M., Miguela, V., Whiting, M.F., Woodruff, R.C., Dominguez, M., 2011. Intron retention in the *Drosophila melanogaster* Rieske Iron Sulphur Protein gene generated a new protein. *Nat. Commun.* 2, 323. <https://doi.org/10.1038/ncomms1328>
- Gordon, F.E., Nutt, C.L., Cheunsuchon, P., Nakayama, Y., Provencher, K.A., Rice, K.A., Zhou, Y., Zhang, X., Klibanski, A., 2010. Increased Expression of Angiogenic Genes in the Brains of Mouse Meg3-Null Embryos. *Endocrinology* 151, 2443–2452. <https://doi.org/10.1210/en.2009-1151>
- Gore, A.V., Monzo, K., Cha, Y.R., Pan, W., Weinstein, B.M., 2012. Vascular development in the zebrafish. *Cold Spring Harb. Perspect. Med.* 2, a006684. <https://doi.org/10.1101/cshperspect.a006684>
- Grabski, D.F., Broseus, L., Kumari, B., Rekosh, D., Hammarskjold, M.-L., Ritchie, W., 2021. Intron retention and its impact on gene expression and protein diversity: A review and a practical guide. *Wiley Interdiscip. Rev. RNA* 12, e1631. <https://doi.org/10.1002/wrna.1631>
- Grassini, D.R., Silva, J., Hall, T.E., Baillie, G.J., Simons, C., Parton, R.G., Hogan, B.M., Smith, K.A., 2019. Myosin Vb is required for correct trafficking of N-cadherin and cardiac chamber ballooning. *Dev. Dyn.* 248, 284–295. <https://doi.org/10.1002/dvdy.19>
- Grego-Bessa, J., Luna-Zurita, L., del Monte, G., Bolós, V., Melgar, P., Arandilla, A., Garratt, A.N., Zang, H., Mukoyama, Y., Chen, H., Shou, W., Ballestar, E., Esteller, M., Rojas, A., Pérez-Pomares, J.M., de la Pompa, J.L., 2007. Notch Signaling Is Essential for Ventricular Chamber Development. *Dev. Cell* 12, 415–429. <https://doi.org/10.1016/j.devcel.2006.12.011>
- Gridley, T., 2007. Notch signaling in vascular development and physiology. *Development* 134, 2709–2718. <https://doi.org/10.1242/dev.004184>
- Günthel, M., Barnett, P., Christoffels, V.M., 2018. Development, Proliferation, and Growth of the Mammalian Heart. *Mol. Ther.* 26, 1599–1609. <https://doi.org/10.1016/j.ymthe.2018.05.022>
- Gupta, D., Bhattacharjee, O., Mandal, D., Sen, M.K., Dey, D., Dasgupta, A., Kazi, T.A., Gupta, R., Sinharoy, S., Acharya, K., Chattopadhyay, D., Ravichandiran, V., Roy, S., Ghosh, D., 2019. CRISPR-Cas9 system: A new-fangled dawn in gene editing. *Life Sci.* 232, 116636. <https://doi.org/10.1016/j.lfs.2019.116636>
- Hadji, F., Boulanger, M.-C., Guay, S.-P., Gaudreault, N., Amellah, S., Mkannez, G., Bouchareb, R., Marchand, J.T., Nsaibia, M.J., Guauque-Olarte, S., Pibarot, P., Bouchard, L., Bossé, Y., Mathieu, P., 2016. Altered DNA Methylation of Long Noncoding RNA *H19* in Calcific Aortic Valve Disease Promotes Mineralization by Silencing *NOTCH1*. *Circulation* 134, 1848–1862. <https://doi.org/10.1161/CIRCULATIONAHA.116.023116>
- Haga, R.B., Ridley, A.J., 2016. Rho GTPases: Regulation and roles in cancer cell biology. *Small GTPases* 7, 207–221. <https://doi.org/10.1080/21541248.2016.1232583>
- Hall, A., 1998. Rho GTPases and the Actin Cytoskeleton. *Science* 279, 509–514. <https://doi.org/10.1126/science.279.5350.509>
- Harvey, B.M., Rana, N.A., Moss, H., Leonardi, J., Jafar-Nejad, H., Haltiwanger, R.S., 2016. Mapping Sites of O-Glycosylation and Fringe Elongation on *Drosophila* Notch. *J. Biol. Chem.* 291, 16348–16360. <https://doi.org/10.1074/jbc.M116.732537>
- Harvey, D.C., De Zoysa, P., Toubat, O., Choi, J., Kishore, J., Tsukamoto, H., Kumar, S.R., 2022. Concomitant genetic defects potentiate the adverse impact of

- prenatal alcohol exposure on cardiac outflow tract maturation. *Birth Defects Res.* 114, 105–115. <https://doi.org/10.1002/bdr2.1968>
- Hassed, S., Li, S., Mulvihill, J., Aston, C., Palmer, S., 2017. Adams–Oliver syndrome review of the literature: Refining the diagnostic phenotype. *Am. J. Med. Genet. A.* 173, 790–800. <https://doi.org/10.1002/ajmg.a.37889>
- Hassed, S.J., Wiley, G.B., Wang, S., Lee, J.-Y., Li, S., Xu, W., Zhao, Z.J., Mulvihill, J.J., Robertson, J., Warner, J., Gaffney, P.M., 2012. RBPJ Mutations Identified in Two Families Affected by Adams-Oliver Syndrome. *Am. J. Hum. Genet.* 91, 391–395. <https://doi.org/10.1016/j.ajhg.2012.07.005>
- Henderson, D.J., Chaudhry, B., 2011. Getting to the heart of planar cell polarity signaling. *Birt. Defects Res. A. Clin. Mol. Teratol.* 91, 460–467. <https://doi.org/10.1002/bdra.20792>
- Henry, C.A., McNulty, I.M., Durst, W.A., Munchel, S.E., Amacher, S.L., 2005. Interactions between muscle fibers and segment boundaries in zebrafish. *Dev. Biol.* 287, 346–360. <https://doi.org/10.1016/j.ydbio.2005.08.049>
- Herbert, S.P., Stainier, D.Y.R., 2011. Molecular control of endothelial cell behaviour during blood vessel morphogenesis. *Nat. Rev. Mol. Cell Biol.* 12, 551–564. <https://doi.org/10.1038/nrm3176>
- Hobuß, L., Bär, C., Thum, T., 2019. Long Non-coding RNAs: At the Heart of Cardiac Dysfunction? *Front. Physiol.* 10, 30. <https://doi.org/10.3389/fphys.2019.00030>
- Hoffman, J.I.E., Kaplan, S., 2002. The incidence of congenital heart disease. *J. Am. Coll. Cardiol.* 39, 1890–1900. [https://doi.org/10.1016/S0735-1097\(02\)01886-7](https://doi.org/10.1016/S0735-1097(02)01886-7)
- Hu, N., Sedmera, D., Yost, H.J., Clark, E.B., 2000. Structure and function of the developing zebrafish heart. *Anat. Rec.* 260, 148–157. [https://doi.org/10.1002/1097-0185\(20001001\)260:2<148::AID-AR50>3.0.CO;2-X](https://doi.org/10.1002/1097-0185(20001001)260:2<148::AID-AR50>3.0.CO;2-X)
- Huang, C.-J., Tu, C.-T., Hsiao, C.-D., Hsieh, F.-J., Tsai, H.-J., 2003. Germ-line transmission of a myocardium-specific GFP transgene reveals critical regulatory elements in the cardiac myosin light chain 2 promoter of zebrafish. *Dev. Dyn.* 228, 30–40. <https://doi.org/10.1002/dvdy.10356>
- Huang, Y., 2018. The novel regulatory role of lncRNA-miRNA-mRNA axis in cardiovascular diseases. *J. Cell. Mol. Med.* 22, 5768–5775. <https://doi.org/10.1111/jcmm.13866>
- Hwang, Woong Y., Fu, Y., Reyon, D., Maeder, M.L., Kaini, P., Sander, J.D., Joung, J.K., Peterson, R.T., Yeh, J.-R.J., 2013. Heritable and Precise Zebrafish Genome Editing Using a CRISPR-Cas System. *PLoS ONE* 8, e68708. <https://doi.org/10.1371/journal.pone.0068708>
- Isidor, B., Lindenbaum, P., Pichon, O., Bézieau, S., Dina, C., Jacquemont, S., Martin-Coignard, D., Thauvin-Robinet, C., Le Merrer, M., Mandel, J.-L., David, A., Faivre, L., Cormier-Daire, V., Redon, R., Le Caignec, C., 2011. Truncating mutations in the last exon of NOTCH2 cause a rare skeletal disorder with osteoporosis. *Nat. Genet.* 43, 306–308. <https://doi.org/10.1038/ng.778>
- Iso, T., Hamamori, Y., Kedes, L., 2003. Notch Signaling in Vascular Development. *Arterioscler. Thromb. Vasc. Biol.* 23, 543–553. <https://doi.org/10.1161/01.ATV.0000060892.81529.8F>
- Isogai, S., Horiguchi, M., Weinstein, B.M., 2001. The Vascular Anatomy of the Developing Zebrafish: An Atlas of Embryonic and Early Larval Development. *Dev. Biol.* 230, 278–301. <https://doi.org/10.1006/dbio.2000.9995>
- Izumi, K., Hayashi, D., Grochowski, C.M., Kubota, N., Nishi, E., Arakawa, M., Hiroma, T., Hatata, T., Ogiso, Y., Nakamura, T., Falsey, A.M., Hidaka, E., Spinner, N.B.,

2016. Discordant clinical phenotype in monozygotic twins with Alagille syndrome: Possible influence of non-genetic factors. *Am. J. Med. Genet. A.* 170, 471–475. <https://doi.org/10.1002/ajmg.a.37429>
- Jacob, A.G., Smith, C.W.J., 2017. Intron retention as a component of regulated gene expression programs. *Hum. Genet.* 136, 1043–1057. <https://doi.org/10.1007/s00439-017-1791-x>
- Jaillon, O., Bouhouche, K., Gout, J.-F., Aury, J.-M., Noel, B., Saudemont, B., Nowacki, M., Serrano, V., Porcel, B.M., Ségurens, B., Le Mouël, A., Lepère, G., Schächter, V., Bétermier, M., Cohen, J., Wincker, P., Sperling, L., Duret, L., Meyer, E., 2008. Translational control of intron splicing in eukaryotes. *Nature* 451, 359–362. <https://doi.org/10.1038/nature06495>
- Jain, R., Rentschler, S., Epstein, J.A., 2010. Notch and cardiac outflow tract development: Notch and cardiac outflow tract development. *Ann. N. Y. Acad. Sci.* 1188, 184–190. <https://doi.org/10.1111/j.1749-6632.2009.05099.x>
- Jones, K.M., Silfvast-Kaiser, A., Leake, D.R., Diaz, L.Z., Levy, M.L., 2017. Adams–Oliver Syndrome Type 2 in Association with Compound Heterozygous DOCK6 Mutations. *Pediatr. Dermatol.* 34, e249–e253. <https://doi.org/10.1111/pde.13239>
- Kaibuchi, K., Kuroda, S., Fukata, M., Nakagawa, M., 1999. Regulation of cadherin-mediated cell–cell adhesion by the Rho family GTPases. *Curr. Opin. Cell Biol.* 11, 591–596. [https://doi.org/10.1016/S0955-0674\(99\)00014-9](https://doi.org/10.1016/S0955-0674(99)00014-9)
- Kakuda, S., Haltiwanger, R.S., 2017. Deciphering the Fringe-Mediated Notch Code: Identification of Activating and Inhibiting Sites Allowing Discrimination between Ligands. *Dev. Cell* 40, 193–201. <https://doi.org/10.1016/j.devcel.2016.12.013>
- Kalueff, A.V., Stewart, A.M., Gerlai, R., 2014. Zebrafish as an emerging model for studying complex brain disorders. *Trends Pharmacol. Sci.* 35, 63–75. <https://doi.org/10.1016/j.tips.2013.12.002>
- Kardash, E., Bandemer, J., Raz, E., 2011. Imaging protein activity in live embryos using fluorescence resonance energy transfer biosensors. *Nat. Protoc.* 6, 1835–1846. <https://doi.org/10.1038/nprot.2011.395>
- Katano, W., Moriyama, Y., Takeuchi, J.K., Koshiba-Takeuchi, K., 2019. Cardiac septation in heart development and evolution. *Dev. Growth Differ.* 61, 114–123. <https://doi.org/10.1111/dgd.12580>
- Kaushik, K., Leonard, V.E., KV, S., Lalwani, M.K., Jalali, S., Patowary, A., Joshi, A., Scaria, V., Sivasubbu, S., 2013. Dynamic Expression of Long Non-Coding RNAs (lncRNAs) in Adult Zebrafish. *PLoS ONE* 8, e83616. <https://doi.org/10.1371/journal.pone.0083616>
- Kay, M., Soltani, B.M., Nemir, M., Aghagolzadeh, P., Pezzuto, I., Chouvardas, P., Ruberto, F., Movahedi, F., Ansari, H., Baharvand, H., Pedrazzini, T., 2021. The conserved long noncoding RNA CARMA regulates cardiomyocyte differentiation. *Cardiovasc. Res.* cvab281. <https://doi.org/10.1093/cvr/cvab281>
- Kelly, R.G., Buckingham, M.E., Moorman, A.F., 2014. Heart Fields and Cardiac Morphogenesis. *Cold Spring Harb. Perspect. Med.* 4, a015750–a015750. <https://doi.org/10.1101/cshperspect.a015750>
- Keyte, A.L., Alonzo-Johnsen, M., Hutson, M.R., 2014. Evolutionary and developmental origins of the cardiac neural crest: Building a divided outflow tract. *Birth Defects Res. Part C Embryo Today Rev.* 102, 309–323. <https://doi.org/10.1002/bdrc.21076>
- Khandekar, M., Brandt, W., Zhou, Y., Dagenais, S., Glover, T.W., Suzuki, N., Shimizu, R., Yamamoto, M., Lim, K.-C., Engel, J.D., 2007. A *Gata2* intronic enhancer

- confers its pan-endothelia-specific regulation. *Development* 134, 1703–1712. <https://doi.org/10.1242/dev.001297>
- Kim, H.K., Min, S., Song, M., Jung, S., Choi, J.W., Kim, Y., Lee, S., Yoon, S., Kim, H. (Henry), 2018. Deep learning improves prediction of CRISPR–Cpf1 guide RNA activity. *Nat. Biotechnol.* 36, 239–241. <https://doi.org/10.1038/nbt.4061>
- Kimmel, C.B., Ballard, W.W., Kimmel, S.R., Ullmann, B., Schilling, T.F., 1995. Stages of embryonic development of the zebrafish. *Dev. Dyn.* 203, 253–310. <https://doi.org/10.1002/aja.1002030302>
- Kimura, K., Wakamatsu, A., Suzuki, Y., Ota, T., Nishikawa, T., Yamashita, R., Yamamoto, J., Sekine, M., Tsuritani, K., Wakaguri, H., Ishii, S., Sugiyama, T., Saito, K., Isono, Y., Irie, R., Kushida, N., Yoneyama, T., Otsuka, R., Kanda, K., Yokoi, T., Kondo, H., Wagatsuma, M., Murakawa, K., Ishida, S., Ishibashi, T., Takahashi-Fujii, A., Tanase, T., Nagai, K., Kikuchi, H., Nakai, K., Isogai, T., Sugano, S., 2006. Diversification of transcriptional modulation: Large-scale identification and characterization of putative alternative promoters of human genes. *Genome Res.* 16, 55–65. <https://doi.org/10.1101/gr.4039406>
- Kopan, R., Ilagan, M.X.G., 2009. The Canonical Notch Signaling Pathway: Unfolding the Activation Mechanism. *Cell* 137, 216–233. <https://doi.org/10.1016/j.cell.2009.03.045>
- Kozak, M., 1987. An analysis of 5′-noncoding sequences from 699 vertebrate messenger RNAs. *Nucleic Acids Res.* 15, 8125–8148. <https://doi.org/10.1093/nar/15.20.8125>
- Kukimoto-Niino, M., Ihara, K., Murayama, K., Shirouzu, M., 2021. Structural insights into the small GTPase specificity of the DOCK guanine nucleotide exchange factors. *Curr. Opin. Struct. Biol.* 71, 249–258. <https://doi.org/10.1016/j.sbi.2021.08.001>
- Kunimura, K., Uruno, T., Fukui, Y., 2020. DOCK family proteins: key players in immune surveillance mechanisms. *Int. Immunol.* 32, 5–15. <https://doi.org/10.1093/intimm/dxz067>
- Labun, K., Montague, T.G., Krause, M., Torres Cleuren, Y.N., Tjeldnes, H., Valen, E., 2019. CHOPCHOP v3: expanding the CRISPR web toolbox beyond genome editing. *Nucleic Acids Res.* 47, W171–W174. <https://doi.org/10.1093/nar/gkz365>
- Lagendijk, A.K., Smith, K.A., Bakkens, J., 2010. Genetics of Congenital Heart Defects: A Candidate Gene Approach. *Trends Cardiovasc. Med.* 20, 124–128. <https://doi.org/10.1016/j.tcm.2010.10.003>
- Lagendijk, A.K., Yap, A.S., Hogan, B.M., 2014. Endothelial cell–cell adhesion during zebrafish vascular development. *Cell Adhes. Migr.* 8, 136–145. <https://doi.org/10.4161/cam.28229>
- Lawson, N.D., Scheer, N., Pham, V.N., Kim, C.H., Chitnis, A.B., Campos-Ortega, J.A., Weinstein, B.M., 2001. Notch signaling is required for arterial-venous differentiation during embryonic vascular development. *Dev. Camb. Engl.* 128, 3675–3683. <https://doi.org/10.1242/dev.128.19.3675>
- Lawson, N.D., Weinstein, B.M., 2002. In Vivo Imaging of Embryonic Vascular Development Using Transgenic Zebrafish. *Dev. Biol.* 248, 307–318. <https://doi.org/10.1006/dbio.2002.0711>
- le Noble, F., Klein, C., Tintu, A., Pries, A., Buschmann, I., 2008. Neural guidance molecules, tip cells, and mechanical factors in vascular development. *Cardiovasc. Res.* 78, 232–241. <https://doi.org/10.1093/cvr/cvn058>

- Lee, Y., Park, J., Kim, S., Nam, K., Lee, W., Cho, H., Han, I., 2020. Sleep deprivation impairs learning and memory by decreasing protein O -GlcNAcylation in the brain of adult zebrafish. *FASEB J.* 34, 853–864. <https://doi.org/10.1096/fj.201901399RR>
- Lehman, A., Stittrich, A., Glusman, G., Zong, Z., Li, H., Eydoux, P., Senger, C., Lyons, C., Roach, J.C., Patel, M., 2014. Diffuse angiopathy in Adams-Oliver syndrome associated with truncating DOCK6 mutations. *Am. J. Med. Genet. A.* 164, 2656–2662. <https://doi.org/10.1002/ajmg.a.36685>
- Lescroart, F., Wang, X., Lin, X., Swedlund, B., Gargouri, S., Sánchez-Dànes, A., Moignard, V., Dubois, C., Paulissen, C., Kinston, S., Göttgens, B., Blanpain, C., 2018. Defining the earliest step of cardiovascular lineage segregation by single-cell RNA-seq. *Science* 359, 1177–1181. <https://doi.org/10.1126/science.aao4174>
- Leslie, J.D., Ariza-McNaughton, L., Bermange, A.L., McAdow, R., Johnson, S.L., Lewis, J., 2007. Endothelial signalling by the Notch ligand Delta-like 4 restricts angiogenesis. *Development* 134, 839–844. <https://doi.org/10.1242/dev.003244>
- Leung, C., Engineer, A., Kim, M.Y., Lu, X., Feng, Q., 2021. Myocardium-Specific Deletion of Rac1 Causes Ventricular Noncompaction and Outflow Tract Defects. *J. Cardiovasc. Dev. Dis.* 8, 29. <https://doi.org/10.3390/jcdd8030029>
- Leung, C., Liu, Y., Lu, X., Kim, M., Drysdale, T.A., Feng, Q., 2016. Rac1 Signaling Is Required for Anterior Second Heart Field Cellular Organization and Cardiac Outflow Tract Development. *J. Am. Heart Assoc.* 5. <https://doi.org/10.1161/jaha.115.002508>
- Leung, C., Lu, X., Liu, M., Feng, Q., 2014. Rac1 Signaling Is Critical to Cardiomyocyte Polarity and Embryonic Heart Development. *J. Am. Heart Assoc.* 3. <https://doi.org/10.1161/jaha.114.001271>
- Li, B., Hu, Y., Li, X., Jin, G., Chen, X., Chen, G., Chen, Y., Huang, S., Liao, W., Liao, Y., Teng, Z., Bin, J., 2018. Sirt1 Antisense Long Noncoding RNA Promotes Cardiomyocyte Proliferation by Enhancing the Stability of Sirt1. *J. Am. Heart Assoc.* 7. <https://doi.org/10.1161/jaha.118.009700>
- Li, H., Wang, M., Zhou, H., Lu, S., Zhang, B., 2020. Long Noncoding RNA EBLN3P Promotes the Progression of Liver Cancer via Alteration of microRNA-144-3p/DOCK4 Signal. *Cancer Manag. Res.* Volume 12, 9339–9349. <https://doi.org/10.2147/CMAR.S261976>
- Li, Jieli, Liu, Y., Jin, Y., Wang, R., Wang, J., Lu, S., VanBuren, V., Dostal, D.E., Zhang, S.L., Peng, X., 2017. Essential role of Cdc42 in cardiomyocyte proliferation and cell-cell adhesion during heart development. *Dev. Biol.* 421, 271–283. <https://doi.org/10.1016/j.ydbio.2016.12.012>
- Li, Jingjing, Miao, L., Zhao, C., Shaikh Qureshi, W.M., Shieh, D., Guo, H., Lu, Y., Hu, S., Huang, A., Zhang, L., Cai, C., Wan, L.Q., Xin, H., Vincent, P., Singer, H.A., Zheng, Y., Cleaver, O., Fan, Z.-C., Wu, M., 2017. CDC42 is required for epicardial and pro-epicardial development by mediating FGF receptor trafficking to the plasma membrane. *Development* 144, 1635–1647. <https://doi.org/10.1242/dev.147173>
- Li, K., Chowdhury, T., Vakeel, P., Kocejka, C., Sampath, V., Ramchandran, R., 2015. Delta-like 4 mRNA is regulated by adjacent natural antisense transcripts. *Vasc. Cell* 7, 3. <https://doi.org/10.1186/s13221-015-0028-9>
- Li, M., Zhao, L., Page-McCaw, P.S., Chen, W., 2016. Zebrafish Genome Engineering Using the CRISPR–Cas9 System. *Trends Genet.* 32, 815–827. <https://doi.org/10.1016/j.tig.2016.10.005>

- Li, T., Zhu, L., Xiao, B., Gong, Z., Liao, Q., Guo, J., 2019. CRISPR-Cpf1-mediated genome editing and gene regulation in human cells. *Biotechnol. Adv.* 37, 21–27. <https://doi.org/10.1016/j.biotechadv.2018.10.013>
- Li, Y., Zdanowicz, M., Young, L., Kumiski, D., Leatherbury, L., Kirby, M.L., 2003. Cardiac neural crest in zebrafish embryos contributes to myocardial cell lineage and early heart function. *Dev. Dyn.* 226, 540–550. <https://doi.org/10.1002/dvdy.10264>
- Lin, C.-J., Lin, C.-Y., Chen, C.-H., Zhou, B., Chang, C.-P., 2012. Partitioning the heart: mechanisms of cardiac septation and valve development. *Development* 139, 3277–3299. <https://doi.org/10.1242/dev.063495>
- Liu, J., Bressan, M., Hassel, D., Huiskens, J., Staudt, D., Kikuchi, K., Poss, K.D., Mikawa, T., Stainier, D.Y.R., 2010. A dual role for ErbB2 signaling in cardiac trabeculation. *Development* 137, 3867–3875. <https://doi.org/10.1242/dev.053736>
- Liu, J., Stainier, D.Y.R., 2012. Zebrafish in the Study of Early Cardiac Development. *Circ. Res.* 110, 870–874. <https://doi.org/10.1161/circresaha.111.246504>
- Liu, L., Zhang, L., Zhao, S., Zhao, X.-Y., Min, P.-X., Ma, Y.-D., Wang, Y.-Y., Chen, Y., Tang, S.-J., Zhang, Y.-J., Du, J., Gu, L., 2019. Non-canonical Notch Signaling Regulates Actin Remodeling in Cell Migration by Activating PI3K/AKT/Cdc42 Pathway. *Front. Pharmacol.* 10, 370. <https://doi.org/10.3389/fphar.2019.00370>
- Liu, Y., Jin, Y., Li, J., Seto, E., Kuo, E., Yu, W., Schwartz, R.J., Blazo, M., Zhang, S.L., Peng, X., 2013. Inactivation of Cdc42 in neural crest cells causes craniofacial and cardiovascular morphogenesis defects. *Dev. Biol.* 383, 239–252. <https://doi.org/10.1016/j.ydbio.2013.09.013>
- Liu, Y., Wang, J., Li, J., Wang, R., Tharakan, B., Zhang, S.L., Tong, C.W., Peng, X., 2017. Deletion of Cdc42 in embryonic cardiomyocytes results in right ventricle hypoplasia. *Clin. Transl. Med.* 6. <https://doi.org/10.1186/s40169-017-0171-4>
- Lombardo, V.A., Heise, M., Moghtadaei, M., Bornhorst, D., Männer, J., Abdelilah-Seyfried, S., 2019. Morphogenetic control of zebrafish cardiac looping by Bmp signaling. *Development* dev.180091. <https://doi.org/10.1242/dev.180091>
- Luxán, G., D’Amato, G., MacGrogan, D., Pompa, J.L. de la, 2016. Endocardial Notch Signaling in Cardiac Development and Disease. *Circ. Res.* 118, e1–e18. <https://doi.org/10.1161/circresaha.115.305350>
- Ma, Y., Zhang, L., Huang, X., 2014. Genome modification by CRISPR/Cas9. *FEBS J.* 281, 5186–5193. <https://doi.org/10.1111/febs.13110>
- MacGrogan, D., Münch, J., de la Pompa, J.L., 2018. Notch and interacting signalling pathways in cardiac development, disease, and regeneration. *Nat. Rev. Cardiol.* 15, 685–704. <https://doi.org/10.1038/s41569-018-0100-2>
- Mack, N.A., Georgiou, M., 2014. The interdependence of the Rho GTPases and apicobasal cell polarity. *Small GTPases* 5, e973768. <https://doi.org/10.4161/21541248.2014.973768>
- Mallon, A.-M., Iyer, V., Melvin, D., Morgan, H., Parkinson, H., Brown, S.D.M., Flicek, P., Skarnes, W.C., 2012. Accessing data from the International Mouse Phenotyping Consortium: state of the art and future plans. *Mamm. Genome Off. J. Int. Mamm. Genome Soc.* 23, 641–652. <https://doi.org/10.1007/s00335-012-9428-9>
- Männer, J., 2009. The anatomy of cardiac looping: A step towards the understanding of the morphogenesis of several forms of congenital cardiac malformations. *Clin. Anat.* 22, 21–35. <https://doi.org/10.1002/ca.20652>

- Marei, H., Malliri, A., 2016. GEFs: Dual regulation of Rac1 signaling. *Small GTPases* 8, 1–10. <https://doi.org/10.1080/21541248.2016.1202635>
- Mascarenhas, J.B., Tchourbanov, A.Y., Fan, H., Danilov, S.M., Wang, T., Garcia, J.G.N., 2017. Mechanical Stress and Single Nucleotide Variants Regulate Alternative Splicing of the *MYLK* Gene. *Am. J. Respir. Cell Mol. Biol.* 56, 29–37. <https://doi.org/10.1165/rcmb.2016-0053OC>
- Mašek, J., Andersson, E.R., 2017. The developmental biology of genetic Notch disorders. *Development* 144, 1743–1763. <https://doi.org/10.1242/dev.148007>
- Matsumoto, K., Luther, K.B., Haltiwanger, R.S., 2020. Diseases related to Notch glycosylation. *Mol. Aspects Med.* 100938. <https://doi.org/10.1016/j.mam.2020.100938>
- McFadden, D.G., Olson, E.N., 2002. Heart development: learning from mistakes. *Curr. Opin. Genet. Dev.* 12, 328–335. [https://doi.org/10.1016/s0959-437x\(02\)00306-4](https://doi.org/10.1016/s0959-437x(02)00306-4)
- Meester, J.A.N., Southgate, L., Stittrich, A.-B., Venselaar, H., Beekmans, S.J.A., den Hollander, N., Bijlsma, E.K., Helderma-van den Enden, A., Verheij, J.B.G.M., Glusman, G., Roach, J.C., Lehman, A., Patel, M.S., de Vries, B.B.A., Ruivenkamp, C., Itin, P., Prescott, K., Clarke, S., Trembath, R., Zenker, M., Sukalo, M., Van Laer, L., Loeys, B., Wuyts, W., 2015. Heterozygous Loss-of-Function Mutations in *DLL4* Cause Adams-Oliver Syndrome. *Am. J. Hum. Genet.* 97, 475–482. <https://doi.org/10.1016/j.ajhg.2015.07.015>
- Meester, J.A.N., Sukalo, M., Schröder, K.C., Schanze, D., Baynam, G., Borck, G., Bramswig, N.C., Duman, D., Gilbert-Dussardier, B., Holder-Espinasse, M., Itin, P., Johnson, D.S., Joss, S., Koillinen, H., McKenzie, F., Morton, J., Nelle, H., Reardon, W., Roll, C., Salih, M.A., Savarirayan, R., Scurr, I., Splitt, M., Thompson, E., Titheradge, H., Travers, C.P., Van Maldergem, L., Whiteford, M., Wiczorek, D., Vandeweyer, G., Trembath, R., Van Laer, L., Loeys, B.L., Zenker, M., Southgate, L., Wuyts, W., 2018. Elucidating the genetic architecture of Adams-Oliver syndrome in a large European cohort. *Hum. Mutat.* 39, 1246–1261. <https://doi.org/10.1002/humu.23567>
- Meester, J.A.N., Verstraeten, A., Alaerts, M., Schepers, D., Laer, L.V., Loeys, B.L., 2019a. Overlapping but distinct roles for NOTCH receptors in human cardiovascular disease. *Clin. Genet.* 95, 85–94. <https://doi.org/10.1111/cge.13382>
- Miyamoto, Y., Torii, T., Yamamori, N., Ogata, T., Tanoue, A., Yamauchi, J., 2013. Akt and PP2A reciprocally regulate the guanine nucleotide exchange factor Dock6 to control axon growth of sensory neurons. *Sci. Signal.* 6, ra15. <https://doi.org/10.1126/scisignal.2003661>
- Miyamoto, Y., Yamauchi, J., 2010. Cellular signaling of Dock family proteins in neural function. *Cell. Signal.* 22, 175–182. <https://doi.org/10.1016/j.cellsig.2009.09.036>
- Miyamoto, Y., Yamauchi, J., Sanbe, A., Tanoue, A., 2007. Dock6, a Dock-C subfamily guanine nucleotide exchanger, has the dual specificity for Rac1 and Cdc42 and regulates neurite outgrowth. *Exp. Cell Res.* 313, 791–804. <https://doi.org/10.1016/j.yexcr.2006.11.017>
- Mohammed, H., Hernando-Herraez, I., Savino, A., Scialdone, A., Macaulay, I., Mulas, C., Chandra, T., Voet, T., Dean, W., Nichols, J., Marioni, J.C., Reik, W., 2017. Single-Cell Landscape of Transcriptional Heterogeneity and Cell Fate Decisions during Mouse Early Gastrulation. *Cell Rep.* 20, 1215–1228. <https://doi.org/10.1016/j.celrep.2017.07.009>

- Moore, J.C., Sheppard-Tindell, S., Shestopalov, I.A., Yamazoe, S., Chen, J.K., Lawson, N.D., 2013. Post-transcriptional mechanisms contribute to Etv2 repression during vascular development. *Dev. Biol.* 384, 128–140. <https://doi.org/10.1016/j.ydbio.2013.08.028>
- Moreno-Mateos, M.A., Fernandez, J.P., Rouet, R., Vejnar, C.E., Lane, M.A., Mis, E., Khokha, M.K., Doudna, J.A., Giraldez, A.J., 2017. CRISPR-Cpf1 mediates efficient homology-directed repair and temperature-controlled genome editing. *Nat. Commun.* 8, 2024. <https://doi.org/10.1038/s41467-017-01836-2>
- Mosaddeghzadeh, N., Ahmadian, M.R., 2021. The RHO Family GTPases: Mechanisms of Regulation and Signaling. *Cells* 10, 1831. <https://doi.org/10.3390/cells10071831>
- Müller, R., Jenny, A., Stanley, P., 2013. The EGF Repeat-Specific O-GlcNAc-Transferase Eogt Interacts with Notch Signaling and Pyrimidine Metabolism Pathways in *Drosophila*. *PLoS ONE* 8, e62835. <https://doi.org/10.1371/journal.pone.0062835>
- Naito, H., Iba, T., Takakura, N., 2020. Mechanisms of new blood-vessel formation and proliferative heterogeneity of endothelial cells. *Int. Immunol.* 32, 295–305. <https://doi.org/10.1093/intimm/dxaa008>
- Nielsen, B.S., 2012. MicroRNA in situ hybridization. *Methods Mol. Biol.* Clifton NJ 822, 67–84. https://doi.org/10.1007/978-1-61779-427-8_5
- Nigam, V., Srivastava, D., 2009. Notch1 represses osteogenic pathways in aortic valve cells. *J. Mol. Cell. Cardiol.* 47, 828–834. <https://doi.org/10.1016/j.yjmcc.2009.08.008>
- Nishikimi, A., Kukimoto-Niino, M., Yokoyama, S., Fukui, Y., 2013. Immune regulatory functions of DOCK family proteins in health and disease. *Exp. Cell Res.* 319, 2343–2349. <https://doi.org/10.1016/j.yexcr.2013.07.024>
- Norden, P.R., Kim, D.J., Barry, D.M., Cleaver, O.B., Davis, G.E., 2016. Cdc42 and k-Ras Control Endothelial Tubulogenesis through Apical Membrane and Cytoskeletal Polarization: Novel Stimulatory Roles for GTPase Effectors, the Small GTPases, Rac2 and Rap1b, and Inhibitory Influence of Arhgap31 and Rasa1. *PLOS ONE* 11, e0147758. <https://doi.org/10.1371/journal.pone.0147758>
- Novodvorsky, P., Watson, O., Gray, C., Wilkinson, R.N., Reeve, S., Smythe, C., Beniston, R., Plant, K., Maguire, R., M. K. Rothman, A., Elworthy, S., van Eeden, F.J.M., Chico, T.J.A., 2015. klf2ash317 Mutant Zebrafish Do Not Recapitulate Morpholino-Induced Vascular and Haematopoietic Phenotypes. *PLOS ONE* 10, e0141611. <https://doi.org/10.1371/journal.pone.0141611>
- Nus, M., MacGrogan, D., Martínez-Poveda, B., Benito, Y., Casanova, J.C., Fernández-Avilés, F., Bermejo, J., de la Pompa, J.L., 2011a. Diet-Induced Aortic Valve Disease in Mice Haploinsufficient for the Notch Pathway Effector RBPJK/CSL. *Arterioscler. Thromb. Vasc. Biol.* 31, 1580–1588. <https://doi.org/10.1161/ATVBAHA.111.227561>
- Ogawa, M., Okajima, T., 2019. Structure and function of extracellular O-GlcNAc. *Curr. Opin. Struct. Biol.* 56, 72–77. <https://doi.org/10.1016/j.sbi.2018.12.002>
- Ogawa, M., Sawaguchi, S., Kawai, T., Nadano, D., Matsuda, T., Yagi, H., Kato, K., Furukawa, K., Okajima, T., 2015. Impaired O -Linked N -Acetylglucosaminylation in the Endoplasmic Reticulum by Mutated Epidermal Growth Factor (EGF) Domain-specific O -Linked N -Acetylglucosamine Transferase Found in Adams-Oliver Syndrome. *J. Biol. Chem.* 290, 2137–2149. <https://doi.org/10.1074/jbc.M114.598821>

- Ogawa, M., Tashima, Y., Sakaguchi, Y., Takeuchi, H., Okajima, T., 2020. Contribution of extracellular O-GlcNAc to the stability of folded epidermal growth factor-like domains and Notch1 trafficking. *Biochem. Biophys. Res. Commun.* <https://doi.org/10.1016/j.bbrc.2020.03.066>
- Okido, M.M., Ragazini, C.S., Duarte, G., Coutinho, C.M., Marcolin, A.C., 2022. Severe Adams-Oliver Syndrome after Maternal COVID-19 Infection Could Be Another Effect of the SARS-CoV-2 Inflammatory Storm? Case Report. *Fetal Pediatr. Pathol.* 1–6. <https://doi.org/10.1080/15513815.2022.2064018>
- Olson, E.N., 2006. Gene Regulatory Networks in the Evolution and Development of the Heart. *Science* 313, 1922–1927. <https://doi.org/10.1126/science.1132292>
- Ota, S., Kawahara, A., 2014. Zebrafish: A model vertebrate suitable for the analysis of human genetic disorders: Zebrafish suitable for genetic analysis. *Congenit. Anom.* 54, 8–11. <https://doi.org/10.1111/cga.12040>
- Panni, S., Lovering, R.C., Porras, P., Orchard, S., 2020. Non-coding RNA regulatory networks. *Biochim. Biophys. Acta Gene Regul. Mech.* 1863, 194417. <https://doi.org/10.1016/j.bbagrm.2019.194417>
- Papoutsis, T., Luna-Zurita, L., Prados, B., Zaffran, S., de la Pompa, J.L., 2018. Bmp2 and Notch cooperate to pattern the embryonic endocardium. *Development* 163378. <https://doi.org/10.1242/dev.163378>
- Parisot, P., Mesbah, K., Théveniau-Ruissy, M., Kelly, R.G., 2011. Tbx1, subpulmonary myocardium and conotruncal congenital heart defects. *Birt. Defects Res. A. Clin. Mol. Teratol.* 91, 477–484. <https://doi.org/10.1002/bdra.20803>
- Parsons, M.J., Pisharath, H., Yusuff, S., Moore, J.C., Siekmann, A.F., Lawson, N., Leach, S.D., 2009. Notch-responsive cells initiate the secondary transition in larval zebrafish pancreas. *Mech. Dev.* 126, 898–912. <https://doi.org/10.1016/j.mod.2009.07.002>
- Pater, E. de, Clijsters, L., Marques, S.R., Lin, Y.-F., Garavito-Aguilar, Z.V., Yelon, D., Bakkens, J., 2009. Distinct phases of cardiomyocyte differentiation regulate growth of the zebrafish heart. *Development* 136, 1633–1641. <https://doi.org/10.1242/dev.030924>
- Paul, B., Montoya, G., 2020. CRISPR-Cas12a: Functional overview and applications. *Biomed. J.* 43, 8–17. <https://doi.org/10.1016/j.bj.2019.10.005>
- Penucci, R., Talpo, F., Astro, V., Montinaro, V., Morè, L., Cursi, M., Castoldi, V., Chiaretti, S., Bianchi, V., Marenga, S., Cambiaghi, M., Tonoli, D., Leocani, L., Biella, G., D'Adamo, P., de Curtis, I., 2015. Loss of Either Rac1 or Rac3 GTPase Differentially Affects the Behavior of Mutant Mice and the Development of Functional GABAergic Networks. *Cereb. Cortex* bhv274. <https://doi.org/10.1093/cercor/bhv274>
- Pereira-Da-Silva, L., Leal, F., Santos, G.C., Videira Amaral, J.M., Feijóo, M.J., 2000a. Clinical evidence of vascular abnormalities at birth in Adams-Oliver syndrome: report of two further cases. *Am. J. Med. Genet.* 94, 75–76. [https://doi.org/10.1002/1096-8628\(20000904\)94:1<75::aid-ajmg15>3.0.co;2-3](https://doi.org/10.1002/1096-8628(20000904)94:1<75::aid-ajmg15>3.0.co;2-3)
- Pickar-Oliver, A., Gersbach, C.A., 2019. The next generation of CRISPR–Cas technologies and applications. *Nat. Rev. Mol. Cell Biol.* 20, 490–507. <https://doi.org/10.1038/s41580-019-0131-5>
- Polacheck, W.J., Kutys, M.L., Yang, J., Eyckmans, J., Wu, Y., Vasavada, H., Hirschi, K.K., Chen, C.S., 2017. A non-canonical Notch complex regulates adherens junctions and vascular barrier function. *Nature* 552, 258–262. <https://doi.org/10.1038/nature24998>

- Pollard, T.D., Borisy, G.G., 2003. Cellular Motility Driven by Assembly and Disassembly of Actin Filaments. *Cell* 112, 453–465. [https://doi.org/10.1016/S0092-8674\(03\)00120-X](https://doi.org/10.1016/S0092-8674(03)00120-X)
- Poller, W., Dimmeler, S., Heymans, S., Zeller, T., Haas, J., Karakas, M., Leistner, D.-M., Jakob, P., Nakagawa, S., Blankenberg, S., Engelhardt, S., Thum, T., Weber, C., Meder, B., Hajjar, R., Landmesser, U., 2018. Non-coding RNAs in cardiovascular diseases: diagnostic and therapeutic perspectives. *Eur. Heart J.* 39, 2704–2716. <https://doi.org/10.1093/eurheartj/ehx165>
- Poon, K.L., Brand, T., 2013. The zebrafish model system in cardiovascular research: A tiny fish with mighty prospects. *Glob. Cardiol. Sci. Pract.* 2013, 4. <https://doi.org/10.5339/gcsp.2013.4>
- Portales-Casamar, E., Briançon-Marjollet, A., Fromont, S., Triboulet, R., Debant, A., 2006. Identification of novel neuronal isoforms of the Rho-GEF Trio. *Biol. Cell* 98, 183–193. <https://doi.org/10.1042/BC20050009>
- Qiao, X.-H., Wang, F., Zhang, X.-L., Huang, R.-T., Xue, S., Wang, J., Qiu, X.-B., Liu, X.-Y., Yang, Y.-Q., 2017. MEF2C loss-of-function mutation contributes to congenital heart defects. *Int. J. Med. Sci.* 14, 1143–1153. <https://doi.org/10.7150/ijms.21353>
- Quinn, J.J., Chang, H.Y., 2016. Unique features of long non-coding RNA biogenesis and function. *Nat. Rev. Genet.* 17, 47–62. <https://doi.org/10.1038/nrg.2015.10>
- Rambeau, P., Faure, E., Théron, A., Avierinos, J.-F., Jopling, C., Zaffran, S., Faucherre, A., 2017. Reduced aggrecan expression affects cardiac outflow tract development in zebrafish and is associated with bicuspid aortic valve disease in humans. *Int. J. Cardiol.* 249, 340–343. <https://doi.org/10.1016/j.ijcard.2017.09.174>
- Reicher, A., Foßelteder, J., Kwong, L.N., Pichler, M., 2018. Crosstalk between the Notch signaling pathway and long non-coding RNAs. *Cancer Lett.* 420, 91–96. <https://doi.org/10.1016/j.canlet.2018.01.070>
- Reischauer, S., Arnaout, R., Ramadass, R., Stainier, D.Y.R., 2014. Actin Binding GFP Allows 4D In Vivo Imaging of Myofilament Dynamics in the Zebrafish Heart and the Identification of Erbb2 Signaling as a Remodeling Factor of Myofibril Architecture. *Circ. Res.* 115, 845–856. <https://doi.org/10.1161/circresaha.115.304356>
- Rekosh, D., Hammarskjöld, M., 2018. Intron retention in viruses and cellular genes: Detention, border controls and passports. *WIREs RNA* 9. <https://doi.org/10.1002/wrna.1470>
- Ridley, A.J., 2015. Rho GTPase signalling in cell migration. *Curr. Opin. Cell Biol.* 36, 103–112. <https://doi.org/10.1016/j.ceb.2015.08.005>
- Ristori, T., Sjöqvist, M., Sahlgren, C.M., 2021. *Ex Vivo* Models to Decipher the Molecular Mechanisms of Genetic Notch Cardiovascular Disorders. *Tissue Eng. Part C Methods* 27, 167–176. <https://doi.org/10.1089/ten.tec.2020.0327>
- Roman, B.L., Pham, V.N., Lawson, N.D., Kulik, M., Childs, S., Lekven, A.C., Garrity, D.M., Moon, R.T., Fishman, M.C., Lechleider, R.J., Weinstein, B.M., 2002. Disruption of *acvr1* increases endothelial cell number in zebrafish cranial vessels. *Development* 129, 3009–3019. <https://doi.org/10.1242/dev.129.12.3009>
- Rottbauer, W., Saurin, A.J., Lickert, H., Shen, X., Burns, C.G., Wo, Z.G., Kemler, R., Kingston, R., Wu, C., Fishman, M., 2002. Reptin and Pontin Antagonistically Regulate Heart Growth in Zebrafish Embryos. *Cell* 111, 661–672. [https://doi.org/10.1016/S0092-8674\(02\)01112-1](https://doi.org/10.1016/S0092-8674(02)01112-1)

- Rottner, K., Faix, J., Bogdan, S., Linder, S., Kerkhoff, E., 2017. Actin assembly mechanisms at a glance. *J. Cell Sci.* 130, 3427–3435. <https://doi.org/10.1242/jcs.206433>
- Rual, J.-F., Hirozane-Kishikawa, T., Hao, T., Bertin, N., Li, S., Dricot, A., Li, N., Rosenberg, J., Lamesch, P., Vidalain, P.-O., Clingingsmith, T.R., Hartley, J.L., Esposito, D., Cheo, D., Moore, T., Simmons, B., Sequerra, R., Bosak, S., Doucette-Stamm, L., Le Peuch, C., Vandenhoute, J., Cusick, M.E., Albala, J.S., Hill, D.E., Vidal, M., 2004. Human ORFeome version 1.1: a platform for reverse proteomics. *Genome Res.* 14, 2128–2135. <https://doi.org/10.1101/gr.2973604>
- Sacilotto, N., Monteiro, R., Fritzsche, M., Becker, P.W., Sanchez-del-Campo, L., Liu, K., Pinheiro, P., Ratnayaka, I., Davies, B., Goding, C.R., Patient, R., Bou-Gharios, G., De Val, S., 2013. Analysis of *Dll4* regulation reveals a combinatorial role for Sox and Notch in arterial development. *Proc. Natl. Acad. Sci.* 110, 11893–11898. <https://doi.org/10.1073/pnas.1300805110>
- Sakaidani, Y., Ichianagi, N., Saito, C., Nomura, T., Ito, M., Nishio, Y., Nadano, D., Matsuda, T., Furukawa, K., Okajima, T., 2012. O-linked-N-acetylglucosamine modification of mammalian Notch receptors by an atypical O-GlcNAc transferase Eogt1. *Biochem. Biophys. Res. Commun.* 419, 14–19. <https://doi.org/10.1016/j.bbrc.2012.01.098>
- Sakaidani, Y., Nomura, T., Matsuura, A., Ito, M., Suzuki, E., Murakami, K., Nadano, D., Matsuda, T., Furukawa, K., Okajima, T., 2011. O-Linked-N-acetylglucosamine on extracellular protein domains mediates epithelial cell–matrix interactions. *Nat. Commun.* 2, 583. <https://doi.org/10.1038/ncomms1591>
- Sampaolo, S., Napolitano, F., Tirozzi, A., Reccia, M.G., Lombardi, L., Farina, O., Barra, A., Cirillo, F., Melone, M.A.B., Gianfrancesco, F., Iorio, G.D., Esposito, T., 2017. Identification of the first dominant mutation of LAMA5 gene causing a complex multisystem syndrome due to dysfunction of the extracellular matrix. *J. Med. Genet.* 54, 710–720. <https://doi.org/10.1136/jmedgenet-2017-104555>
- Sánchez-Posada, J., 2022. Dissecting the Links between Morphology and ECM Dynamics in the Developing Zebrafish Heart. University of Sheffield.
- Savage, A.M., Kurusamy, S., Chen, Y., Jiang, Z., Chhabria, K., MacDonald, R.B., Kim, H.R., Wilson, H.L., van Eeden, F.J.M., Armesilla, A.L., Chico, T.J.A., Wilkinson, R.N., 2019. *tmem33* is essential for VEGF-mediated endothelial calcium oscillations and angiogenesis. *Nat. Commun.* 10, 732. <https://doi.org/10.1038/s41467-019-08590-7>
- Savolainen, S.M., Foley, J.F., Elmore, S.A., 2009. Histology Atlas of the Developing Mouse Heart with Emphasis on E11.5 to E18.5. *Toxicol. Pathol.* 37, 395–414. <https://doi.org/10.1177/0192623309335060>
- Sawaguchi, S., Varshney, S., Ogawa, M., Sakaidani, Y., Yagi, H., Takeshita, K., Murohara, T., Kato, K., Sundaram, S., Stanley, P., Okajima, T., 2017. O-GlcNAc on NOTCH1 EGF repeats regulates ligand-induced Notch signaling and vascular development in mammals. *eLife* 6, e24419. <https://doi.org/10.7554/elife.24419>
- Schleich, J.-M., Abdulla, T., Summers, R., Houyel, L., 2013. An overview of cardiac morphogenesis. *Arch. Cardiovasc. Dis.* 106, 612–623. <https://doi.org/10.1016/j.acvd.2013.07.001>
- Schmidt, A., Hall, A., 2002. Guanine nucleotide exchange factors for Rho GTPases: turning on the switch. *Genes Dev.* 16, 1587–1609. <https://doi.org/10.1101/gad.1003302>

- Schröder, K.C., Duman, D., Tekin, M., Schanze, D., Sukalo, M., Meester, J., Wuyts, W., Zenker, M., 2019. Adams–Oliver syndrome caused by mutations of the *EOGT* gene. *Am. J. Med. Genet. A.* 179, 2246–2251. <https://doi.org/10.1002/ajmg.a.61313>
- Sehnert, A.J., Huq, A., Weinstein, B.M., Walker, C., Fishman, M., Stainier, D.Y.R., 2002. Cardiac troponin T is essential in sarcomere assembly and cardiac contractility. *Nat. Genet.* 31, 106–110. <https://doi.org/10.1038/ng875>
- Servián-Morilla, E., Takeuchi, H., Lee, T.V., Clarimon, J., Mavillard, F., Area-Gómez, E., Rivas, E., Nieto-González, J.L., Rivero, M.C., Cabrera-Serrano, M., Gómez-Sánchez, L., Martínez-López, J.A., Estrada, B., Márquez, C., Morgado, Y., Suárez-Calvet, X., Pita, G., Bigot, A., Gallardo, E., Fernández-Chacón, R., Hirano, M., Haltiwanger, R.S., Jafar-Nejad, H., Paradas, C., 2016. A *POGLUT 1* mutation causes a muscular dystrophy with reduced Notch signaling and satellite cell loss. *EMBO Mol. Med.* 8, 1289–1309. <https://doi.org/10.15252/emmm.201505815>
- Shaheen, R., Aglan, M., Keppler-Noreuil, K., Faqeih, E., Ansari, S., Horton, K., Ashour, A., Zaki, M.S., Al-Zahrani, F., Cueto-González, A.M., Abdel-Salam, G., Temtamy, S., Alkuraya, F.S., 2013. Mutations in *EOGT* Confirm the Genetic Heterogeneity of Autosomal-Recessive Adams-Oliver Syndrome. *Am. J. Hum. Genet.* 92, 598–604. <https://doi.org/10.1016/j.ajhg.2013.02.012>
- Shaheen, R., Faqeih, E., Sunker, A., Morsy, H., Al-Sheddi, T., Shamseldin, H.E., Adly, N., Hashem, M., Alkuraya, F.S., 2011a. Recessive Mutations in *DOCK6*, Encoding the Guanidine Nucleotide Exchange Factor *DOCK6*, Lead to Abnormal Actin Cytoskeleton Organization and Adams-Oliver Syndrome. *Am. J. Hum. Genet.* 89, 328–333. <https://doi.org/10.1016/j.ajhg.2011.07.009>
- Shaheen, R., Faqeih, E., Sunker, A., Morsy, H., Al-Sheddi, T., Shamseldin, H.E., Adly, N., Hashem, M., Alkuraya, F.S., 2011b. Recessive mutations in *DOCK6*, encoding the guanidine nucleotide exchange factor *DOCK6*, lead to abnormal actin cytoskeleton organization and Adams-Oliver syndrome. *Am. J. Hum. Genet.* 89, 328–333. <https://doi.org/10.1016/j.ajhg.2011.07.009>
- Shi, S., Stanley, P., 2003. Protein O -fucosyltransferase 1 is an essential component of Notch signaling pathways. *Proc. Natl. Acad. Sci.* 100, 5234–5239. <https://doi.org/10.1073/pnas.0831126100>
- Shoji, W., Sato-Maeda, M., 2008. Application of heat shock promoter in transgenic zebrafish. *Dev. Growth Differ.* 50, 401–406. <https://doi.org/10.1111/j.1440-169X.2008.01038.x>
- Siebel, C., Lendahl, U., 2017. Notch Signaling in Development, Tissue Homeostasis, and Disease. *Physiol. Rev.* 97, 1235–1294. <https://doi.org/10.1152/physrev.00005.2017>
- Snape, K.M.G., Ruddy, D., Zenker, M., Wuyts, W., Whiteford, M., Johnson, D., Lam, W., Trembath, R.C., 2009. The spectra of clinical phenotypes in aplasia cutis congenita and terminal transverse limb defects. *Am. J. Med. Genet. A.* 149A, 1860–1881. <https://doi.org/10.1002/ajmg.a.32708>
- Southgate, L., Machado, R.D., Snape, K.M., Primeau, M., Dafou, D., Ruddy, D.M., Branney, P.A., Fisher, M., Lee, G.J., Simpson, M.A., He, Y., Bradshaw, T.Y., Blaumeiser, B., Winship, W.S., Reardon, W., Maher, E.R., FitzPatrick, D.R., Wuyts, W., Zenker, M., Lamarche-Vane, N., Trembath, R.C., 2011. Gain-of-Function Mutations of *ARHGAP31*, a *Cdc42/Rac1* GTPase Regulator, Cause Syndromic Cutis Aplasia and Limb Anomalies. *Am. J. Hum. Genet.* 88, 574–585. <https://doi.org/10.1016/j.ajhg.2011.04.013>

- Southgate, L., Sukalo, M., Karountzos, A.S.V., Taylor, E.J., Collinson, C.S., Ruddy, D., Snape, K.M., Dallapiccola, B., Tolmie, J.L., Joss, S., Brancati, F., Digilio, M.C., Graul-Neumann, L.M., Salviati, L., Coerdts, W., Jacquemin, E., Wuyts, W., Zenker, M., Machado, R.D., Trembath, R.C., 2015. Haploinsufficiency of the NOTCH1 Receptor as a Cause of Adams–Oliver Syndrome With Variable Cardiac Anomalies. *Circ. Cardiovasc. Genet.* 8, 572–581. <https://doi.org/10.1161/circgenetics.115.001086>
- Srinivas, B.P., Woo, J., Leong, W.Y., Roy, S., 2007. A conserved molecular pathway mediates myoblast fusion in insects and vertebrates. *Nat. Genet.* 39, 781–786. <https://doi.org/10.1038/ng2055>
- Srivastava, D., Olson, E.N., 2000. A genetic blueprint for cardiac development. *Nature* 407, 35025190. <https://doi.org/10.1038/35025190>
- Stainier, D.Y., Weinstein, B.M., Detrich, H.W., Zon, L.I., Fishman, M.C., 1995. Cloche, an early acting zebrafish gene, is required by both the endothelial and hematopoietic lineages. *Development* 121, 3141–3150. <https://doi.org/10.1242/dev.121.10.3141>
- Staudt, D., Stainier, D., 2012. Uncovering the Molecular and Cellular Mechanisms of Heart Development Using the Zebrafish. *Annu. Rev. Genet.* 46, 397–418. <https://doi.org/10.1146/annurev-genet-110711-155646>
- Stittrich, A.-B., Lehman, A., Bodian, D.L., Ashworth, J., Zong, Z., Li, H., Lam, P., Khromykh, A., Iyer, R.K., Vockley, J.G., Baveja, R., Silva, E.S., Dixon, J., Leon, E.L., Solomon, B.D., Glusman, G., Niederhuber, J.E., Roach, J.C., Patel, M.S., 2014. Mutations in NOTCH1 Cause Adams-Oliver Syndrome. *Am. J. Hum. Genet.* 95, 275–284. <https://doi.org/10.1016/j.ajhg.2014.07.011>
- Sukalo, M., Tilsen, F., Kayserili, H., Müller, D., Tüysüz, B., Ruddy, D.M., Wakeling, E., Ørstavik, K.H., Snape, K.M., Trembath, R., Smedt, M., Aa, N., Skalej, M., Mundlos, S., Wuyts, W., Southgate, L., Zenker, M., 2015. DOCK6 Mutations Are Responsible for a Distinct Autosomal-Recessive Variant of Adams–Oliver Syndrome Associated with Brain and Eye Anomalies. *Hum. Mutat.* 36, 593–598. <https://doi.org/10.1002/humu.22795>
- Suzuki, D., Yamada, A., Kamijo, R., 2013. The essential roles of the small GTPase Rac1 in limb development. *J. Oral Biosci.* 55, 116–121. <https://doi.org/10.1016/j.job.2013.05.002>
- Swartz, E.N., Sanatani, S., Sandor, G.G., Schreiber, R.A., 1999. Vascular abnormalities in Adams-Oliver syndrome: cause or effect? *Am. J. Med. Genet.* 82, 49–52. [https://doi.org/10.1002/\(sici\)1096-8628\(19990101\)82:1<49::aid-ajmg10>3.0.co;2-m](https://doi.org/10.1002/(sici)1096-8628(19990101)82:1<49::aid-ajmg10>3.0.co;2-m)
- Swope, D., Kramer, J., King, T.R., Cheng, Y.-S., Kramer, S.G., 2014. Cdc42 is required in a genetically distinct subset of cardiac cells during *Drosophila* dorsal vessel closure. *Dev. Biol.* 392, 221–232. <https://doi.org/10.1016/j.ydbio.2014.05.024>
- Sylva, M., Hoff, M.J.B. van den, Moorman, A.F.M., 2014. Development of the human heart. *Am. J. Med. Genet. A.* 164, 1347–1371. <https://doi.org/10.1002/ajmg.a.35896>
- Taminato, T., Yokota, D., Araki, S., Ovara, H., Yamasu, K., Kawamura, A., 2016. Enhancer activity-based identification of functional enhancers using zebrafish embryos. *Genomics* 108, 102–107. <https://doi.org/10.1016/j.ygeno.2016.05.005>

- Tan, W., Palmby, T.R., Gavard, J., Amornphimoltham, P., Zheng, Y., Gui, J.S., 2008. An essential role for Rac1 in endothelial cell function and vascular development. *FASEB J.* 22, 1829–1838. <https://doi.org/10.1096/fj.07-096438>
- Tashima, Y., Okajima, T., 2018. Congenital diseases caused by defective O-glycosylation of Notch receptors. *Nagoya J. Med. Sci.* 80, 299–307. <https://doi.org/10.18999/nagjms.80.3.299>
- Tessadori, F., Roessler, H.I., Savelberg, S.M.C., Chocron, S., Kamel, S.M., Duran, K.J., Haelst, M.M. van, Haafte, G. van, Bakkers, J., 2018. Effective CRISPR/Cas9-based nucleotide editing in zebrafish to model human genetic cardiovascular disorders. *Dis. Model. Mech.* 11, dmm035469. <https://doi.org/10.1242/dmm.035469>
- Timmerman, L.A., Grego-Bessa, J., Raya, A., Bertrán, E., Pérez-Pomares, J.M., Díez, J., Aranda, S., Palomo, S., McCormick, F., Izpisua-Belmonte, J.C., de la Pompa, J.L., 2004. Notch promotes epithelial-mesenchymal transition during cardiac development and oncogenic transformation. *Genes Dev.* 18, 99–115. <https://doi.org/10.1101/gad.276304>
- Torrado, M., Iglesias, R., Nespereira, B., Centeno, A., López, E., Mikhailov, A.T., 2009a. Intron retention generates ANKRD1 splice variants that are co-regulated with the main transcript in normal and failing myocardium. *Gene* 440, 28–41. <https://doi.org/10.1016/j.gene.2009.03.017>
- Trevarrow, B., Marks, D.L., Kimmel, C.B., 1990. Organization of hindbrain segments in the zebrafish embryo. *Neuron* 4, 669–679. [https://doi.org/10.1016/0896-6273\(90\)90194-K](https://doi.org/10.1016/0896-6273(90)90194-K)
- Tu, S., Chi, N.C., 2012. Zebrafish models in cardiac development and congenital heart birth defects. *Differentiation* 84, 4–16. <https://doi.org/10.1016/j.diff.2012.05.005>
- Ullrich, S., Guigó, R., 2020. Dynamic changes in intron retention are tightly associated with regulation of splicing factors and proliferative activity during B-cell development. *Nucleic Acids Res.* 48, 1327–1340. <https://doi.org/10.1093/nar/gkz1180>
- Van Aelst, L., D'Souza-Schorey, C., 1997. Rho GTPases and signaling networks. *Genes Dev.* 11, 2295–2322. <https://doi.org/10.1101/gad.11.18.2295>
- van der Oost, J., Jore, M.M., Westra, E.R., Lundgren, M., Brouns, S.J.J., 2009. CRISPR-based adaptive and heritable immunity in prokaryotes. *Trends Biochem. Sci.* 34, 401–407. <https://doi.org/10.1016/j.tibs.2009.05.002>
- Vanichkina, D.P., Schmitz, U., Wong, J.J.-L., Rasko, J.E.J., 2018. Challenges in defining the role of intron retention in normal biology and disease. *Semin. Cell Dev. Biol.* 75, 40–49. <https://doi.org/10.1016/j.semcdb.2017.07.030>
- Varadkar, P., Kraman, M., Despres, D., Ma, G., Lozier, J., McCright, B., 2008. Notch2 is required for the proliferation of cardiac neural crest-derived smooth muscle cells. *Dev. Dyn.* 237, 1144–1152. <https://doi.org/10.1002/dvdy.21502>
- Varshney, S., Stanley, P., 2017. EOGT and O-GlcNAc on secreted and membrane proteins. *Biochem. Soc. Trans.* 45, 401–408. <https://doi.org/10.1042/bst20160165>
- Vermot, J., Forouhar, A.S., Liebling, M., Wu, D., Plummer, D., Gharib, M., Fraser, S.E., 2009. Reversing Blood Flows Act through *klf2a* to Ensure Normal Valvulogenesis in the Developing Heart. *PLoS Biol.* 7, e1000246. <https://doi.org/10.1371/journal.pbio.1000246>
- Vogler, G., Liu, J., Iafe, T.W., Migh, E., Mihály, J., Bodmer, R., 2014. Cdc42 and formin activity control non-muscle myosin dynamics during *Drosophila* heart

- morphogenesis. *J. Cell Biol.* 206, 909–922. <https://doi.org/10.1083/jcb.201405075>
- Wang, B., Rekosh, D., Hammarskjold, M.-L., 2015. Evolutionary conservation of a molecular machinery for export and expression of mRNAs with retained introns. *RNA N. Y. N* 21, 426–437. <https://doi.org/10.1261/rna.048520.114>
- Wang, T., Chen, Lizhang, Yang, T., Huang, P., Wang, L., Zhao, L., Zhang, S., Ye, Z., Chen, Letao, Zheng, Z., Qin, J., 2019. Congenital Heart Disease and Risk of Cardiovascular Disease: A Meta-Analysis of Cohort Studies. *J. Am. Heart Assoc.* 8, e012030. <https://doi.org/10.1161/jaha.119.012030>
- Wang, Y., Fang, Y., Lu, P., Wu, B., Zhou, B., 2021. NOTCH Signaling in Aortic Valve Development and Calcific Aortic Valve Disease. *Front. Cardiovasc. Med.* 8, 682298. <https://doi.org/10.3389/fcvm.2021.682298>
- Williams, K., Carson, J., Lo, C., 2019. Genetics of Congenital Heart Disease. *Biomolecules* 9, 879. <https://doi.org/10.3390/biom9120879>
- Wong, J.J.-L., Au, A.Y.M., Ritchie, W., Rasko, J.E.J., 2016. Intron retention in mRNA: No longer nonsense: Known and putative roles of intron retention in normal and disease biology. *BioEssays News Rev. Mol. Cell. Dev. Biol.* 38, 41–49. <https://doi.org/10.1002/bies.201500117>
- Xiao, Y., Gao, M., Gao, L., Zhao, Y., Hong, Q., Li, Z., Yao, J., Cheng, H., Zhou, R., 2016. Directed Differentiation of Zebrafish Pluripotent Embryonic Cells to Functional Cardiomyocytes. *Stem Cell Rep.* 7, 370–382. <https://doi.org/10.1016/j.stemcr.2016.07.020>
- Yalcin, H.C., Amindari, A., Butcher, J.T., Althani, A., Yacoub, M., 2017. Heart function and hemodynamic analysis for zebrafish embryos. *Dev. Dyn.* 246, 868–880. <https://doi.org/10.1002/dvdy.24497>
- Yang, C., Hu, J.-F., Zhan, Q., Wang, Z.-W., Li, G., Pan, J.-J., Huang, L., Liao, C.-Y., Huang, Y., Tian, Y.-F., Shen, B.-Y., Chen, J.-Z., Wang, Y.-D., Chen, S., 2021. SHCBP1 interacting with EOGT enhances O-GlcNAcylation of NOTCH1 and promotes the development of pancreatic cancer. *Genomics* 113, 827–842. <https://doi.org/10.1016/j.ygeno.2021.01.010>
- Yang, C., Svitkina, T., 2011. Filopodia initiation: Focus on the Arp2/3 complex and formins. *Cell Adhes. Migr.* 5, 402–408. <https://doi.org/10.4161/cam.5.5.16971>
- Yang, J., Bücker, S., Jungblut, B., Böttger, T., Cinnamon, Y., Tchorz, J., Müller, M., Bettler, B., Harvey, R., Sun, Q.-Y., Schneider, A., Braun, T., 2012. Inhibition of Notch2 by Numb/Numbl-like controls myocardial compaction in the heart. *Cardiovasc. Res.* 96, 276–285. <https://doi.org/10.1093/cvr/cvs250>
- Yelon, D., Horne, S.A., Stainier, D.Y.R., 1999. Restricted Expression of Cardiac Myosin Genes Reveals Regulated Aspects of Heart Tube Assembly in Zebrafish. *Dev. Biol.* 214, 23–37. <https://doi.org/10.1006/dbio.1999.9406>
- Yue, L., Wan, R., Luan, S., Zeng, W., Cheung, T.H., 2020. Dek Modulates Global Intron Retention during Muscle Stem Cells Quiescence Exit. *Dev. Cell* 53, 661–676.e6. <https://doi.org/10.1016/j.devcel.2020.05.006>
- Zepeda-Romero, L.C., Zenker, M., Schanze, D., Schanze, I., Peña-Padilla, C., Quezada-Salazar, C.A., Pacheco-Torres, P.A., Rivera-Montellano, M.L., Aguirre-Guillén, R.L., Bobadilla-Morales, L., Corona-Rivera, A., Corona-Rivera, J.R., 2022. Intrafamilial phenotypic variability in autosomal recessive DOCK6-related Adams-Oliver syndrome. *Eur. J. Med. Genet.* 65, 104653. <https://doi.org/10.1016/j.ejmg.2022.104653>
- Zhang, Z.-Y., Sun, Y.-Y., Wang, H.-C., Fu, W.-N., Sun, C.-F., 2022. Overexpression of DOCK6 in oral squamous cell cancer promotes cellular migration and

- invasion and is associated with poor prognosis. *Arch. Oral Biol.* 133, 105297. <https://doi.org/10.1016/j.archoralbio.2021.105297>
- Zhou, B., Lin, W., Long, Y., Yang, Y., Zhang, H., Wu, K., Chu, Q., 2022. Notch signaling pathway: architecture, disease, and therapeutics. *Signal Transduct. Target. Ther.* 7, 95. <https://doi.org/10.1038/s41392-022-00934-y>
- Zhou, S., Wang, Q., Meng, Z., Peng, J., Zhou, Y., Song, W., Wang, J., Chen, S., Sun, K., 2020. Mutations in fibroblast growth factor (FGF8) and FGF10 identified in patients with conotruncal defects. *J. Transl. Med.* 18, 283. <https://doi.org/10.1186/s12967-020-02445-2>
- Zhou, Y., Cashman, T.J., Nevis, K.R., Obregon, P., Carney, S.A., Liu, Y., Gu, A., Mosimann, C., Sondalle, S., Peterson, R.E., Heideman, W., Burns, C.E., Burns, C.G., 2011. Latent TGF- β binding protein 3 identifies a second heart field in zebrafish. *Nature* 474, 645–648. <https://doi.org/10.1038/nature10094>
- Zhou, Y., Fan, R.-G., Qin, C.-L., Jia, J., Wu, X.-D., Zha, W.-Z., 2019. LncRNA-H19 activates CDC42/PAK1 pathway to promote cell proliferation, migration and invasion by targeting miR-15b in hepatocellular carcinoma. *Genomics* 111, 1862–1872. <https://doi.org/10.1016/j.ygeno.2018.12.009>
- Zoysa, P.D., Liu, J., Toubat, O., Choi, J., Moon, A., Gill, P.S., Duarte, A., Sucov, H.M., Kumar, S.R., 2020. Delta-like ligand 4-mediated Notch signaling controls proliferation of second heart field progenitor cells by regulating Fgf8 expression 13.